

SYNTHESIS OF SEISMICITY AND GEOLOGICAL DATA IN CALIFORNIA

John G. Anderson

University of California, San Diego
La Jolla, California 92093

U.S.G.S. CONTRACT NO. 14-08-0001-19766
Supported by the EARTHQUAKE HAZARDS REDUCTION PROGRAM

OPEN-FILE NO. 84-424

U.S. Geological Survey
OPEN FILE REPORT

This report was prepared under contract to the U.S. Geological Survey and has not been reviewed for conformity with USGS editorial standards and stratigraphic nomenclature. Opinions and conclusions expressed herein do not necessarily represent those of the USGS. Any use of trade names is for descriptive purposes only and does not imply endorsement by the USGS.

CONTENTS

Cover page

Contents

Technical Report Summary

Appendix I: **Comparison of instrumentally recorded seismicity
in California with predictions based on geological
slip rates.**

Appendix II: **Consequence of slip rate constraints on
earthquake occurrence relations.**

SYNTHESIS OF SEISMICITY AND GEOLOGICAL DATA IN CALIFORNIA

USGS USDI 14-08-0001-6-501

John G. Anderson

Institute of Geophysics and Planetary Physics (A025)

Scripps Institution of Oceanography

University of California, San Diego

La Jolla, California 92093

(619) 452-2424

Investigations

- (1) Compile as complete as possible a set of slip rates for major faults in California.
- (2) Compare the historical seismicity on each of these faults with activity rates which are needed to maintain the slip rate.
- (3) Determine if this information will be useful for predicting earthquakes.

Results

Geological slip rates have been compiled for 69 faults in the state of California, United States of America. Furthermore, bounds on the instrumentally recorded occurrence rate of earthquakes in the vicinity of each of these faults and additional observational parameters have also been compiled, including fault length, and instrumentally observed maximum magnitude on the fault and seismic slip rate.

Based on these data, several relationships have been investigated. The maximum observed magnitude M on each fault but one is bounded by $M = \frac{4}{3} (\log L + 3.29)$, where L is the total length of the fault and the relationship is derived from the scaling of Scholz (1982). Attention has been paid to the ratio R of observed occurrence rate of events to the rate predicted from the seismic slip rate. Most of the observations show R between 0.1 and 10, but several cases of R as small as 0.01 have been observed. On those faults which have apparently seen a 1000 year earthquake during the period of instrumental observations, R is about 10 at all magnitudes, implying that aftershocks are sufficient to assure that the Gutenberg-Richter relationship between the logarithms of occurrence rates and magnitude holds at small magnitudes when occurrence rates are averaged over a complete seismic cycle involving long periods of quiescence. Thus currently quiescent faults, such as segments of the San Andreas fault, are not evidence for the failure of the Gutenberg-Richter relationship on individual faults.

The ratio R was also investigated as a possible predictor for earthquakes, but it does not appear to be particularly good. In particular, the criteria $R > 1$ appears to have a missed forecast rate of about 75%, and a false forecast rate of about 90%. However, detailed study with better constrained slip rates might eventually allow this criterion to help with the earthquake prediction problem on some faults.

A study has been made on the theoretical distributions of seismicity which will generate a given slip rate. This study (Anderson and Luco, 1983) extends the methods of Anderson (1979) to another form for the distribution curve of the number of earthquakes at each magnitude, and investigates the sensitivity of seismicity estimates to the estimate for maximum magnitude. It also explores ways in which point observations of historical seismicity such as those of Siesh (1978) at Pallett Creek can be interpreted. One interpretation of the Pallett Creek earthquake sequence could imply that the distribution of magnitudes recorded in the record is consistent with a $\log n = a - bM$ distribution as used by Anderson (1979), but with a very low b-value not distinguishable from zero.

Although not required for the completion of this contract, a study was made on how to use precursor observations to obtain predictions. Anderson (1982) treats, in a statistical manner, the class of geophysical observations that sometimes are precursors to a large earthquake, but at other times occur apparently unrelated to any earthquakes in time or space. Each such observation is handled by associating it with the largest ensuing earthquake in a definite time and spatial window; then the probability that the observation is useful is estimated from the difference between this extreme value distribution and the long-term average extreme value distribution for the same region. This probability that the precursor is useful can then be incorporated into calculations of the revised probability of an earthquake following observation of one (a trivial case) or several unreliable precursors to derive the revised probability of a significant earthquake. The model takes full account of the magnitude distribution of earthquakes and of discrete levels of precursor observations. The United States earthquake prediction program is still many years from being able to obtain the full benefits of the model. However, the model suggests useful statistics the program should gather on unreliable precursors.

References

Anderson, J.G. (1979). Estimating the seismicity from geological structure for seismic risk studies, Bull. Seism. Soc. Am., 69, 135-158.

Anderson, J.G. (1981). A simple way to look at a Bayesian model for the statistics of earthquake prediction, Bull. Seism. Soc. Am., 71, 1929-1931.

Anderson, J.G. (1982). Revised estimates for the probabilities of earthquakes following observations of unreliable precursors, Bull. Seism. Soc. Am., 72, 879-888.

Anderson, J.G. (1983). Comparison of instrumentally recorded seismicity in California with predictions based on geological slip rates, (in preparation).

Anderson, J.G. and J.E. Luco (1983). Consequences of slip rate constraints on earthquake occurrence relations, Bull. Seism. Soc. Am., (in press, April).

Sieh, K.E. (1978). Prehistoric large earthquakes produced by slip on the San Andreas fault at Pallett Creek, California, J. Geophys. Res., 83, 3907-3939.

COMPARISON OF INSTRUMENTALLY RECORDED SEISMICITY IN CALIFORNIA
WITH PREDICTIONS BASED ON GEOLOGICAL SLIP RATES

John G. Anderson
Institute of Geophysics and Planetary Physics,
Scripps Institution of Oceanography, (A025)
University of California, San Diego
La Jolla, California, 92093

Abstract

Geological slip rates have been compiled for 69 faults in the state of California, United States of America. Furthermore, bounds on the instrumentally recorded occurrence rate of earthquakes in the vicinity of each of these faults and additional observational parameters have also been compiled, including fault length, and instrumentally observed maximum magnitude on the fault and seismic slip rate.

Based on these data, several relationships have been investigated. The maximum observed magnitude M on each fault but one is bounded by $M = \frac{4}{3} (\log L + 3.29)$, where L is the total length of the fault and the relationship is derived from the scaling of Scholz (1982). Attention has been paid to the ratio R of observed occurrence rate of events to the rate predicted from the seismic slip rate. Most of the observations show R between 0.1 and 10, but several cases of R as small as 0.01 have been observed. On those faults which have apparently seen a 1000 year earthquake during the period of instrumental observations, R is about 10 at all magnitudes, implying that aftershocks are sufficient to assure that the Gutenberg-Richter relationship between the logarithms of occurrence rates and magnitude holds at small magnitudes when occurrence rates are averaged over a complete seismic cycle involving long periods of quiescence. Thus currently quiescent faults, such as segments of the San Andreas fault, are not evidence for the failure of the Gutenberg-Richter relationship on individual faults.

The ratio R was also investigated as a possible predictor for earthquakes, but it does not appear to be particularly good. In particular, the criterion $R > 1$ appears to have a missed forecast rate of about 75%, and a false forecast rate of about 90%. However, detailed study with better constrained slip rates might eventually allow this criterion to help with the earthquake prediction problem on some faults.

Introduction

It is well established that the slip rate on a fault is correlated with the average occurrence rate of large earthquakes on the fault. Brune (1968) and Davies and Brune (1971) established this on a worldwide

Appendix I

basis. Anderson (1979) and Molnar (1979) have shown how slip rates can be inverted to constrain occurrence relations. Anderson and Luco (1982) have generalized that procedure to several occurrence relations. Anderson (1979), Greensfelder *et al.*, (1980), and Doser and Smith (1982) have used slip rates to study regional seismicity.

While the method works well on a regional to global scale, inspection of results by Anderson (1979) indicate that for individual faults, geological and instrumental seismicity often differ considerably. This should come as no surprise, for the duration of instrumental records is short compared to the repeat times of large earthquakes on many faults. One reasonable hypothesis would be that on faults with long recurrence times, the instrumental seismicity should be larger than geological seismicity if a major earthquake has occurred, and smaller if it has not occurred. There would be no discrepancy only when the observation period compares with or exceeds the recurrence interval.

The possibility that the discrepancy is systematic like that raises several questions, also. One possibility would be that the ratio of low level seismicity to theory is predictable, or can be bounded, based on the slip rate, even in the interval between major earthquakes. If this were proven, it could have an important effect by allowing bounds on the usually poorly defined inputs to seismic risk analysis. Another useful observation would be if this discrepancy were some function of the part of the seismicity cycle on the fault, and thus could be used in a predictive capacity.

This paper undertakes to investigate the discrepancy between geological and instrumental seismicity on a fault by fault basis in California. The region is excellent for such a study, as detailed earthquake catalogs exist and as there is a wealth of geological data pertaining to slip rates on many major faults.

Geological Slip Rates

There are now several compilations of estimates for the geological slip rate on the major faults of California. These include Anderson (1979), Herd (1979), Woodward-Clyde Consultants (1979), Eguchi *et al.* (1979), and Bird (1982). Slip rate estimates for a few additional faults are presented in Table 1. Table 2 lists the slip rate bounds and best estimates for many of the important faults in California, as given in each of the above compilations.

Inspection of Table 2 shows that there is general agreement of these sources for faults with a large slip rate. We note, however, that these are secondary sources, and the consistency may result only from consulting the same primary sources. In general, for faults with smaller slip rates, the consistency is not as good. Also, for strike-slip faults, the scatter in estimates tends to be lower than for thrust

Appendix I

or normal faults. The estimates given by Eguchi *et al.* (1979), based on "expert opinion", cannot be verified by normal scientific procedures and are therefore given less weight than other estimates during further studies. A subjective "best" estimate, and reasonable bounds on the slip rates of each fault was culled from Table 2, and is listed in Table 4.

Instrumental Seismicity

Instrumental occurrence rates have been determined in quadrilateral areas surrounding each of 72 faults. Figure 1 shows an index map which locates each of the eight regions in California considered. Figure 2 A-H show these eight regions, major faults, and quadrilateral boundaries. Figure 3 A-B repeat these regions and show the instrumental epicenters for $M \geq 4$. Table 3 lists the quadrilateral corner coordinates for each of the faults shown on Figures 2 or 3.

Quadrilaterals were drawn on the Fault Map of California (Jennings, 1975) without specific reference to the seismicity maps. Some attempt was made to avoid overlapping regions where that was reasonable. In the Transverse Ranges (Map 3), that became impossible without causing the zone to be excessively narrow, and there, in particular, the zones overlap considerably. After the zones were defined in this manner, boundaries were adjusted only to incorporate any significant earthquakes which were initially excluded. On Figures 2 and 3, names followed by an asterisk were motivated by some geographical factor other than the fault name itself on Jennings (1975), as the fault is unnamed on Jennings (1975).

Earthquake epicenters were read from the EDIS (Earthquake Data Information Service) data tape (Meyers and Von Hake, 1976) complete through December 1979. Output of each seismicity search included a plot of cumulative moment versus time, and a plot from which occurrence rates were measured. The cumulative moment was defined by assigning to each earthquake of magnitude M_L a moment $M_0 = 10^{16+1.5M_L}$.

The procedure for the determination of occurrence rates deserves some more detailed explanation. It is assumed that one does not have a fundamental basis for selection of the appropriate time interval to determine the average occurrence rate but that the most recent data is most likely to give complete coverage of a given magnitude interval. One expects that the time interval is variable between magnitude classes on any individual fault. Furthermore, it is concluded that reasonable upper and lower bounds on the occurrence rate would be an appropriate way to characterize the occurrence rates for the purposes of this study. Therefore, when earthquakes satisfied the location criteria, they were sorted into magnitude classes ($3.0 \leq M < 3.99$, $4.0 \leq M < 4.99$, etc.) and the number of events per year in each magnitude class was counted. Then a sequence of averages, A_k , was formed: A_1 based on the most recent one

Appendix I

year of data, A_2 based on the most recent two years of data, ..., and A_k based on the most recent k years of data. The plots from which earthquake occurrence rates are calculated show $\log A_k$ as a function of $\log k$. These plots were used to choose upper and lower bounds on instrumental occurrence rates.

It was found that these plots, giving average rate versus duration of average, take one of five typical shapes. These are illustrated in Figure 4. Shape 1 represents a fairly well-defined average occurrence rate resulting from stable seismicity and good instrumental coverage. The average occurrence rate usually is determined to within a factor of less than 2, regardless of how long the interval which is averaged is chosen to be.

Shape 2 occurs for low occurrence rates, when two or more earthquakes have occurred. The bounds one obtains are wider or narrower depending on when the earthquakes occurred. This shape is recognized when the earthquakes are widely separated in time, so that the bounds correspond to averages over long time periods, as in Figure 4. When the earthquakes occurred close together in time, a different characteristic shape (usually 5) appeared.

Shape 3, shown in Figure 4, results from a recent increase in activity which is small (less than a factor of about 5), resulting in an asymptotic decay toward earlier levels. A lower bound on the activity rate is usually easily selected, but the upper bound is ambiguous. This shape can result from expanding instrumental coverage, as well as the case in which the higher activity rates derived from the shorter averages may represent long-term trends. The upper bound was sometimes chosen by selection of a time interval which caused a relative maximum at other magnitude levels. Shape 4 results when an earthquake early in the record causes very high activity, but subsequent rates have been lower. In Figure 4, a relatively well-determined average, in the most recent years gives the impression that aftershocks of the major event may be over. In other cases, a stable average cannot be recognized because aftershocks are continuing. The upper bound depends on the time the main shock occurred. This shape gives no information about the occurrence rates prior to the main shock.

Shape 5 results when all the earthquakes occurred at nearly the same time (often there is only one). In this case additional assumptions are needed to define the lower bound (we usually took 50 or 100 years, depending on magnitude level), while the upper bound depends on when the earthquake occurred, and probably overestimates the occurrence rate.

Table 4 lists on a fault by fault basis, the occurrence rate bounds and the type of curve which the earthquakes caused to define these bounds. The complete set of occurrence rate plots, and the

Appendix I

interpretations, are shown in Appendix I-1.

There are several additional observations which are listed in Table 4. The seismic slip rate is derived by summing assumed moments of historical events, using the assumed moment $M_0 = 10^{(16+1.5M_L)}$ for events with magnitude M_L (Hanks and Kanamori, 1979). The moment is assumed to be released in a fault length, L, given, and a fault width of 10 km. The time interval T is the duration used in this average, with all intervals ending December 1979. The largest magnitude in this time interval is also listed. From the fault length, and the assumption $w/L = 1.25 \times 10^{-5}$ (Scholz, 1982; Anderson and Luco, 1983), a theoretical maximum moment was derived, and converted to the theoretical maximum magnitude by the relation given above. The maximum magnitudes in Table 4 sometimes differ from this estimate for faults which required more than one quadrilateral to carry out the search. The empirical b-value was derived from a plot of the bounds on seismicity rates against magnitude and a visual fit through the data. Rigorous estimates of the b-values (eg. Knopoff *et al.*, 1982) would necessarily include the estimates in Table 4 within formal error limits.

Characteristics of Observed Occurrence Rates

Figure 5 illustrates how the estimated upper and lower bounds on occurrence rates which are given in Table 4 compare. Many of the points show an upper bound equal to about twice the lower bound, but upper bounds of ten times the lower bound are seen in a few cases. The observed occurrence rates are all between 10^{-2} and 30 events/year, or about 3.5 orders of magnitude. Obviously, larger occurrence rates would occur if larger regions had been chosen. The lower limit is simply a result of the short seismicity catalog and not a physical property. Where the rate is in reality less than 10^{-2} /year either there were no events and the estimate is zero, or there were events, and the rate becomes estimated at greater than 10^{-2} /year.

Figure 6 shows incremental occurrence rates (n^I) on each fault for magnitude intervals above $M = 4$ plotted as a function of the occurrence rates for events in the magnitude range $3.0 \leq M \leq 3.99$. For this plot, the upper bound on occurrence rates in each range has been employed. This figure shows, in a compact format, the same information as a Gutenberg-type plot of occurrence rate against magnitude. On this figure, data from each fault appear on a vertical line. If each of these data sets obeyed the law $\log n^I = 10^{a-bM}$, with the same b-value on each fault, then all points would fall on diagonal lines with slope 1; the separation would be determined by the b-value. Such lines are shown for $b = 0.83$, and data cluster in the vicinity of these predictions. Because of the difficulty involved in measuring small occurrence rates with a 50 year time sample, data in the upper right half of this plot are more reliable than data in the lower-left half of the plot. The

Appendix I

choice of $b = 0.83$ is estimated by a visual fitting procedure to these more reliable data.

Characteristics of Maximum Magnitude

Figure 7 compares the total fault length and the maximum observed magnitude for each entry to Table 4. In addition, a theoretical relationship of magnitude and rupture length from Anderson and Luco (1983) has been plotted. This relationship,

$$\log L = 0.75M - 3.29 ,$$

where L is the rupture length in kilometers, was derived on the assumption that the ratio of the average slip (u) to the rupture length is a constant equal to 1.25×10^{-5} (Scholz, 1982), that the rupture width is constant ($w = 10 \text{ km}$) and that the seismic moment is related to the magnitude by $M_0 = 10^{16+1.5M}$ (Hanks and Kanamori, 1979). The one datum to the right of this curve is the 1952 Kern County earthquake on the White Wolf fault. For thrust earthquakes, the ratio u/L is typically greater than for strike slip events (Scholz, 1982), and for this particular event, based on parameters compiled by Papageorgiou and Aki, (1982), $u/L \approx 3.6 \times 10^{-5}$. Furthermore, the fault width, 20 km, exceeds the assumed 10 km width which was used to prepare the theoretical curve. Finally, the surface wave magnitude, $M_s = 7.7$, for this event exceeds best estimates of the moment magnitude, $M = 7.3$ to 7.5, based on moment estimates compiled by Papageorgiou and Aki (1982). For strike-slip California earthquakes, it appears that as yet there are no known exceptions to the bound shown in Figure 7.

Figure 8 compares the magnitude of the maximum observed earthquake and the seismic slip rate each fault in Table 4. As expected, the two parameters are correlated. This correlation results because the largest earthquakes are the ones which cause most of the slip. Scatter is introduced by the different fault lengths and to some extent by the distribution of smaller earthquakes on each fault.

Figure 9 shows the maximum observed magnitude plotted against the best estimate of geological slip rate. Woodward Clyde Consultants (1979) have previously prepared such a plot, for strike-slip faults worldwide. Based on an assumed occurrence-rate relationship, Anderson and Luco (1982) have derived a theoretical relationship between these two parameters also, as a function of the average recurrence time of the maximum magnitude event. We note that these theoretical curves assume a particular shape of the occurrence rate relationship near the maximum magnitude earthquake, but that alternative shapes yield similar predictions (Anderson and Luco, 1982). Figure 9 shows six events which apparently have recurrence times of 1000 years or more. These six faults are designated as follows on Table 4: White Wolf, Newport-Inglewood, Stampede, Honey Lake Valley, Honey Lake, and Genoa. We note

Appendix I

that for a 69 fault data set and about 100 years of seismic history, depending on the fault, six observations of a 1000 year event on the fault is about what one would expect.

At the small magnitude extreme, 12 faults, or 20%, appear below the 10-year contour on Figure 9. These 12 faults are designated as follows on Table 4: San Andreas 2,5,6, and 7; Garlock East, Garlock West, Cucamonga, Oakridge, Rose Canyon, Raymond, Big Pine, San Juan. In addition Santa Monica and Santa Susana are on the borderline of this group. Formally this only means that if the maximum earthquake on the fault were the maximum observed, then earthquakes of this size would have to occur more frequently, and in some cases significantly more frequently, than once every 10 years to achieve the slip rate which has been designated. Therefore, one cannot make a statistical inference, based on this figure, that faults in this group have had unusually low activity and are statistically due for a larger earthquake. However, Figure 8 shows at most under 2 magnitude units of scatter at a given seismic slip rate, while Figure 9 shows typically 3 to 4 magnitude units of scatter. Because the geological and seismic slip rates must be the same over a sufficiently long observation period, it is reasonable to infer that the data at frequent recurrence contours in Figure 4 do not represent situations in which large slip rates are achieved by frequent small earthquakes, but rather situations in which large earthquakes have not been recorded in the earthquake catalog.

To establish whether the maximum observed earthquake is unusually small, a different type of procedure is needed. This is pursued in Table 4 which gives a theoretical estimate for the mean expected recurrence time of the largest observed earthquake on each fault, $T(M^0)$. These estimates are based on Eq. II.9 of Anderson and Luco (1983) and incorporate the value of M_{\max} which has been assumed on Table 4. One third of the faults have an expected recurrence time of the largest observed earthquake being less than 10 years; seven of these recurrence times (10% of all faults) are estimated to be less than two years, and three of these (4% of all faults) are estimated to be less than one year. One would not expect such large fractions of the total data to appear in these categories if earthquakes were randomly distributed in time. However, it is reasonable to explain these fractions by a tendency for earthquakes to occur in aftershock sequences or swarms during active periods on a fault. Those faults on which the $T(M^0)$ is less than one year are designated San Juan, San Andreas 5, and Big Pine on Table 4; those with $T(M^0)$ between one year and two years are the Hayward, Oakridge, Raymond, and Rose Canyon faults.

Comparison of Observed and Predicted Occurrence Rates

Predicted occurrence rates of earthquakes in magnitude intervals 3.0 to 3.99, 4.0 to 4.99, etc. were derived by expressions in Anderson and Luco (1982), using occurrence relation $N_2(M)$, with the b-value and

Appendix I

M_{max} for each fault as listed in Table 4. Appendix I-2 contains plots of observed and predicted occurrence rates, as a function of the magnitude range, for each of the faults which is listed in Table 4. To account for the uncertainty, these plots show expected occurrence rates for the maximum and minimum estimate of slip rate, and for estimates of M_{max} of 0.5 units larger or smaller than those given in Table 4. Occurrence rates which correspond to the best estimates appear as larger symbols. These comparisons are summarized in Figures 10 to 14. The error bars on predicted rates on these figures correspond to the range of slip rates in Table 4; the error bars on observed rates span the range between maximum and minimum estimates. The diagonal solid line across each figure shows equality of the rates, and the dashed lines show discrepancies of ± 1 and ± 2 orders of magnitude. Figure 10 shows data from all faults; Figure 11 shows data from some of the faults which have had a 1000 year earthquake, Figure 12 shows data from faults which appear below the contour on Figure 9, and Figures 13 and 14 show results broken down according to the regional maps.

Figure 10, which contains the entire set of data, shows that in the vast majority of cases, the observed occurrence rates are within a factor of 10 of the predicted rates. Most exceptions to this fall in the range where observations are smaller than the prediction by a factor of 10 to 100. Incomplete recording at the magnitude 3 to 4 level probably contributes to some of these low data points.

Figure 11 compares the observed and predicted occurrence rates for the Newport-Inglewood fault and the White Wolf fault. The observed occurrence rates on these two faults are about ten times larger than the rate predicted from the slip rate. Data for four other faults which have apparently had their 1000 year earthquake (designated Stampede, Honey Lake Valley, Honey Lake, and Genoa) have been left off from Figure 11. When these data are plotted on Figure 11, they overlie the trend defined by the Newport-Inglewood and White Wolf faults. These data have been left off because the slip rates are rather poorly constrained. For the White Wolf fault and the Newport-Inglewood fault, the slip rates are well constrained, and the conclusion is that the earthquakes represent relatively rare occurrences which happened to occur during the observational time period.

Averaged over about a 50-year time period, the average occurrence rate on the Newport-Inglewood and White Wolf faults is about ten times that predicted from the slip rates. Therefore, if all small earthquakes on these two faults were to cease for the next 500 years, the average occurrence rates from the current 50-year interval, including aftershocks would be consistent with the occurrence rate as estimated from the slip rate. Considering that low level activity may continue on these faults, or that additional segments may rupture during cycles of duration $\approx 10^3$ years, it appears reasonable to anticipate that an average of 10^3 years will yield average occurrence rates which are

Appendix I

consistent with the estimated slip rate. The low occurrence rate on faults between main shocks has been cited by Wasnousky *et al.* (1983) as evidence that the Gutenberg-Richter occurrence rate curve does not apply to an individual fault. Figure 11, on the contrary, indicates that the aftershocks of major earthquakes are sufficient to eliminate the deficit which is seen during the low activity periods of the seismic cycle.

Figure 12 shows the faults which are below the 10-year earthquake contour on Figure 9, and does not show the complementary picture of observations all being less than the observed occurrence rates. There are three faults, San Andreas 6, Garlock East, and Garlock West which have more earthquakes than predicted by the theory. Considering that these faults are considered on Figure 12 because they have not had large earthquakes, this observation would seem to contradict the conclusion which was reached in conjunction with Figure 11. The more likely explanation is that the estimated b-values do not apply to complete cycles of seismicity. Figure 12 uses $b = .46$ for San Andreas 6, $b = .50$ for Garlock East, and $b = .52$ for Garlock West. These b-values, while motivated by observations, are quite low. A larger b-value can probably be expected from a main shock and its aftershocks on each of these faults, and can reasonably be expected to eliminate the discrepancy.

Figures 13 a-h show this comparison for each of the sub-regions which have been considered, and allow error bars on each datum to be displayed.

Application to earthquake prediction

It is conceivable that the comparison of occurrence rates with rates predicted from geological slip rate may yield information which is useful to earthquake prediction. For this purpose, occurrence rates were examined up to the year prior to the occurrence of each of the earthquakes in California with magnitude greater than 6.0. Eleven faults representing fifteen earthquakes show enough prior seismicity to establish these prior occurrence rates: Hosgri, Pleito-White Wolf, Sierra Madre, San Andreas 9, San Andreas 10, Imperial, San Jacinto, Sierra Nevada-Owens Valley, Hilton Creek, Stampede, and Mannix. It is convenient to define $R(M)$ as the ratio of the observed occurrence rate at magnitude M to the occurrence rate at magnitude M which is predicted from the slip rate. On four of the above-named faults $R(M) > 1$ for M less than 5, on the others $R(M) < 1$. The faults with low observed occurrence rates indicate that if $R(M) > 1$ ($M < 5$) is used as an earthquake predictor, there would be a significant rate of missed forecasts (about 75%), at least on a survey level such as this.

The faults with high occurrence rates relative to the slip rate estimates are San Andreas 10, Stampede, Sierra Nevada-Owens Valley, and Hilton. If a high rate of earthquakes relative to the slip rate estimate, in the absence of an aftershock sequence, could be used as a

Appendix I

precursor for even 25% of the earthquakes in California, this would be a helpful observation for the earthquake prediction problem. Therefore, an effort was made to determine which faults, at the end of December 1979, had occurrence rates at the magnitude 3 to 5 level which were larger than expected from the slip rate estimates. Of the 69 on Figure 10, 26 (about 40%) fall into this category. In 1980 or 1981, only one of these faults (Hilton Creek) had earthquakes with $M \geq 6$. About 30 to 50 percent of the high ratios can be attributed to previous aftershock sequences. The Hilton Creek fault showed increasing seismicity (type 3), but seven other faults did also. Consequently, $R(M) > 1$, if it can be regarded as a predictor, is likely to have a large rate of false alarms (greater than 90%) on a time scale of one or two years. This conclusion is weak, primarily because of the large uncertainties which are present in the data.

Conclusions

This paper has compared observed occurrence rates of earthquakes in the vicinity of active faults in California, United States of America, with occurrence rates which have been estimated from slip rates on these faults. The observed occurrence rates seem to be bounded, between one order of magnitude larger than predicted to two orders of magnitude smaller than predicted. Most of the observed rates are within one order of magnitude of the predicted rates. There are important, but uncertain, parameters which enter to affect the estimate of occurrence rates from the slip rate: the maximum moment earthquake, the b-value, and the slip rate itself. However, relatively well-constrained data from some of the faults suggest that the scatter about the predicted occurrence rate is a real phenomenon for observed rates averaged for a 50-year time interval. No cases have appeared in which a linear relationship between magnitude and the logarithm of occurrence rate is seriously inadequate.

There are now several studies of the seismic hazard in which slip rates or strain rates are converted to earthquake occurrence rates with methods similar to those which have been employed by this study (e.g. Campbell, 1977; Anderson, 1979; Papastamatiou, 1980; Greensfelder *et al.*, 1980; Doser and Smith, 1982; and Wesnousky, 1982). Figure 10 indicates that such seismic hazard studies may arrive at expected earthquake recurrence rates up to a factor of 10 different from comparable studies which use instrumentally recorded earthquakes as a basis for the input. We note from Tables 2 and 4 that the subjective uncertainty in the slip rate on the fault is considerably smaller than a multiplication factor of 10 ± 1 . Campbell (1977) has employed a procedure in which the geological estimate is used as a prior model in a Bayesian procedure, and observed earthquakes are used as supplementary data to update the prior model. The updated model tends to yield risk estimates which are intermediate between the slip-rate based estimate and the historical seismicity based estimate. In view of the results of this paper, it is not unlikely that the updated occurrence rates obtained by the Bayesian

Appendix I

procedure will be inconsistent with extreme estimates of the slip rate based on geological observations.

One interesting result is that on faults where a 1000 year earthquake has occurred, the observed average occurrence rates, over 50 years, at all magnitudes are about 10 times the rates predicted from slip rate. Therefore, these faults can undergo 500 years of quiescence, after which the observed rate would agree with the prediction. It would, however, be premature to use a statistical conclusion such as this as justification for assuming that these faults may be neglected in seismic hazard assessments of structures with shorter lifetimes. In particular, these earthquakes have not always ruptured the entire lengths of the fault. Furthermore, not enough is known to justify an assumption that a fault is strained at a constant rate in time.

An attempt has been made to determine if a high level of small earthquake occurrence relative to the slip rate estimates is helpful for the problem of predicting earthquakes. Preliminary results are discouraging, in that they imply that this indicator may be present before only a small fraction of the earthquakes (~ 25%), and that the presence of this indicator may have a large false alarm rate (~ 90%). However, it may be valuable to consider different ways of determining the average occurrence rates, in conjunction with better established slip rates as these become available. Furthermore, it is possible that this indicator could be helpful in the future at faults where it has been valid in the past.

Acknowledgments

This research was supported by the United States Geological Survey Contract No. 14-08-0001-19766.

Appendix I

References

Anderson, J.G. (1979). Estimating the seismicity from geological structure for seismic-risk studies, Bull. Seism. Soc. Am., **69**, 135-158.

Anderson, J.G. and J.E. Luco (1983). Consequences of slip rate constraints on earthquake occurrence relations, Bull. Seism. Soc. Am., in press, April.

Bateman, P.C. and C. Wahrhaftig (1966). Geology of the Sierra Nevada, in Geology of Northern California, Bull. 190, Calif. Div. of Mines and Geology, 107-172.

Bird, P. (1982). Kinematics of present crust and mantle flow in southern California, Geol. Soc. of Am. Bull. (in press).

Brune (1968). Seismic moment, seismicity, and rate of slip along major fault zones, J. Geophys. Res., **73**, 777-784.

Bryant, W.A. (1979). Earthquakes near Honey Lake, Lassen County, California, California Geology, May 1979, 106-109.

Campbell, K.W. (1977). The use of seismotectonics in the Bayesian estimation of seismic risk, Rept. No. UCLA-ENG-7744, School of Eng. and Applied Sciences, Univ. of California, Los Angeles.

Davies, G.F. and J.N. Brune (1971). Regional and global fault slip rates from seismicity, Nature, **229**, 101-107.

Doser, D. and R.B. Smith (1982). Seismic moment rates in the Utah region, Bull. Seism. Soc. Am., **72**, 597-614.

Durrel, C. (1966). Tertiary and Quaternary geology of the northern Sierra Nevada, in Geology of Northern California, Bull. 190, Calif. Div. of Mines and Geology, 185-197.

Eguchi, R.T., K.W. Campbell, and J.H. Wiggins (1979). A survey of expert opinion on active and potentially active faults in California, Nevada, Arizona, and northern Baja California, Technical Report No. 79-1328-2, J.H. Wiggins Co., Redondo Beach, Calif.

Ellsworth, W.L., A.G. Lindh, W.H. Prescott and D.G. Herd (1981). The 1906 San Francisco earthquake and the seismic cycle, in Earthquake Prediction: An International Review.

Greensfelder, R., F.C. Kintzer, and M.R. Summerville (1980). Seismotectonic regionalization of the Great Basin, and comparison of moment rates computed from Holocene strain and historic seismicity, in

Appendix I

Proc. of Conf. X, Earthquake Hazards along the Wasatch and Sierra Nevada Frontal Fault Zones, Open File Report 80-801, U.S. Geol. Survey, Menlo Park, Calif., 533-493.

Hanks, T. and H. Kanamori (1979). A moment magnitude scale, J. Geophys. Res., 84, 2348-2350.

Herd, D.G. (1979). Neotectonic framework of central coastal California and its implications to microzonation of the San Francisco Bay region, in Brabb, E.E. (editor), Progress on seismic zonation in the San Francisco Bay region, U.S. Geol. Survey Circular 807, 3-12.

Knopoff, L., Y.Y. Kagan, and R. Knopoff (1982). b-values for foreshocks and aftershocks in real and simulated earthquake sequences, Bull. Seism. Soc. Am., 72, 1663-1676.

Myers, H. and C.A. VonHake (1976). Earthquake Data File Summary, National Geophysical and Solar-Terrestrial Data Center, Boulder, Co.

Molnar, P.E. (1979). Earthquake recurrence intervals and plate tectonics, Bull. Seism. Soc. Am., 69, 115-133.

Papastamatiou, D. (1980). Incorporation of crustal deformation to seismic hazard analysis, Bull. Seism. Soc. Am., 70, 1321-1335.

Papageorgiou, A.S. and K. Aki (1982). A specific barrier model for the quantitative description of inhomogenous faulting and the prediction of strong ground motion II. Description of the model, Proceedings of Workshop XVI, The Dynamic Characteristics of Faulting Inferred from Recordings of Strong Ground Motion, Open File Report 82-591, U.S. Geol. Survey, Menlo Park, Calif., 311-352.

Sharp, R.V. (1981). Variable Rates of late Quaternary strike slip on the San Jacinto fault zone, southern California, J. Geophys. Res., 86, 1754-1762.

Slemmons, D.B., D. Van Wormer, E.J. Bell, and M.L. Silberman (1979). Recent crustal movements in the Sierra Nevada - Walker Lake region of California - Nevada. Part I, Rate and style of deformation, Tectonophysics, 52, 561-570.

Sylvester, A.G. and A.C. Darrow (1979). Structure and neotectonics of the western Santa Ynez fault system in southern California, Tectonophysics, 52, 389-405.

Taylor, G.C. and W.A. Bryant (1980). Surface rupture associated with the Mammoth Lakes earthquakes of 25 and 27 May 1980, in Mammoth

Appendix I

Lakes, California earthquakes of May 1980. Special Report 150,
Calif. Div. of Mines and Geology, 49-67.

Weber, G.E., K.R. Lajoie, and J.F. Wohmiller (1979). Quaternary crustal deformation along a major branch of the San Andreas fault in central California. Tectonophysics, 52, 378-379.

Wesnouski, S.G. (1982). Crustal deformation and earthquake risk in Japan, Ph.D. Thesis, Columbia University, New York.

Wesnouski, S.G., C.H. Scholz, K. Shimazaki, and T. Matsuda (1983). Earthquake frequency distribution and the mechanics of faulting (preprint).

Woodward-Clyde Consultants (1979). Report of the evaluation of maximum earthquake and site ground motion parameters associated with the offshore zone of deformation San Onofre Nuclear Generating Station, prepared for Southern California Edison, Rosemead, California. 1754-1762.

Table 1 - Supplemental slip rate estimates.

Reference	Fault/Region	Offset	Dir. [†]	Age	Rate mm/yr
Taylor and Bryant (1980)	Hilton Creek	1.1 km	N	0.72-2.5 my*	0.44-1.57
		15 m		10,000-60,000 y	0.25-1.50
	Hartley Springs (June Lake)	300 m	N	0.7 my*	0.43
		15 m		0.2 my	0.075
		10 m		0.1 my	0.10
		5 m		650 y	7.7
Slemmons <i>et al.</i> (1979)	Donner Summit area (Stampede)	compilation of geology			0.10-0.24
		geodetic	N		4.5-9.2
	Carson Pass -	comp. of			0.06-0.16
	Sonora Pass area	geology			
Bryant (1979)	Honey Lake	>2000 ft total offset	N	10 my upper from Slemmons	>0.06
St. Amans and Roquemore (1979)	Sierra Nevada	3000-5000 ft	N	2 my	0.45-0.76
Sylvester and Darrow (1979)	Santa Ynez (E. of Lake Cachuma)	1.6-3.0	LL	38-53 my	0.030-0.079
		11-14 km	LL	38-53 my	0.21-0.37
		35 km	LL	26-38 my	0.92-1.35
		60 km	LL	20-26 my	2.3-3.0
Wehmiller <i>et al.</i> (1979)	Ventura - Santa Barbara coast		T	1-6	
Yeats (1977)	Oakridge		Normal		3.3-7.6
Sharpe (1981)	San Jacinto (Anza)	5.7-8.6 km	RL	0.73 my	8-12

*Ages based on chronology of Bateman and Wahhaftig (1966).

**Additional estimates in this.

†Direction

N = normal

RL = right lateral

LL = left lateral

T = thrust

TABLE 2
GEOLOGICAL SLIP RATES (MM/YEAR) OBTAINED FROM SEVERAL COMPILED

NAME	---ANDERSON---			HERD		-WIGGINS-			++WOOD, CLYDE++		BIRD....			----NEW----			
	MIN	MAX	BEST			MIN	MAX		MIN	MAX	BEST	MIN	MAX	MODL	MIN	MAX	EST	
MAP 1																		
SAN ANDREAS 1						30.0	30.0	50.0	20.0	20.0	20.0							
SAN ANDREAS 2						20.0	30.0	50.0										
PALO COLORADO - SAN GREGORIO	6.00	23.0	10.0			10.0			9.00	16.0	16.0					16.0		
HEALDSBURG - ROGERS CREEK						7.50												
HAYWARD						7.50			5.00	7.50	6.00							
GREEN VALLEY - CALAVERAS						7.50			6.00	8.00	6.00							
CALAVERAS - HAYWARD						15.0			5.00	15.0	12.0							
MAP 2																		
SAN ANDREAS 3				29.0	35.0	37.0	20.0	30.0	50.0									
SAN ANDREAS 4				32.0	40.0	37.0	37.0	20.0	40.0	34.0	41.0	37.0	21.3	40.0	36.0			
HOSGRI				6.00	23.0	10.0	10.0	0.30	16.0				2.00	26.0	16.0			
RINCONADA				3.00	3.00	3.00				1.00	2.00	1.50	2.40	12.0	2.50			
ORTIGALITA																		
SAN JUAN																		
MAP 3																		
SAN ANDREAS 5				34.0	40.0	37.0	37.0	20.0	40.0	3.00	52.0	37.0	34.0	40.3	36.0			
SAN ANDREAS 6						37.0		20.0	40.0						42.0			
SAN ANDREAS 7				34.0	60.0	37.0		20.0	40.0				17.0	42.0	43.0			
PLEITO - WHITE WOLF				0.40	0.40	0.40		0.40	10.0				3.00	8.50	7.00			
OZENA																		
PINE MOUNTAIN																		
BIG PINE				1.00	2.00	2.00		2.00	2.00	2.10	2.70	2.40	1.40		2.00			
SANTA YNEZ						2.00							0.50	0.30	0.00	.030	3.00	
ARROYO PARRIDA				0.05	0.05	0.05												
OAKRIDGE				0.20	0.50	0.30												
SANTA BARBARA CHANNEL																		
SANTA CRUZ ISLAND																		
SANTA SUSANA				1.20	1.20	1.20				8.00	8.00							
SIERRA MADRE				8.00	24.0	8.00		0.00	10.0				0.70	3.00	17.0			
CUCAMONGA				8.00	24.0	8.00							0.70	3.00	17.0			
MALIBU COAST						0.15									1.50			
SANTA MONICA				0.13	0.15	0.15		0.13	0.13				0.18	1.00	1.00			
RAYMOND				0.13	0.17	0.15							0.12	0.24	1.70			
MAP 4																		
SAN ANDREAS 8						15.0		10.0	40.0				17.0	36.0	22.0			
SAN ANDREAS 9						15.0		10.0	40.0				10.0	46.0	22.0			
SAN ANDREAS 10						15.0		30.0	32.0				21.0	49.0	22.0			
IMPERIAL				40.0	40.0	15.0		40.0	40.0						22.0			
SAN JACINTO ZONE				2.50	26.0	20.0		1.00	20.0	1.00	12.0	8.00	18.0		34.0			
EL SINORE				0.60	4.00	1.00		0.40	1.00	1.80	7.10	2.30	0.80	9.00	1.00			
PINTO MOUNTAIN				0.30	2.00	1.00				2.00	4.00	3.00	5.30	6.00				
BLUE CUT										1.00	2.50	1.80	0.00	0.00				
MAP 5																		
SURPRISE VALLEY								0.10	5.00									
LIKELY								0.10	10.0									
HONEY LAKE VALLEY								0.10	0.10						0.06			
HONEY LAKE															0.10	0.24		
STAMPEDE RESERVOIR																		
MAP 6																		
DEATH VALLEY				0.50	1.00	1.00		0.10	5.00				3.70	5.70	4.00			
PANAMINT VALLEY				1.00	2.00	1.50		0.10	0.50				1.00	2.00	2.00			
SIERRA NEVADA - OWENS VALLEY				0.40	4.00	4.10		0.10	1.00				0.30	1.40	0.40			
MONO LAKE REGION															0.40			
JUNE LAKE REGION															0.40	.075	7.70	
HILTON CREEK REGION															0.40	0.25	1.57	
TOPAZ *								0.15	5.00						.060	0.16	0.12	
GENOA *															.060	0.16	0.12	
MAP 7																		
GARLOCK WEST				4.00	9.00	8.00		0.80	8.00	3.40	12.9	8.00	5.40	5.40	7.00			
GARLOCK EAST				4.00	9.00	8.00		0.80	8.00	3.40	12.9	8.00	5.40	5.40	5.00			
BICYCLE LAKE *																		
DRINKWATER LAKE *																		
MANNIX																		
LUDLOW																		
PISGAH - BULLION				1.50	5.00	2.00												
BLACKWATER																		
CALICO				0.60	2.40	1.00												
HARPER																		
CAMP ROCK - EMERSON				0.60	1.20	1.00				1.10	1.30	1.20	0.10	0.70				
LOCKHART				0.90	2.50	1.50		0.13	0.13	0.50	1.50	1.00						
LENWOOD				0.90	2.50	1.50		0.13	0.13	1.00	5.00		0.10	0.70				
HELENDALE				0.50	1.70	1.00				2.00	4.00	3.00						
THRUST UNNAMED															2.00			
MAP 8																		
NEWPORT-INGLEWOOD				0.30	0.60	0.60		0.30	1.00	0.38	0.68	0.50	0.40	0.80	0.90			
OFFSHORE ZONE OF DEFORMATION								0.30	1.00						0.90			
ROSE CANYON				1.00	2.00	1.50		0.30	1.00				1.00	2.20	0.90			
PALOS VERDES				0.70	0.70	0.70		0.50	1.00				0.30	0.60	0.80			
SAN CLEMENTE															1.50			

TABLE 3
COORDINATES OF CORNERS OF ZONES USED FOR SEISMICITY SEARCHES

	CORNER 1 LAT	CORNER 1 LONG	CORNER 2 LAT	CORNER 2 LONG	CORNER 3 LAT	CORNER 3 LONG	CORNER 4 LAT	CORNER 4 LONG
SAN ANDREAS 1	37.68	-123.17	39.83	-124.66	40.18	-123.89	37.96	-122.57
SAN ANDREAS 2	37.05	-122.14	37.98	-122.68	37.22	-121.80	37.22	-121.80
SAN ANDREAS 3	36.37	-121.13	37.11	-122.83	36.52	-122.94	36.52	-122.94
SAN ANDREAS 4	35.65	-120.31	36.37	-121.13	36.49	-121.75	35.88	-120.13
PALO COLORADO-SAN GREGORIO	36.35	-122.11	37.82	-122.87	37.98	-122.68	36.48	-121.78
HOSGRI	34.69	-120.76	36.35	-122.11	36.88	-121.78	34.91	-120.29
RINCONADA	35.14	-120.53	36.71	-121.96	35.84	-120.87	35.31	-120.24
HEALDSBURG - ROGERS CREEK	37.96	-122.57	38.79	-123.12	38.88	-122.93	38.17	-122.26
HAYWARD	37.38	-121.95	37.99	-122.54	38.16	-122.27	37.44	-121.84
CALAVERAS - GREEN VALLEY	37.44	-121.84	38.23	-122.32	38.36	-122.83	37.50	-121.64
CALAVERAS - HAYWARD	36.82	-121.41	37.38	-121.95	37.50	-121.64	36.88	-121.27
ORTIGALITA	36.59	-120.97	37.12	-121.31	37.21	-121.86	36.72	-120.73
SAN JUAN	35.68	-120.26	35.17	-119.86	35.84	-120.87	35.63	-120.43
SAN ANDREAS 5	35.79	-120.12	34.99	-119.38	34.81	-119.47	35.61	-120.34
SAN ANDREAS 6	34.99	-119.38	34.98	-118.85	34.73	-118.94	34.81	-119.47
SAN ANDREAS 7	34.90	-118.85	34.39	-117.37	34.21	-117.57	34.73	-118.94
WHITE WOLF AND PLEITO	35.50	-118.48	35.31	-118.22	34.85	-119.83	34.95	-119.34
OZENA	35.12	-119.94	34.75	-119.21	34.59	-119.53	34.99	-120.15
PINE MOUNTAIN	34.65	-118.82	34.52	-118.75	34.61	-119.47	34.68	-119.22
BIG PINE	34.83	-119.11	34.74	-118.92	34.55	-119.74	34.71	-119.78
SANTA YNEZ	34.66	-118.82	34.48	-118.78	34.41	-120.33	34.63	-120.33
ARROYO PARIDA - SAN CAYATANO	34.51	-118.78	34.42	-118.78	34.33	-120.88	34.47	-120.88
OAKRIDGE	34.45	-118.78	34.37	-118.78	34.18	-119.25	34.31	-119.38
SANTA CRUZ ISLAND	34.28	-120.11	34.11	-119.33	33.86	-119.35	33.98	-120.13
SANTA SUSANA	34.48	-118.47	34.24	-118.51	34.31	-118.77	34.56	-118.78
SIERRA MADRE	34.48	-118.47	34.35	-118.08	34.11	-118.82	34.24	-118.58
CUCAMONGA	34.35	-118.08	34.24	-117.55	34.11	-117.38	34.89	-118.82
MALIBU COAST	34.19	-118.56	33.97	-118.47	33.97	-119.34	34.21	-119.34
SANTA BARBARA CHANNEL	34.32	-120.13	34.39	-119.34	34.11	-119.34	34.28	-120.13
SANTA MONICA	34.18	-118.29	34.05	-118.24	34.00	-118.48	34.19	-118.55
RAYMOND	34.18	-118.15	34.08	-117.97	34.05	-118.24	34.18	-118.29
SAN ANDREAS 8	34.34	-117.41	33.99	-116.34	33.81	-116.54	34.24	-117.52
SAN ANDREAS 9	33.99	-116.35	33.44	-115.61	33.30	-115.86	33.82	-116.53
SAN ANDREAS 10	33.43	-115.61	32.97	-115.36	32.95	-115.67	33.31	-115.86
IMPERIAL	32.97	-115.36	32.47	-114.98	32.37	-115.27	32.95	-115.67
SAN JACINTO	34.28	-117.35	32.87	-115.58	32.73	-115.75	34.18	-117.57
EL SINORE	34.05	-117.70	32.65	-115.71	32.49	-115.91	34.05	-118.15
PINTO MOUNTAIN	34.28	-115.82	33.99	-115.65	33.99	-116.34	34.14	-116.80
BLUT CUT	33.99	-116.35	33.99	-115.29	33.80	-115.29	33.80	-116.18
SURPRISE VALLEY	41.08	-120.15	42.00	-120.50	42.08	-120.80	41.08	-120.88
LIKELY	40.71	-120.27	41.54	-121.28	41.76	-120.97	40.86	-120.82
HONEY LAKE VALLEY	39.78	-119.84	40.50	-120.56	40.60	-120.44	39.99	-119.58
HONEY LAKE	39.68	-119.98	40.31	-120.80	40.58	-120.56	39.78	-119.84
STAMPEDE RESERVOIR	39.26	-120.15	39.22	-120.42	39.69	-120.09	39.59	-119.93
DEATH VALLEY	35.46	-116.59	38.03	-118.43	36.94	-116.88	35.58	-116.06
PANAMINT VALLEY	35.52	-117.14	37.11	-118.23	37.11	-117.76	35.52	-116.63
SIERRA NEVADA AND OWENS VALLEY	34.97	-118.12	37.89	-118.60	37.89	-118.34	35.16	-117.55
MONO LAKE	37.81	-119.24	38.28	-119.62	37.96	-119.16	37.96	-118.84
JUNE LAKE	37.56	-119.84	37.81	-119.24	37.96	-118.84	37.74	-118.68
HILTON	36.79	-118.41	37.55	-119.84	37.79	-118.68	37.62	-118.55
TOPAZ	38.84	-119.44	38.34	-119.29	38.29	-119.59	38.80	-119.78
GENOA	38.43	-119.89	39.01	-119.99	39.03	-119.75	38.45	-119.62
GARLOCK WEST	35.68	-117.66	35.35	-117.60	34.78	-118.65	34.85	-119.03
GARLOCK EAST	35.65	-116.17	35.53	-116.17	35.35	-117.68	35.60	-117.66
BICYCLE LAKE	35.41	-116.89	35.35	-116.24	35.24	-116.24	35.27	-116.89
DRINKWATER LAKE	35.52	-117.11	35.52	-116.24	35.35	-116.24	35.42	-117.11
MANNIX	35.14	-116.26	35.03	-116.18	34.80	-116.63	35.01	-116.74
LUDLOW	35.03	-116.16	34.41	-115.65	34.30	-115.90	34.95	-116.44
PISGAH	34.95	-116.45	34.15	-115.78	34.18	-116.82	34.88	-116.63
BLACKWATER	35.51	-117.31	35.16	-116.89	35.07	-117.86	35.42	-117.56
CALICO	35.16	-116.87	34.18	-116.82	34.18	-116.88	35.07	-117.84
HARPER	35.43	-117.56	34.89	-116.84	34.81	-116.92	35.31	-117.72
CAMP ROCK	34.88	-116.84	34.18	-116.88	34.28	-116.38	34.81	-116.92
LOCKHART	35.31	-117.71	34.81	-116.94	34.68	-117.11	35.24	-117.81
LENWOOD	34.81	-116.94	34.20	-116.29	34.19	-116.50	34.68	-117.11
HELENDALE	34.93	-117.42	34.19	-116.50	34.20	-116.78	34.84	-117.53
MOJAVE	34.52	-117.36	34.45	-116.54	34.20	-116.43	34.28	-117.36
NEWPORT-INGLEWOOD	34.95	-118.27	33.68	-117.85	33.56	-118.81	33.99	-118.48
OFFSHORE ZONE OF DEFORMATION	33.71	-117.79	33.11	-117.22	33.01	-117.49	33.56	-118.81
ROSE CANYON	33.18	-117.22	32.56	-116.95	32.52	-117.24	33.01	-117.49
PALOS VERDES	33.99	-118.47	33.44	-117.89	33.31	-118.04	33.92	-118.54
SAN CLEMENTE	33.38	-118.61	32.46	-117.63	32.24	-117.89	33.18	-118.87

REPRODUCED FROM BEST AVAILABLE COPY

-18- (23)

TABLE 4
COMPILATION OF GEOLOGICAL AND SEISMICAL PARAMETERS FOR SEVERAL FAULTS

NAME	L	TMX	OMX	T	B	OBSERVED EARTHQUAKE OCCURRENCE RATES *												SLIP RATES (MM/YEAR)									
						N-3			N-4			N-5			N-6			N-7			GEOL			SEIS	MIN	MAX	BEST
						S	MIN	MAX	S	MIN	MAX	S	MIN	MAX	S	MIN	MAX	S	MIN	MAX	S	MIN	MAX	70			
MAP 1																											
SAN ANDREAS 1 &	270	8.0	7.7	80	.88	4	.33	.60	2	.049	.871	2	.025	.871	8	8	8	8	8	8	38.00	28.0	50.0	30.0	365.		
SAN ANDREAS 2	110	8.0	5.3	50	.74	4	.47	.1.6	2	.092	.26	5	.019	.044	8	8	8	8	8	8	8.079	28.0	40.0	28.0	3.2		
PALO COLORADO-SAN GREGORIO	180	7.4	6.1	60	1.16	1	.48	.74	1	.28	.60	5	.020	.038	8	8	8	8	8	8	2.0	.02040	9.00	16.0	13.0	25.	
HEALDSBURG - ROGERS CREEK	70	6.8	5.7	50	.46	1	.84	1.2	2	.30	.40	5	.020	.18	8	8	8	8	8	8	0.5680	5.0	8.00	7.50	2.2		
HAYWARD	80	6.9	4.6	50	.88	1	1.2	.7	1	.16	.22	8	.0	.0	8	8	8	8	8	8	0.8310	1.5	8.00	7.50	1.8		
GREEN VALLEY - CALAVERAS	90	7.0	5.4	50	.94	1	2.1	3.0	1	.19	.31	5	.020	.044	8	8	8	8	8	8	0.1200	2.0	8.00	7.50	8.3		
CALAVERAS - HAYWARD	75	6.9	6.6	70	.76	3	4.5	8.6	3	.60	1.5	3	.084	.34	5	.011	.015	8	8	8	5.5000	3.0	15.0	15.0	96.		
MAP 2																											
SAN ANDREAS 3	110	8.0	5.6	50	.79	1	10	15	1	1.5	2.0	4	.16	.43	8	8	8	8	8	8	8.9300	28.0	40.0	28.0	4.6		
SAN ANDREAS 4	110	8.0	6.5	50	.71	1	3.8	5.2	1	.26	.67	1	.12	.22	2	.016	.036	8	8	8	8	4.1000	34.0	41.0	37.0	15.	
HOSGRI	200	7.5	6.0	50	.91	1	1.3	2.2	4	.059	.37	8	.0	.0	8	8	8	8	8	8	0.3300	9.00	16.0	13.0	25.		
RINCONADA	190	7.4	5.2	50	.80	4	.11	2.7	4	.050	.46	2	.021	.042	8	8	8	8	8	8	0.0630	1.00	3.00	2.50	31.		
ORTIGALITA	50	6.6	3.9	50	.86	4	.074	.66	8	.0	.0	8	.0	.0	8	8	8	8	8	8	0.0862						
SAN JUAN	65	6.8	3.4	50	.86	1	.094	.16	8	.0	.0	8	.0	.0	8	8	8	8	8	8	.00032	0.75	2.50	1.60	8.0		
MAP 3																											
SAN ANDREAS 5	115	8.3	5.5	50	.86	1	.13	.38	8	.0	.0	8	.0	.0	8	8	8	8	8	8	8.0044	34.0	52.0	37.0	.83		
SAN ANDREAS 6	45	8.3	5.5	70	.46	4	.18	1.1	4	.084	.27	1	.087	.070	8	8	8	8	8	8	8.3600	34.0	52.0	37.0	9.0		
SAN ANDREAS 7	145	8.3	5.4	50	.63	1	.74	1.1	2	.14	.18	2	.036	.070	8	8	8	8	8	8	0.0780	34.0	60.0	43.0	2.0		
PLEITO - WHITE WOLF	80	7.7	7.7	50	.76	4	3.5	20	4	.31	.66	4	.956	.7	5	.024	.071	5	.012	.036	298.00	3.0	8.50	7.00	INF		
OZENA	70	6.8	3.5	50	.86	2	.026	.852	8	.0	.0	8	.0	.0	8	8	8	8	8	8	0.0829						
PINE MOUNTAIN	60	6.8	4.7	50	.66	4	.042	.17	2	.026	.058	8	.0	.0	8	8	8	8	8	8	8.0130						
BIG PINE	70	6.8	3.5	50	.66	4	.038	.17	8	.0	.0	8	.0	.0	8	8	8	8	8	8	.0275	1.4	2.70	2.00	8.0		
SANTA YNEZ	130	7.2	4.7	50	.74	4	.22	.68	4	.040	.15	8	.0	.0	8	8	8	8	8	8	8.0150	8.23	3.00	2.00	11.		
ARROYO PARRIDA	120	7.0	4.5	50	.95	3	.95	2.3	2	.027	.082	8	.0	.0	8	8	8	8	8	8	0.0120	0.70	11.0	1.00	4.2		
OAKRIDGE	40	6.5	4.1	50	.82	4	.060	.38	5	.020	.038	8	.0	.0	8	8	8	8	8	8	0.0060	3.30	7.60	5.50	1.1		
SANTA BARBARA CHANNEL	75	6.9	6.2	50	.95	4	.50	.54	5	.19	.22	2	.026	.052	5	.010	.018	8	8	8	2.5000	1.00	13.0	12.0	38.		
SANTA CRUZ ISLAND	60	6.8	5.4	50	.84	2	.21	.43	2	.080	.17	2	.029	.059	8	8	8	8	8	8	0.2300	2.00	5.00	4.00	27.		
SANTA SUSANA	25	6.2	4.9	50	.61	3	.85	3.0	2	.13	.43	8	.0	.0	8	8	8	8	8	8	0.1100	1.0	17.0	9.0	4.7		
SIERRA MADRE	50	6.6	6.4	50	.82	4	1.0	.30	4	.20	4.5	5	.084	.20	5	.028	.11	8	8	8	8	0.8000	1.0	17.0	8.00	189.	
CUCAMONGA	55	6.7	4.7	50	.85	1	1.0	.8	1	.14	.26	8	.0	.0	8	8	8	8	8	8	0.8640	1.0	17.0	8.00	2.3		
MALIBU COAST	75	6.9	5.9	50	.95	3	1.7	3.6	2	.14	.28	5	.02	.15	8	8	8	8	8	8	0.6300	0.15	1.50	1.50	140.		
SANTA MONICA	25	6.2	3.7	50	.86	4	.20	.67	8	.0	.0	8	.0	.0	8	8	8	8	8	8	0.0028	0.15	1.00	1.00	2.0		
RAYMOND	25	6.2	3.7	50	.86	4	.13	.82	8	.0	.0	8	.0	.0	8	8	8	8	8	8	0.0019	0.15	1.70	1.70	1.6		
MAP 4																											
SAN ANDREAS 8	180	8.3	5.5	50	.79	1	4.2	9.2	4	.21	.98	4	.12	.19	8	8	8	8	8	8	8.4400	10.0	45.0	20.0	3.7		
SAN ANDREAS 9	90	8.3	6.5	50	.91	1	1.3	2.4	4	.043	.22	8	.0	.0	8	8	8	8	8	8	4.0000	10.0	45.0	20.0	28.		
SAN ANDREAS 10	50	8.3	6.1	50	.82	3	6.2	26	3	1.3	4.2	1	.085	.17	2	.02	.06	8	8	8	8	2.0000	10.0	45.0	20.0	10.	
IMPERIAL	70	6.8	6.7	50	.81	3	4.7	25	2	.080	1.3	2	.050	.15	2	.026	.044	8	8	8	8	18.0000	10.0	45.0	20.0	320.	
SAN JACINTO ZONE	220	7.5	6.8	70	.97	1	18	24	1	1.5	3.2	1	.016	.40	2	.026	.044	8	8	8	8	6.0000	2.50	34.0	20.0	82.	
EL SINORE	265	7.5	5.5	50	.97	1	7.0	18	4	.44	.93	4	.024	.048	8	8	8	8	8	8	0.0900	0.40	4.00	2.00	27.		
PINTO MOUNTAIN	70	5.8	5.5	50	.85	1	1.0	6.2	4	.13	.93	4	.027	.12	8	8	8	8	8	8	0.0900	2.00	4.00	2.00	73.		
BLUE CUT	80	6.0	4.8	50	.92	4	1.2	2.5	4	.11	.29	8	.0	.0	8	8	8	8	8	8	0.0054	1.0	2.50	1.00	10.		
MAP 5																											
SURPRISE VALLEY	85	7.0	5.2	50	.87	2	.040	.093	8	.0	.0	8	.0	.0	8	8	8	8	8	8	0.0560	0.10	5.00	1.00	44.		
LIVELY	95	7.0	3.9	50	.86	2	.050	.12	8	.0	.0	8	.0	.0	8	8	8	8	8	8	0.0010	0.10	5.00	1.00	33.		
HONEY LAKE VALLEY	20	6.1	5.6	50	.97	4	.30	2.4	5	.18	.38	5	.021	.033	8	8	8	8	8	8	0.0000	0.10	5.00	1.00	2160.		
HONEY LAKE	55	6.7	5.2	50	.82	3	.35	6.1	2	.062	.050	5	.02	.10	8	8	8	8	8	8	0.0000	0.10	5.00	1.00	516.		
STAMPEDE RESERVOIR	15	6.0	6.0	50	.99	4	.25	3.1	4	.082	.05	2	.039	.075	2	.032	.064	8	8	8	8	0.0000	0.10	5.00	0.10	INF	
MAP 6																											
GARLOCK WEST	140	7.6	5.5	70	.52	4	.27	1.9	4	.075	.54	2	.015	.031	8	8	8	8	8	8	0.0980	4.00	9.0	7.00	22.		
GARLOCK EAST	120	7.6	4.2	50	.59	1	.21	.38	2	.072	.10	8	.0	.0	8	8	8	8	8	8	0.0442	4.00	9.0	5.00	6.6		
BICYCLE LAKE	40	6.5	4.0	50	.55	5	.02	.18	8	.0	.0	8	.0	.0	8	8	8	8	8	8	0.0202	0.50	2.00	1.00	4.6		
SPINKWATER LAKE	60	6.8	4.2	50	.55	8	.0	.0	8	.0	.0	8	.0	.0	8	8	8	8	8	8	0.0011		</				

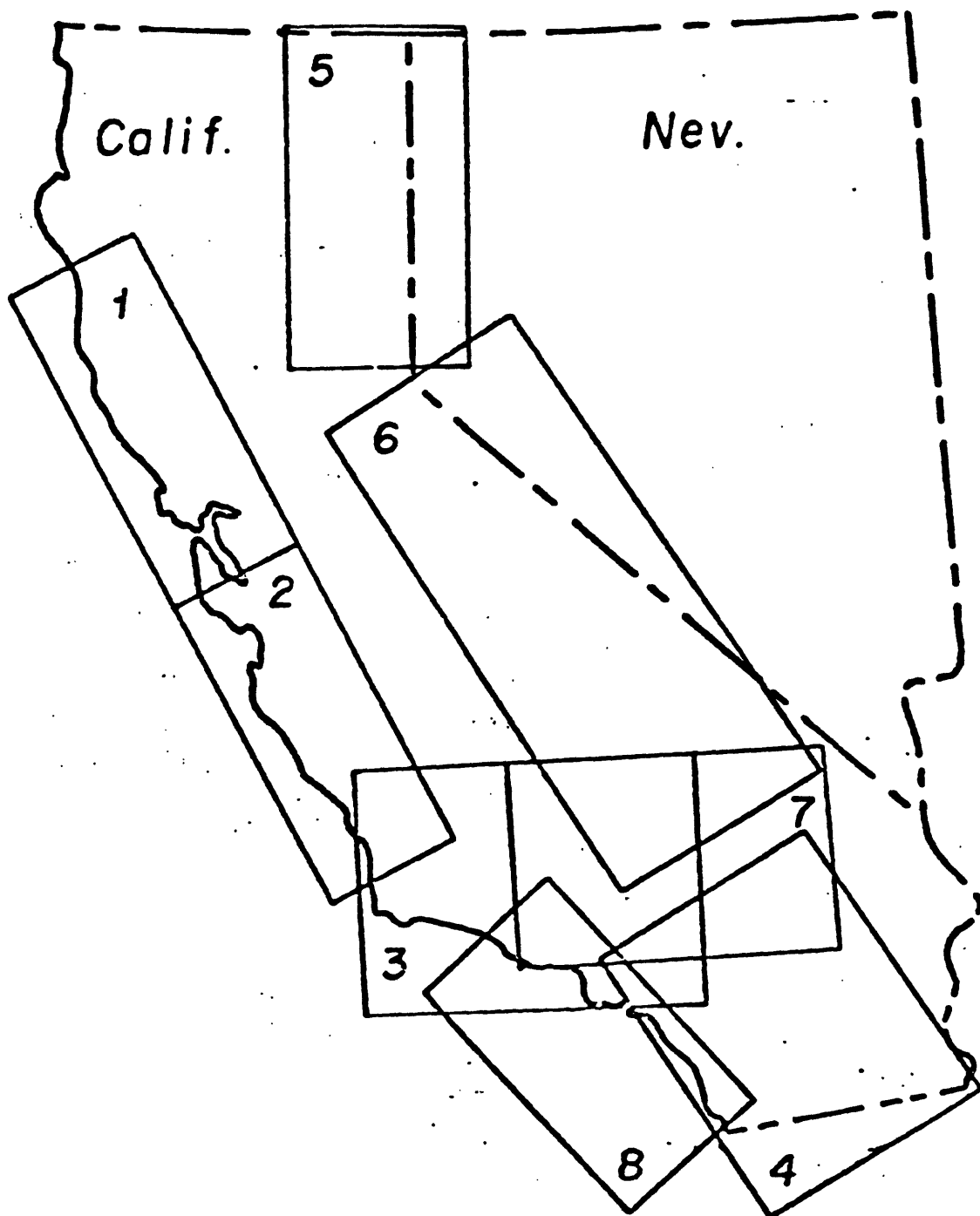


Figure 1. Map of California showing boundaries of detailed maps for regions 1 to 8.

Appendix I

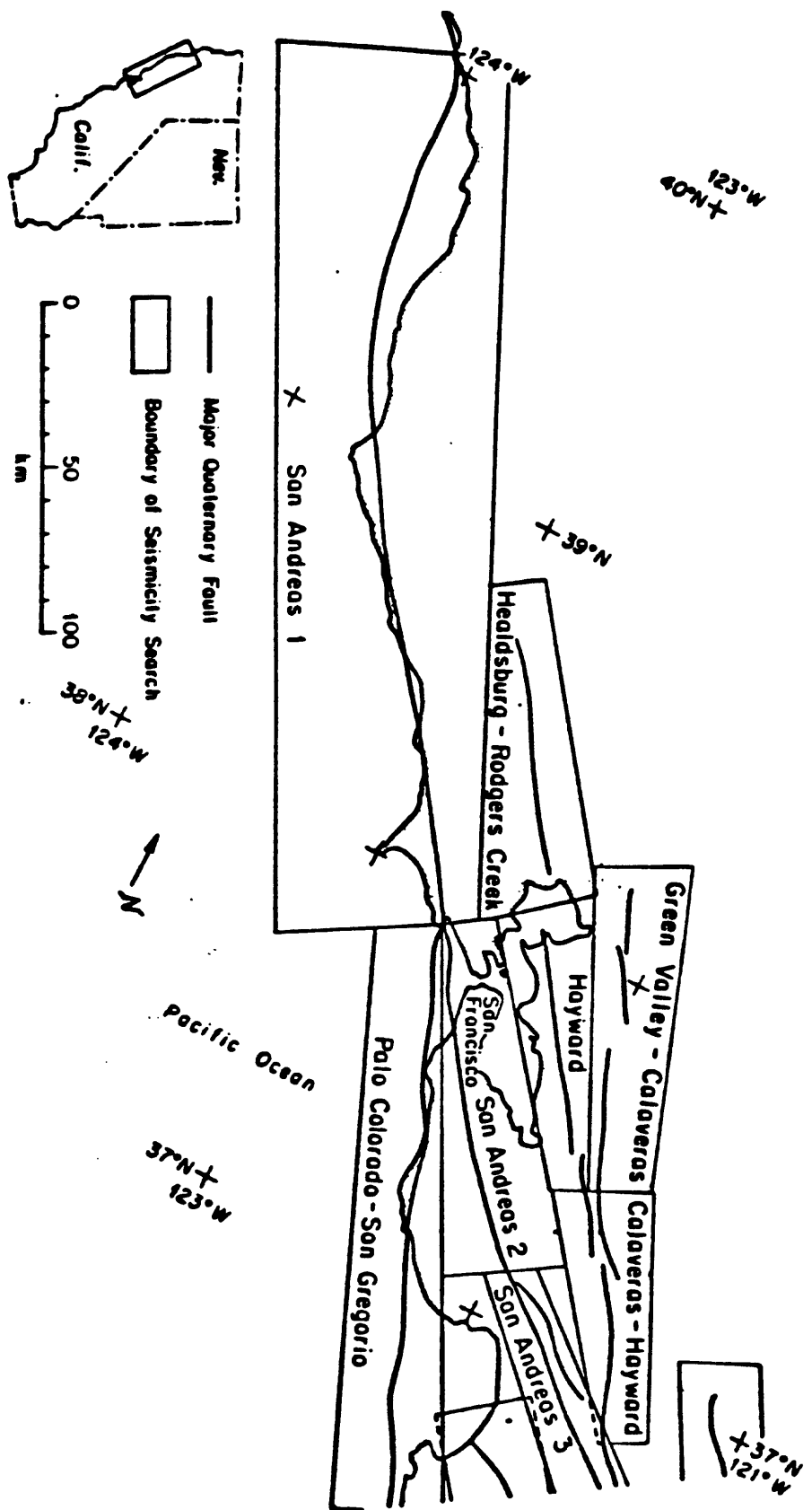


Figure 2. a) Faults and boundaries of seismicity searches for region 1.

Appendix I

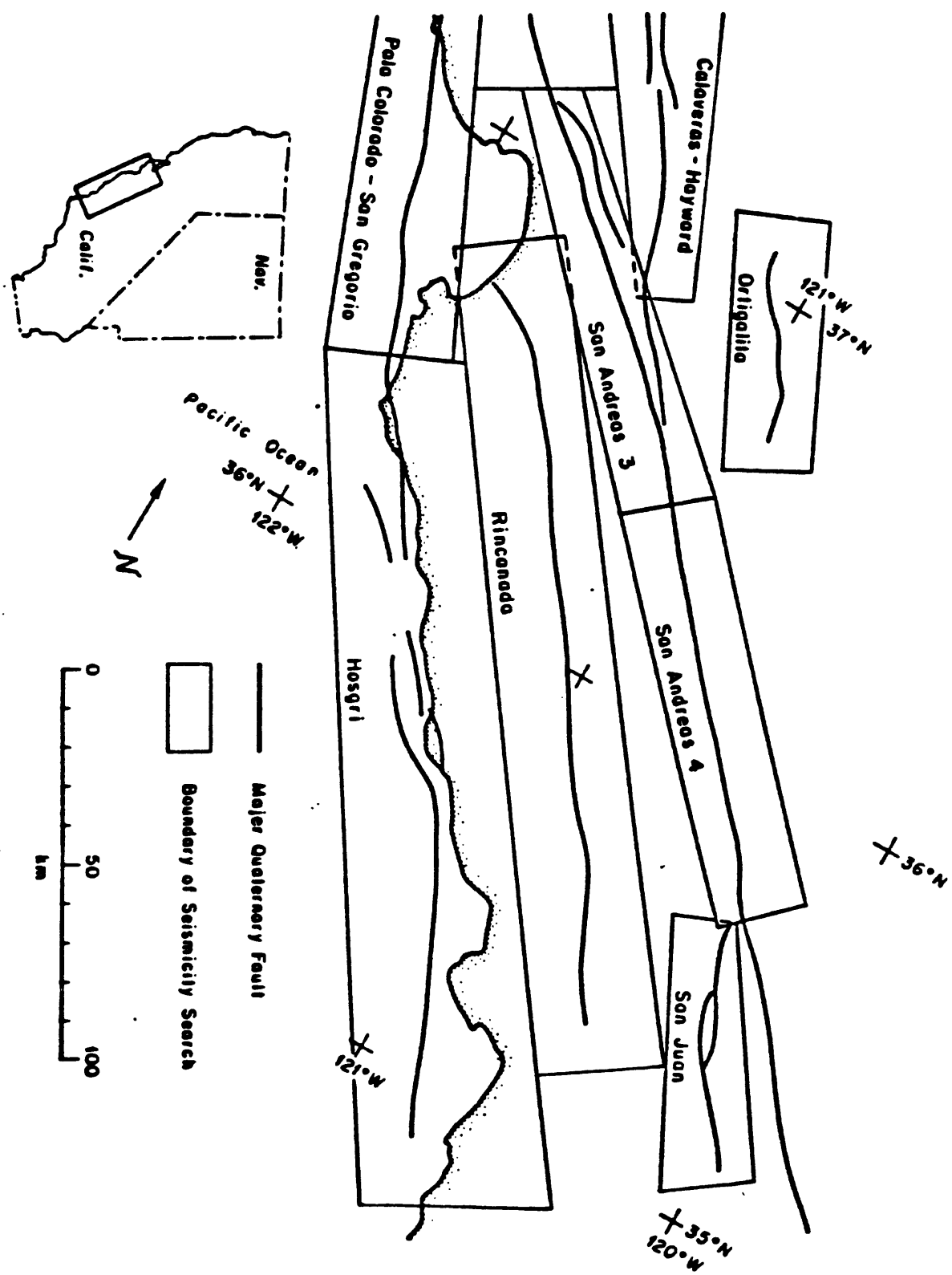


Figure 2. b) Faults and boundaries of seismicity searches for region 2.

Appendix I

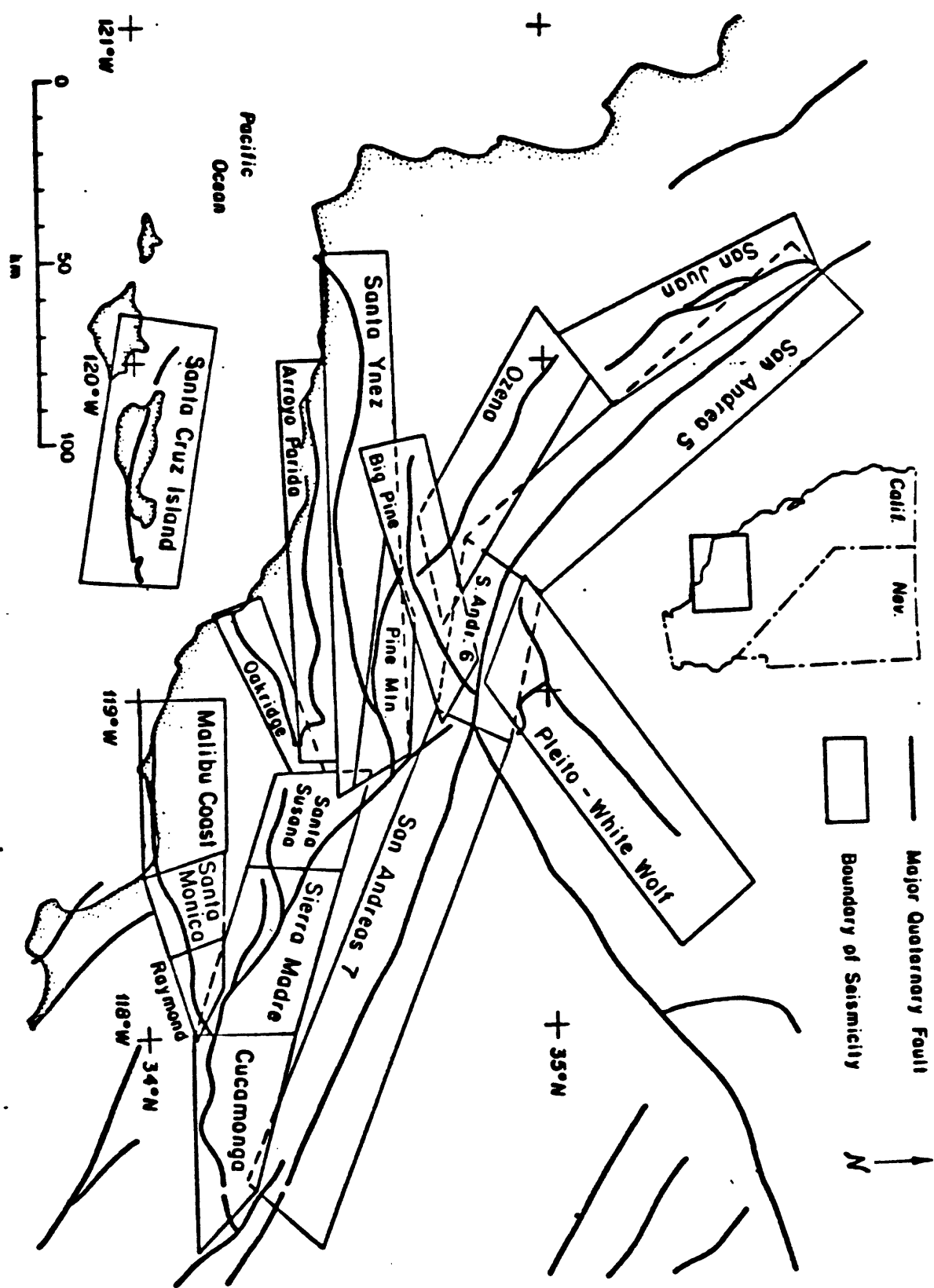


Figure 2. c) Faults and boundaries of seismicity searches for region 3.

Appendix I

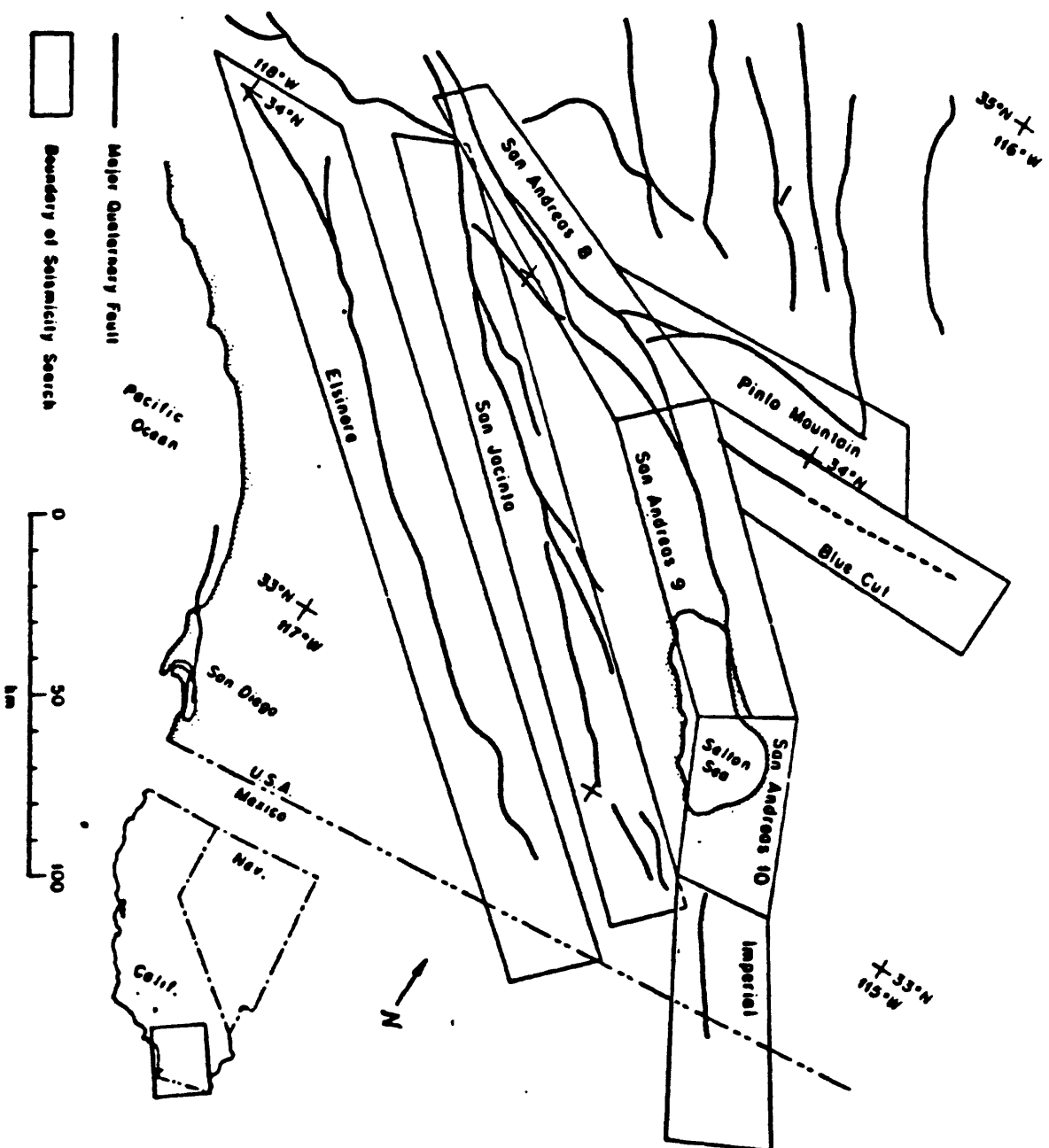


Figure 2. d) Faults and boundaries of seismicity searches for region 4.

Appendix I

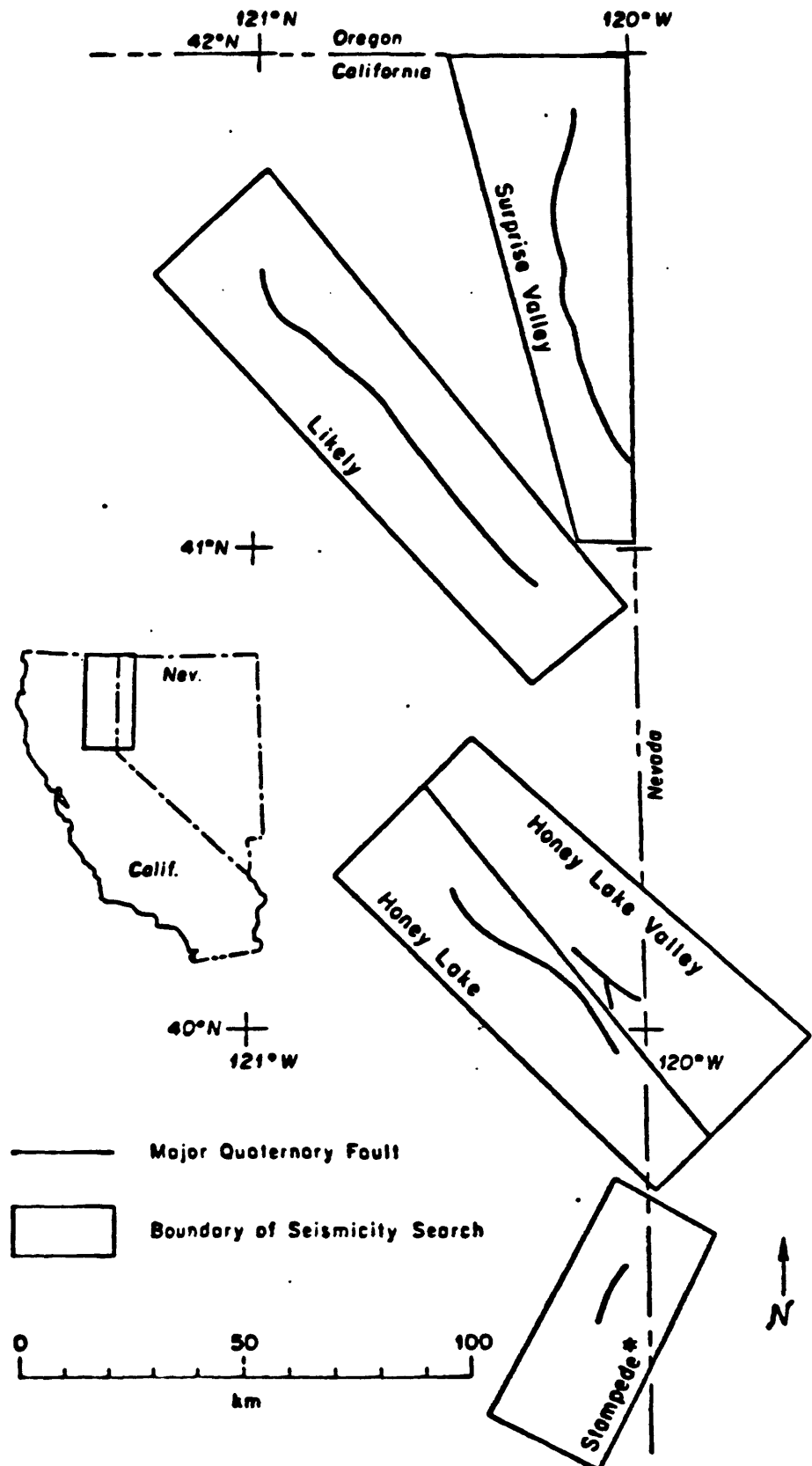


Figure 2. e) Faults and boundaries of seismicity searches for region 5.

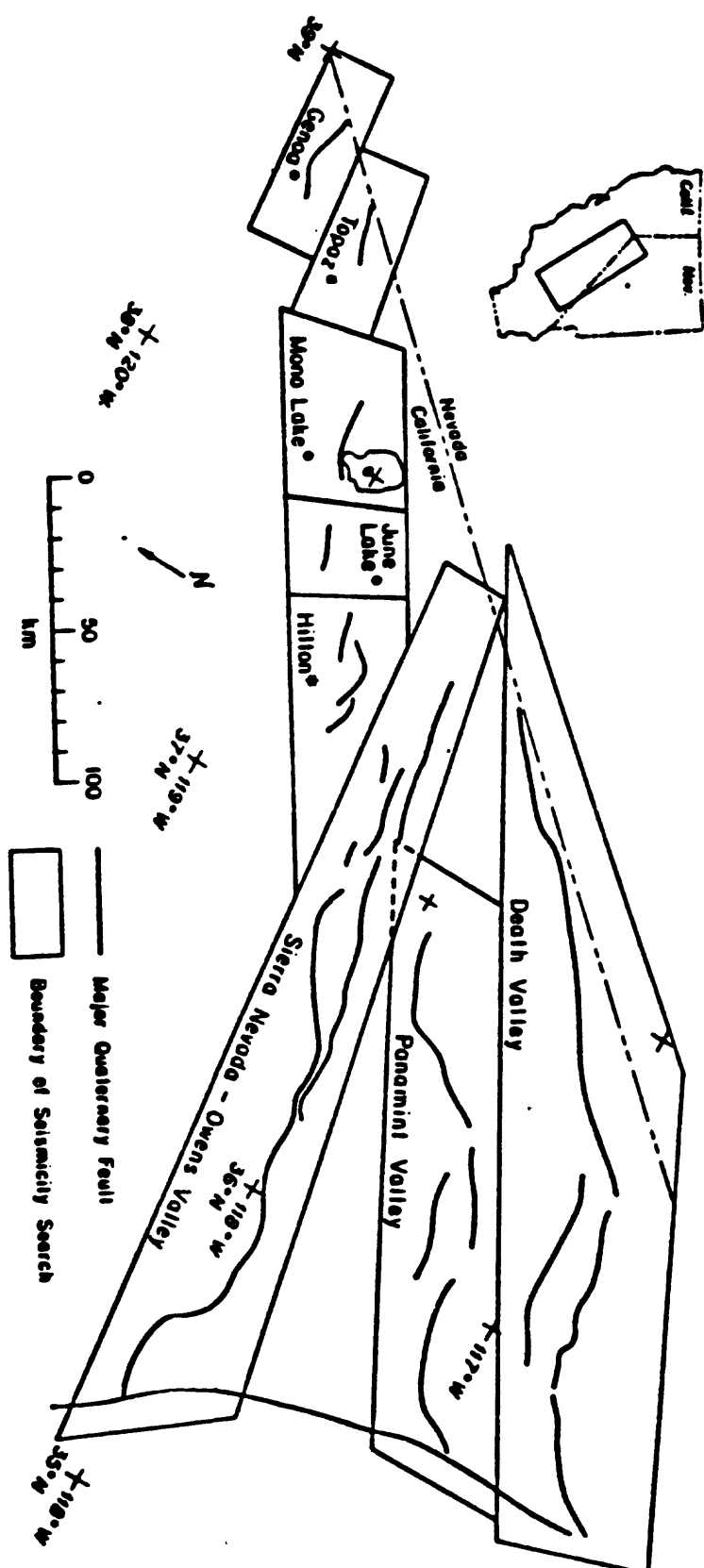


Figure 2. f) Faults and boundaries of seismicity searches for region 6.

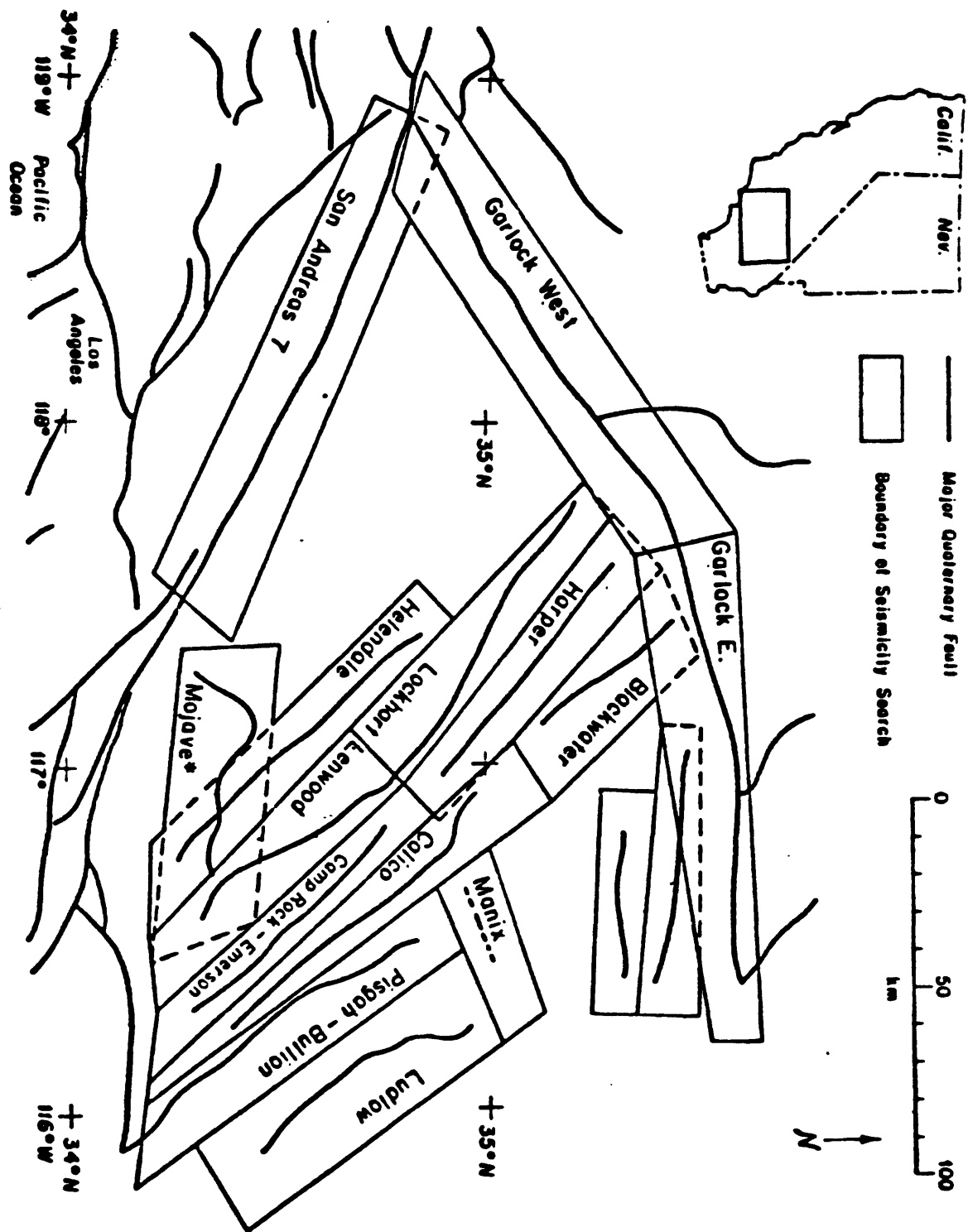


Figure 2. 8) Faults and boundaries of seismicity searches for region 7.

Appendix I

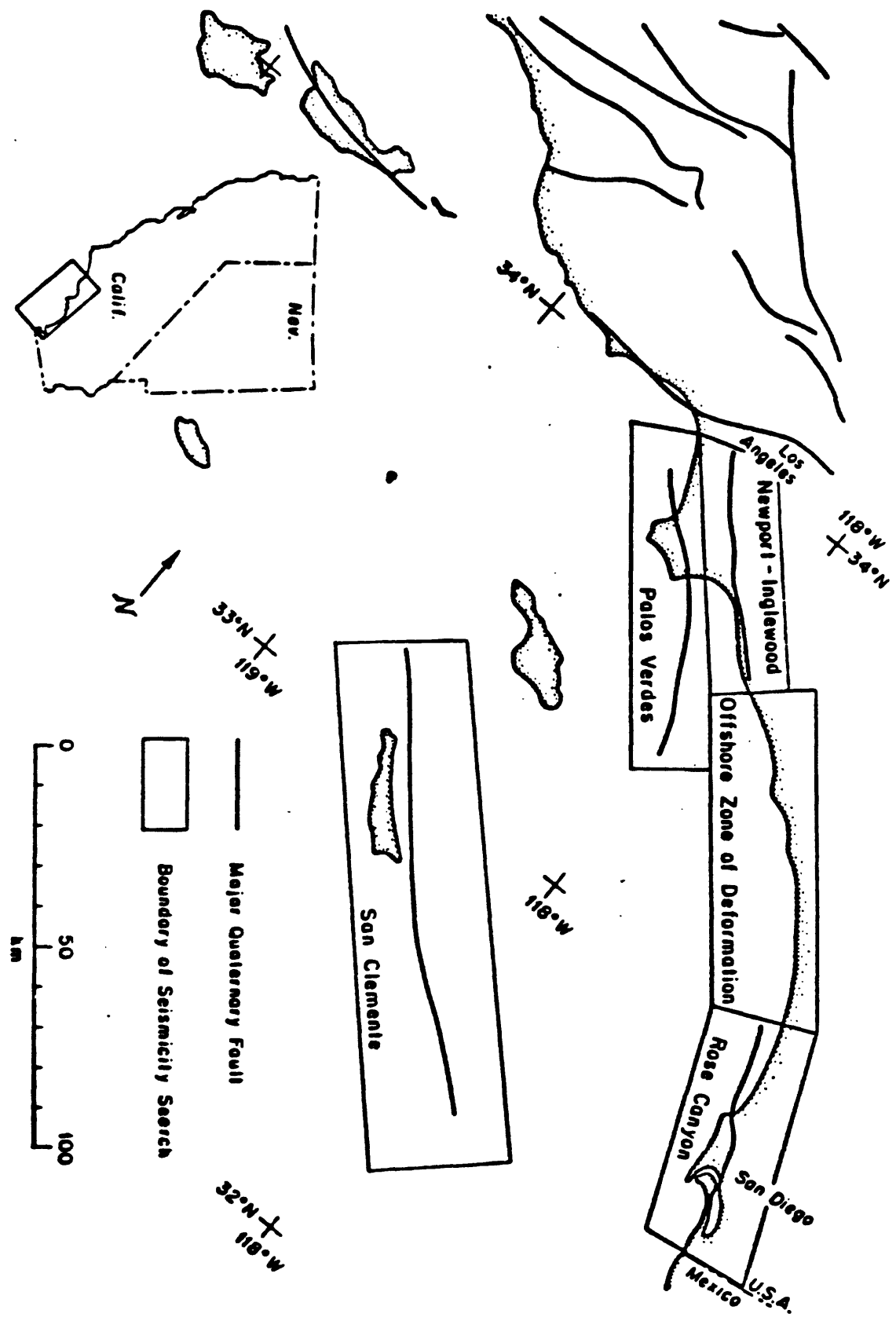


Figure 2. h) Faults and boundaries of seismicity searches for region 8.

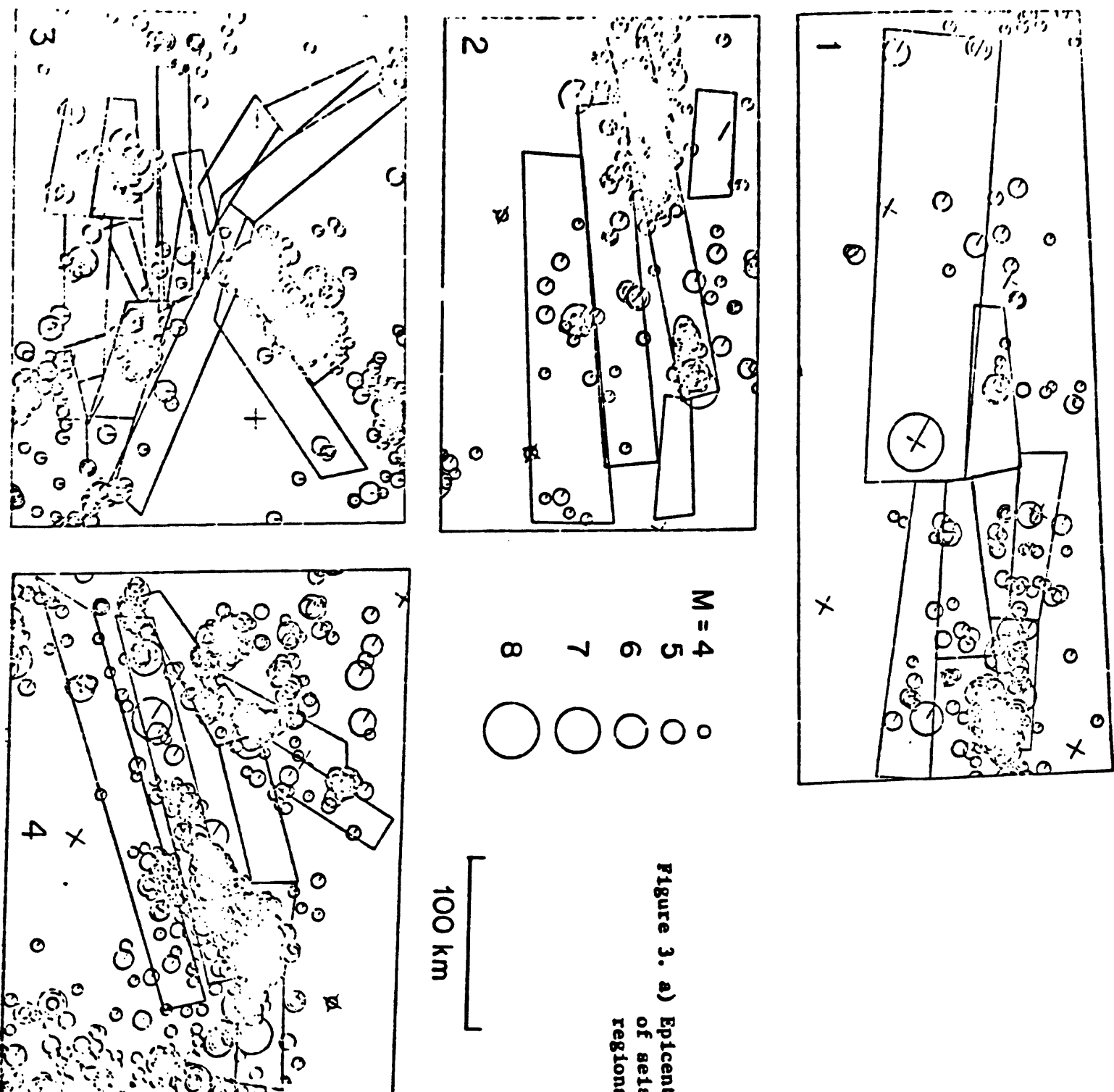
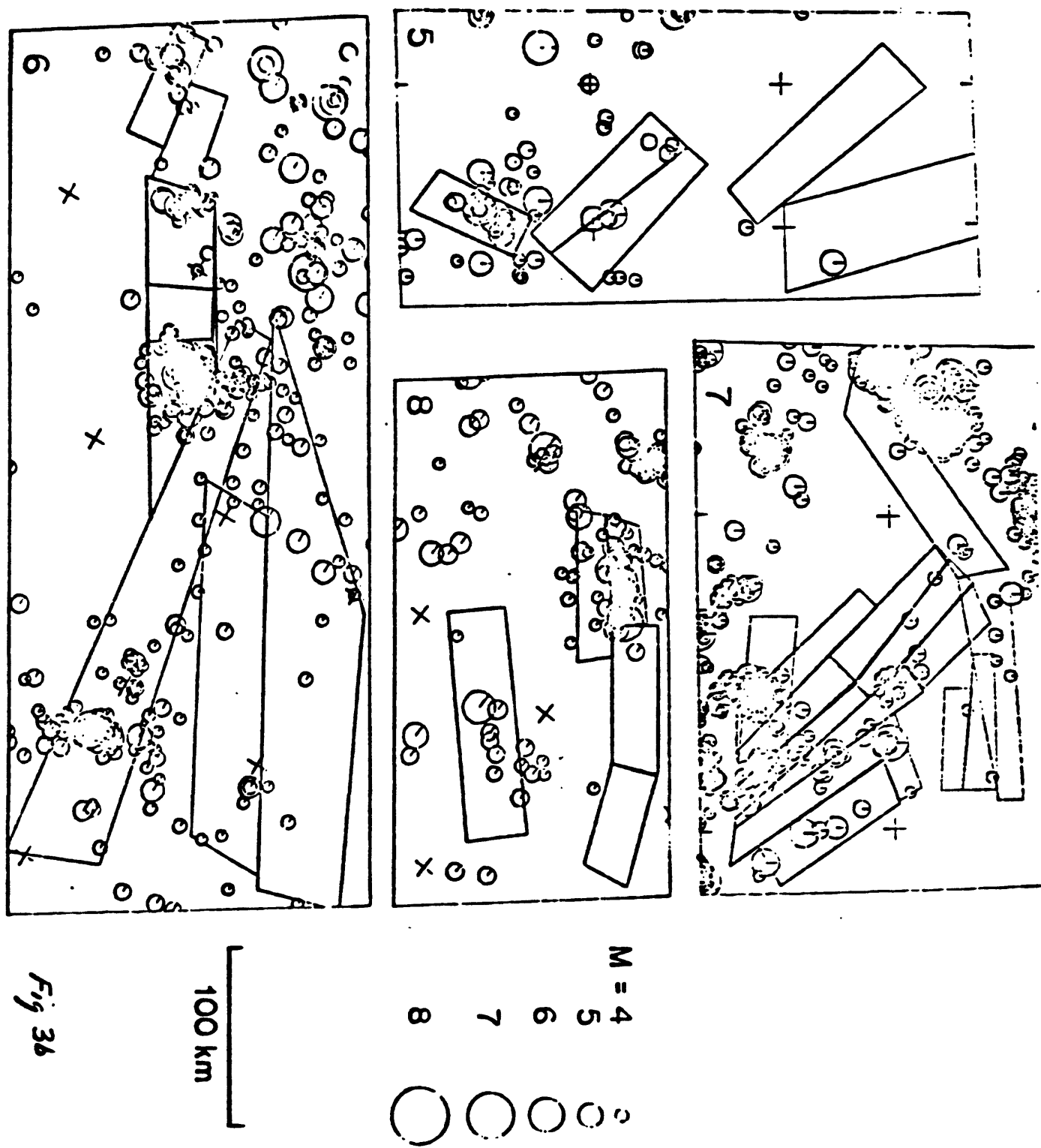


Figure 3. a) Epicenters and boundaries of seismicity searches for regions 1 to 4.

Figure 3. b) Epicenters and boundaries of seismicity searches for regions 5 to 8.



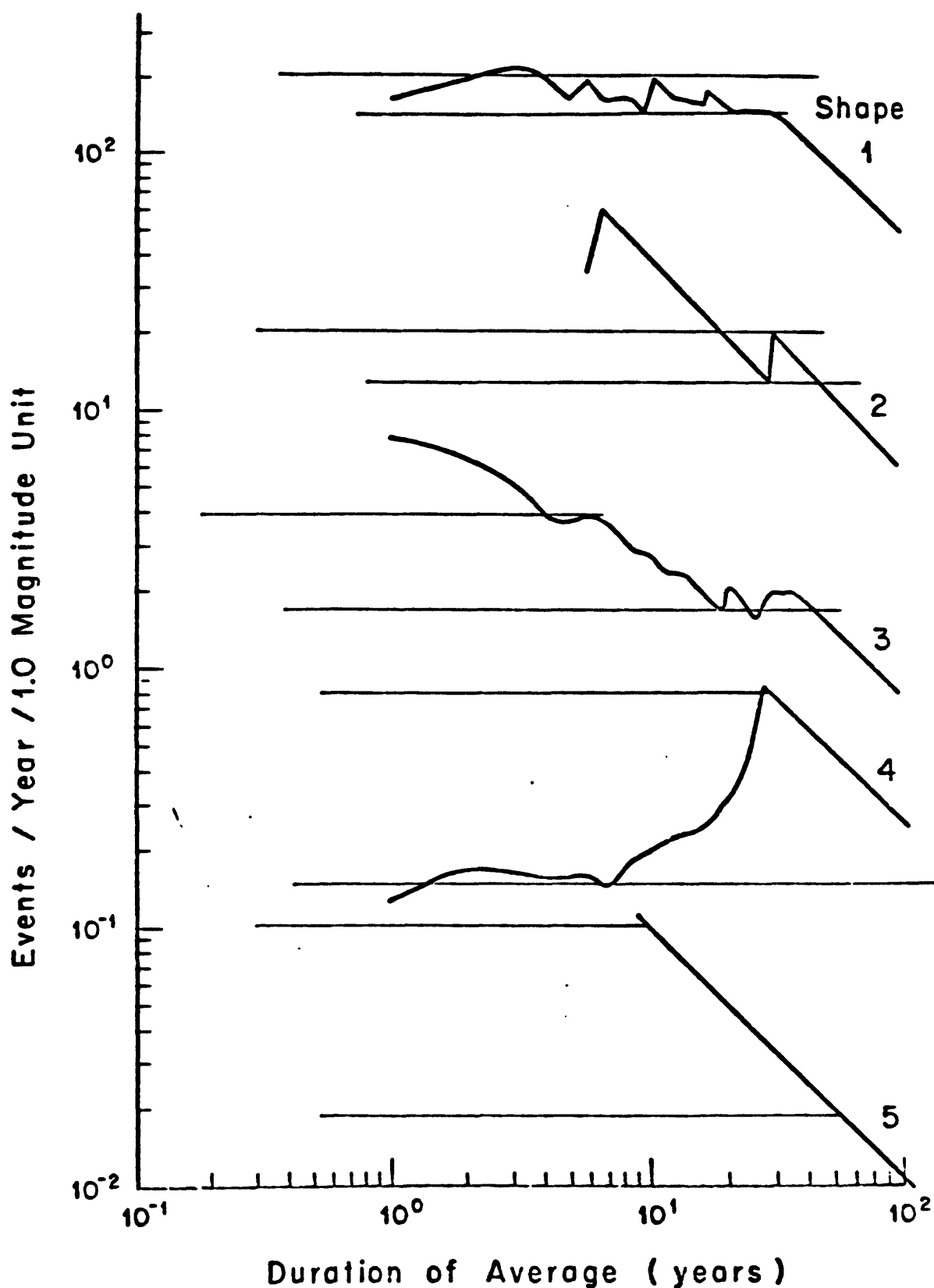


Figure 4. Characteristic shapes for the sequence of averages A_k . The value of A_k for a k -year duration for the average is the number of earthquakes per year listed in the catalog over the most recent k years. Bounds on the average occurrence rate are shown consistent with the way these bounds have been chosen in each of the seismicity searches.

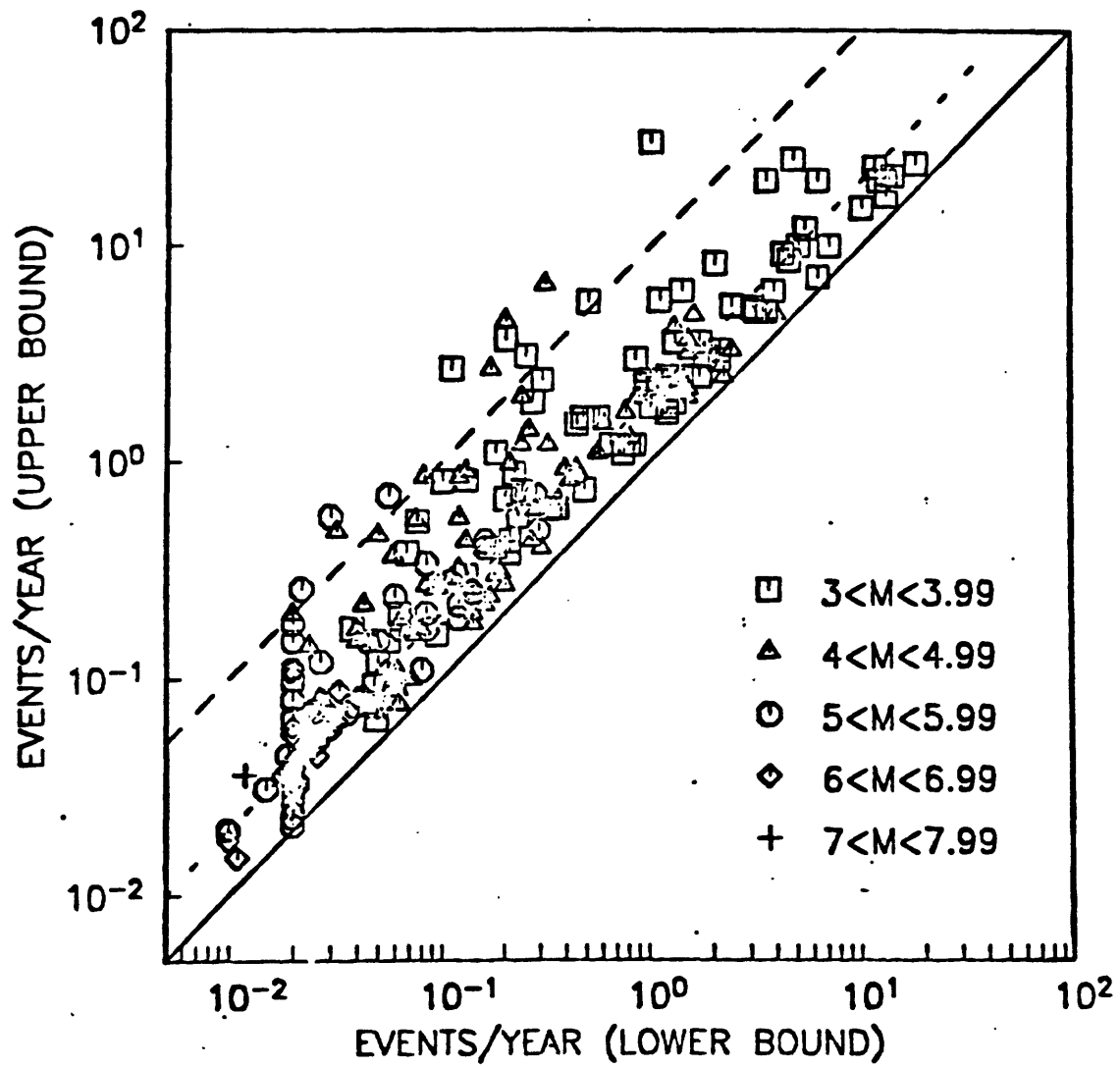


Figure 5. Relationship of upper and lower bounds on occurrence rates for all seismicity zones listed in Table 4 and illustrated in Figure 2.

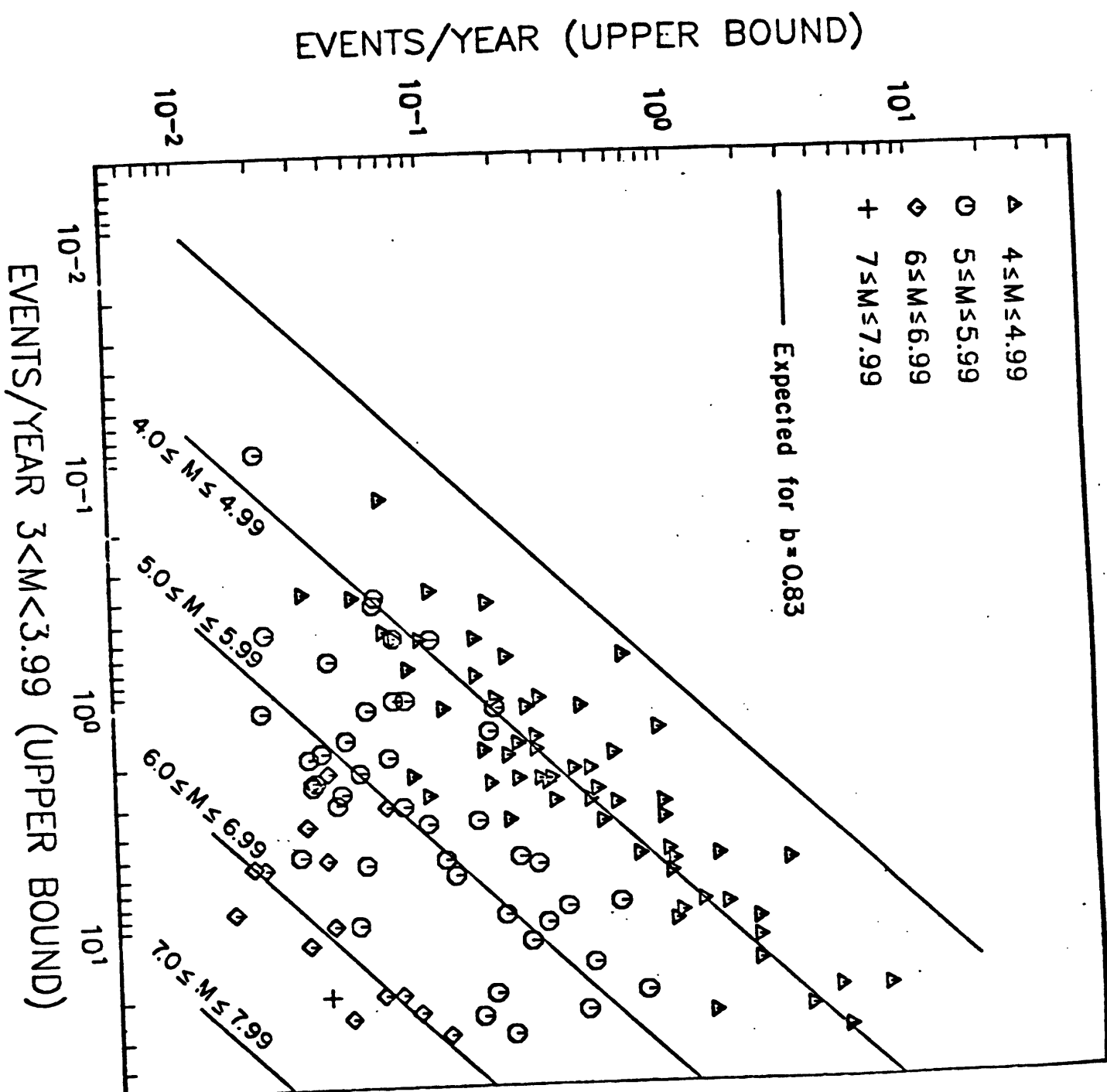


Figure 6. Events per year in each magnitude interval, shown as a function of events per year in the magnitude 3 interval on each fault. The expected trend of data for $b = 0.83$ is shown.

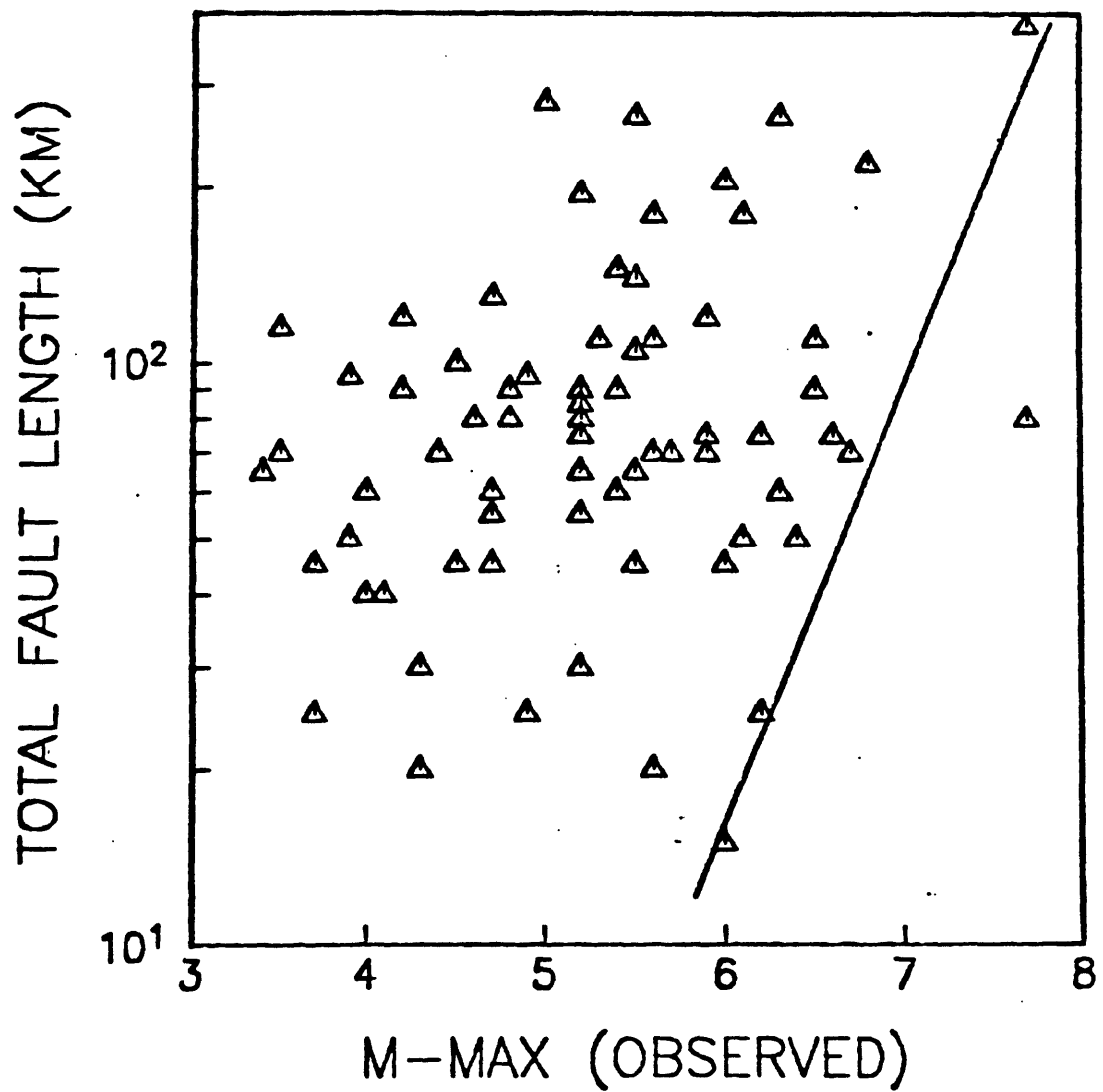


Figure 7. Maximum observed magnitude earthquake on each fault, shown as a function of the length of the zone as defined in Figure 2. The line is a theoretical relationship obtained based on a scaling relationship of Scholz (1982), and with one exception, appears to be a good bound for these data.

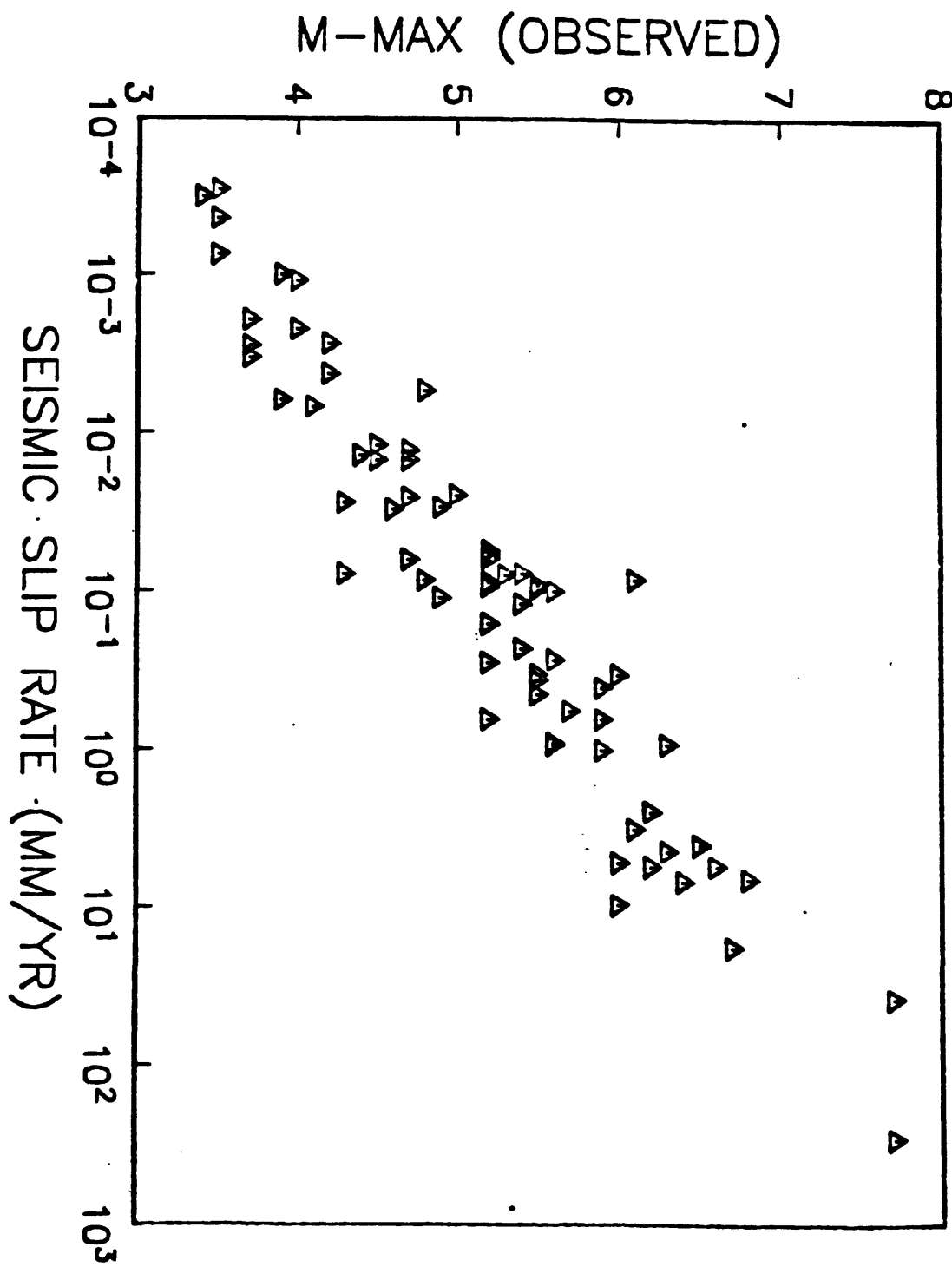


Figure 8. Maximum observed magnitude on each fault shown as a function of the slip rate on the fault due to all catalogued earthquakes. The seismic slip rate is obtained from the catalog through an assumed relationship between magnitude and seismic moment.

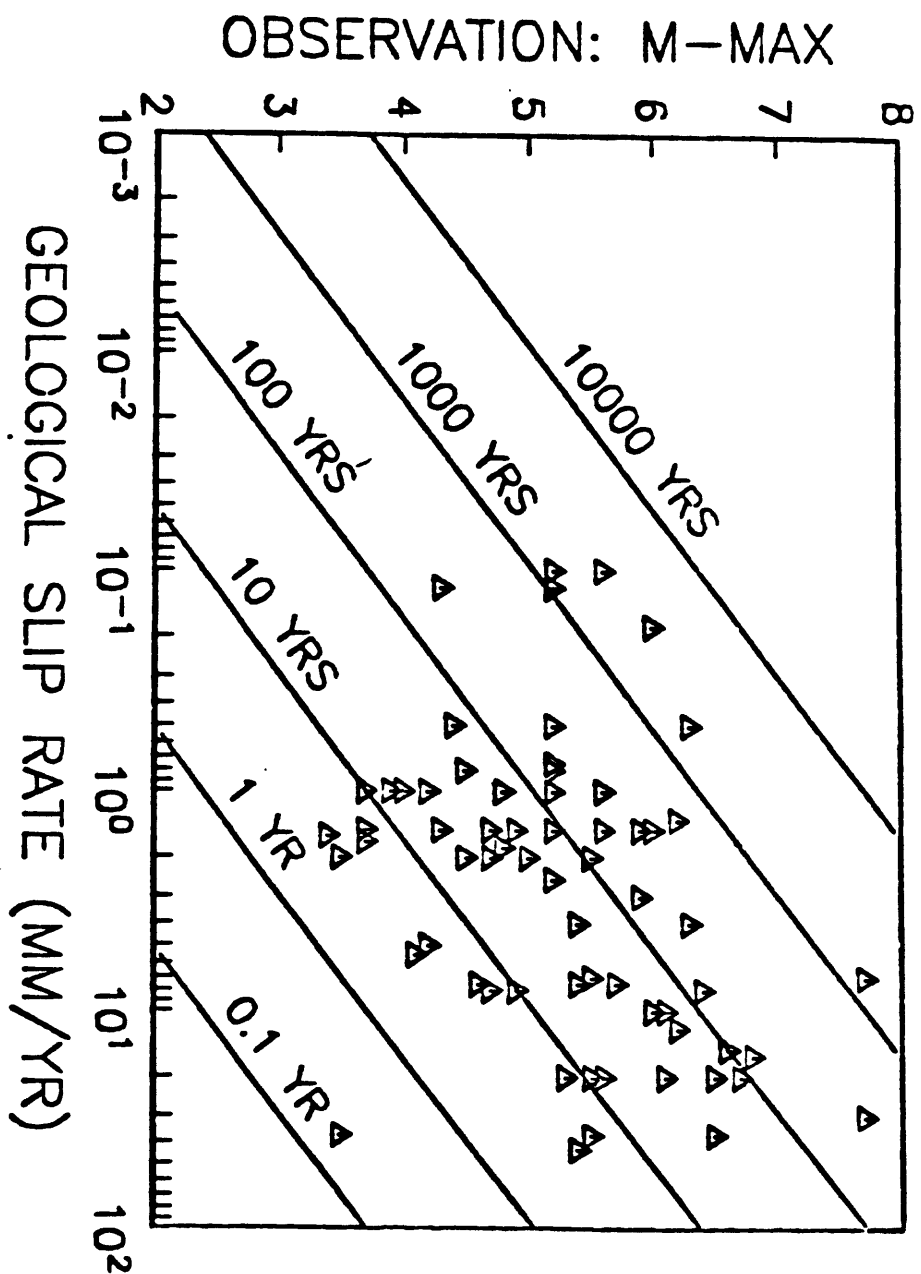


Figure 9. Maximum observed magnitude on each fault segment, shown as a function of the best estimate of geological slip rate (Table 4). The theoretical curves show the frequency with which a particular magnitude earthquakes would have to recur if that magnitude were the largest that the fault ever has, in order for the fault to achieve the given slip rate.

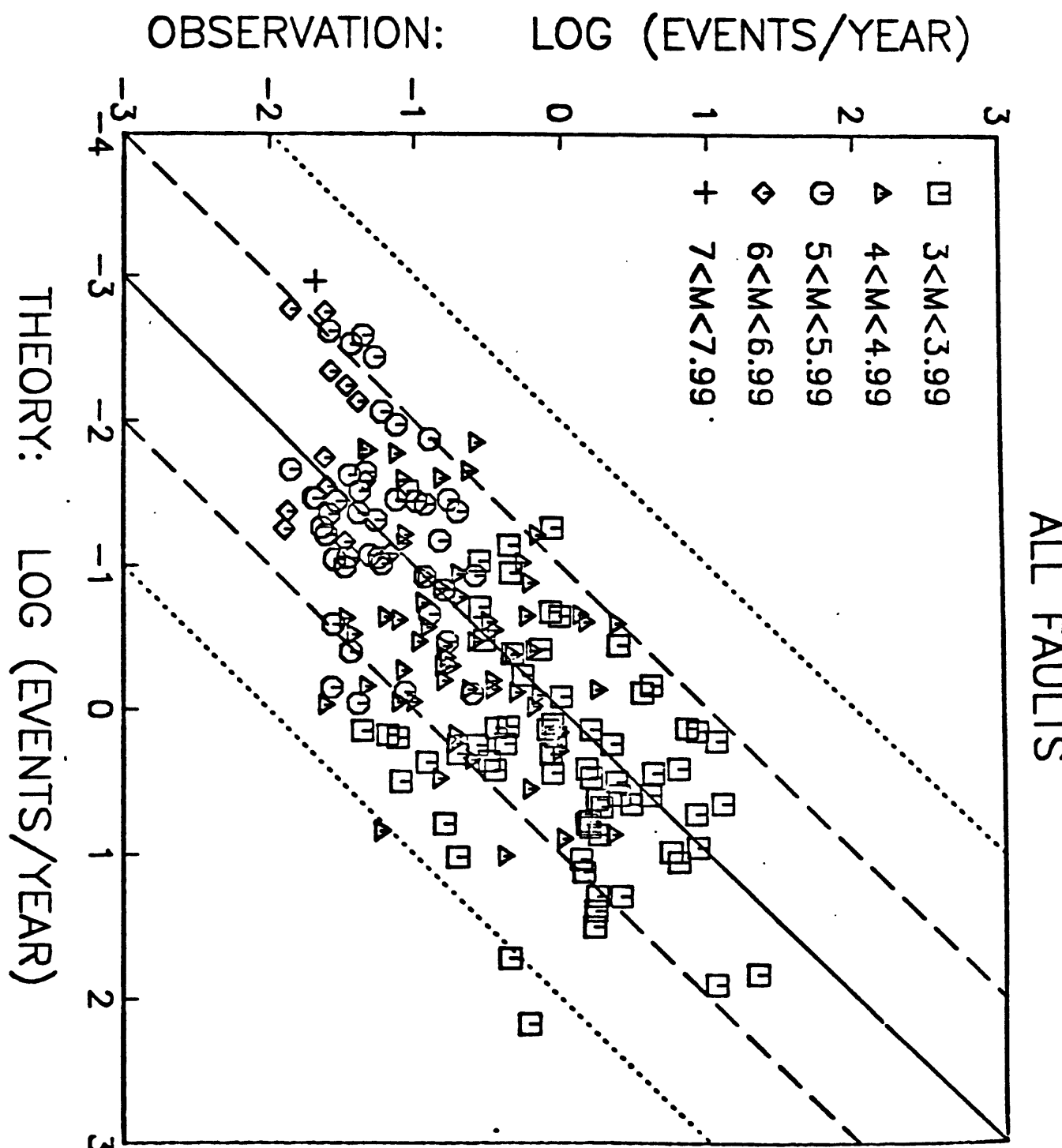


Figure 10. Observed occurrence rates on each fault in Table 4, given as a function of the occurrence rate as predicted from the slip rate, M_{max} , and the b -value. Error bars have been deleted from this figure for clarity, but are shown on subsequent similar figures. Observed rates are plotted at the geometric mean of observed bounds on rates. The theoretical rates are based on the best estimate of slip rate. The solid line shows equality of the two rates, and the dashed and dotted lines show differences of one and two orders of magnitude.

NEWPORT-INGLEWOOD AND WHITE WOLF

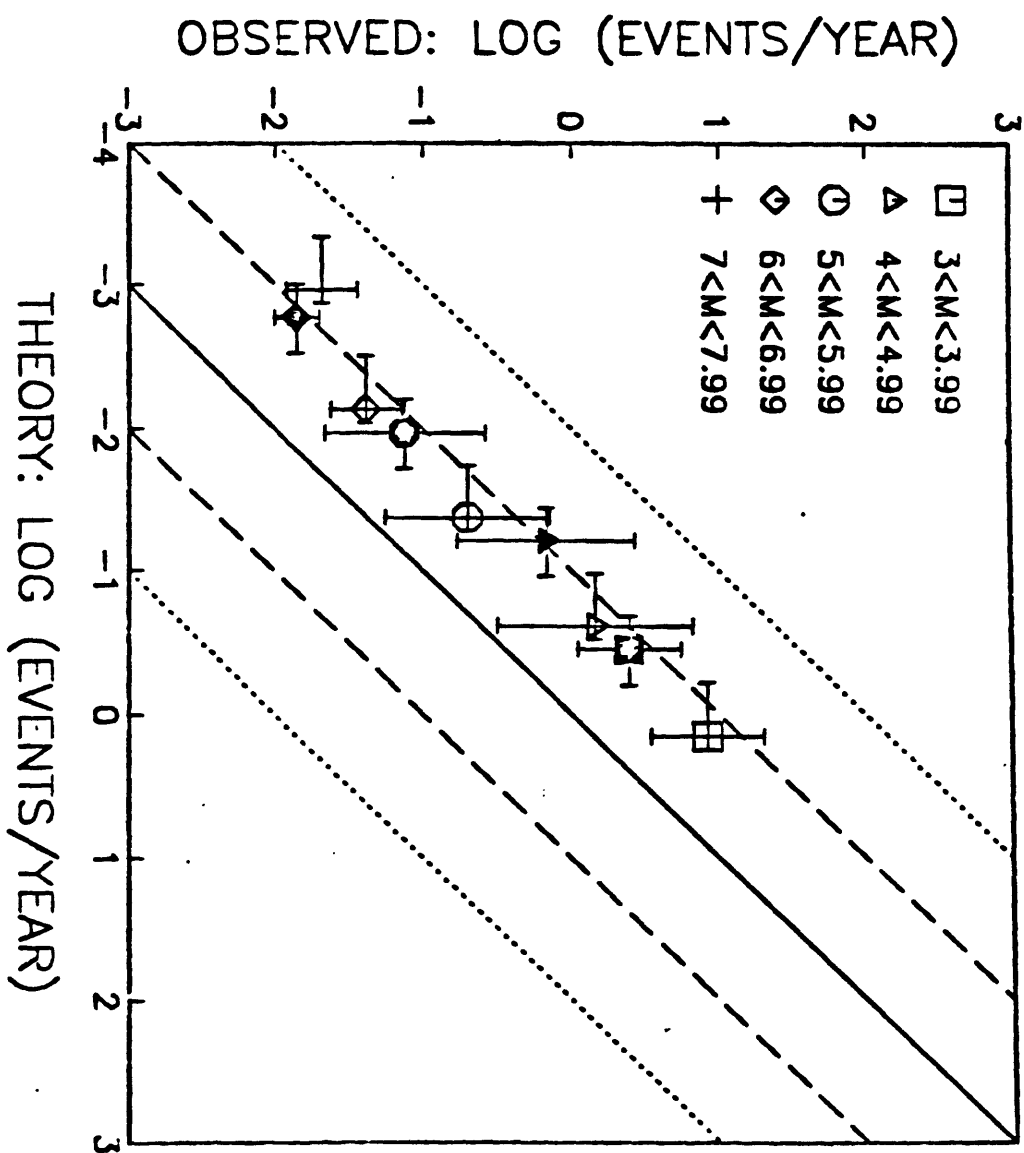


Figure 11. Equivalent of Figure 10, showing only data from the Newport-Inglewood fault (solid symbols) and the White Wolf fault (open symbols). Error bars on observed rates show the upper and lower bounds on occurrence rate estimates. Error bars on theoretical rates show the effects of using the minimum and maximum slip rate estimates which are given in Table 4.

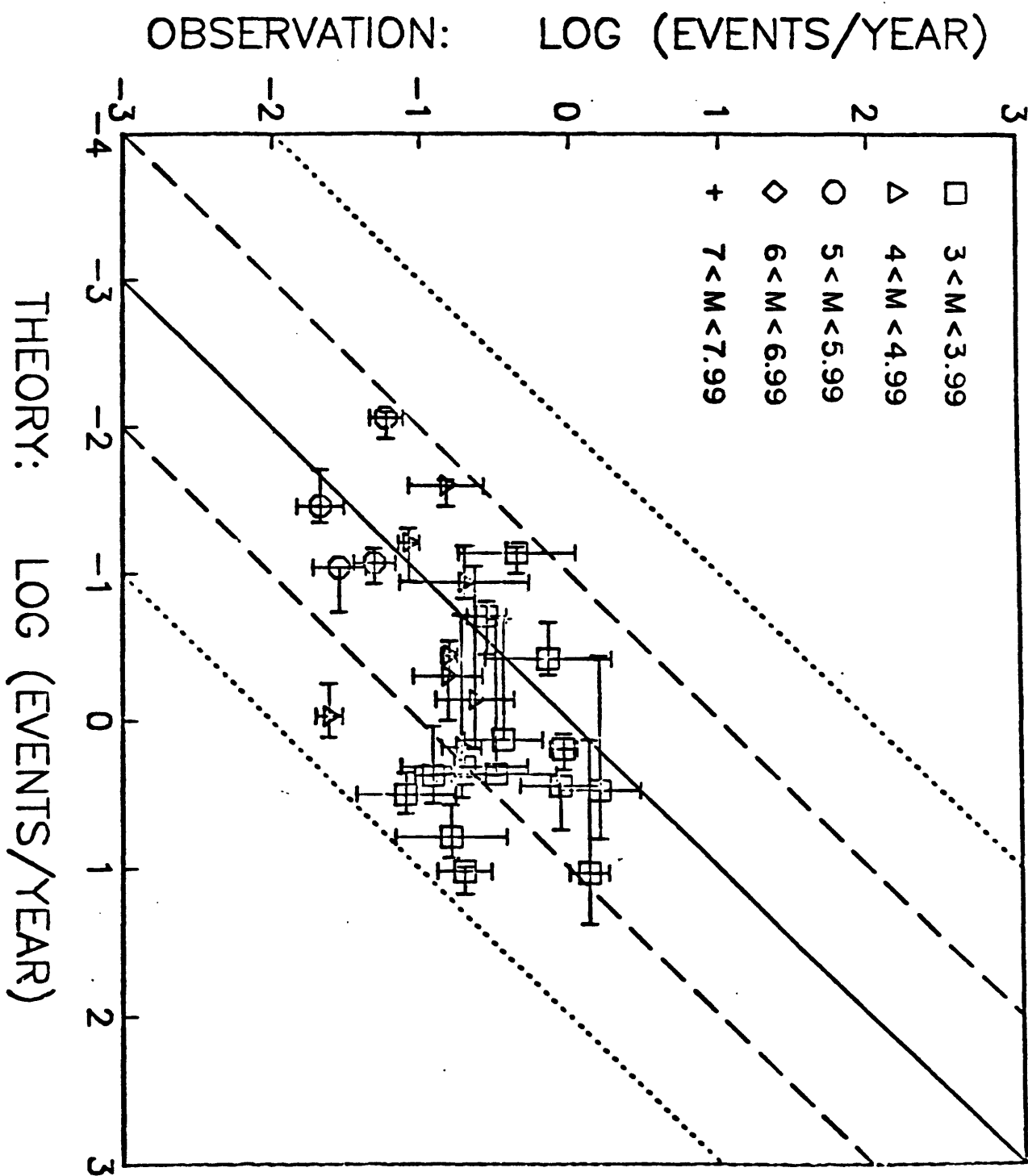


Figure 12. Equivalent of Figures 10 and 11 for those faults which are below the 10-year contour on Figure 9.

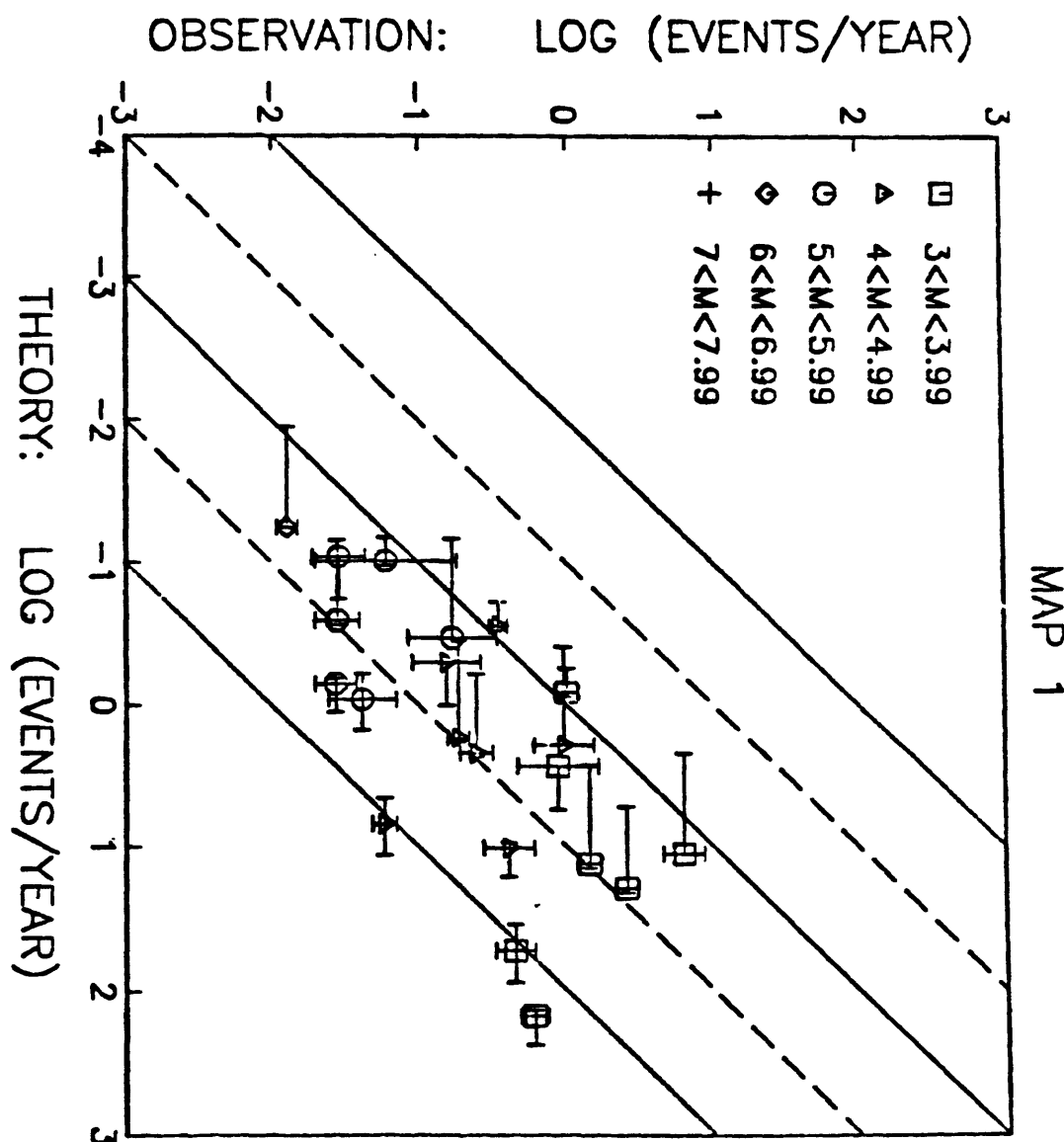


Figure 13. a) Equivalent of Figures 10 and 11 for region 1.

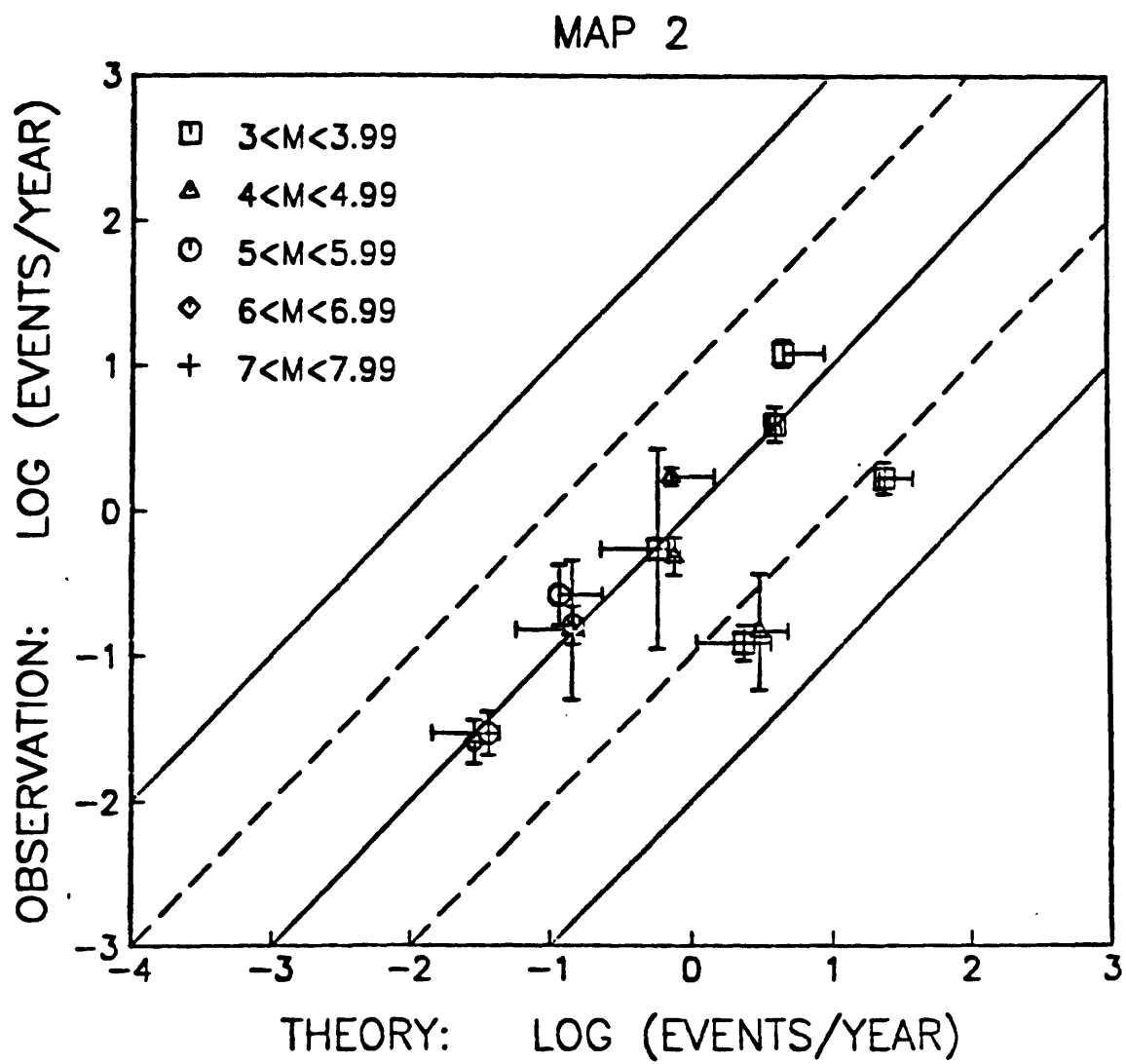


Figure 13. b) Equivalent of Figures 10 and 11 for region 2.

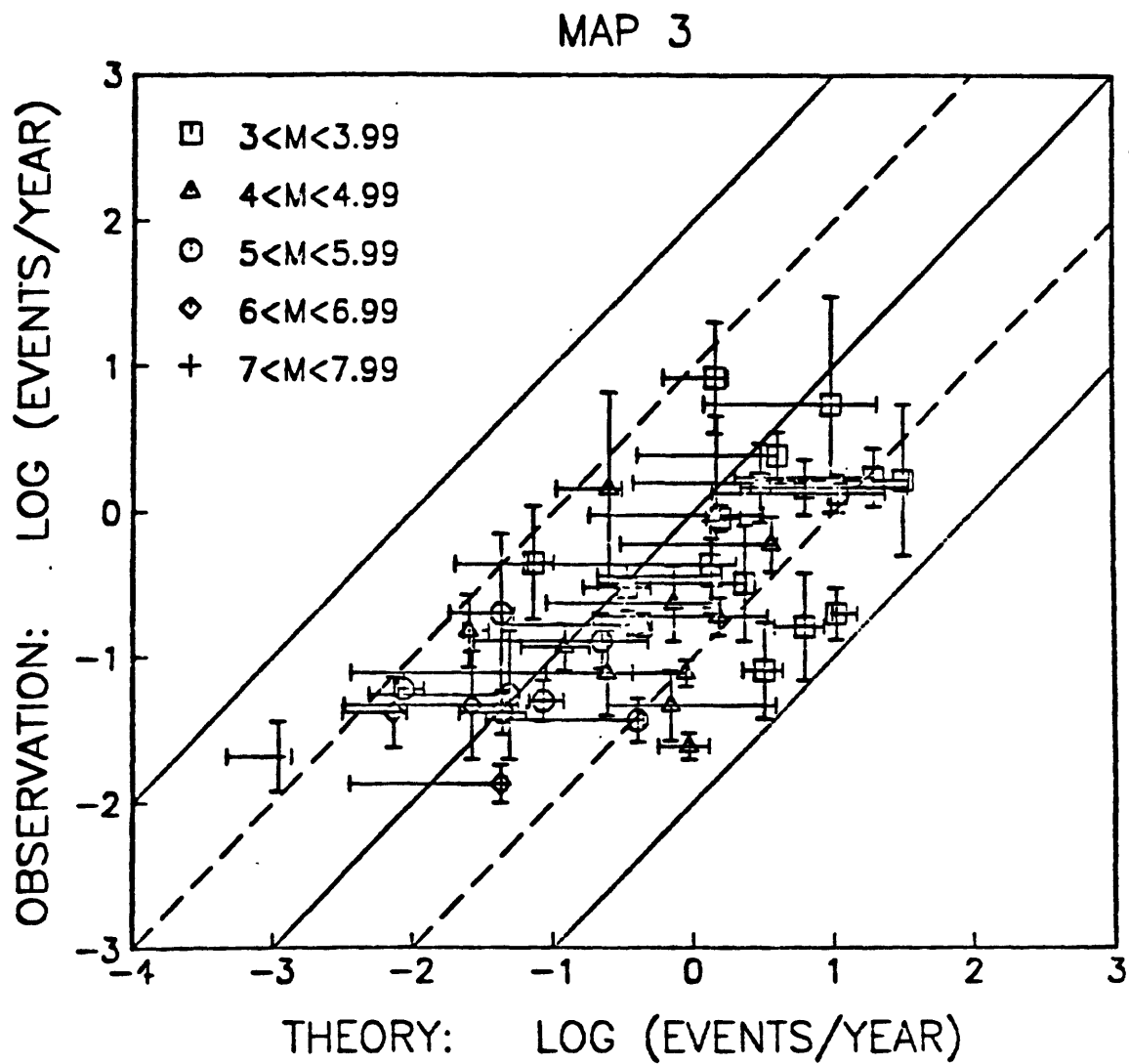


Figure 13. c) Equivalent of Figures 10 and 11 for region 3.

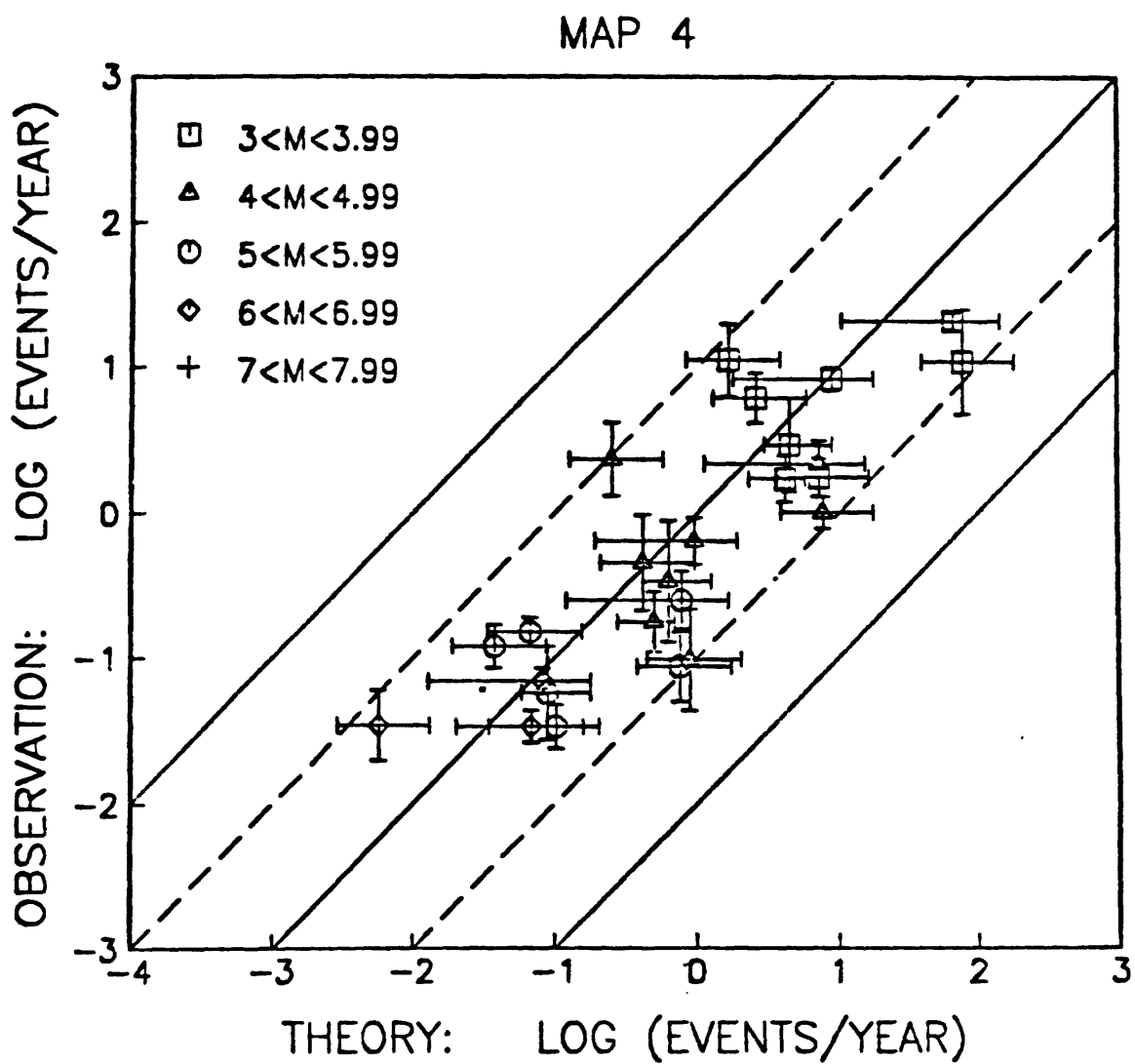


Figure 13. d) Equivalent of Figures 10 and 11 for region 4.

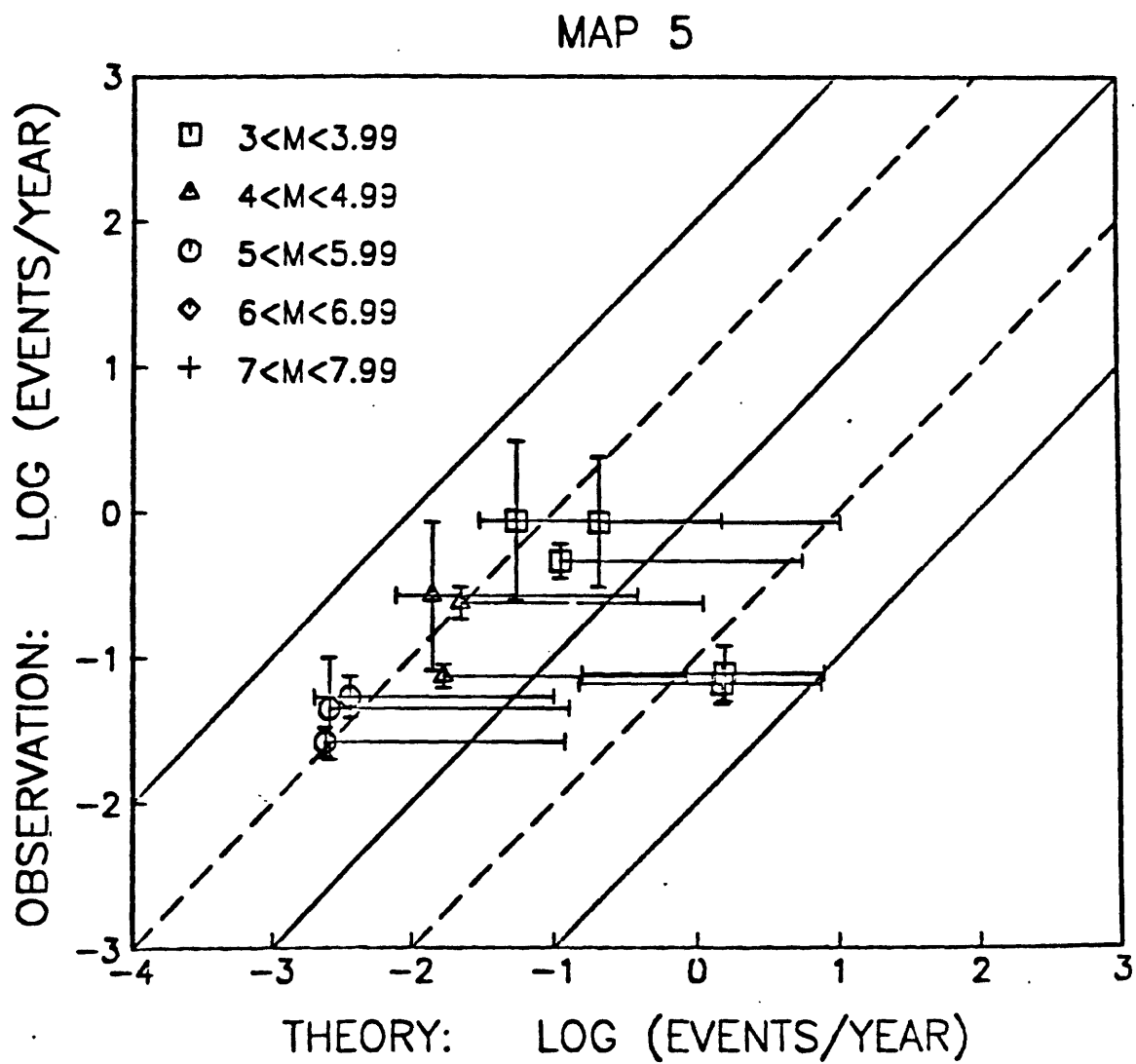


Figure 13. e) Equivalent of Figures 10 and 11 for region 5.

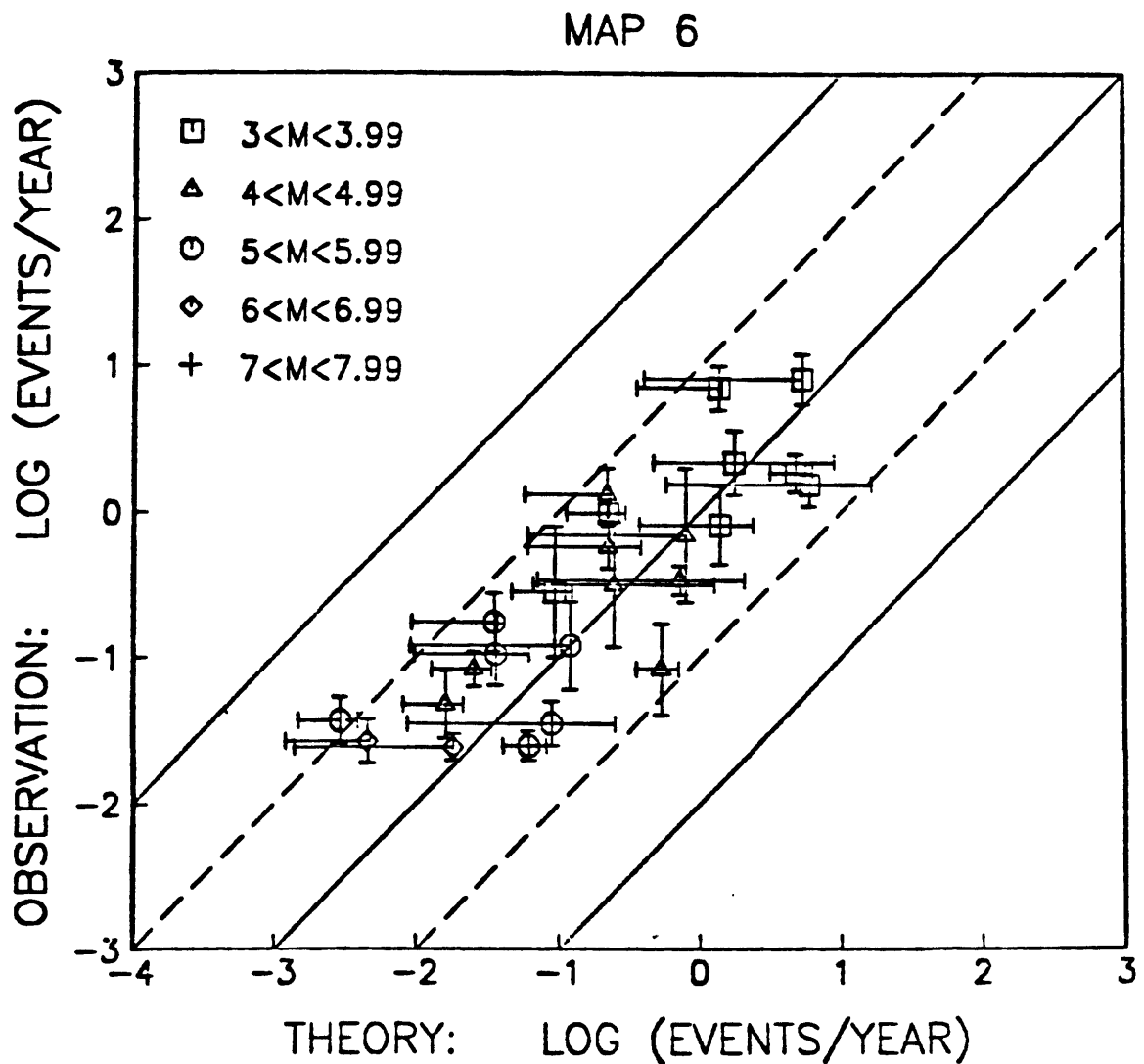


Figure 13. f) Equivalent of Figures 10 and 11 for region 6.

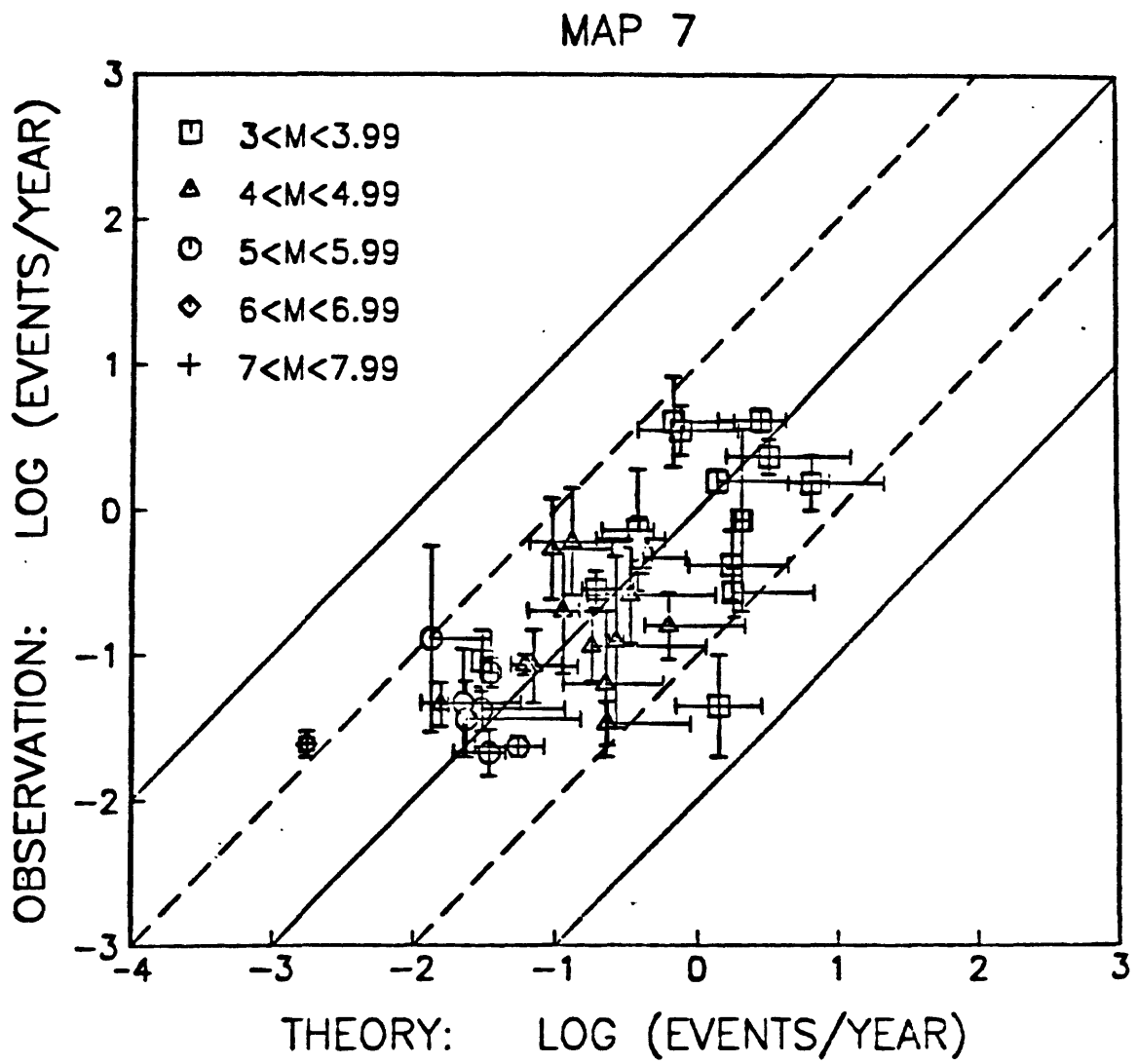


Figure 13. g) Equivalent of Figures 10 and 11 for region 7.

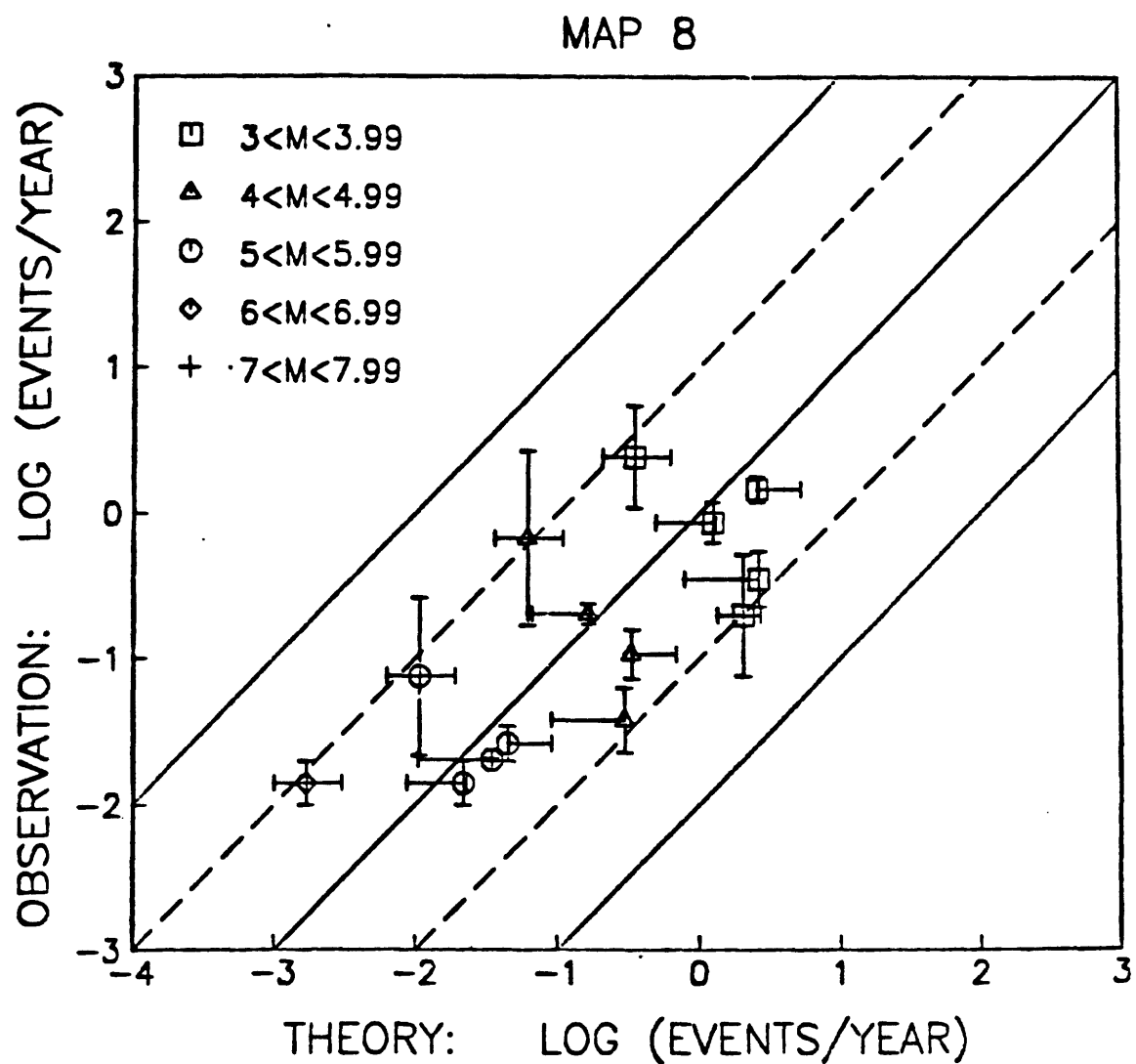


Figure 13. h) Equivalent of Figures 10 and 11 for region 8.

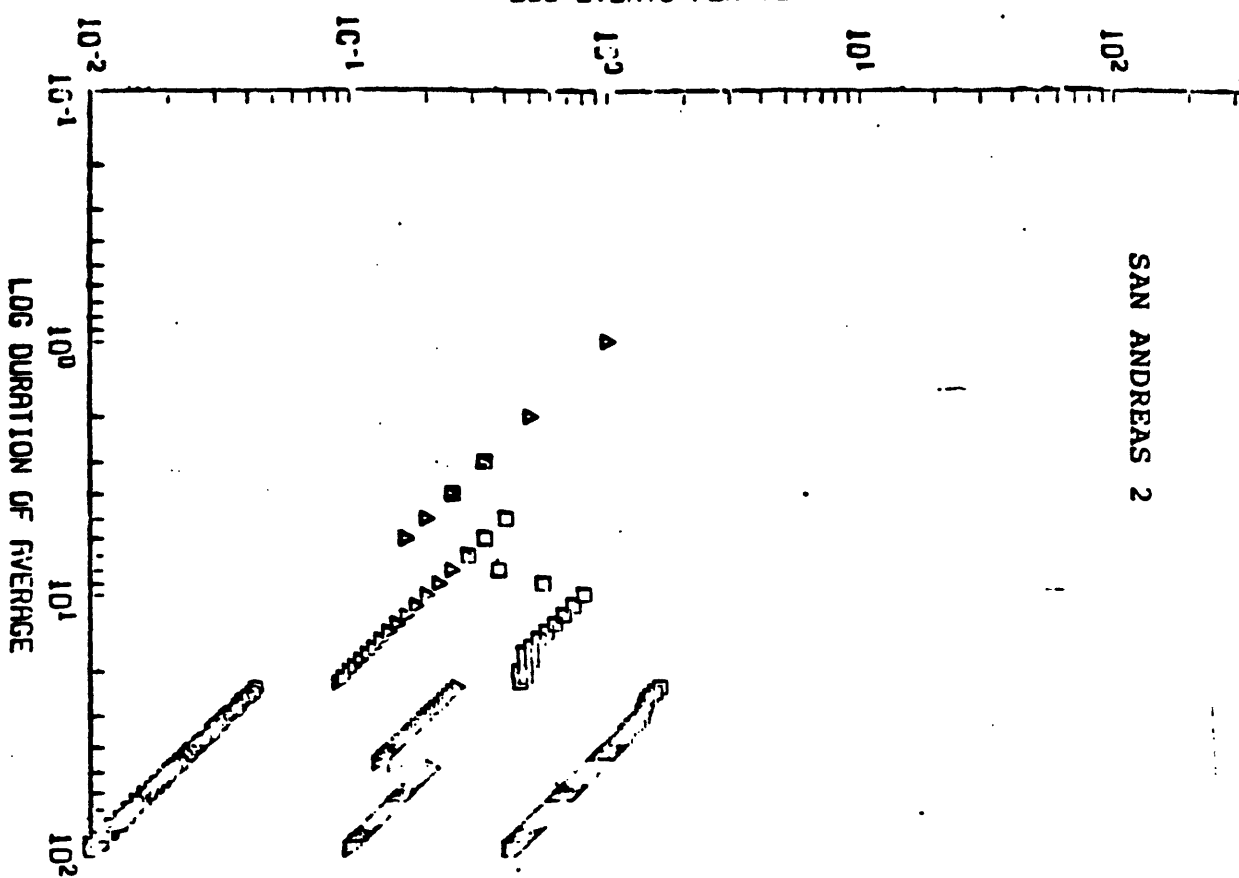
APPENDIX I-1

Plots of average occurrence rates of earthquakes as a function of length of the time period over which the average is defined. All time periods end December 31, 1979.

Symbols correspond to the following magnitude ranges:

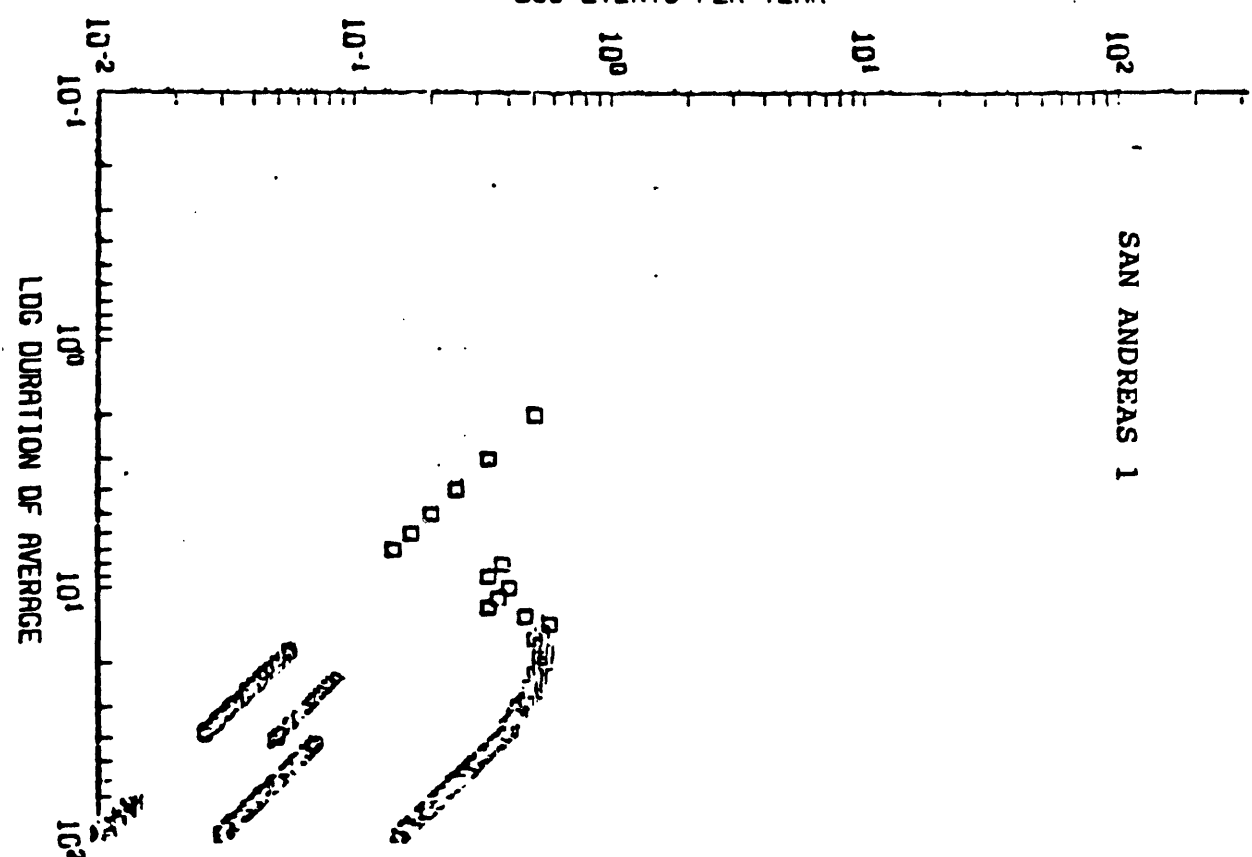
- \square $3.0 \leq M \leq 3.99$
- \triangle $4.0 \leq M \leq 4.99$
- \circlearrowleft $5.0 \leq M \leq 5.99$
- \diamond $6.0 \leq M \leq 6.99$
- \dagger $7.0 \leq M \leq 7.99$

LOG EVENTS PER YEAR



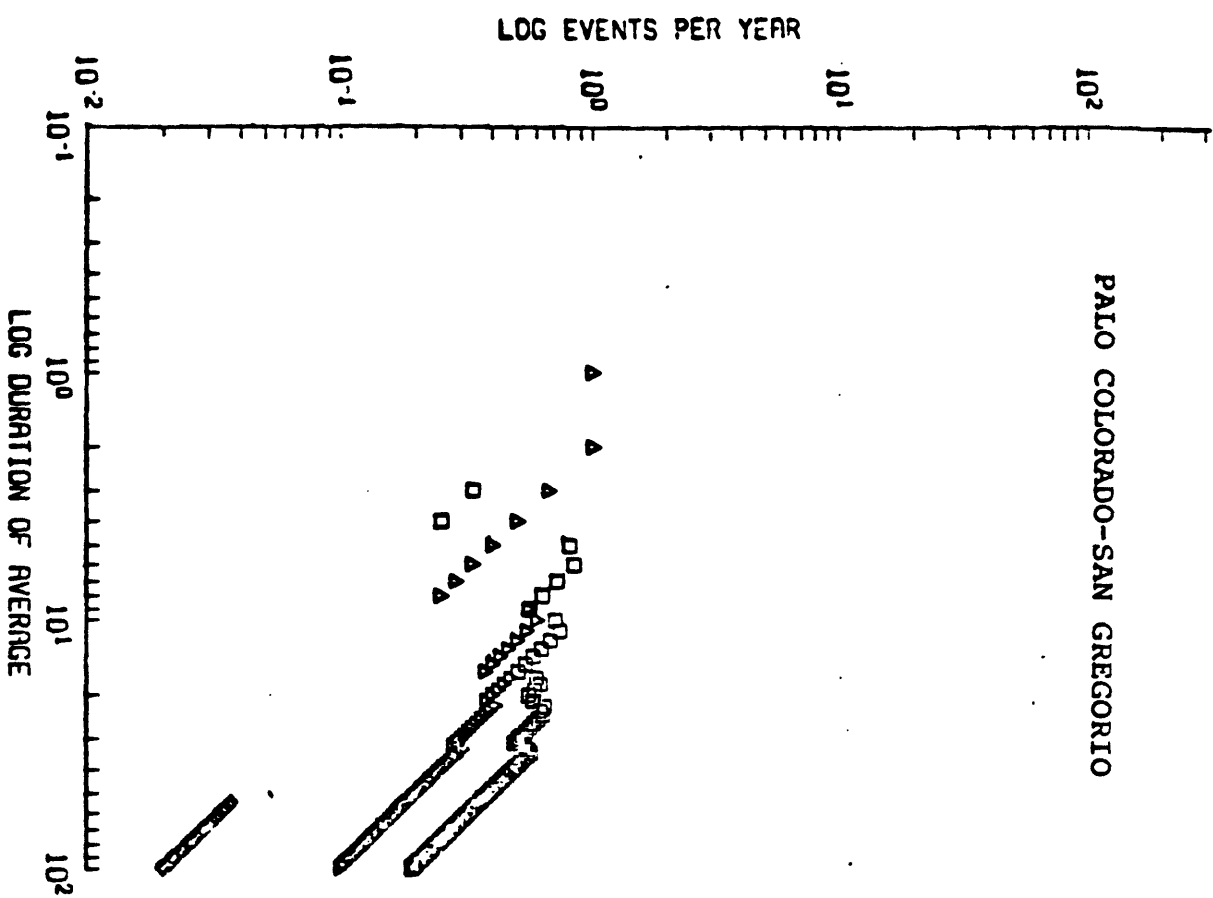
SAN ANDREAS 2

LOG EVENTS PER YEAR

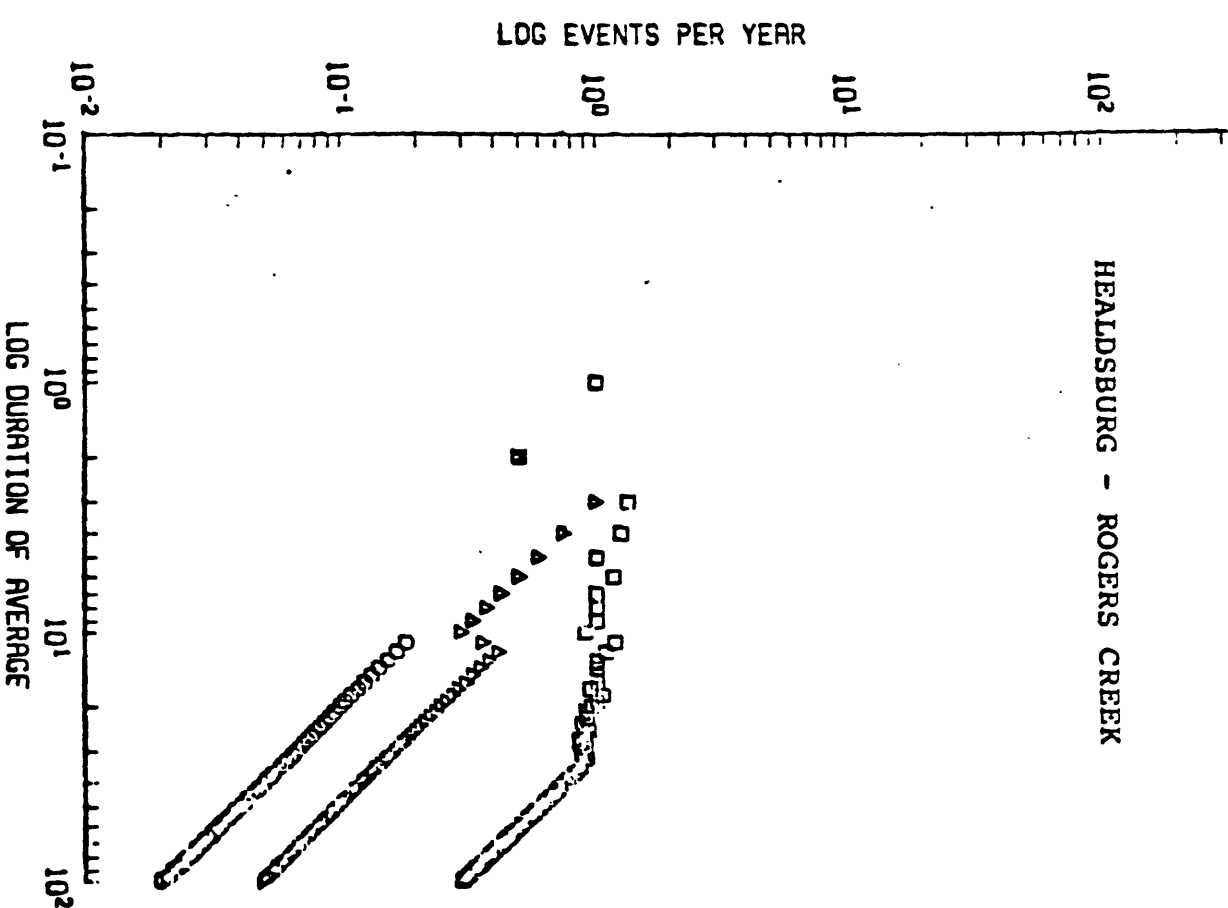


SAN ANDREAS 1

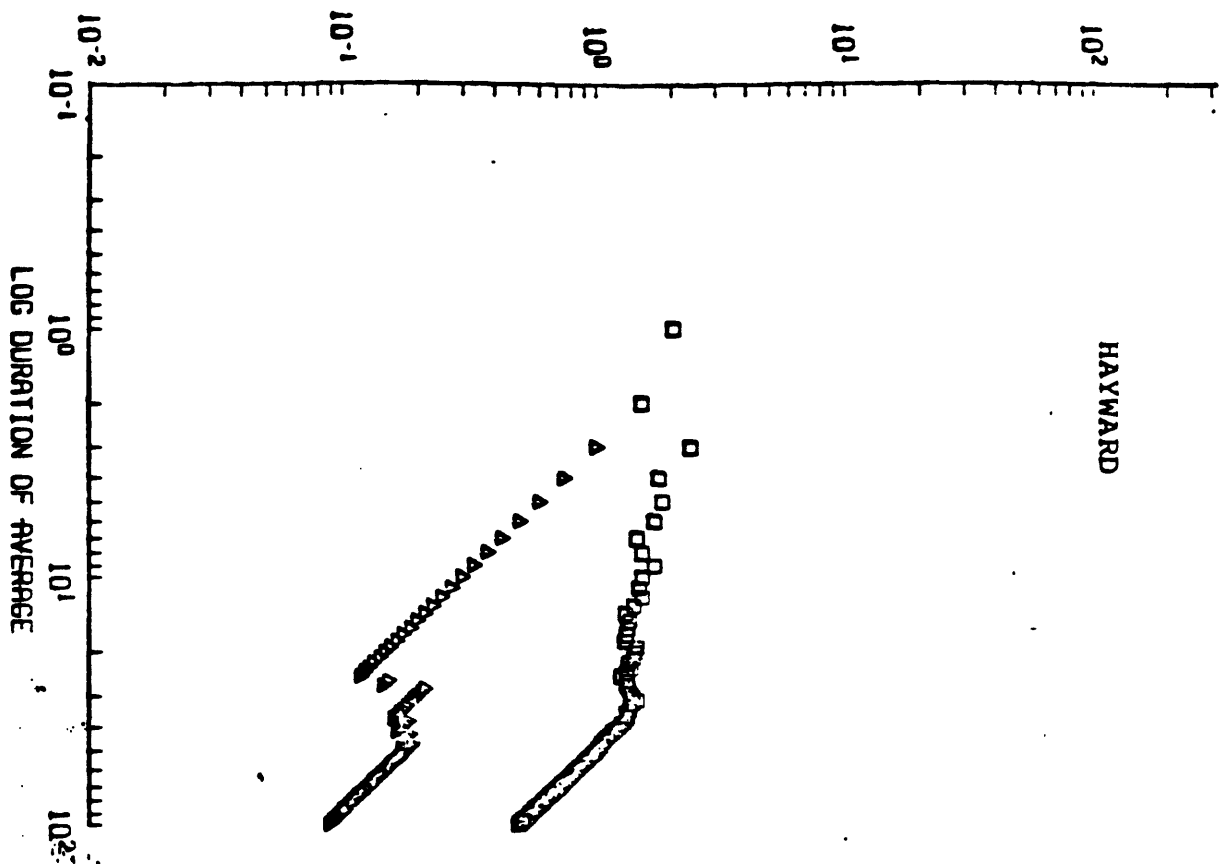
PALO COLORADO-SAN GREGORIO



HEALDSBURG - ROGERS CREEK

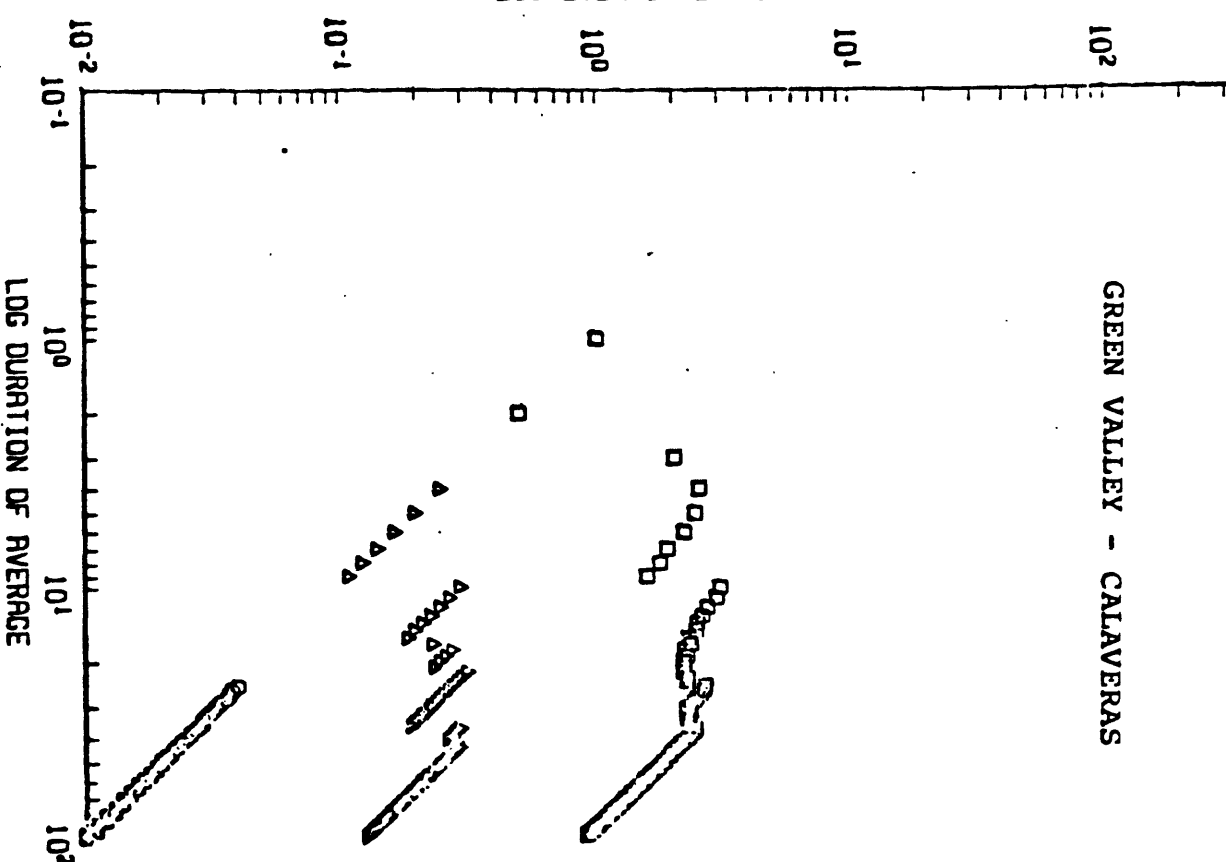


LOG EVENTS PER YEAR



HAYWARD

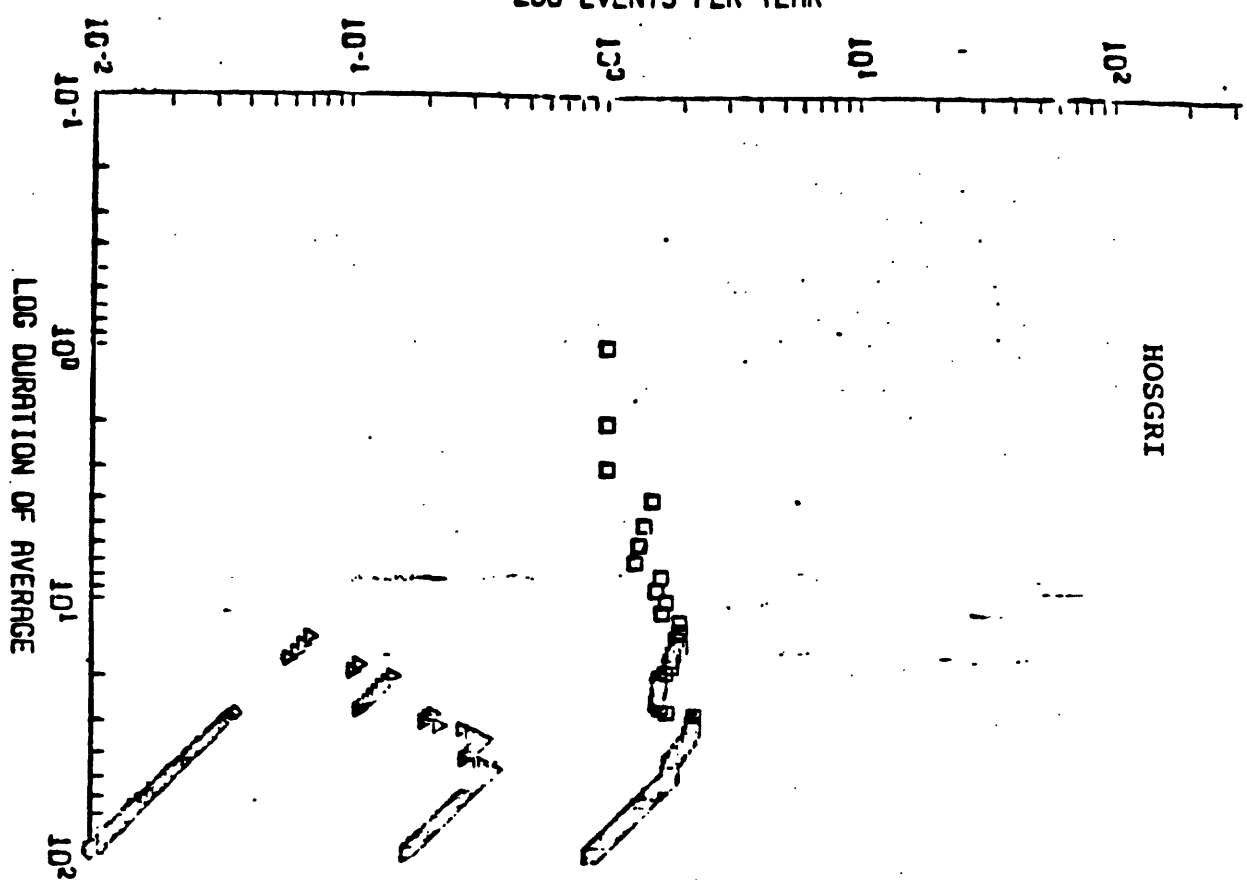
LOG EVENTS PER YEAR



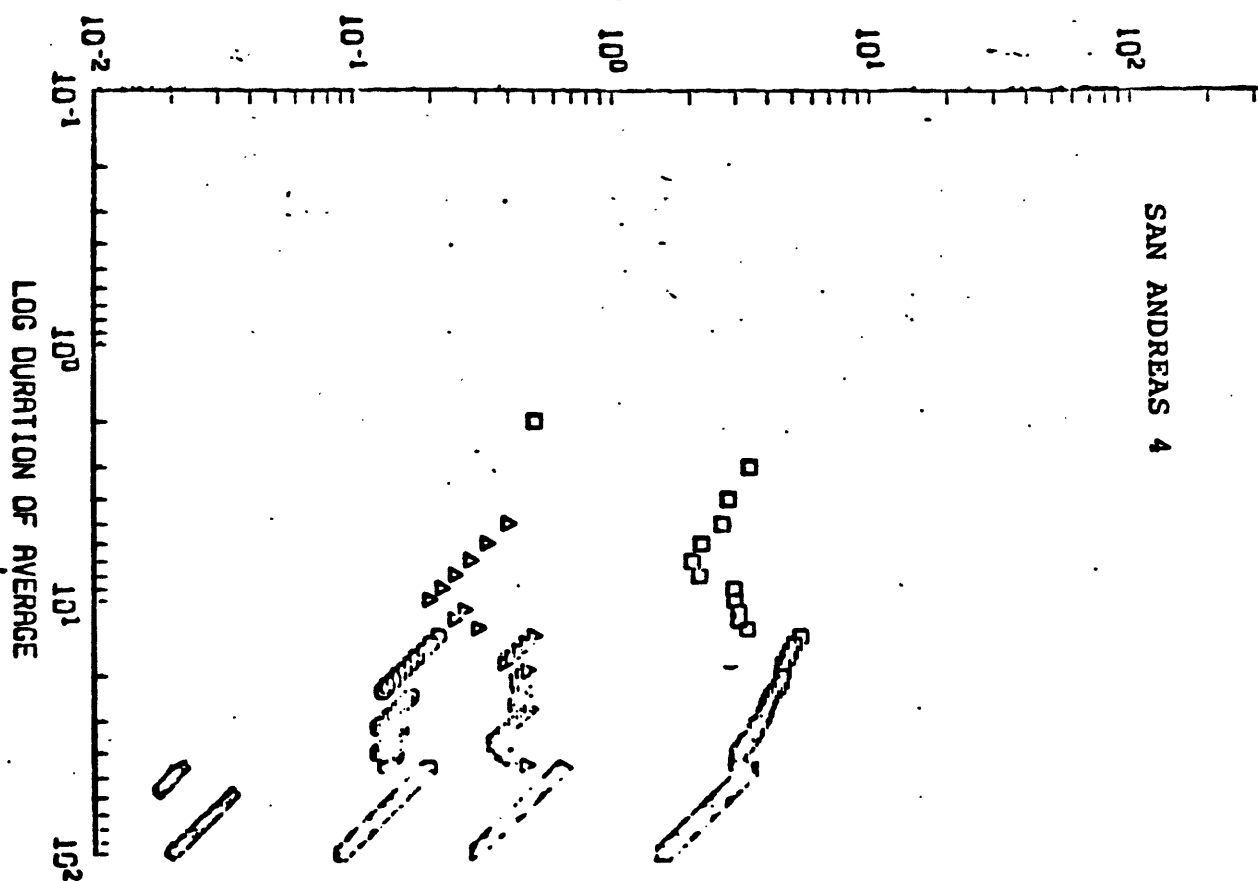
GREEN VALLEY - CALAVERAS



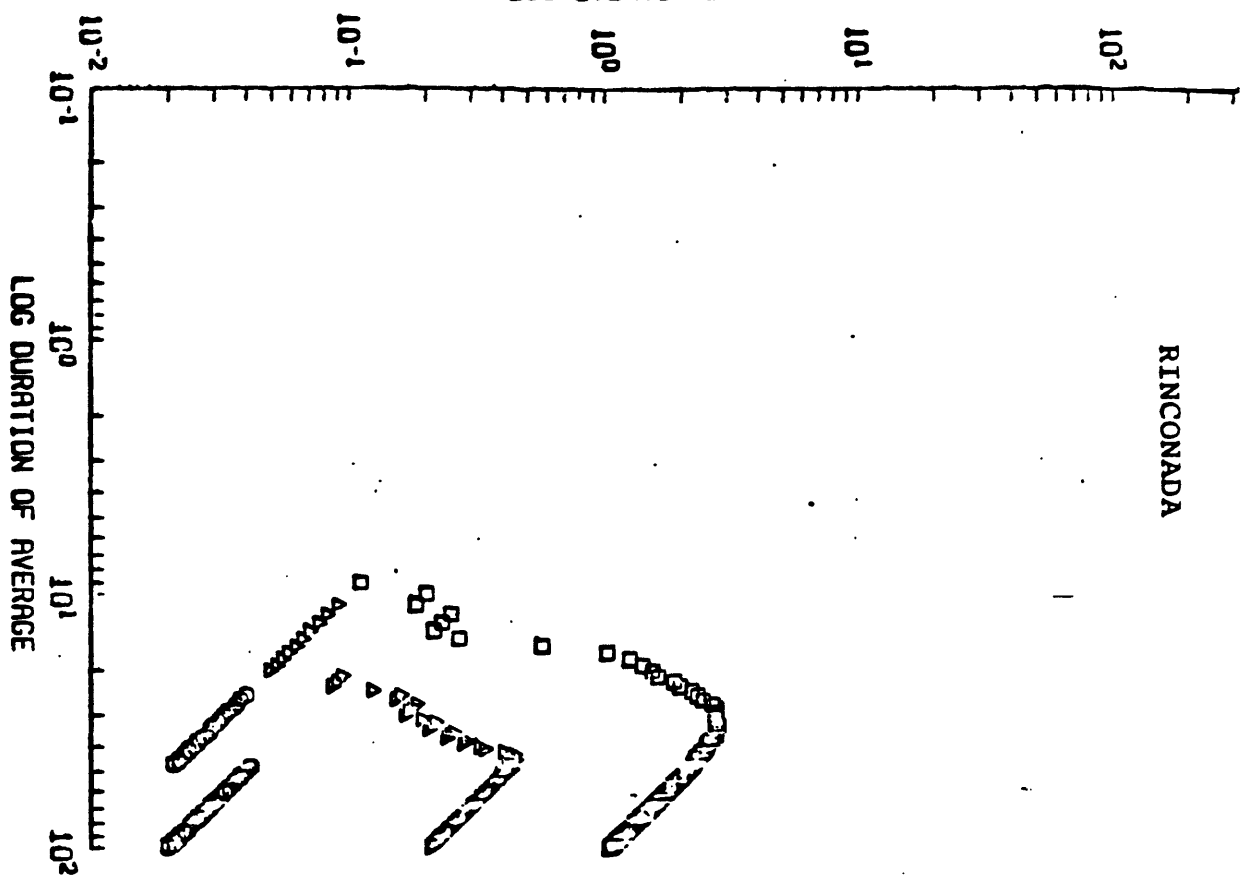
LOG EVENTS PER YEAR



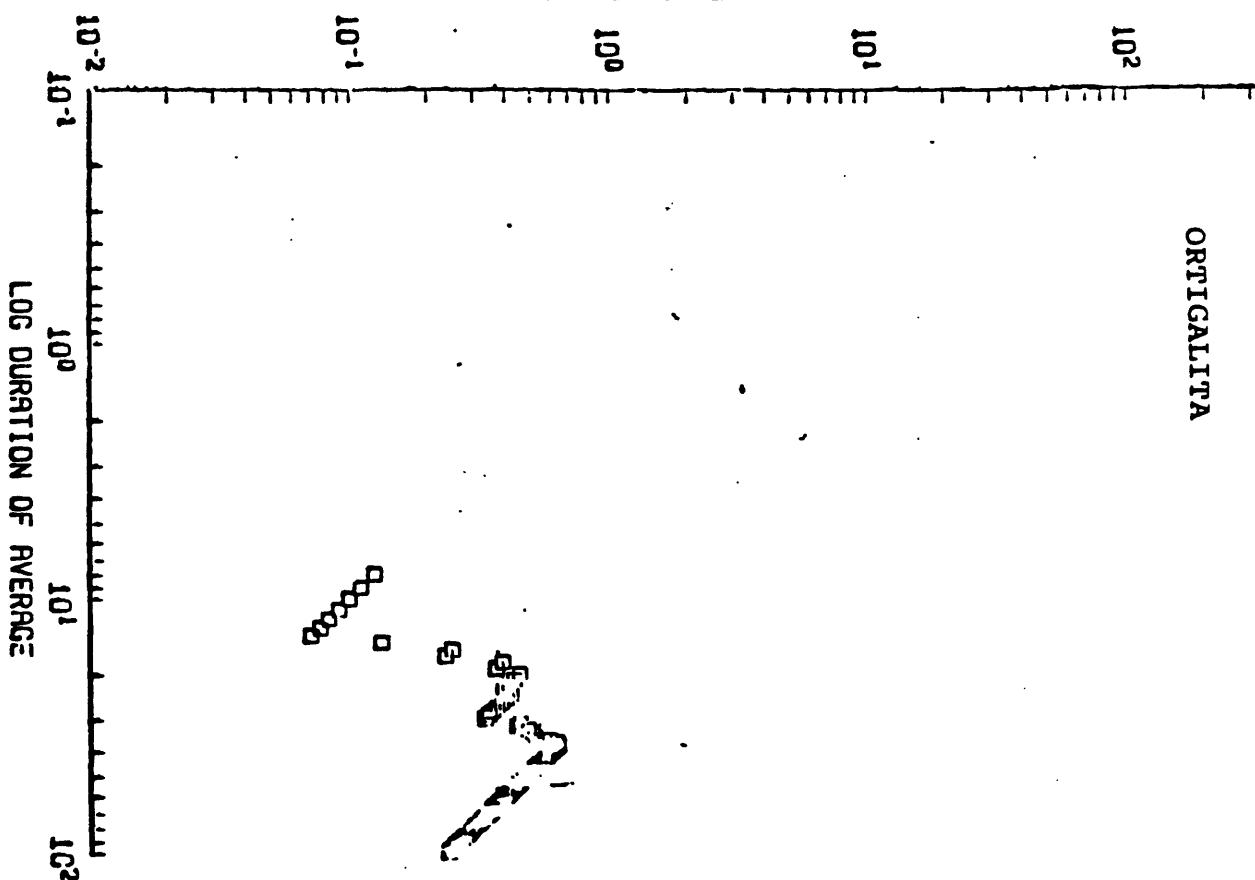
LOG EVENTS PER YEAR



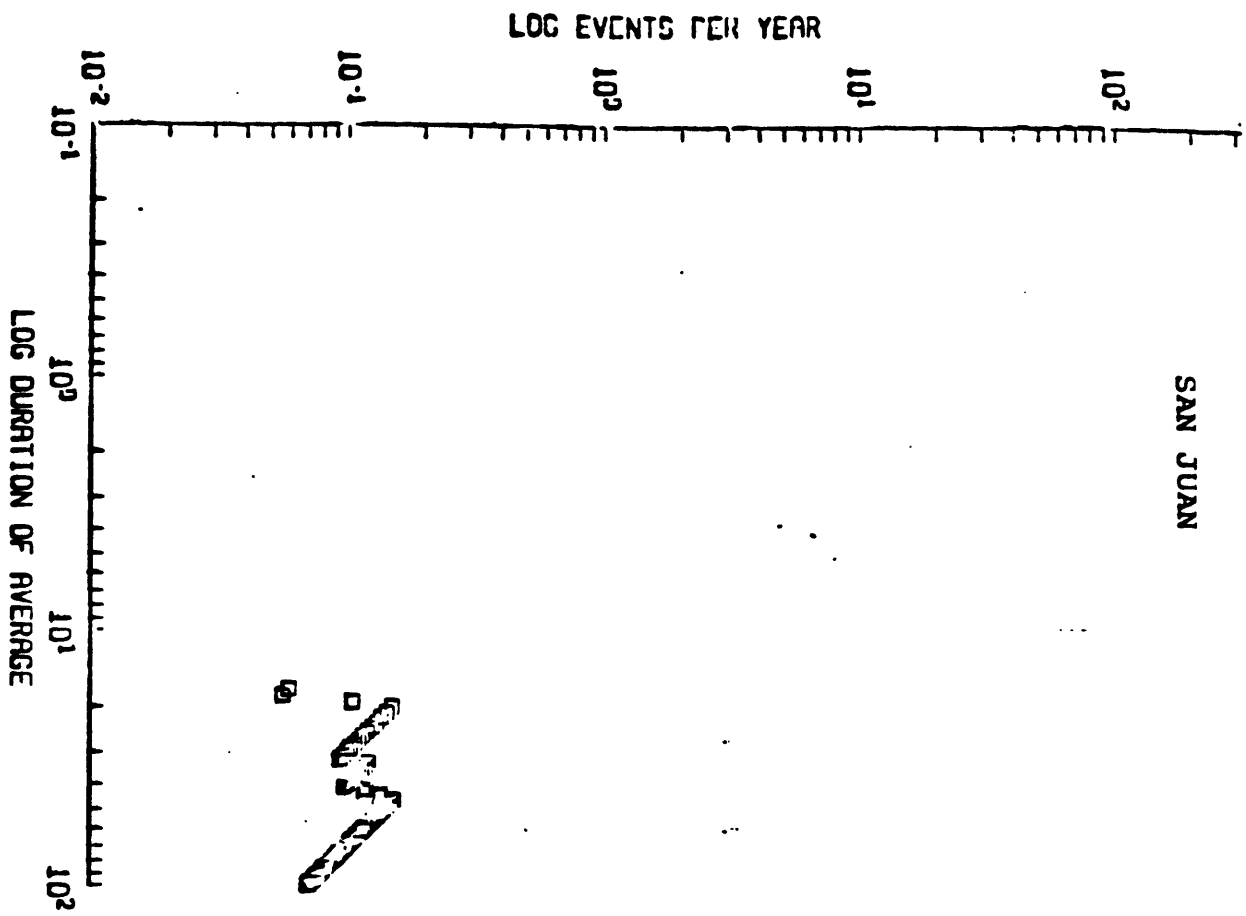
LOG EVENTS PER YEAR



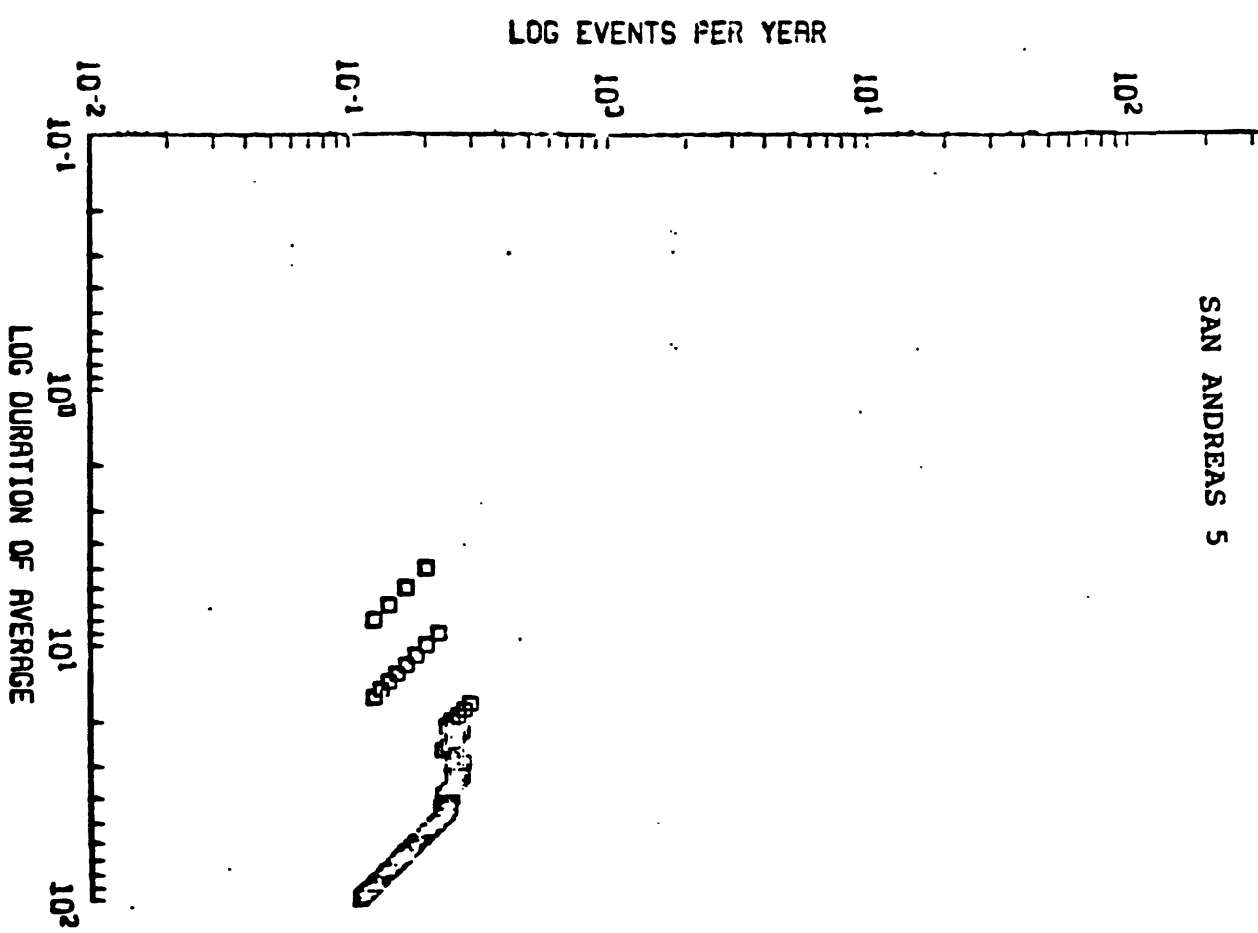
LOG EVENTS PER YEAR



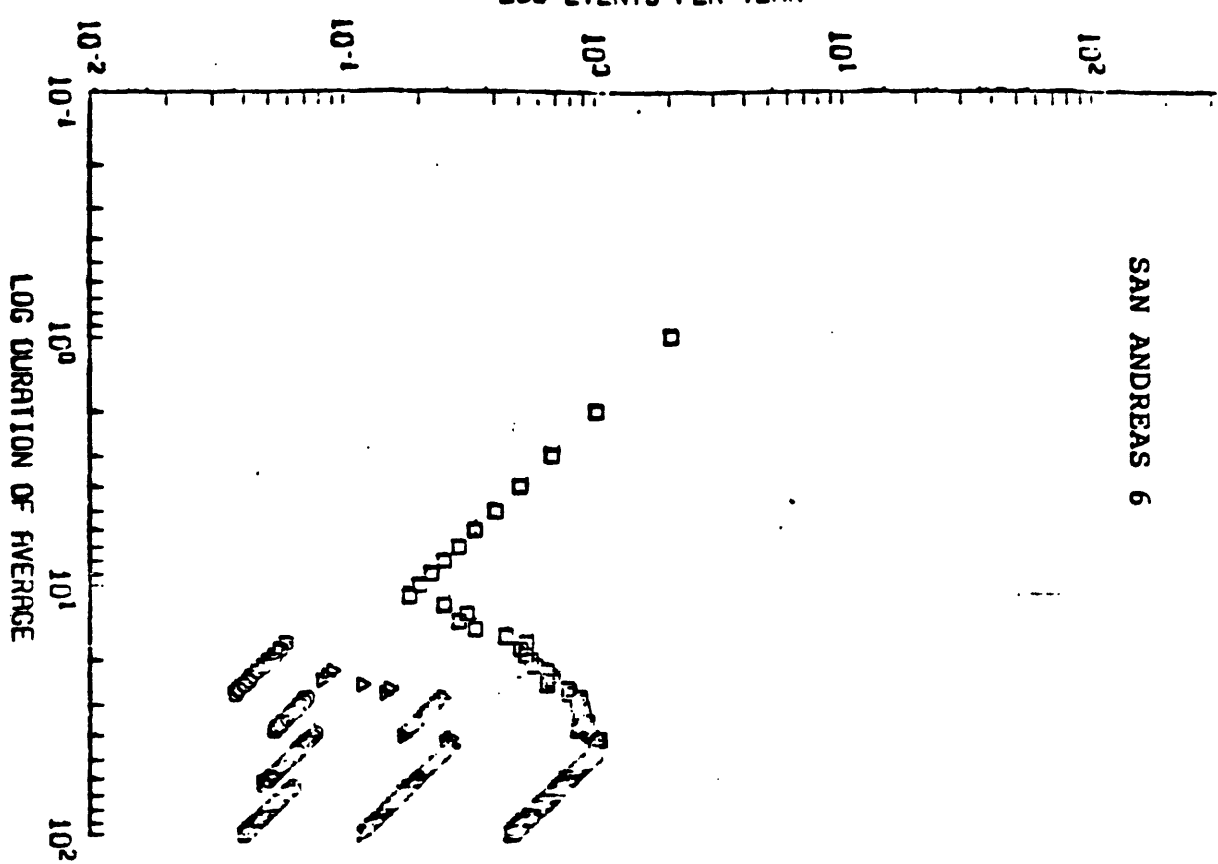
SAN JUAN



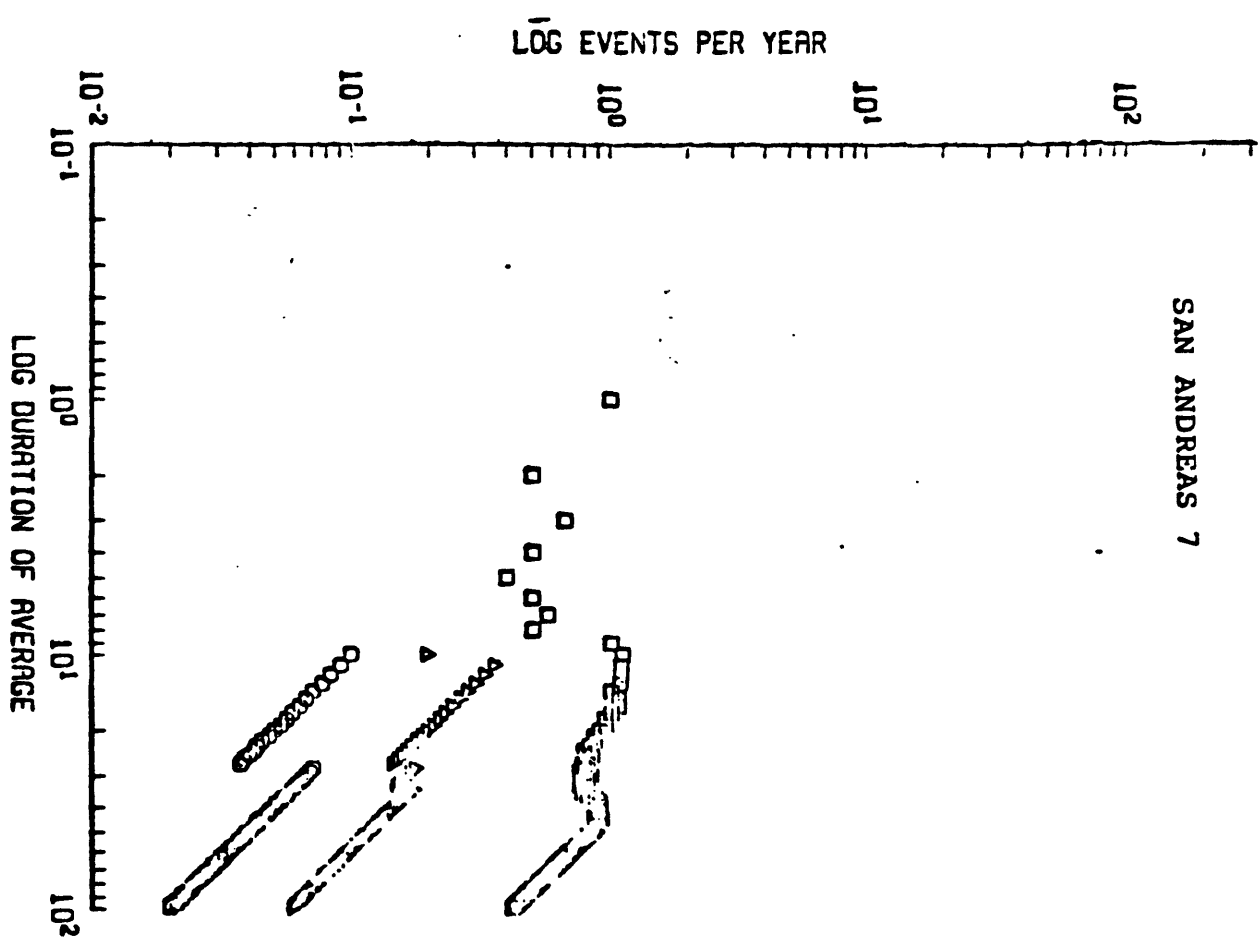
SAN ANDREAS 5



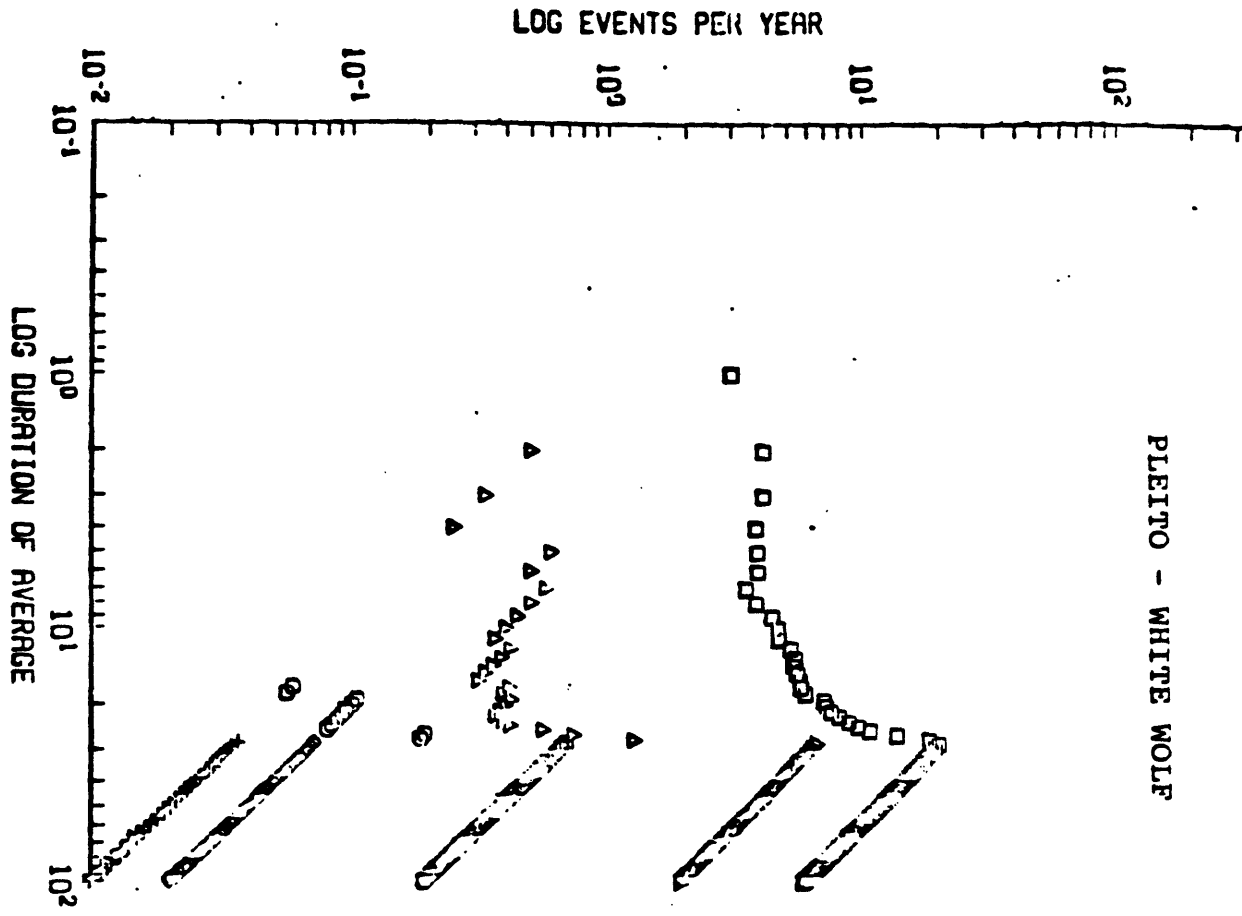
SAN ANDREAS 6



SAN ANDREAS 7

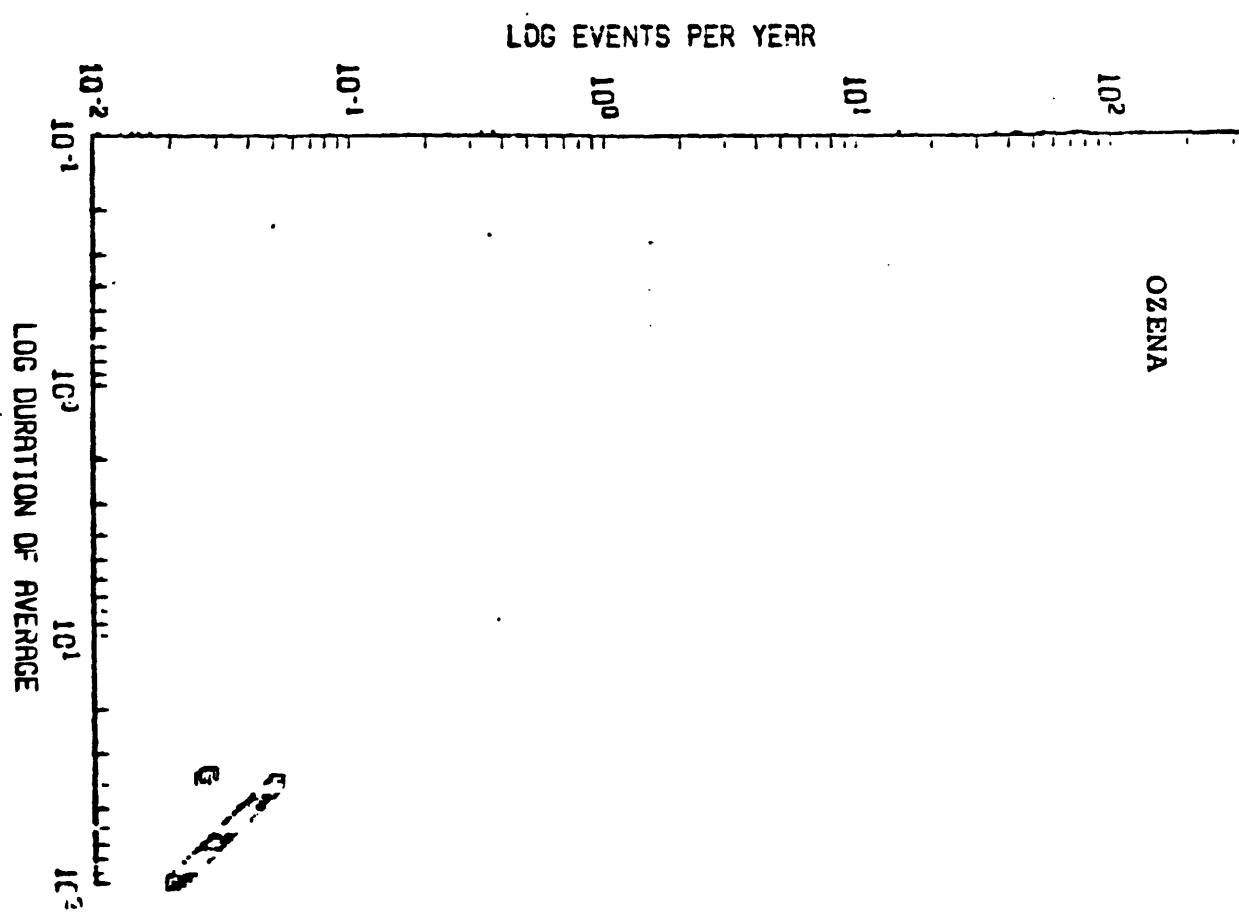


PLEITO - WHITE WOLF

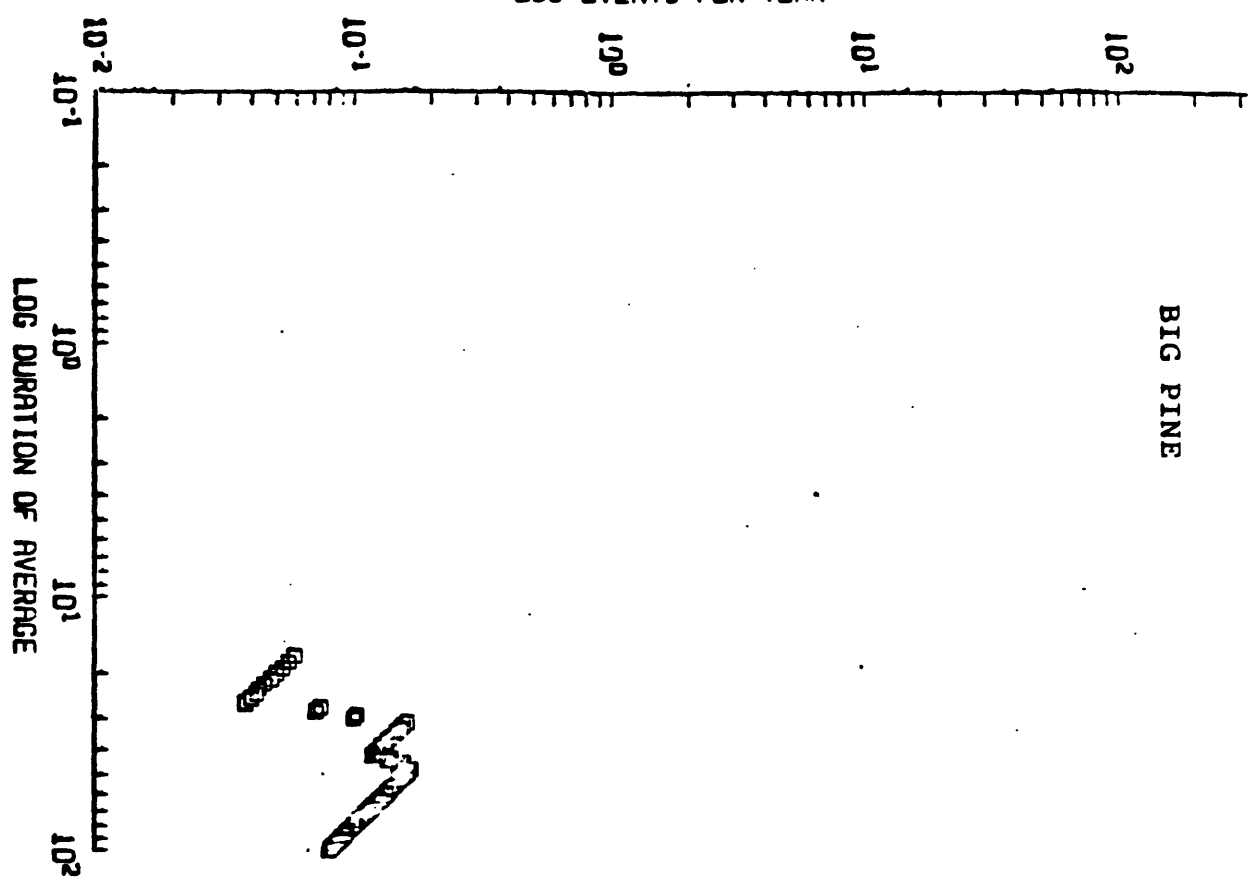


APPENDIX I-1

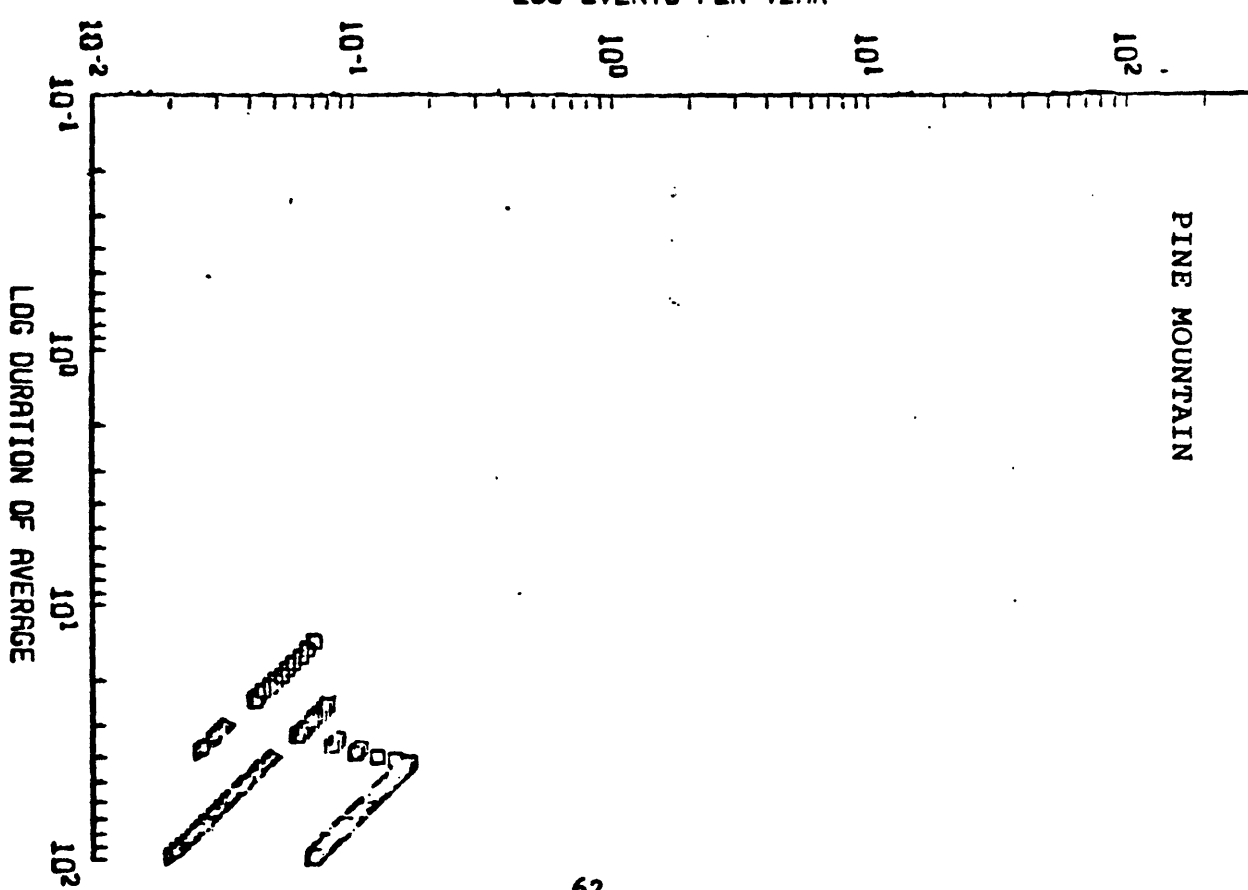
OZENA



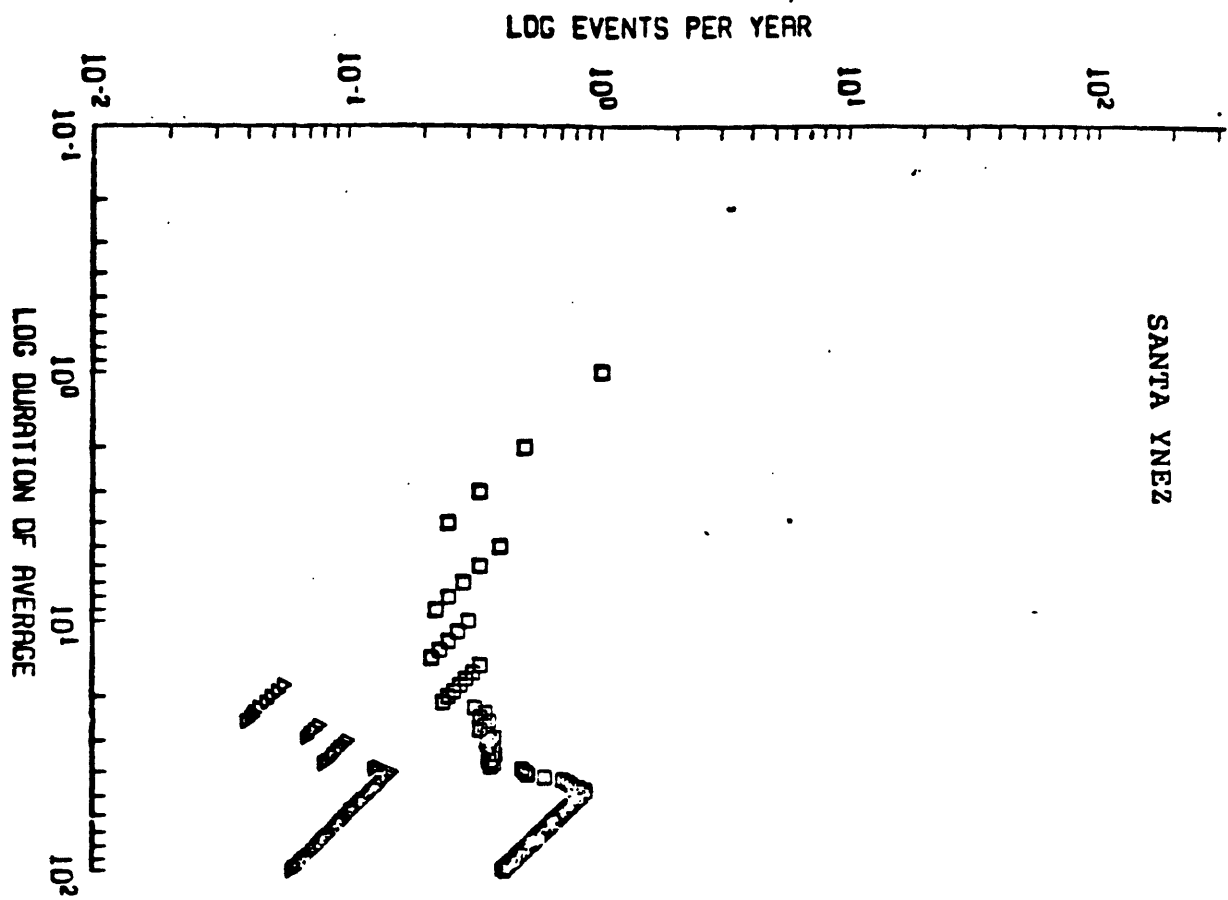
LOG EVENTS PER YEAR



LOG EVENTS PER YEAR

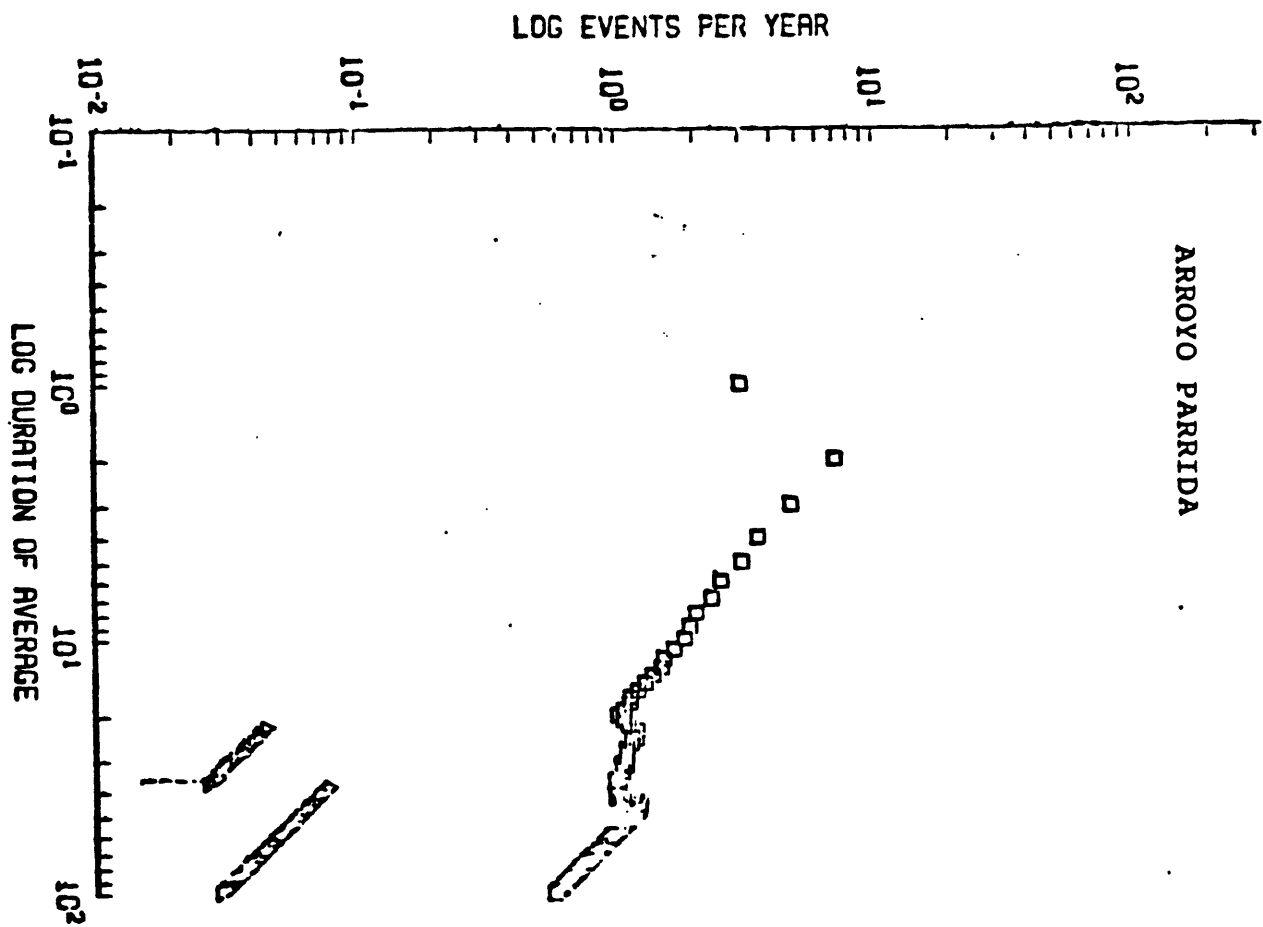


SANTA YNEZ

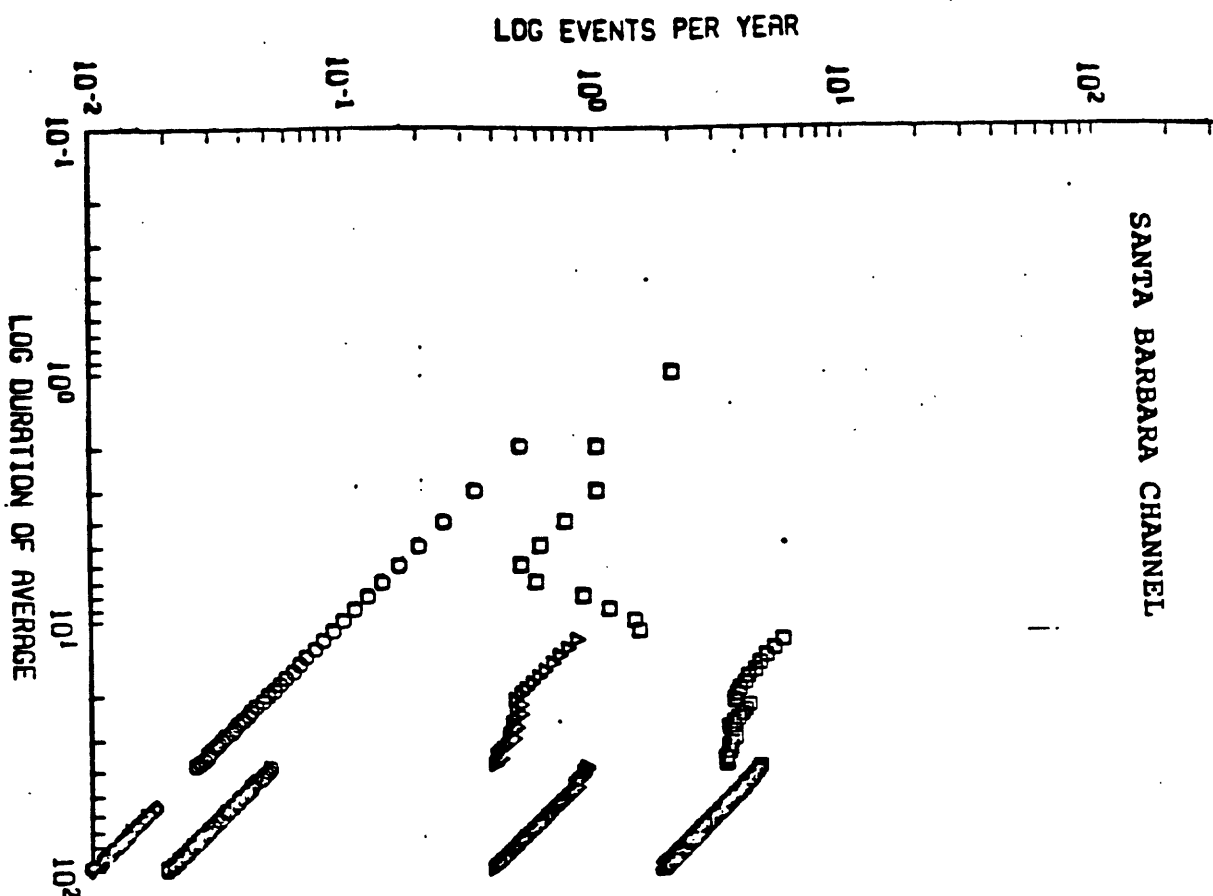


APPENDIX I-1

ARROYO PARRIDA

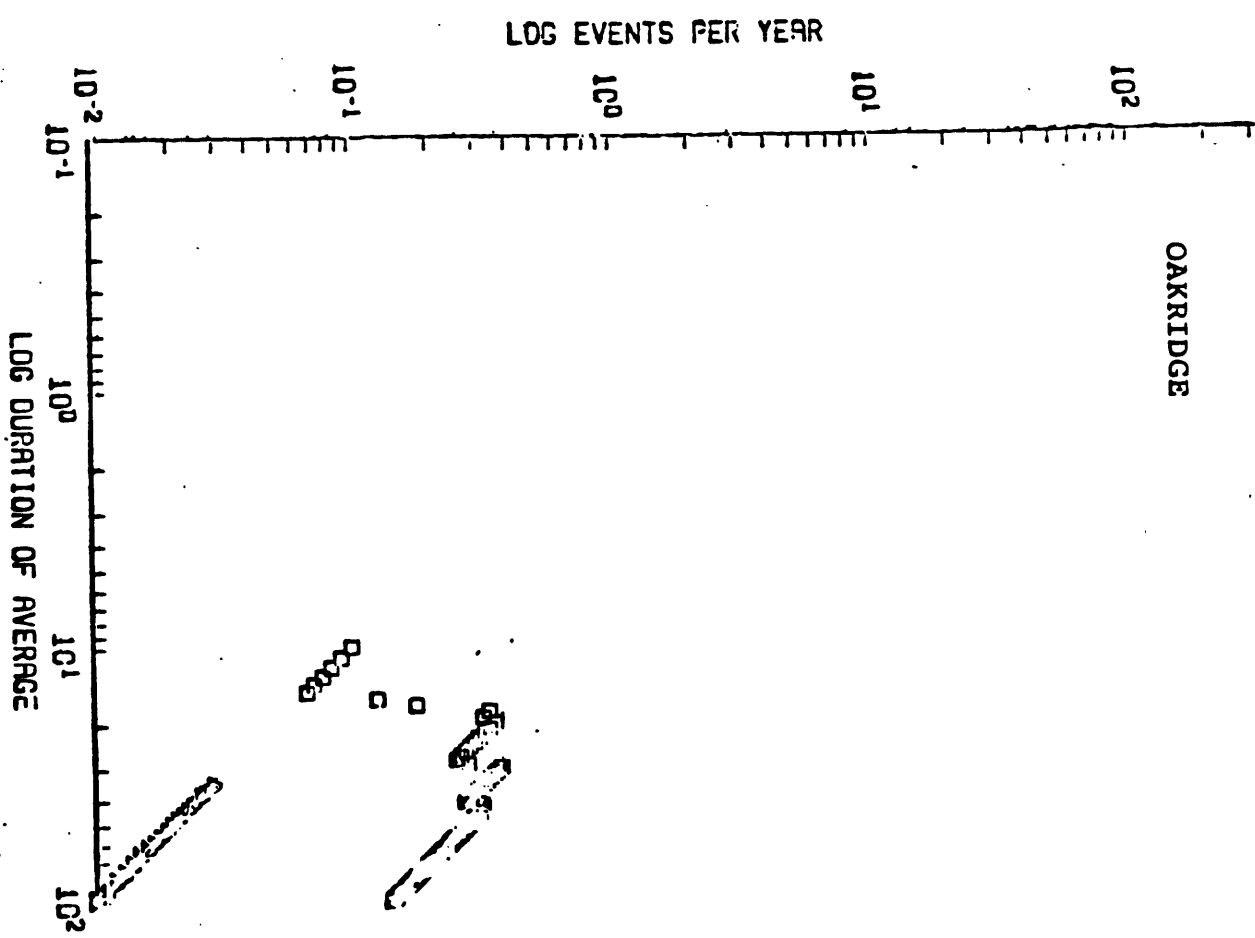


SANTA BARBARA CHANNEL

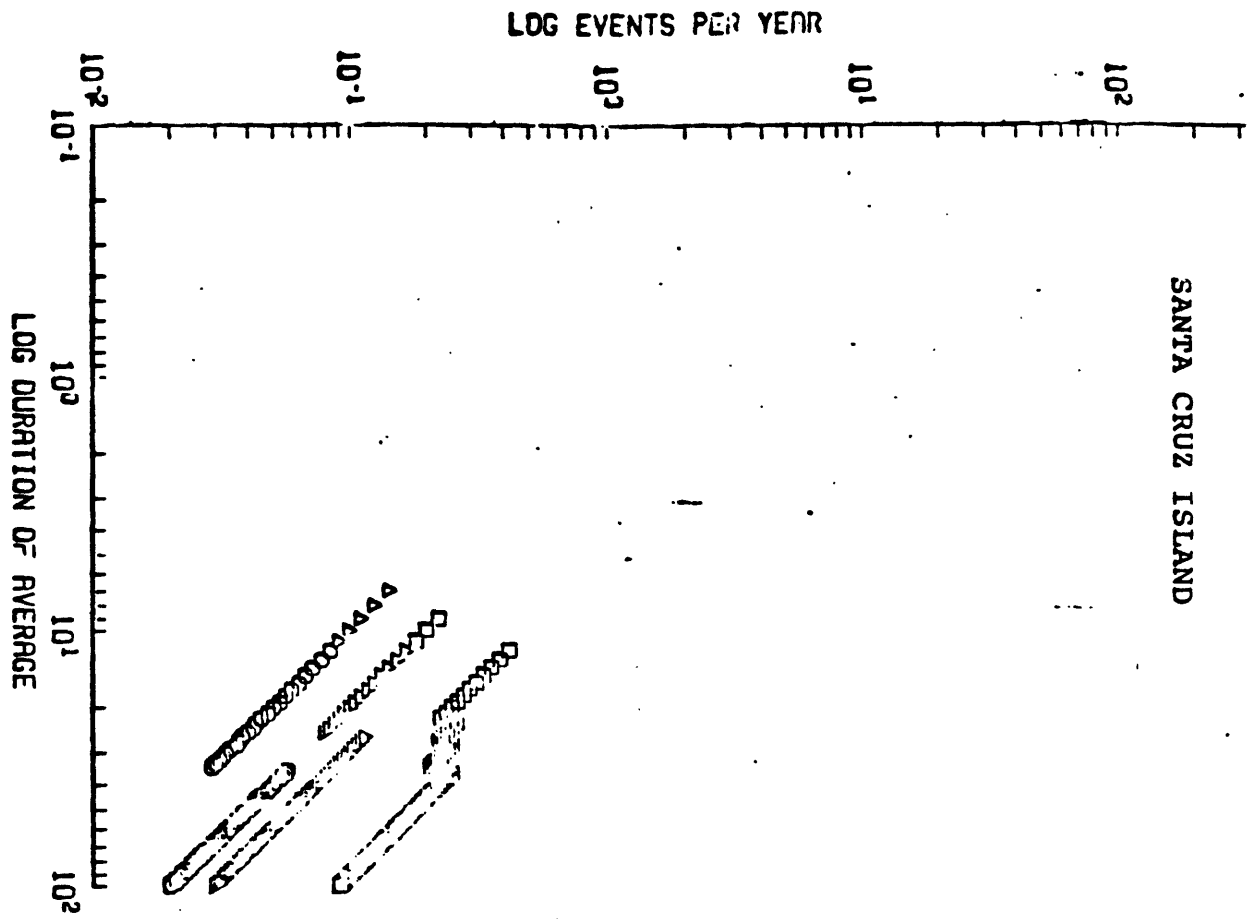


APPENDIX I-1

OAKRIDGE

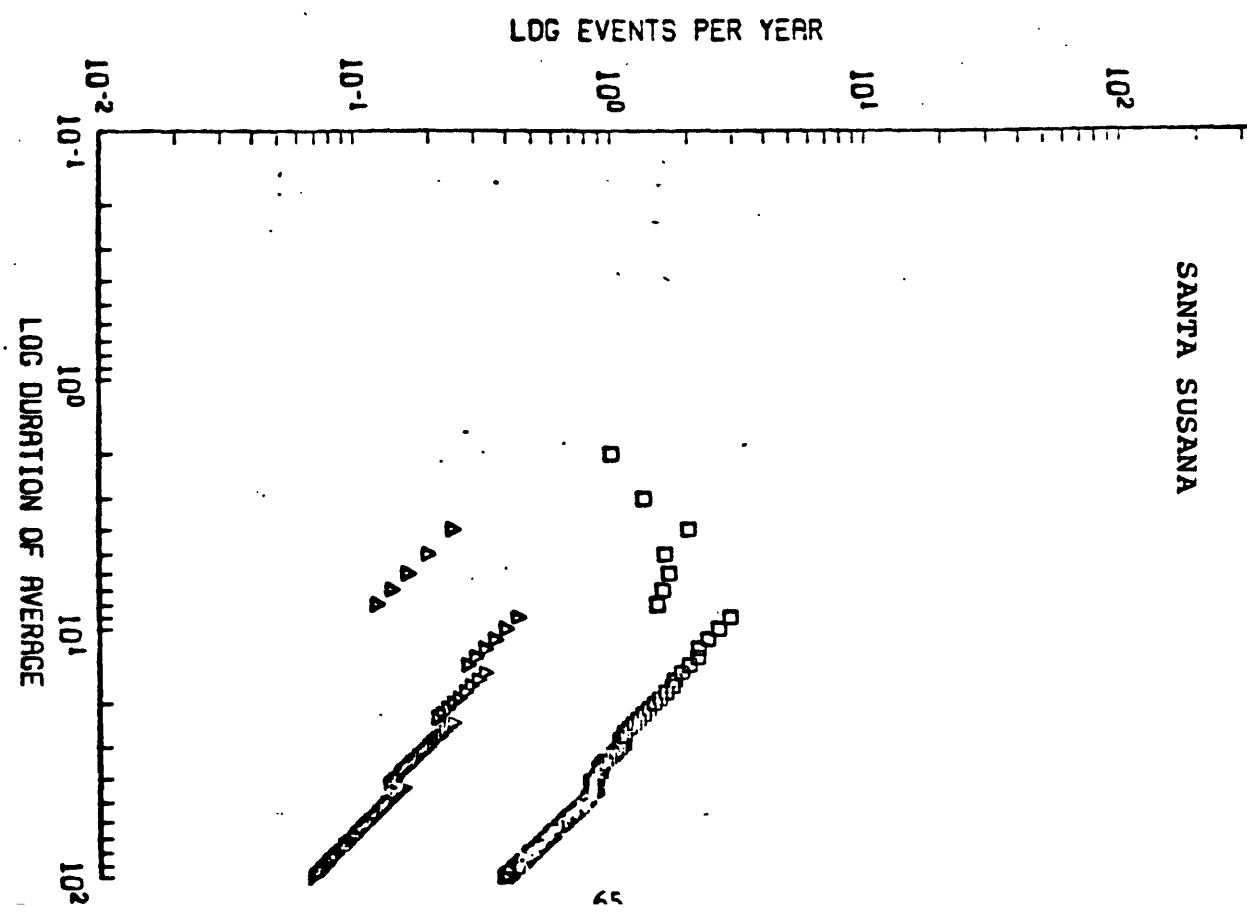


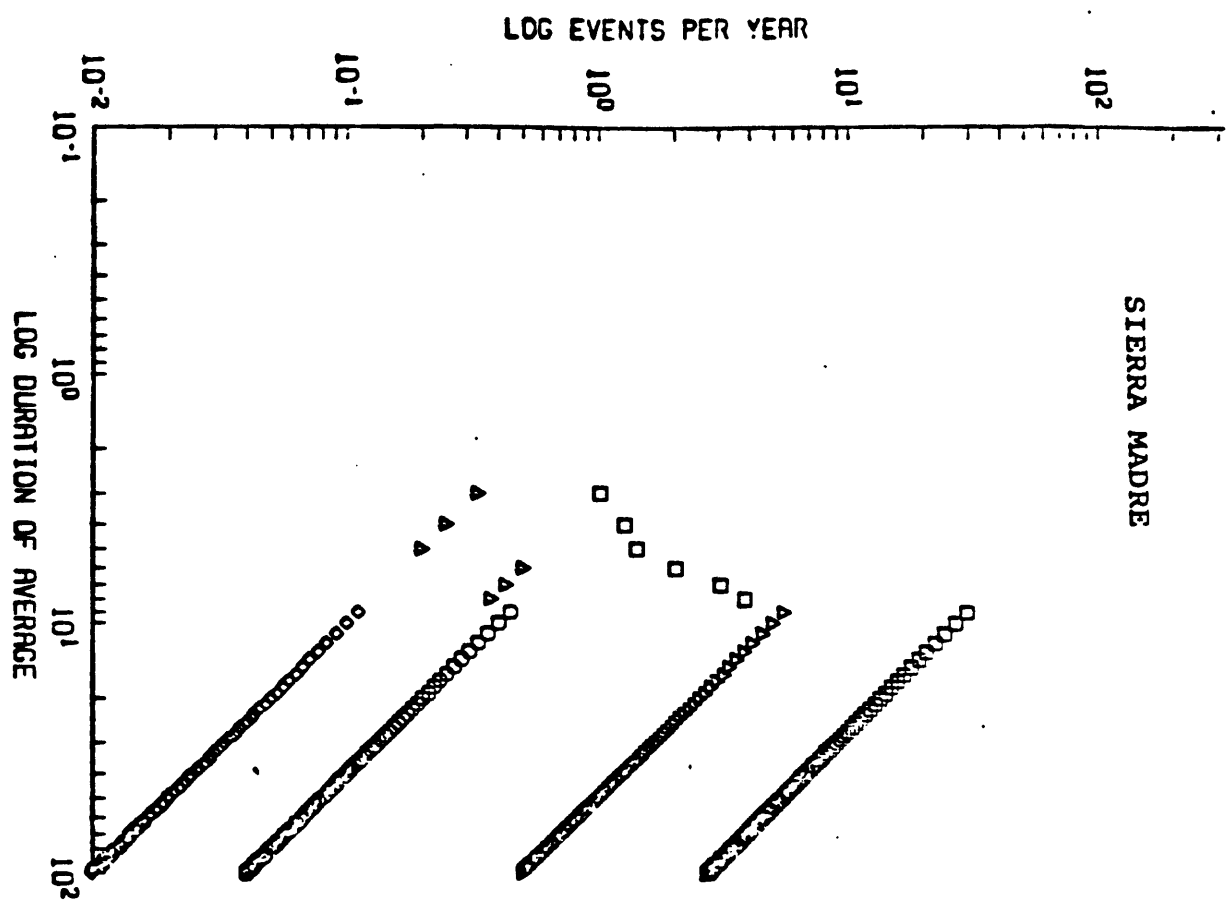
SANTA CRUZ ISLAND



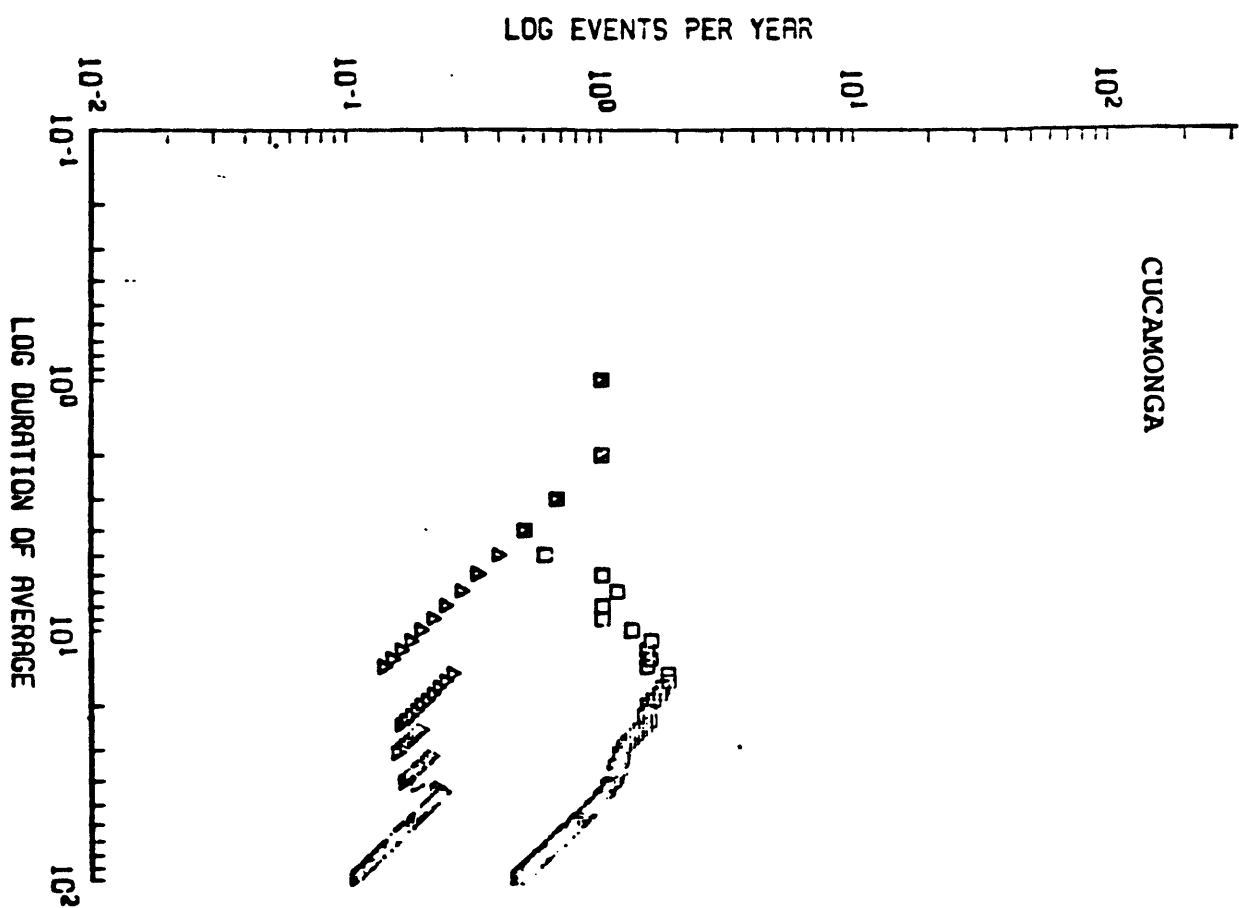
APPENDIX I-1

SANTA SUSANA

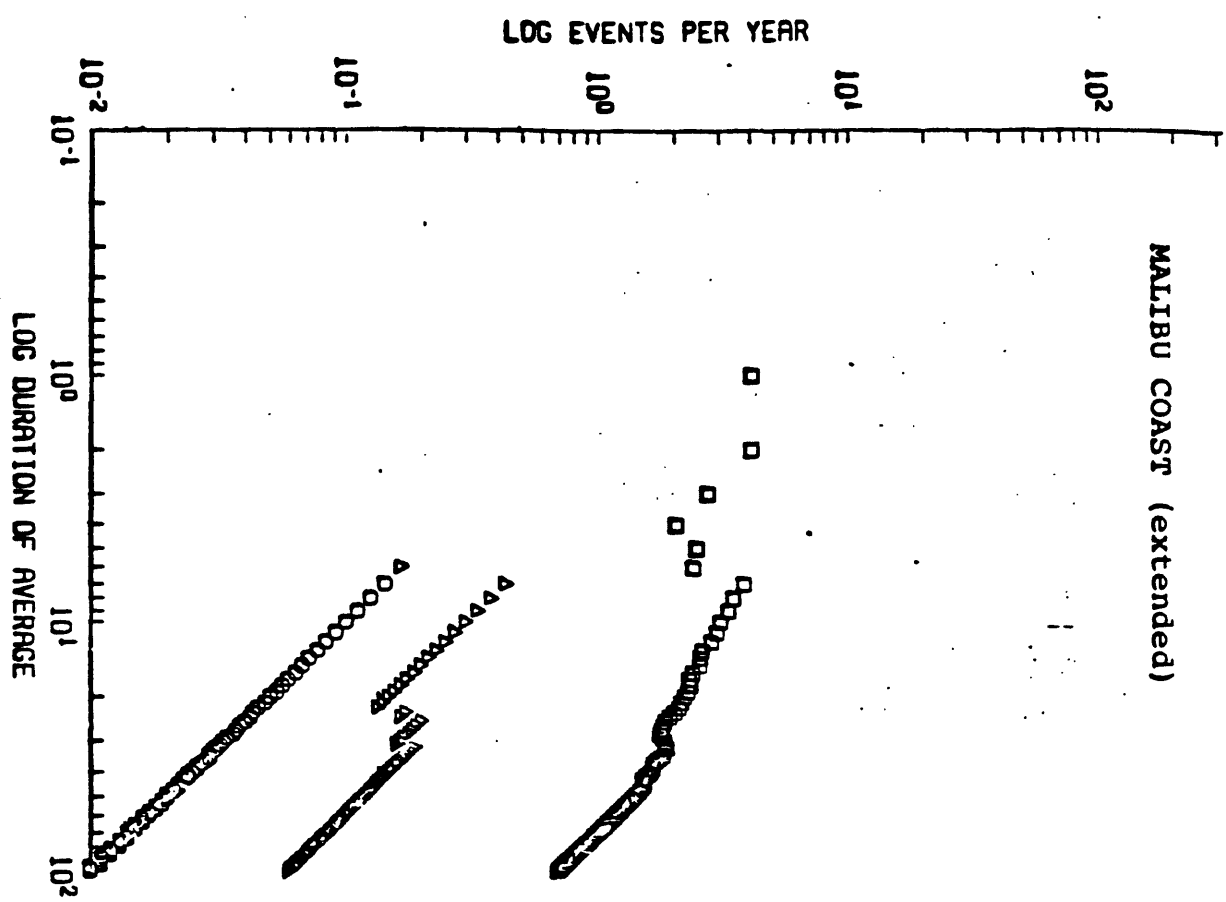




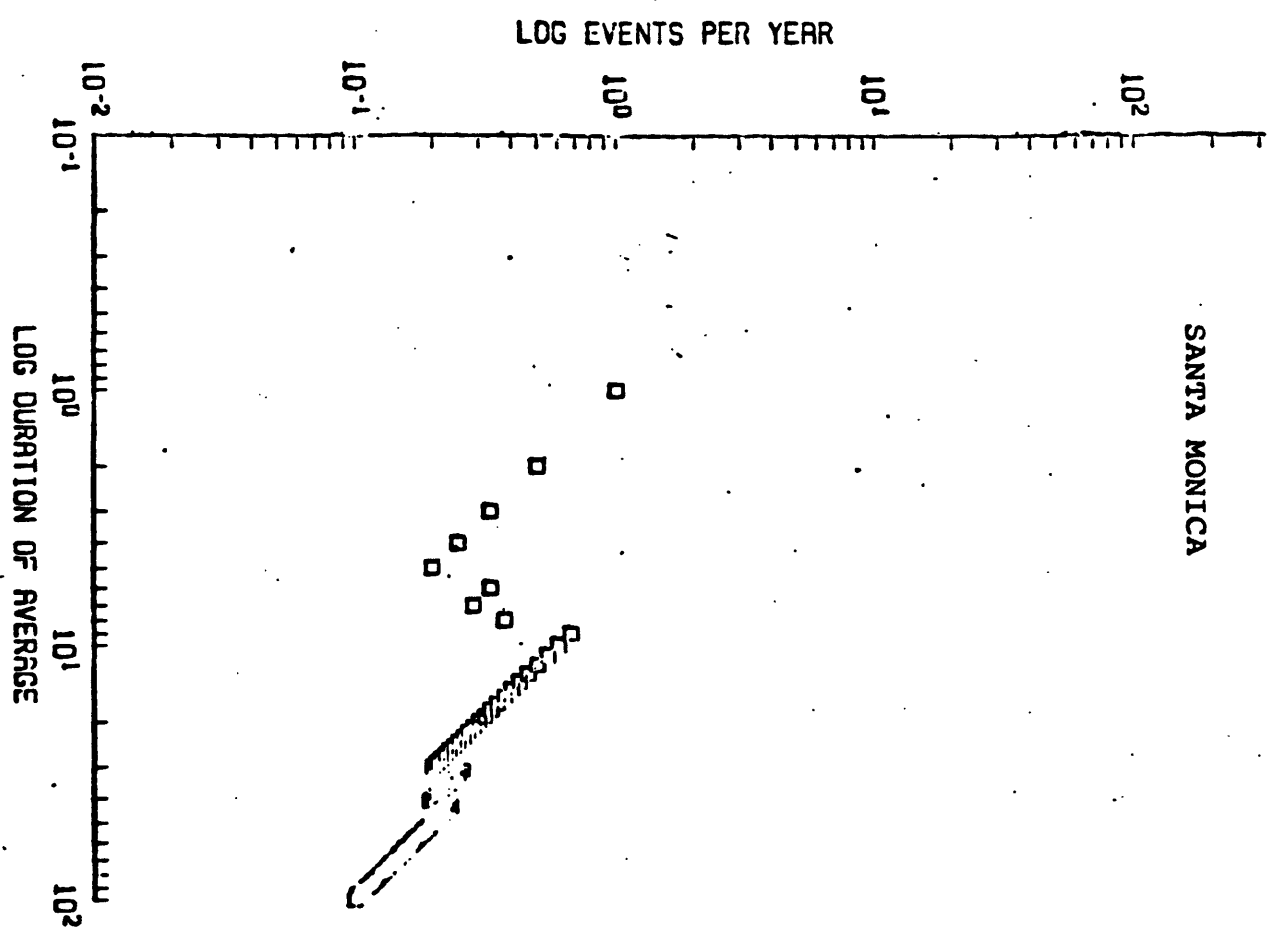
APPENDIX I-1



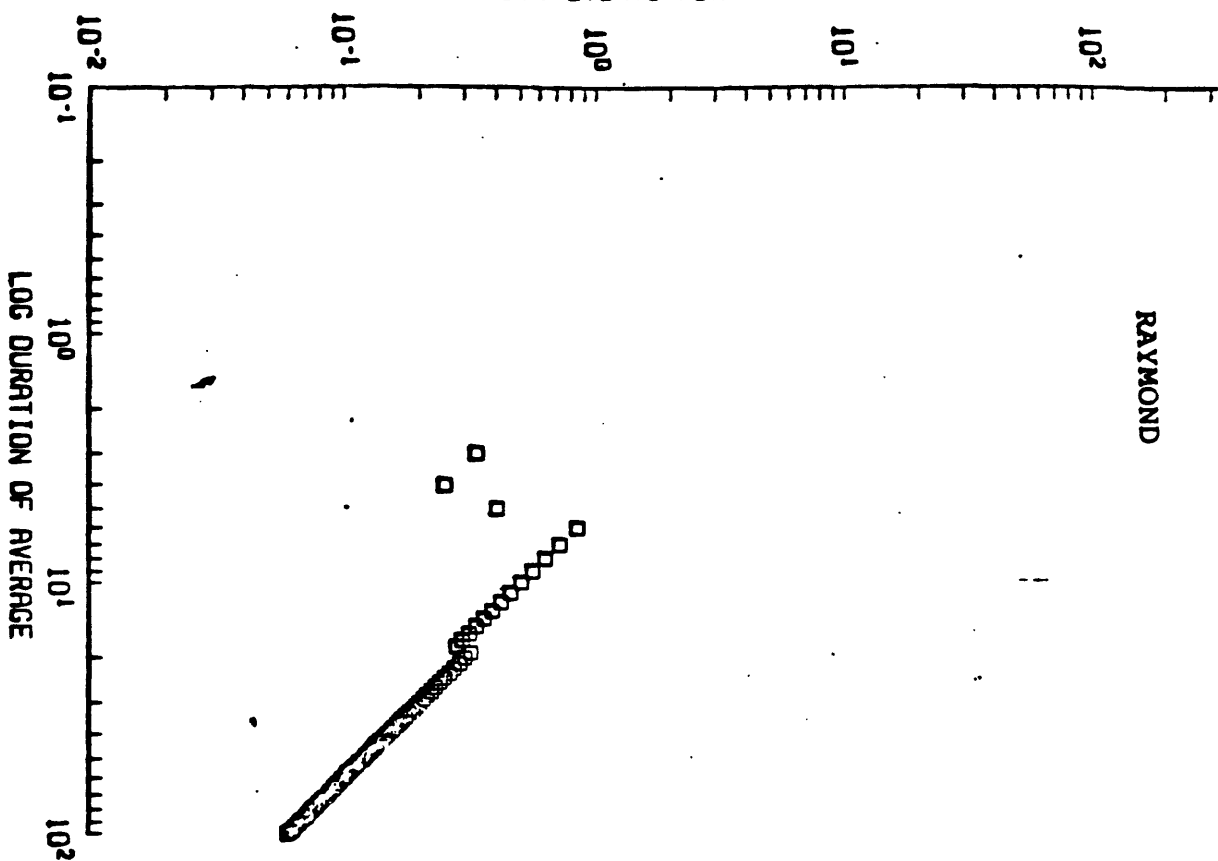
MALIBU COAST (extended)



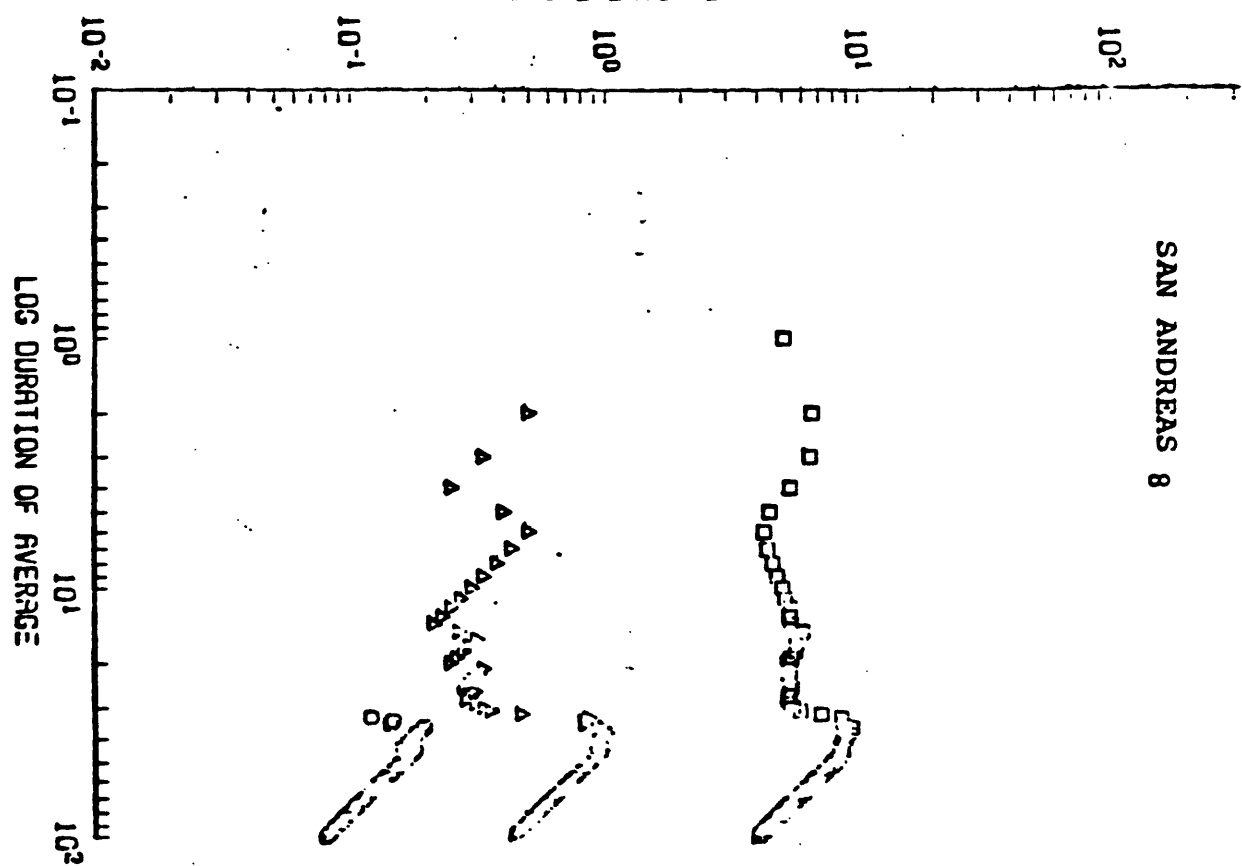
SANTA MONICA



LOG EVENTS PER YEAR

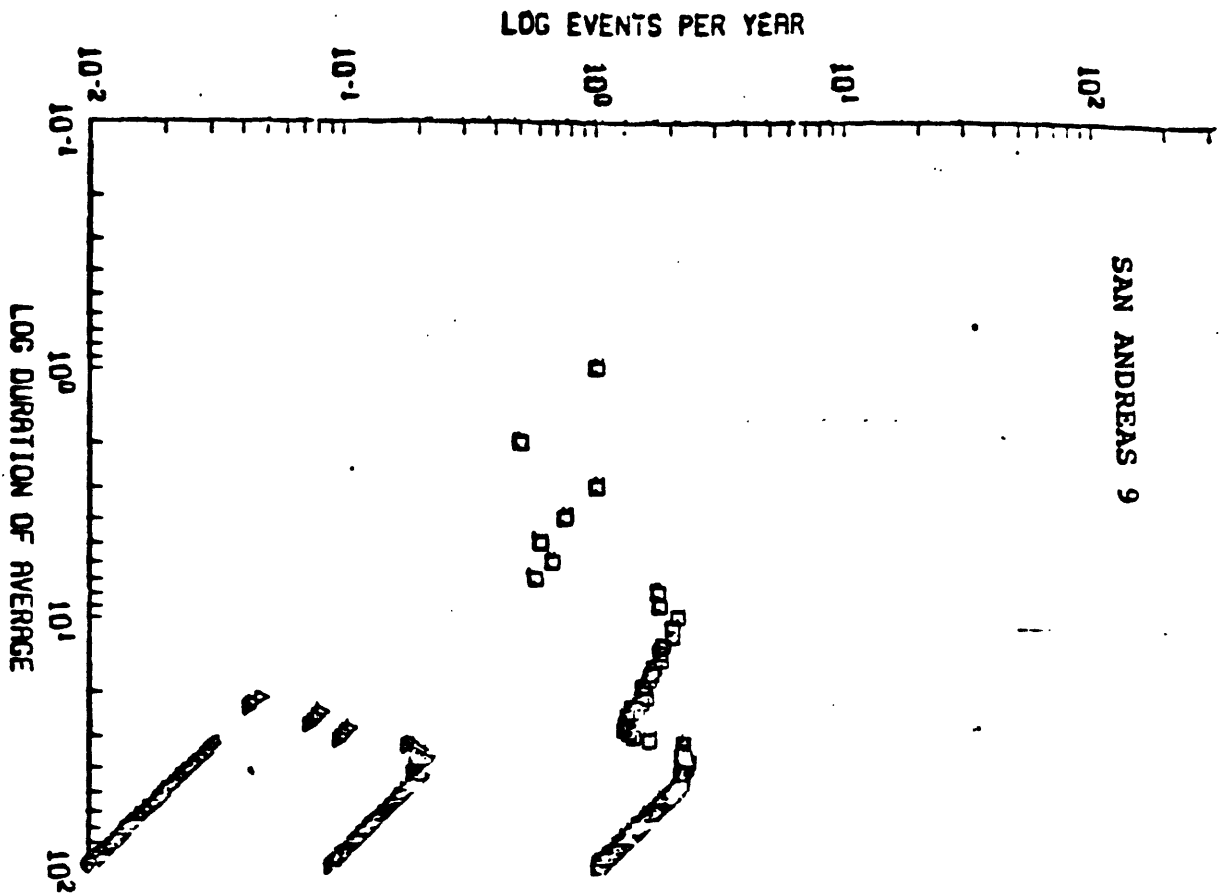


LOG EVENTS PER YEAR



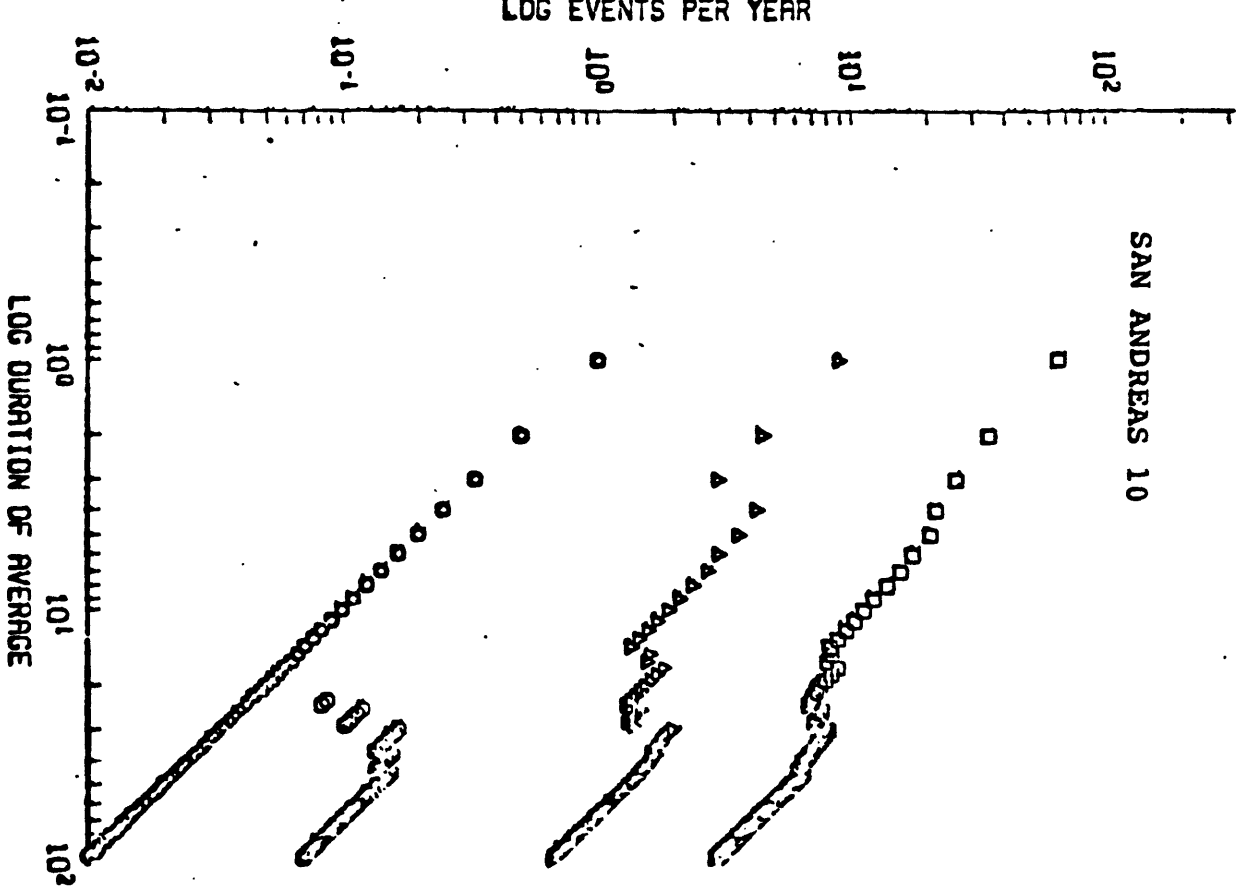
APPENDIX I-1

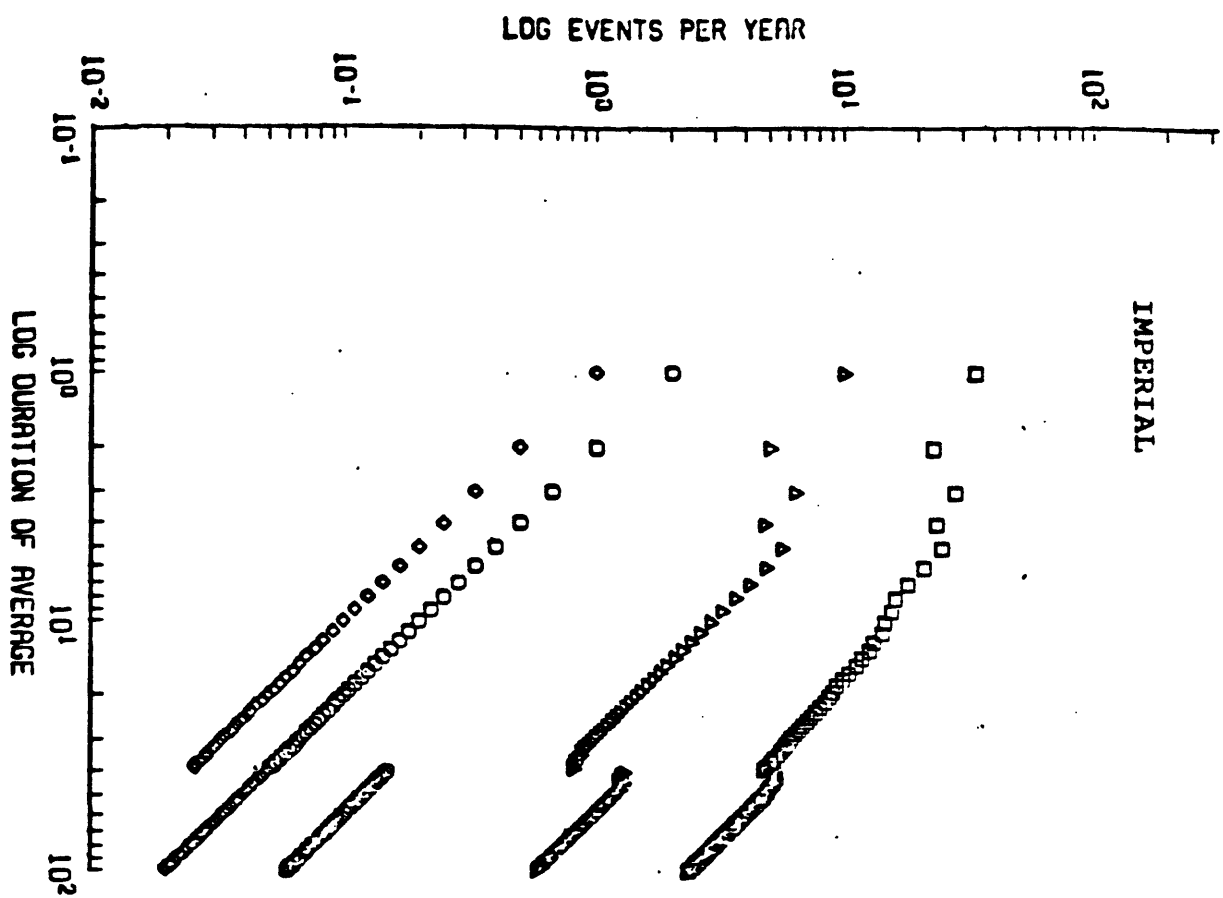
SAN ANDREAS 9



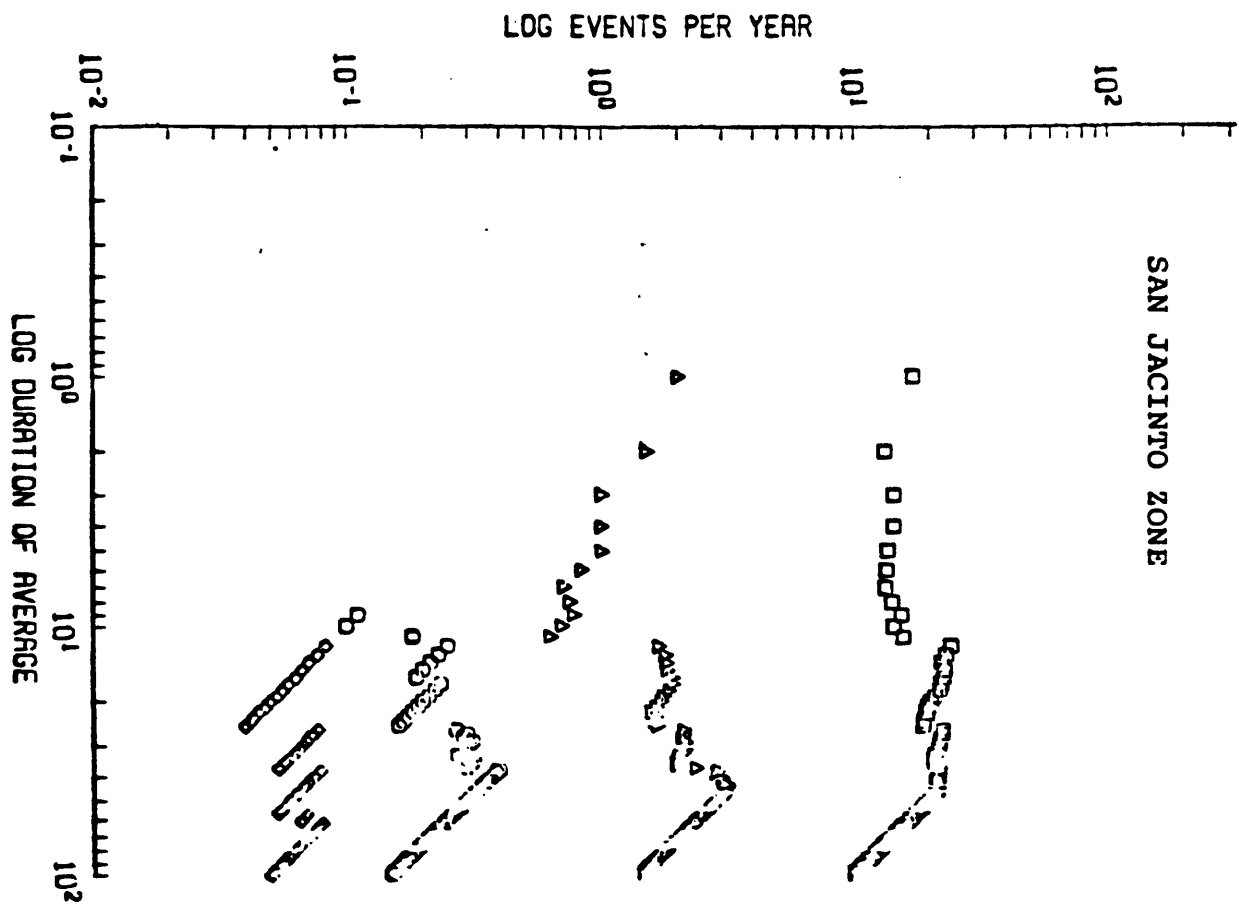
APPENDIX I-1

SAN ANDREAS 10

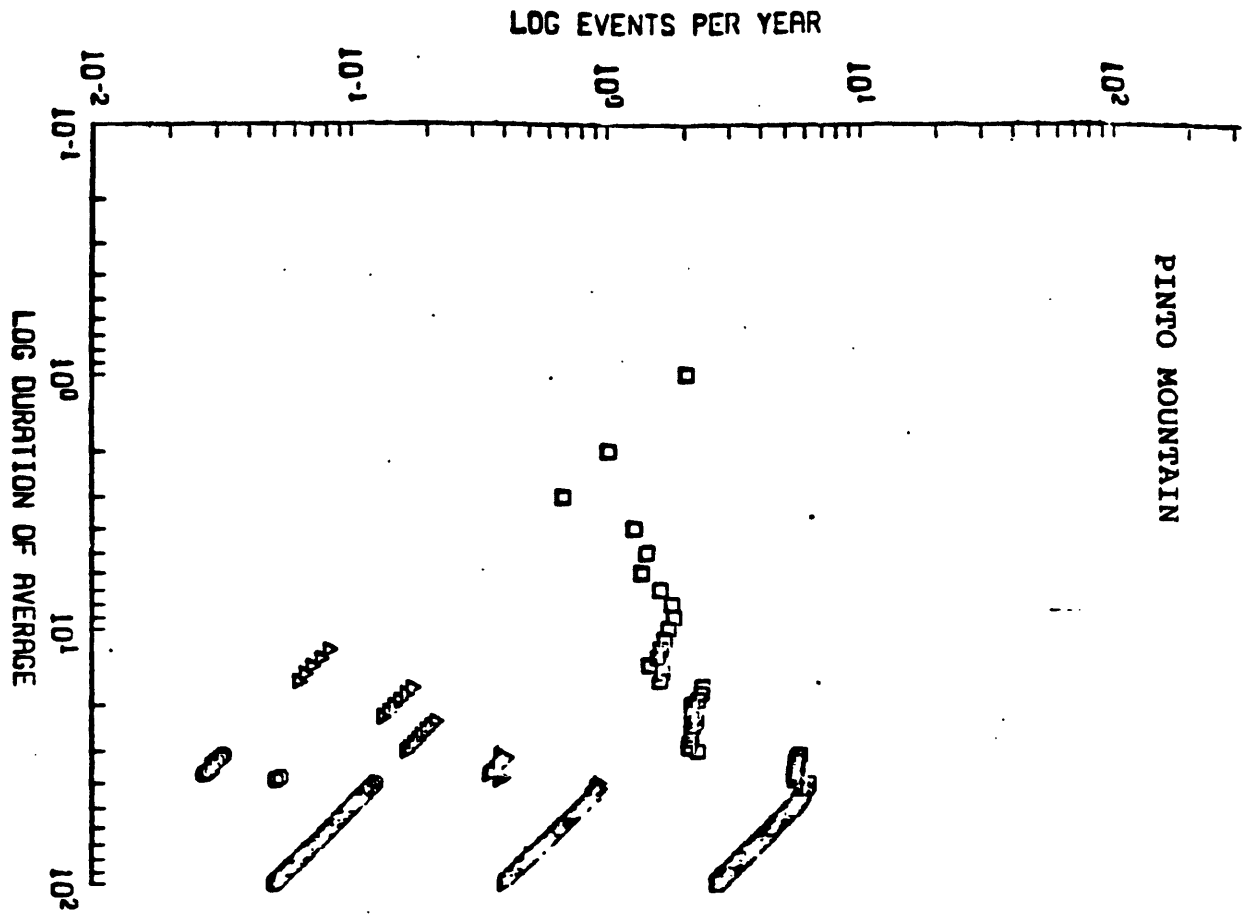




APPENDIX I-1

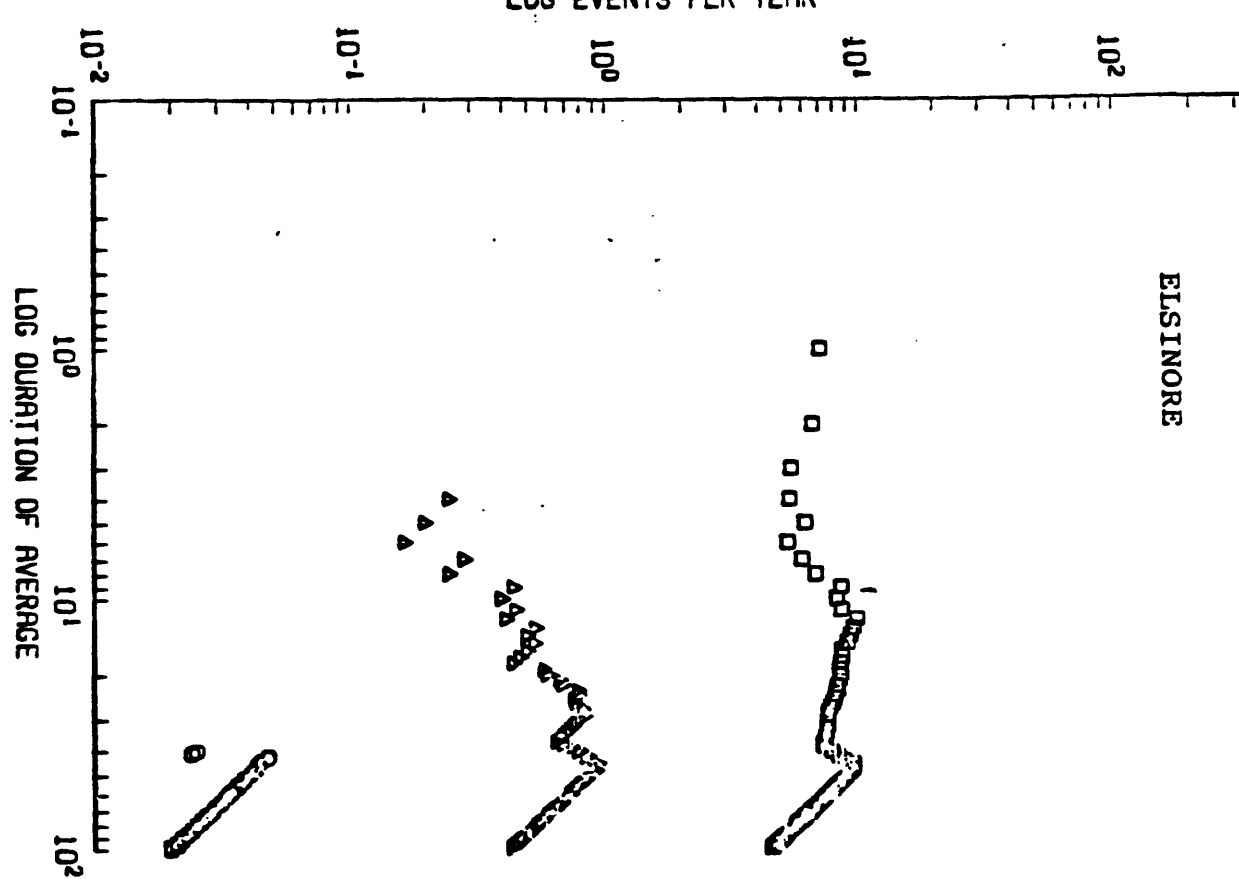


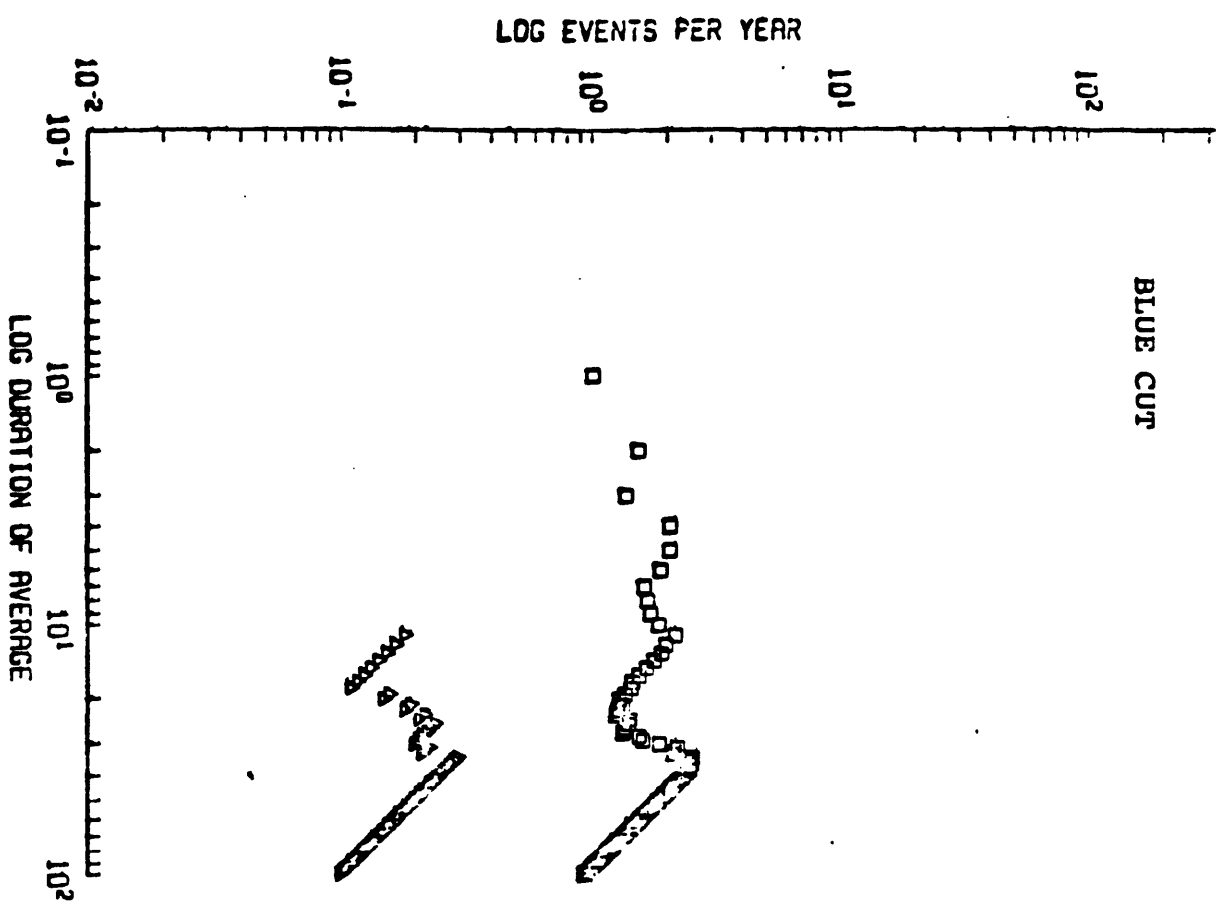
PINTO MOUNTAIN



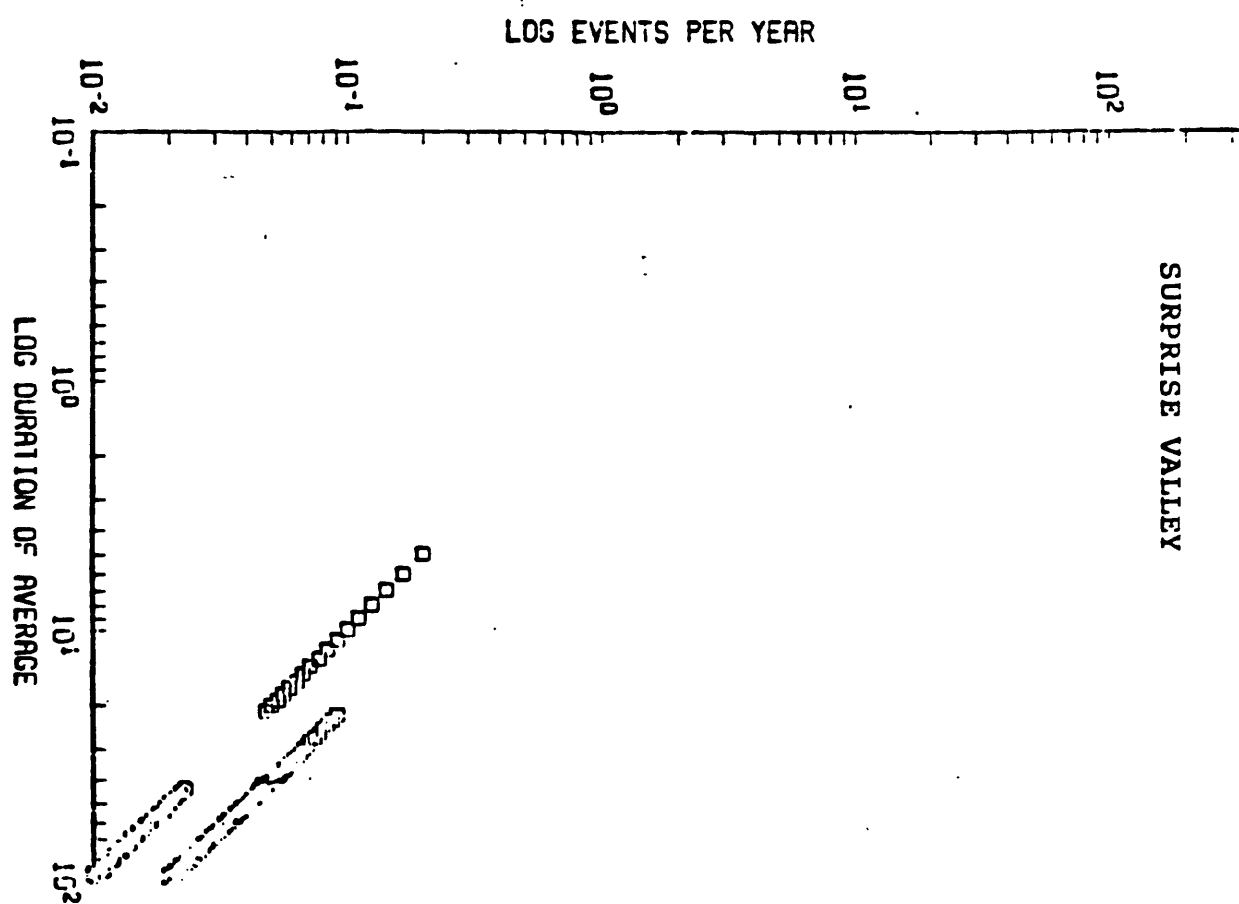
APPENDIX I-1

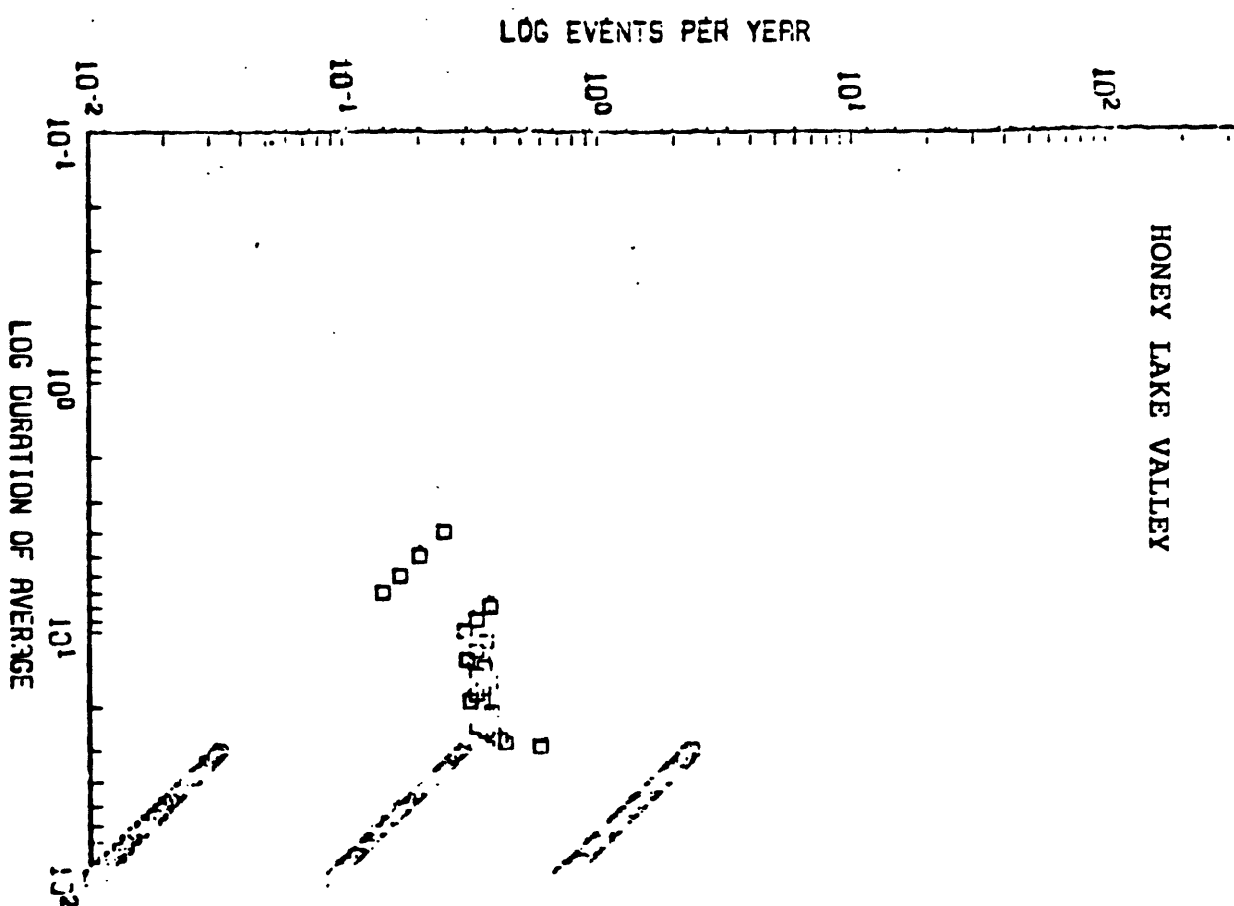
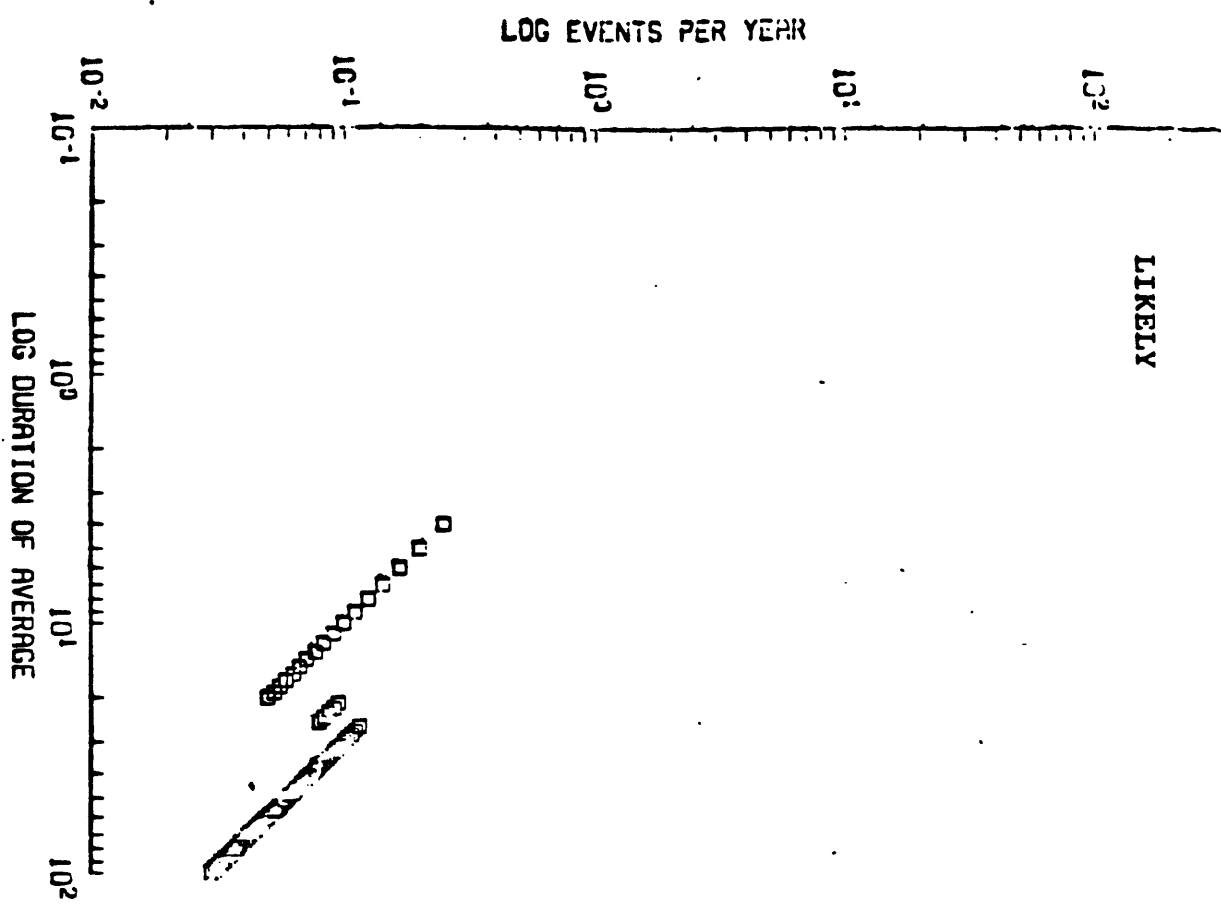
EL SINORE



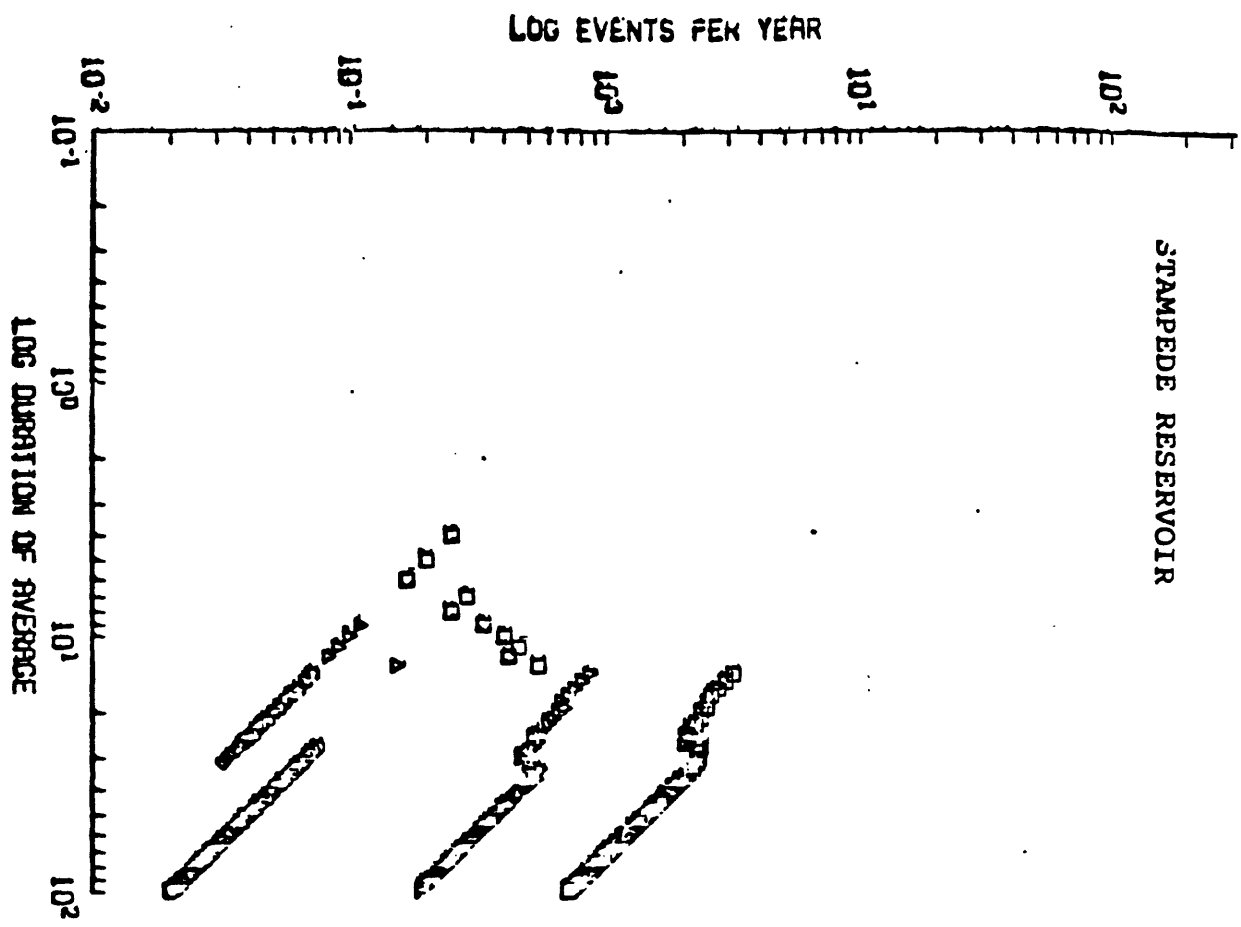


APPENDIX I-1



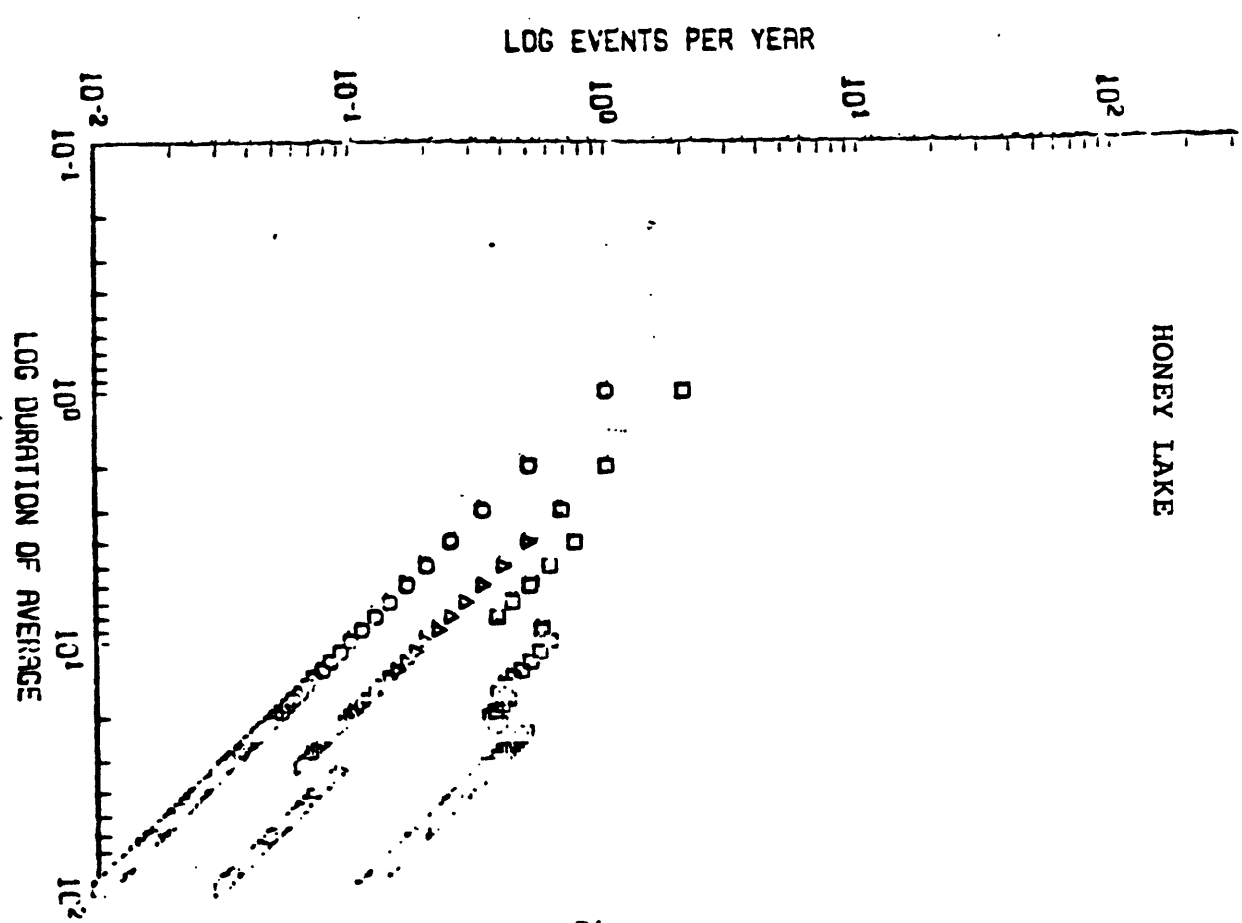


STAMPEDE RESERVOIR

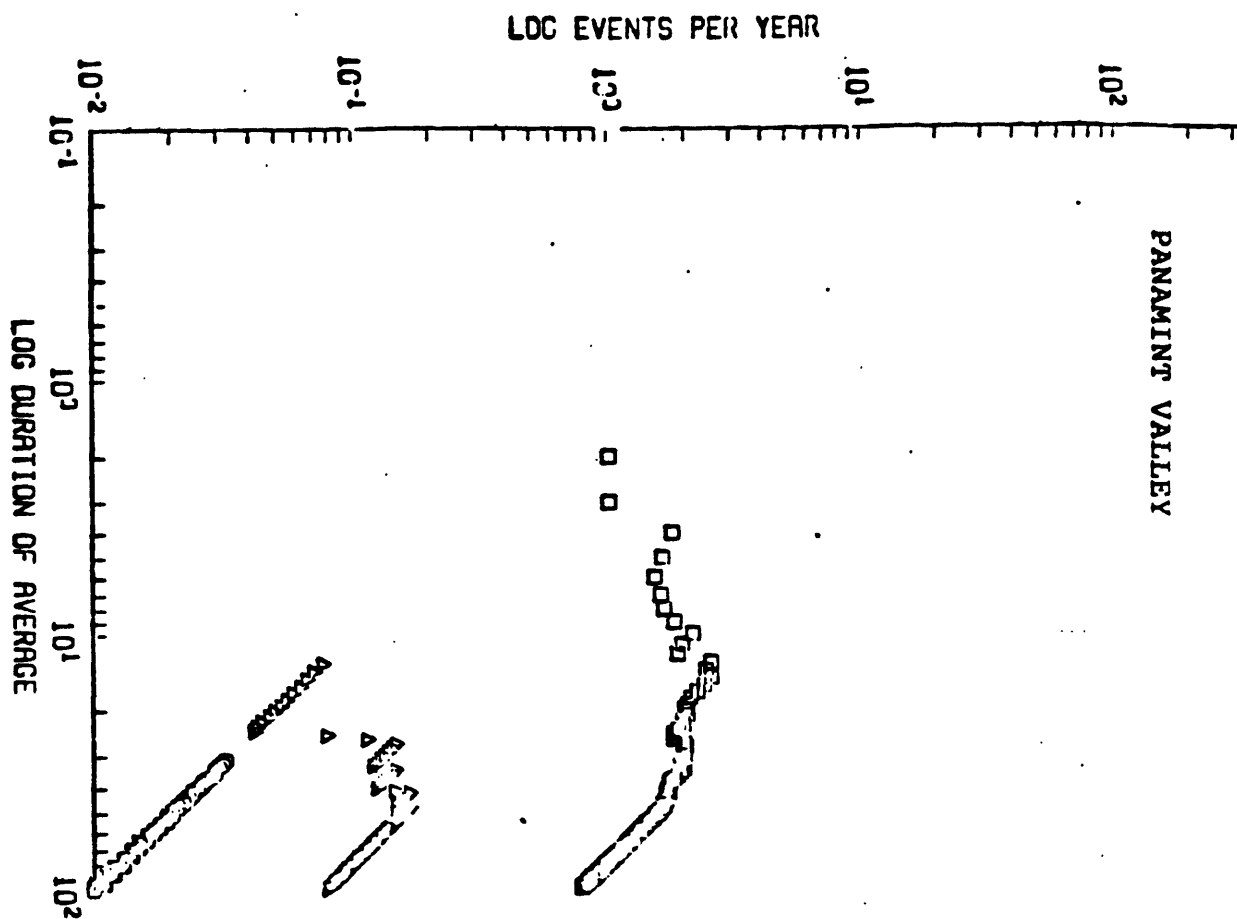


APPENDIX I-1

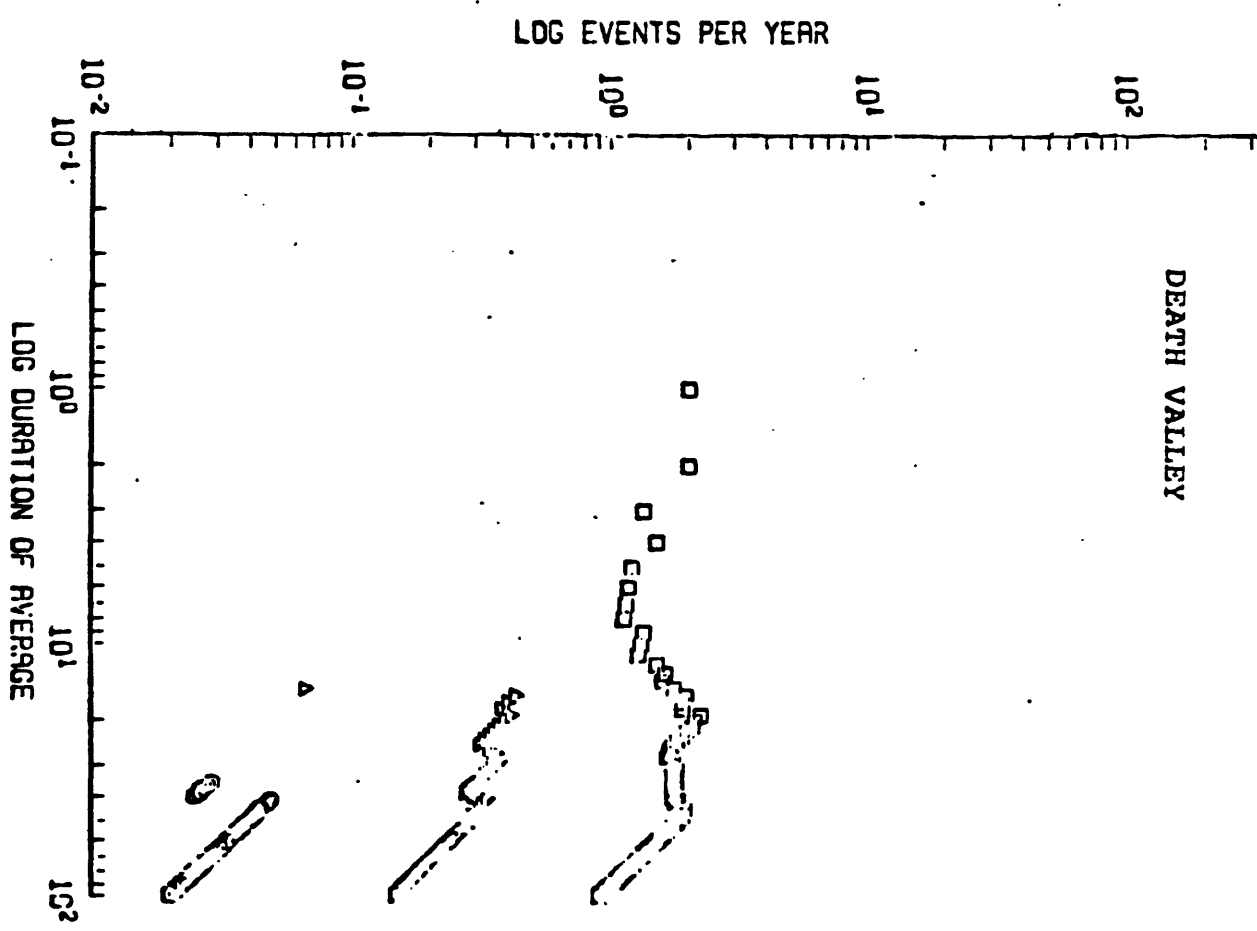
HONEY LAKE



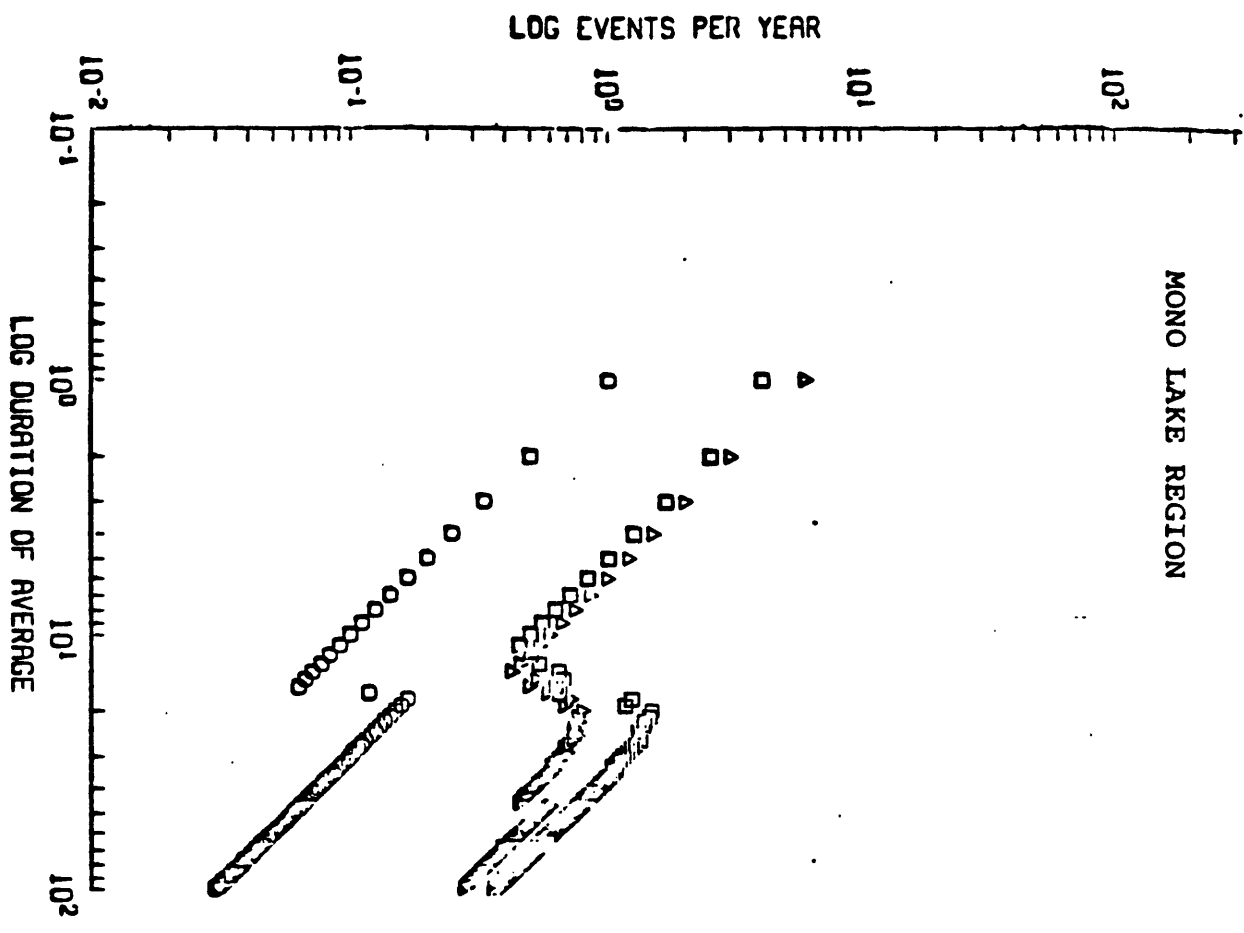
PANAMINT VALLEY



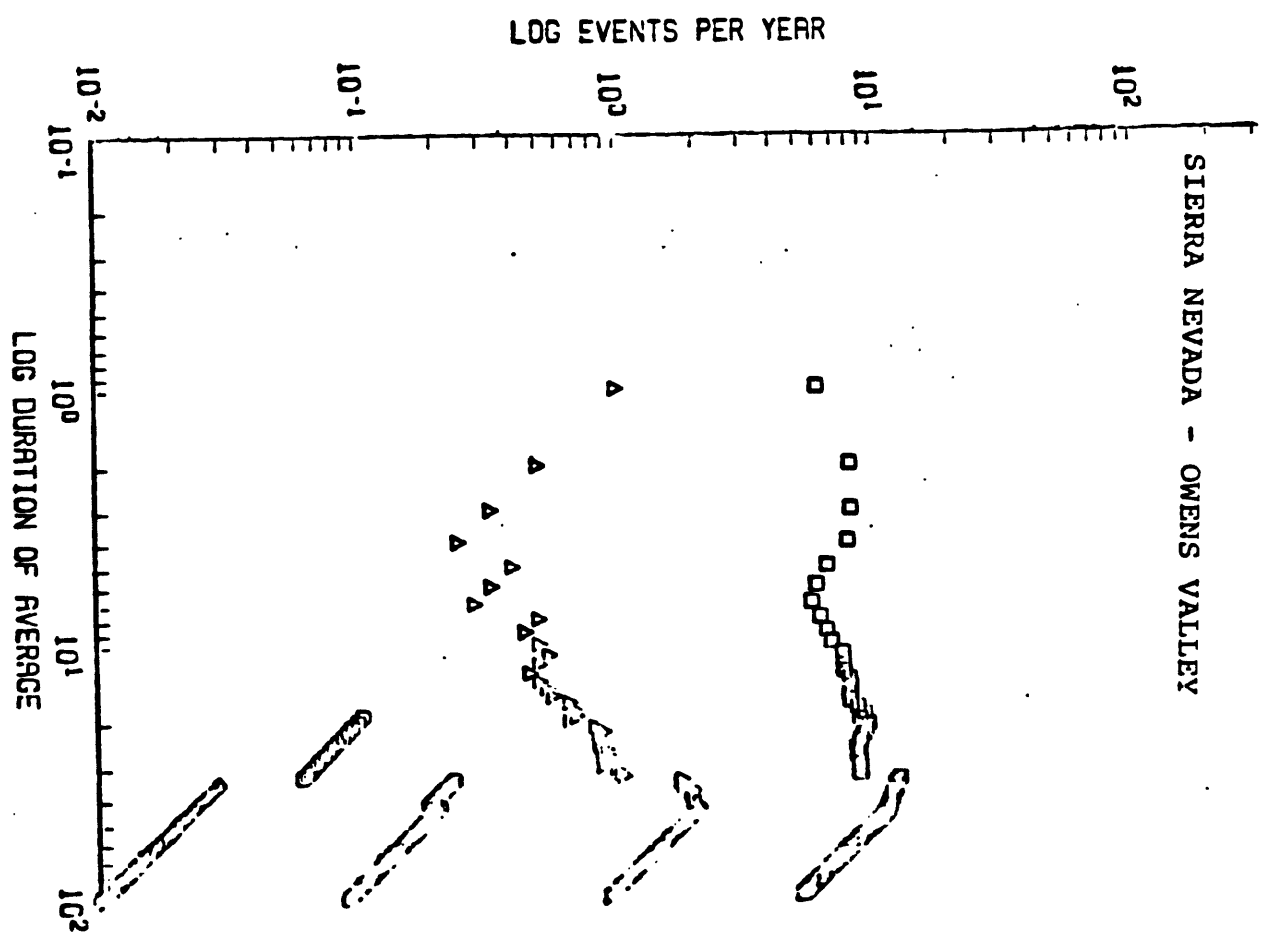
DEATH VALLEY

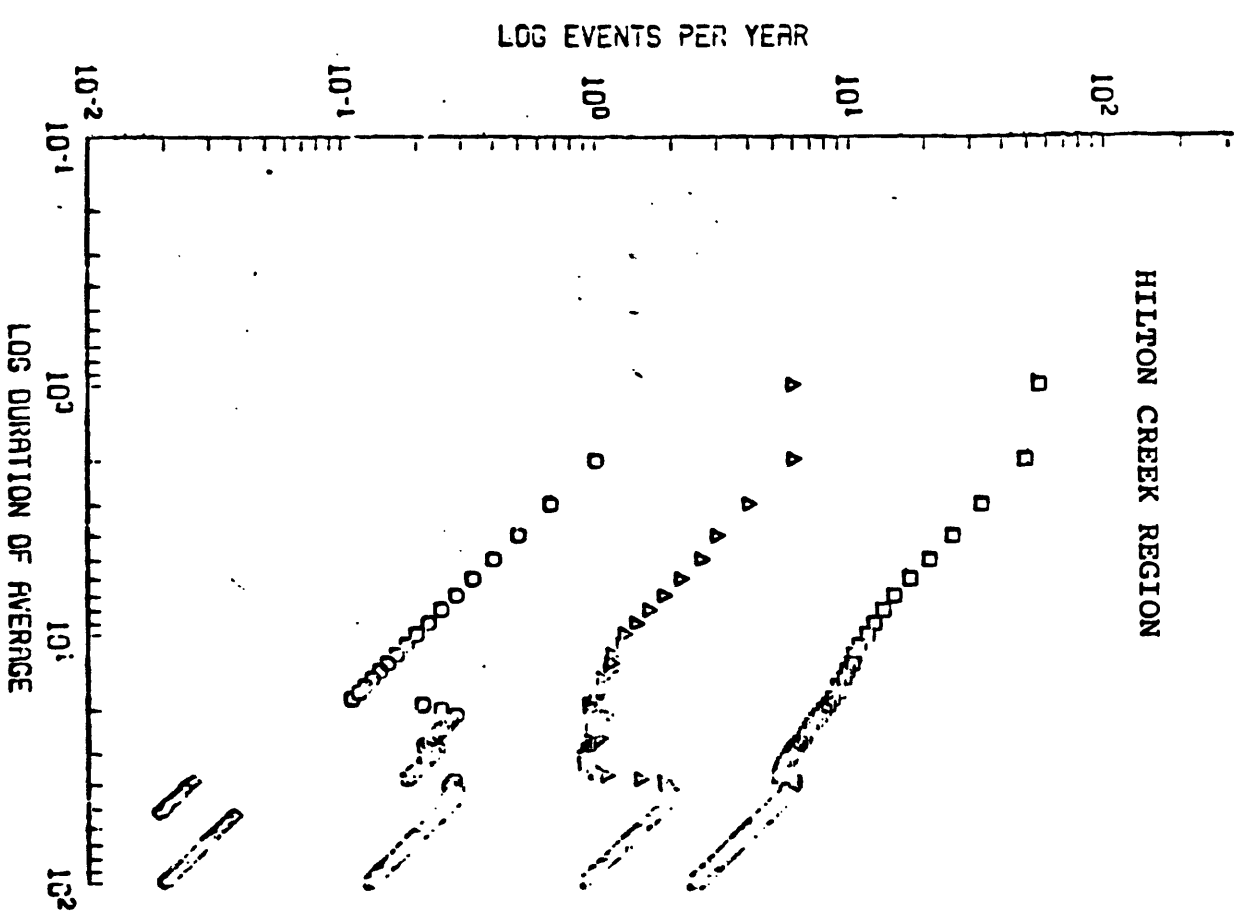
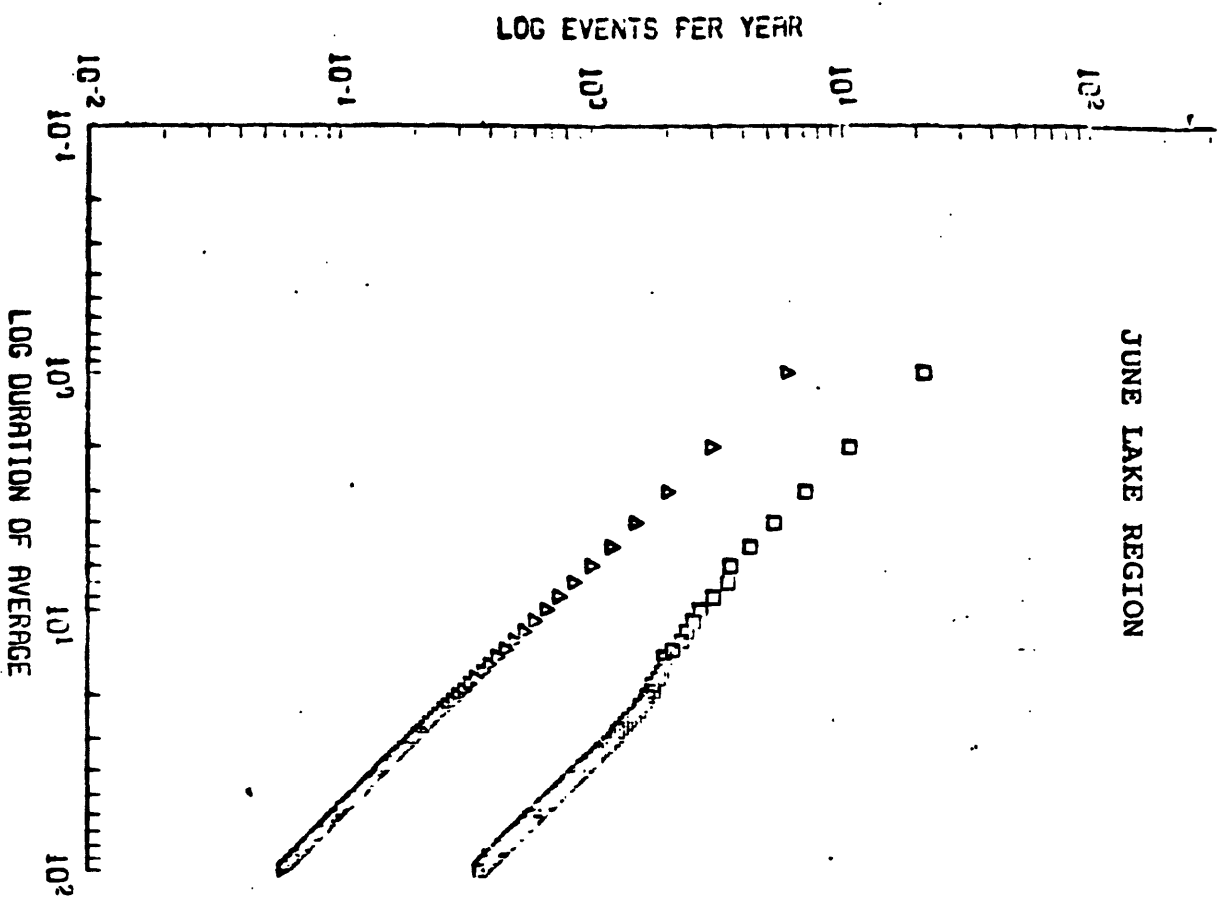


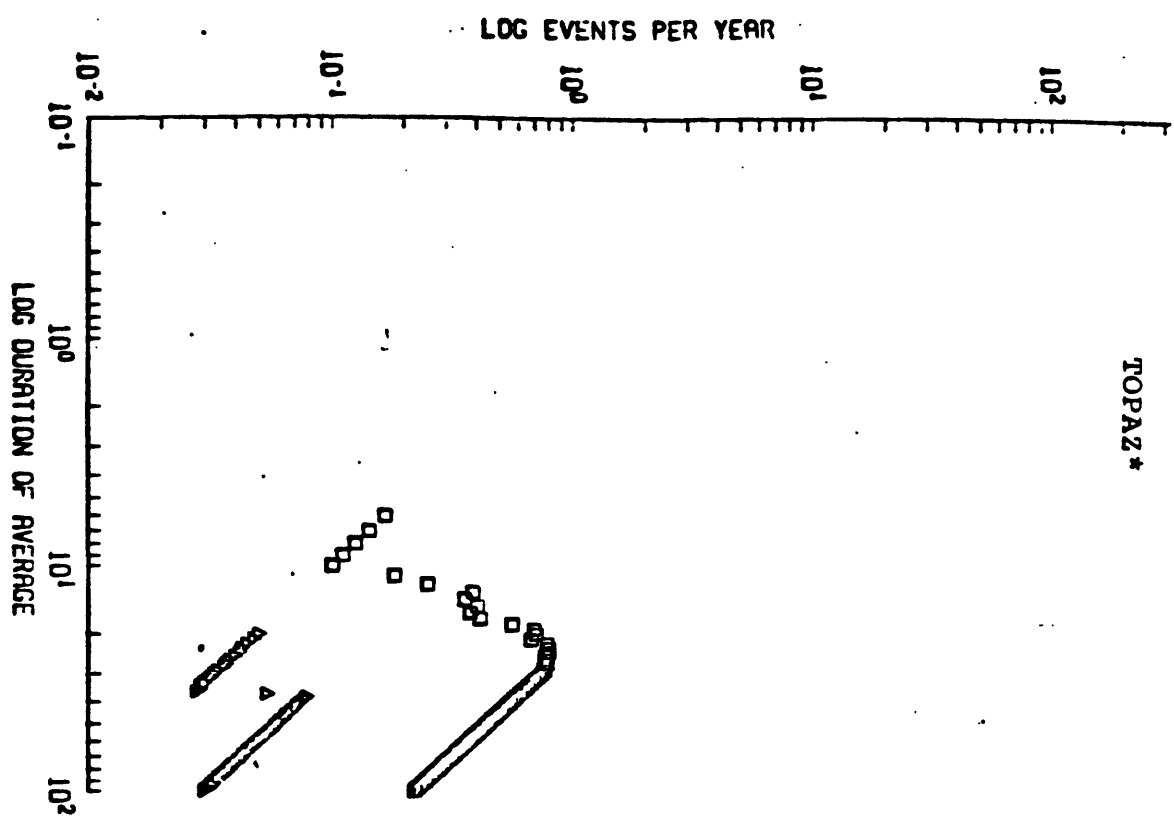
MONO LAKE REGION



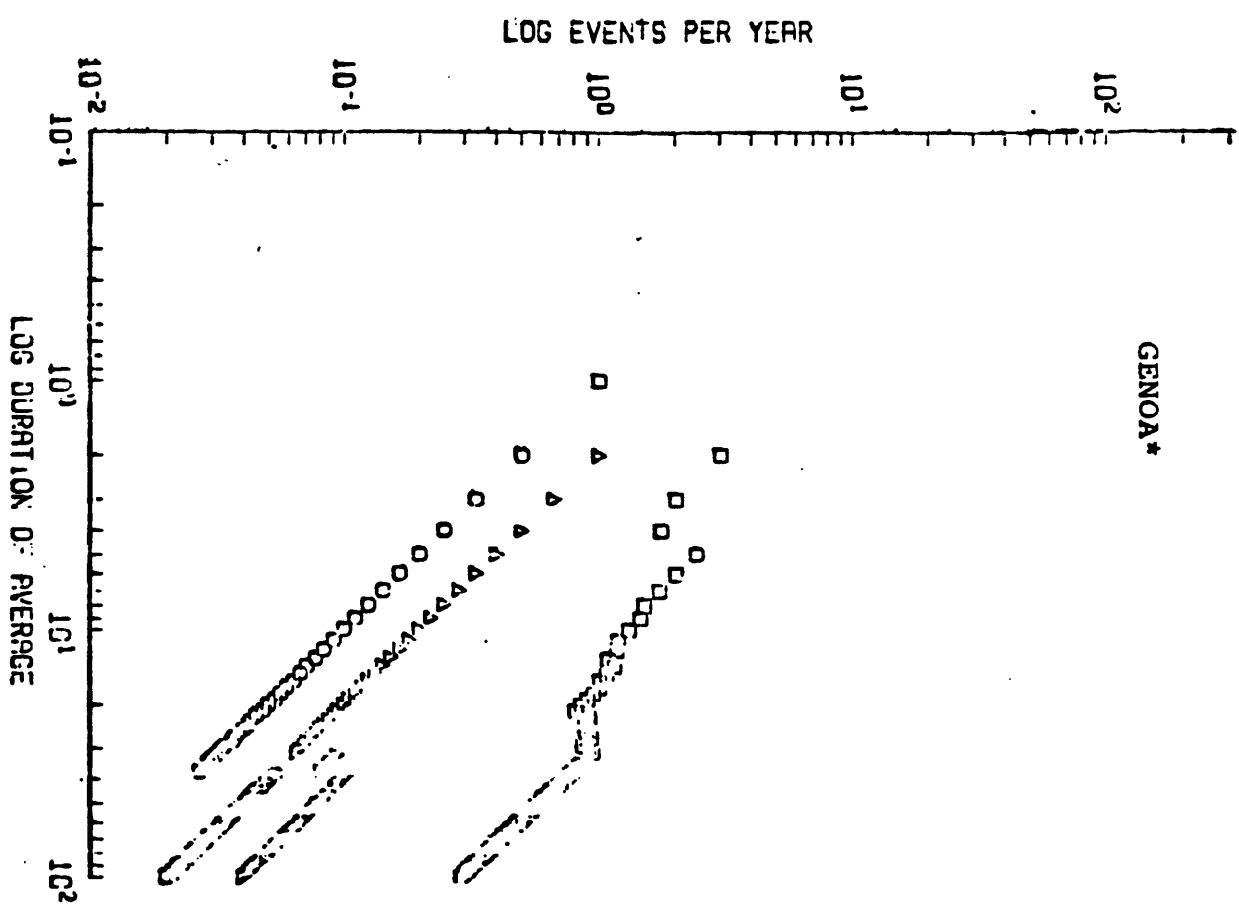
SIERRA NEVADA - OWENS VALLEY

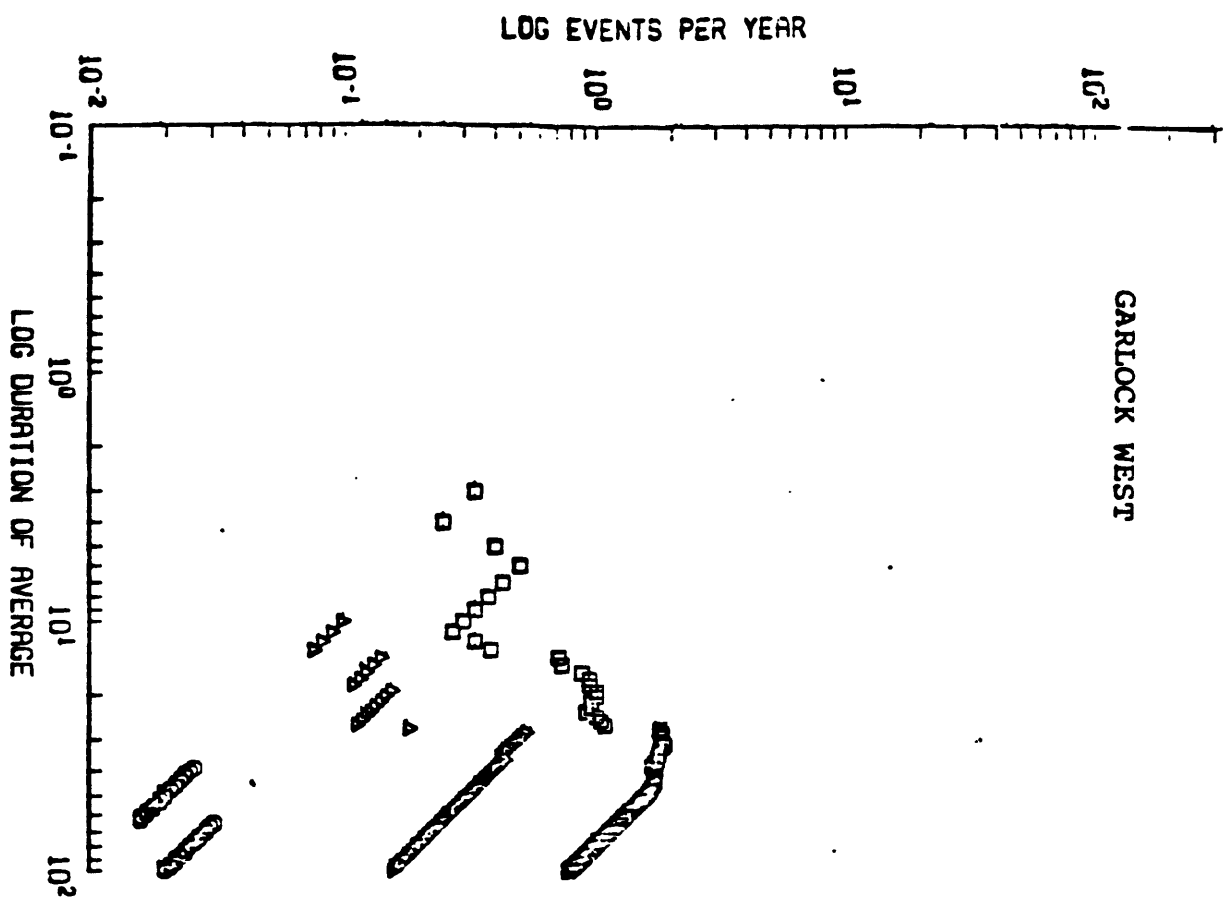




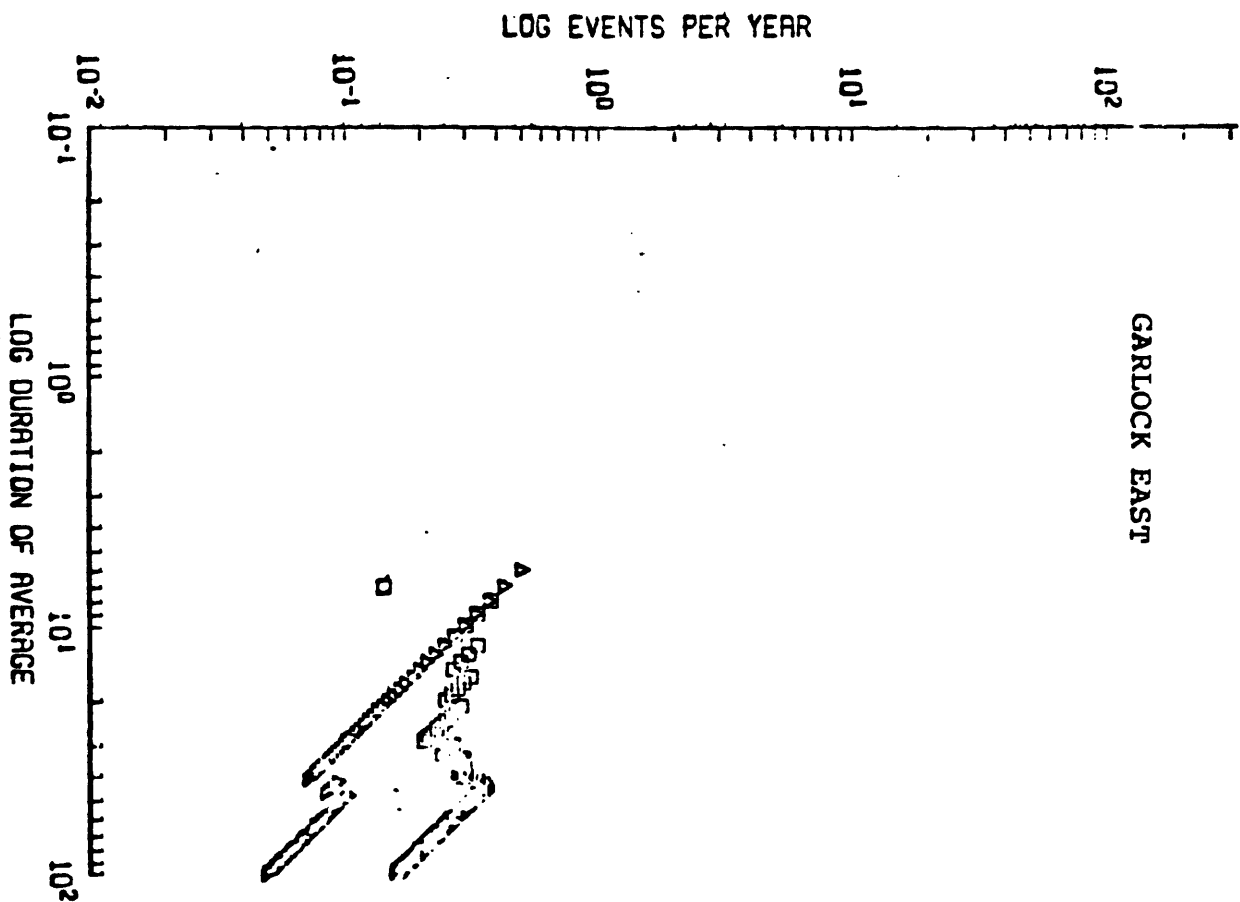


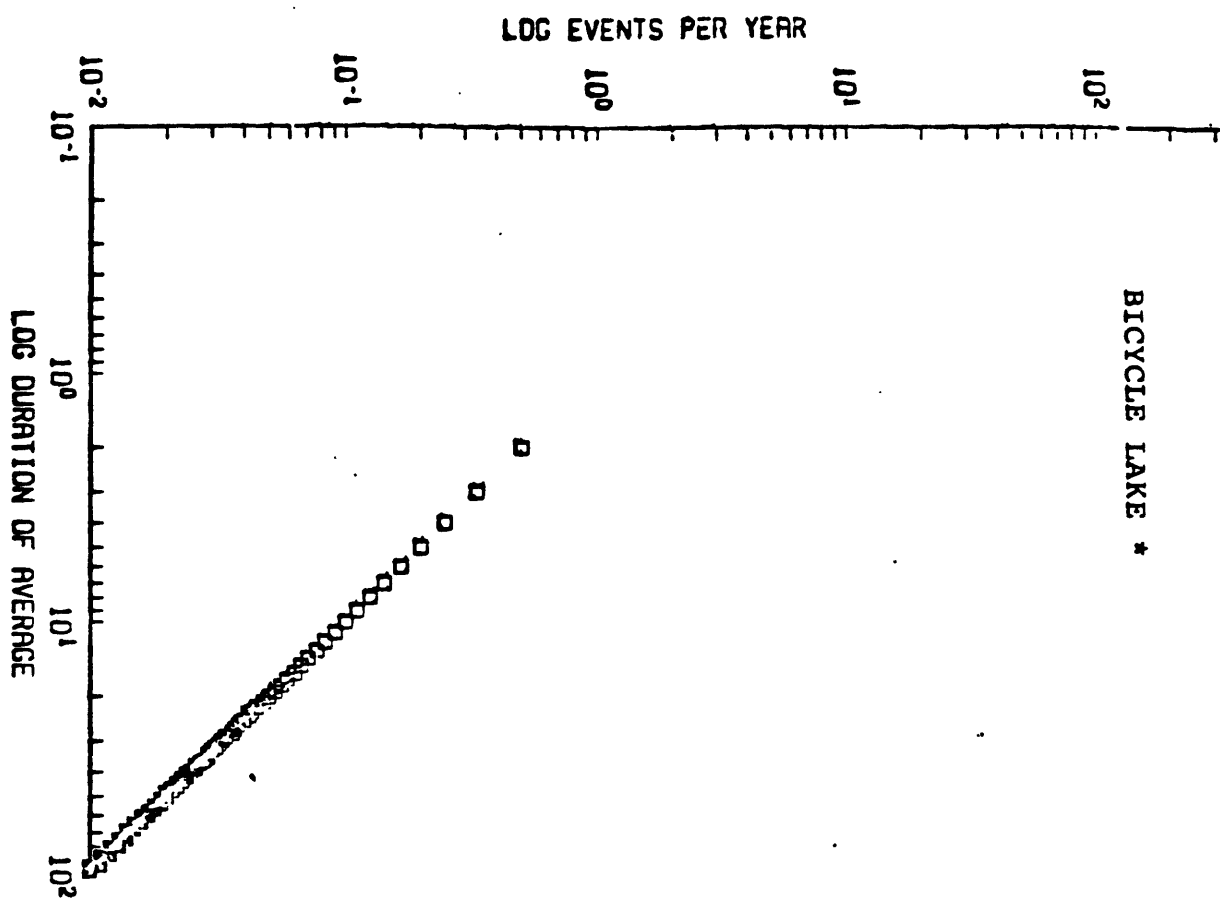
APPENDIX I-1



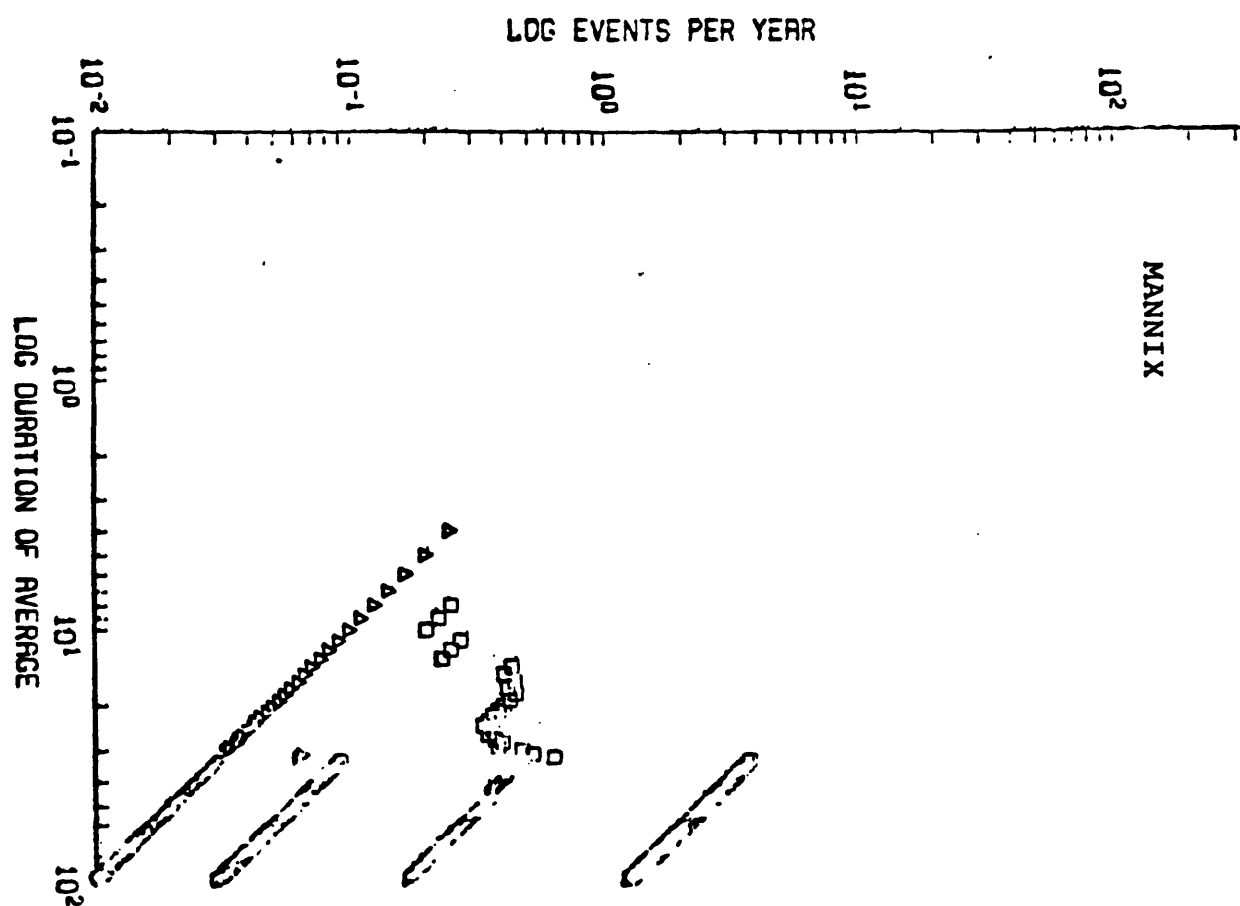


APPENDIX I-1

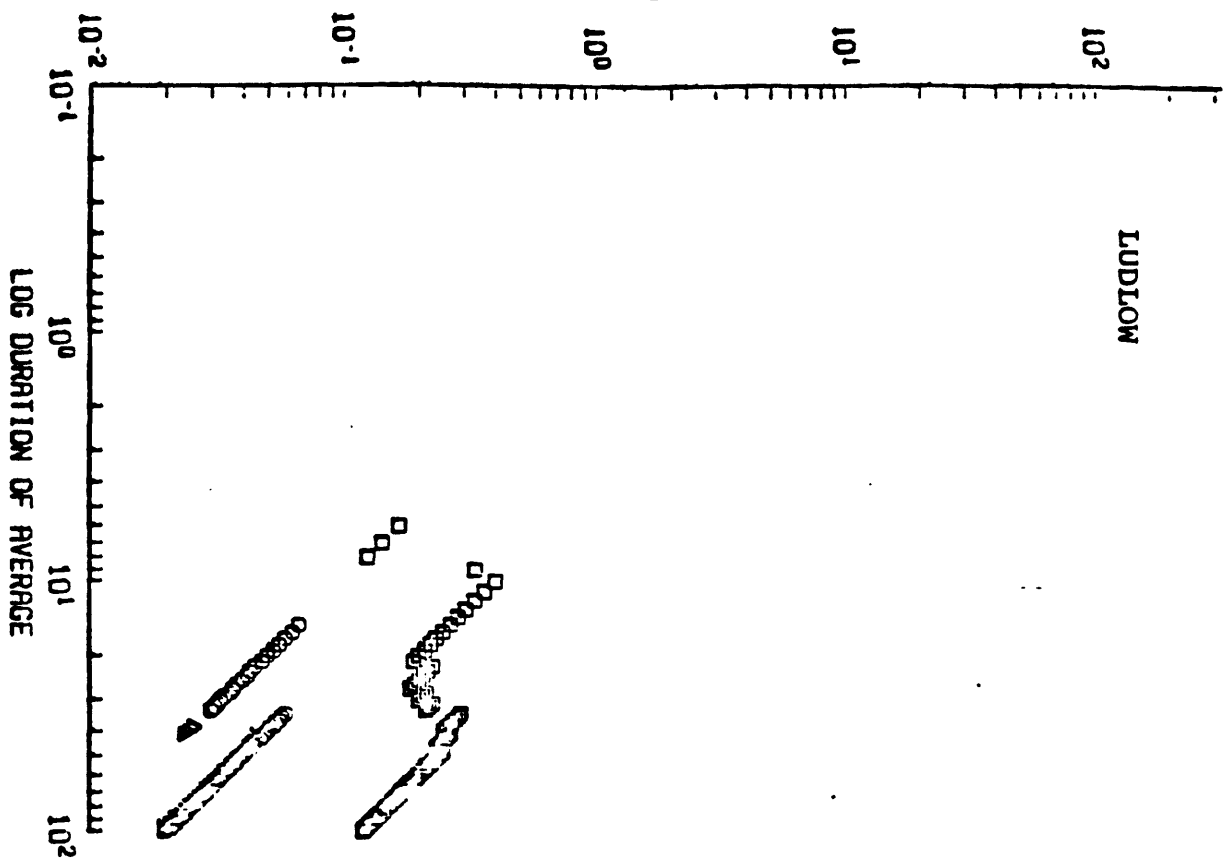




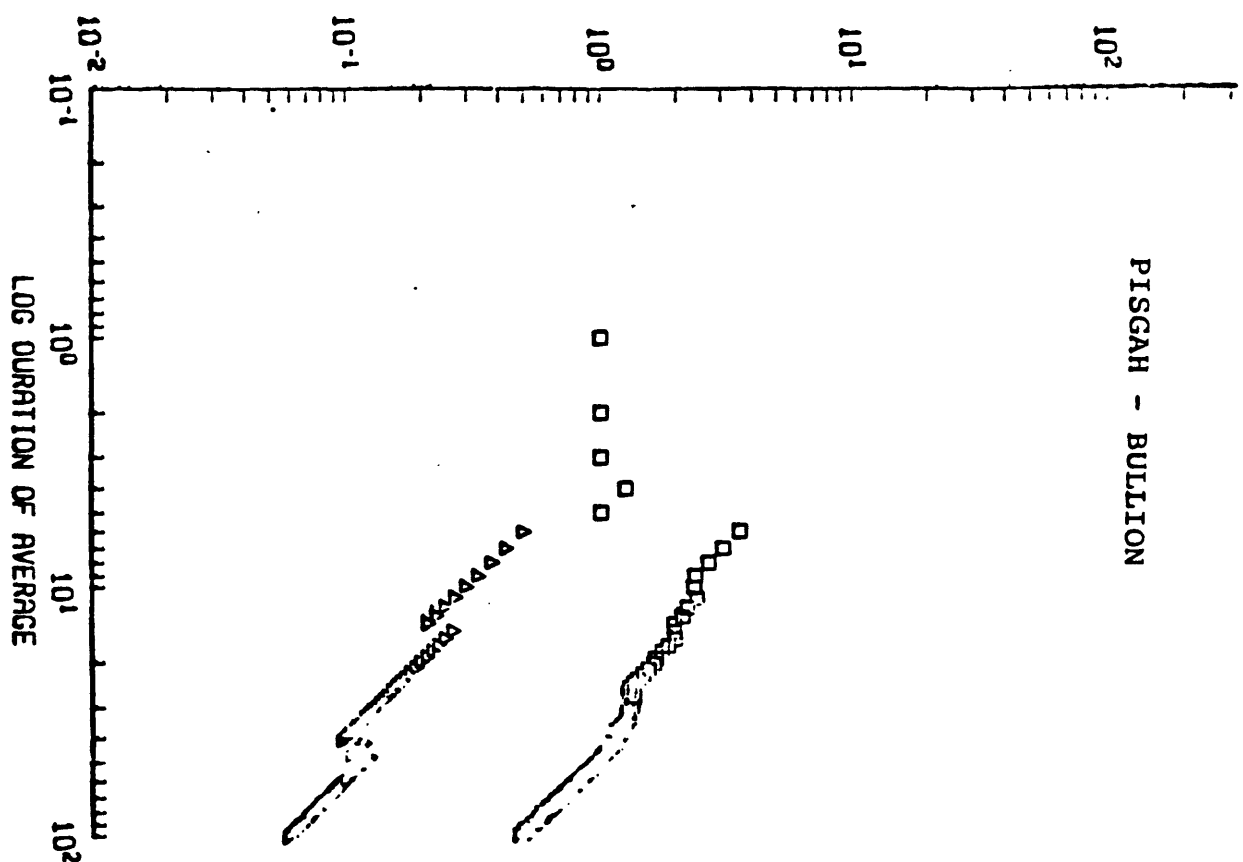
APPENDIX I-1



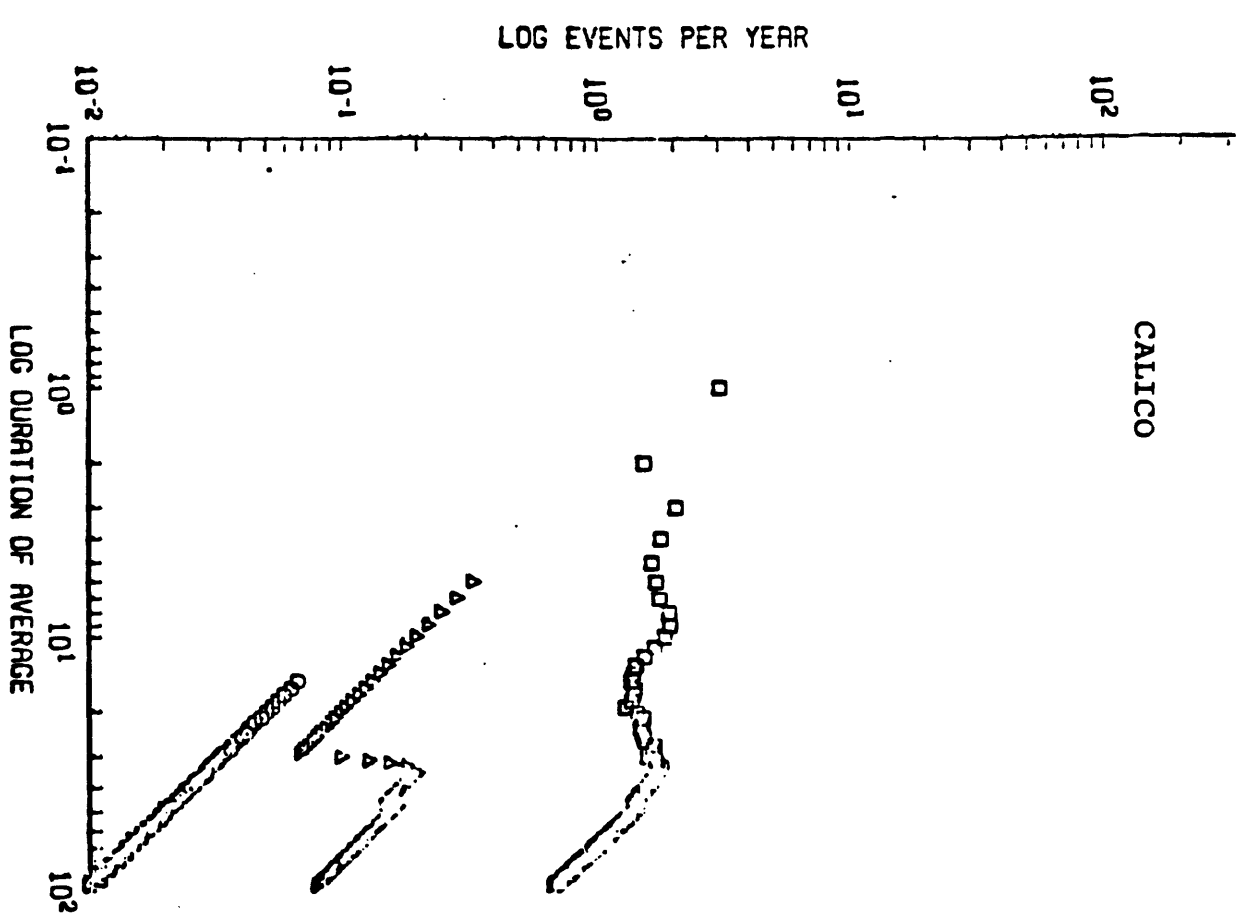
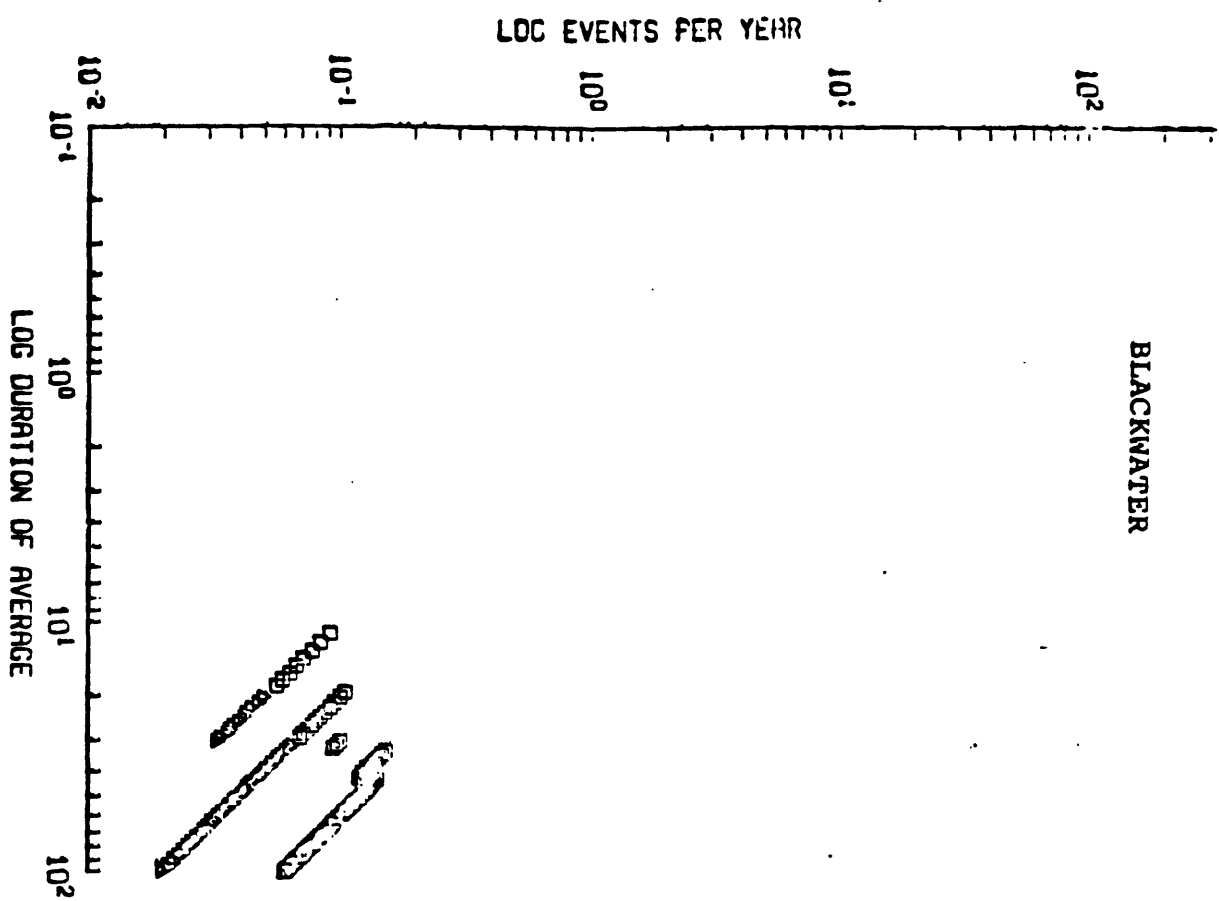
LOG EVENTS PER YEAR



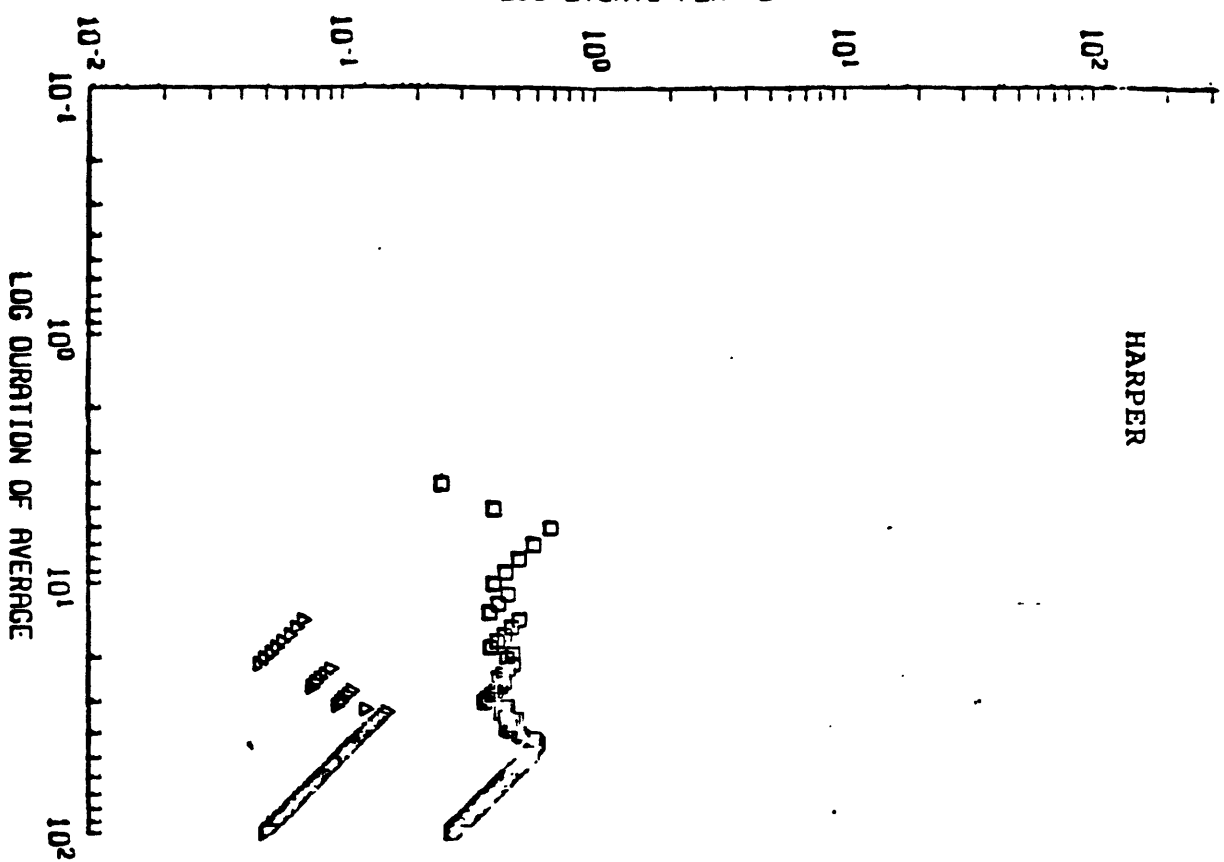
LOG EVENTS PER YEAR



APPENDIX I-1

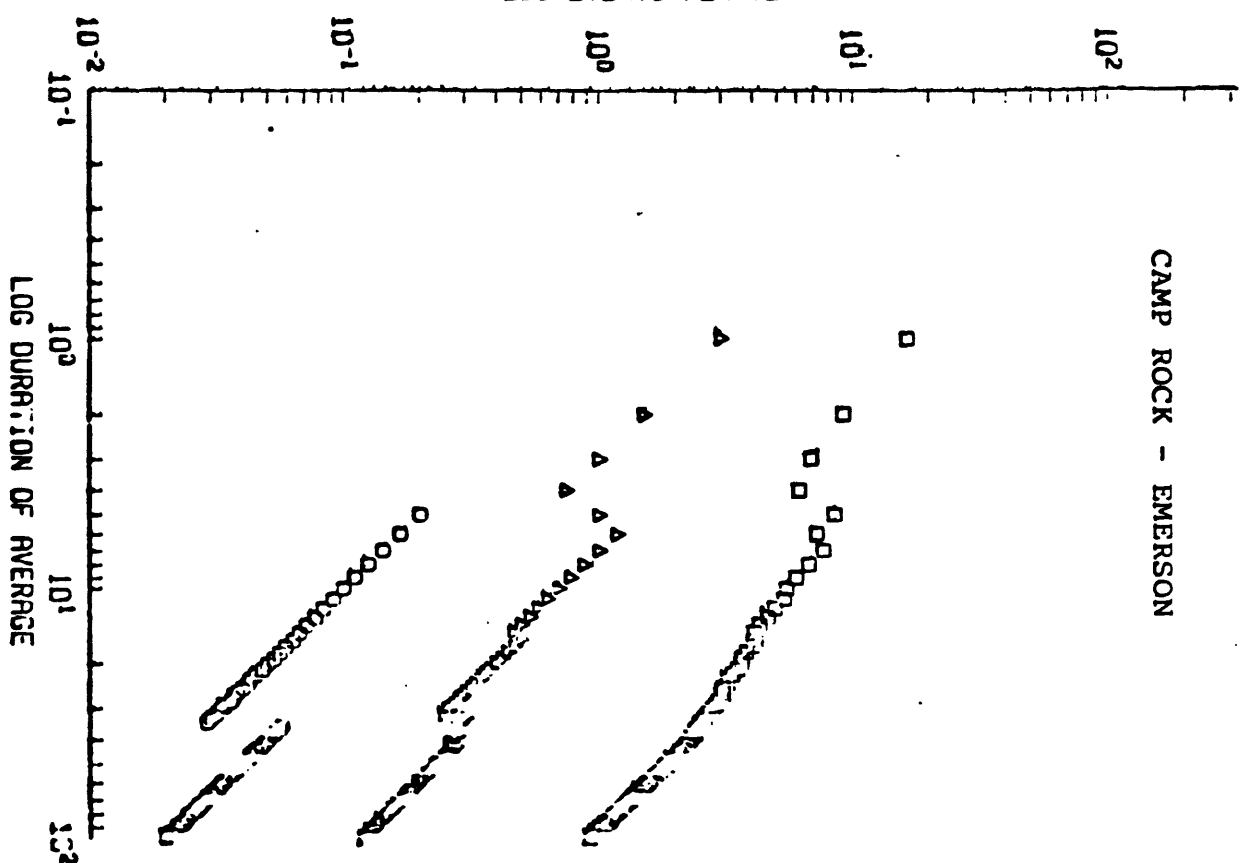


LOG EVENTS PER YEAR



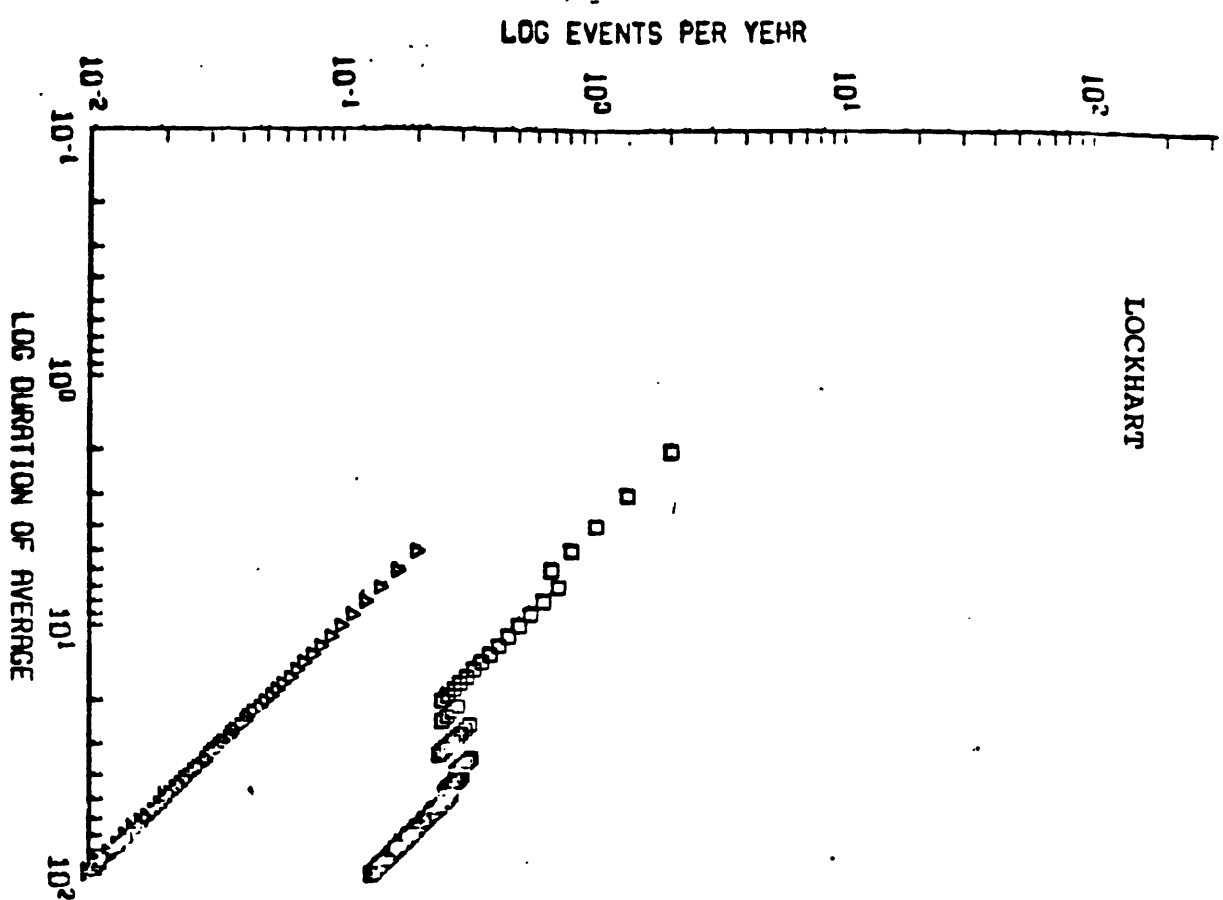
HARPER

LOG EVENTS PER YEAR

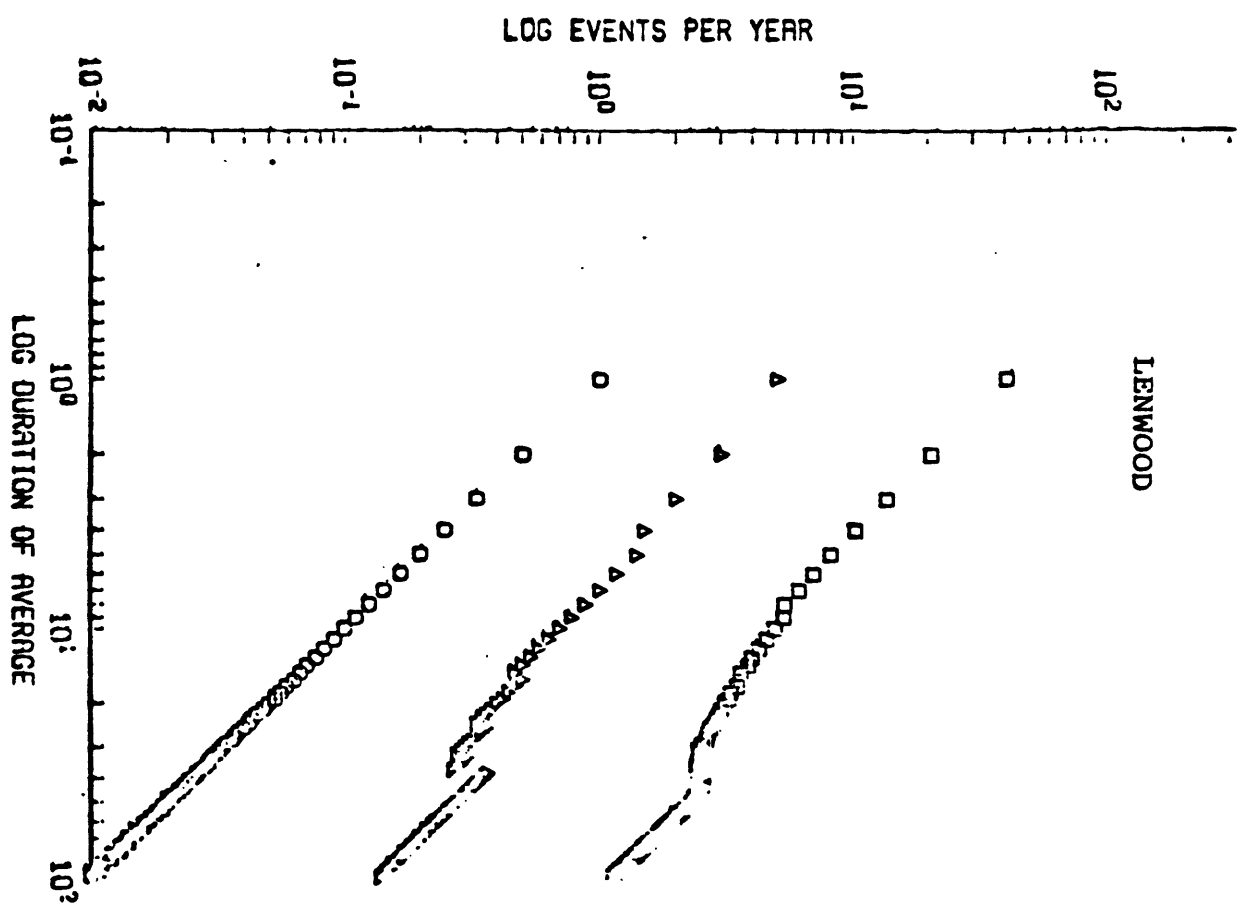


CAMP ROCK - EMERSON

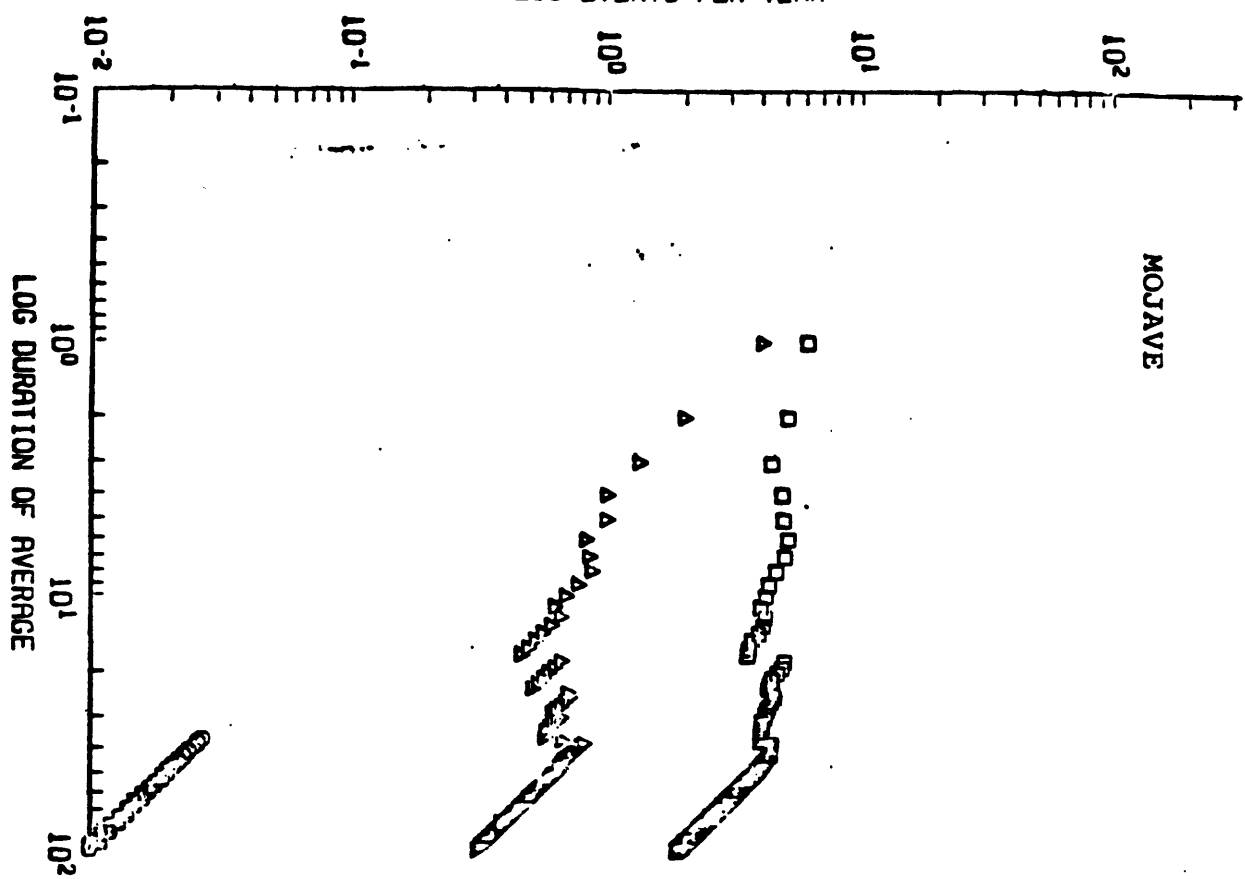
APPENDIX I-1



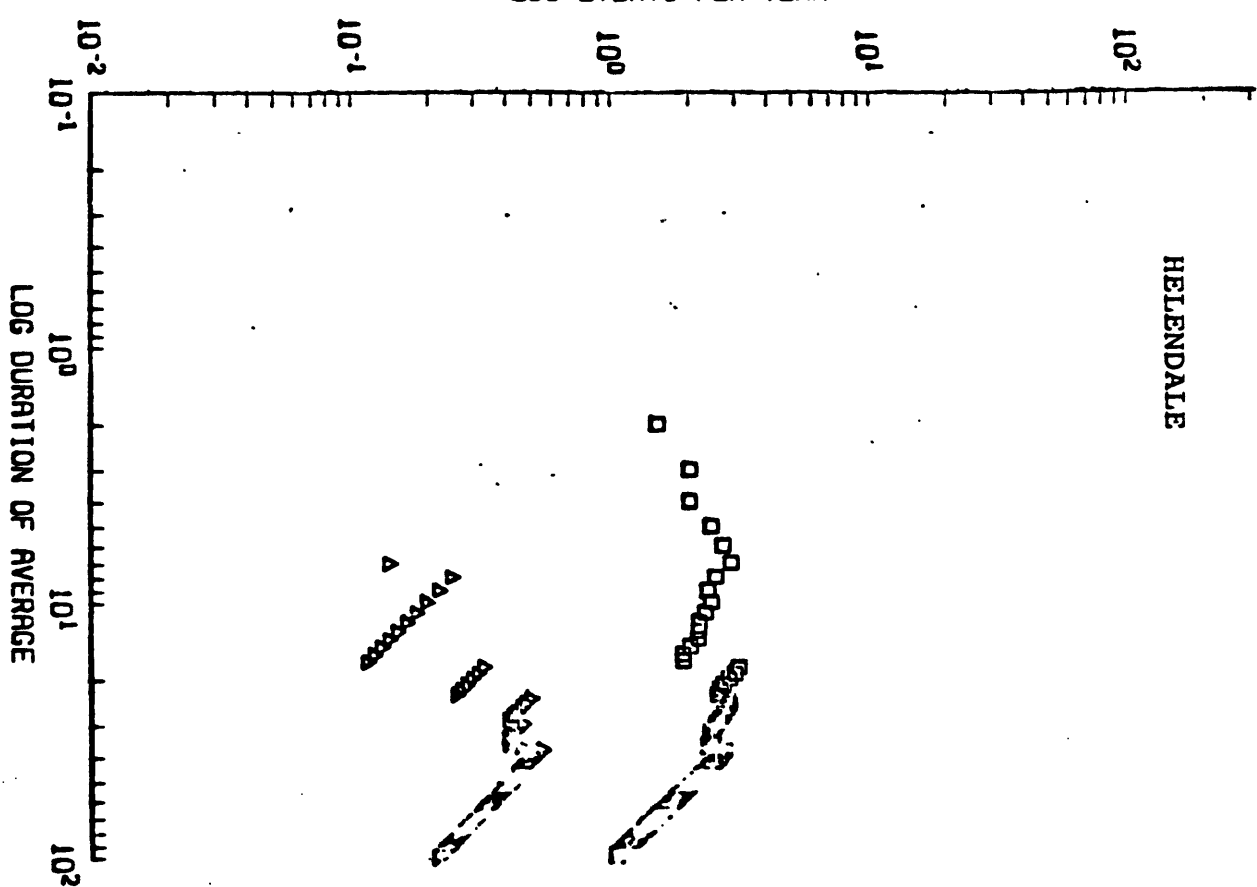
APPENDIX I-1



LOG EVENTS PER YEAR

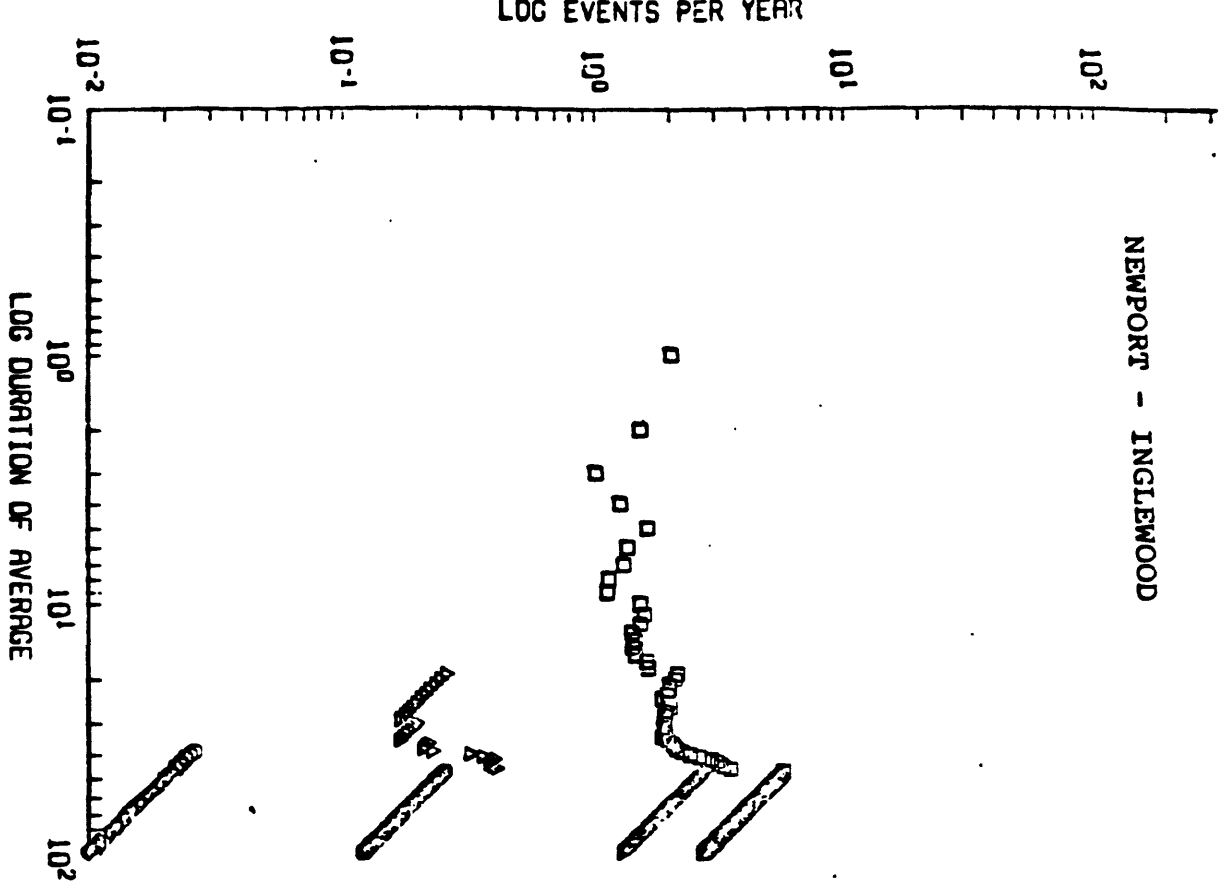


LOG EVENTS PER YEAR

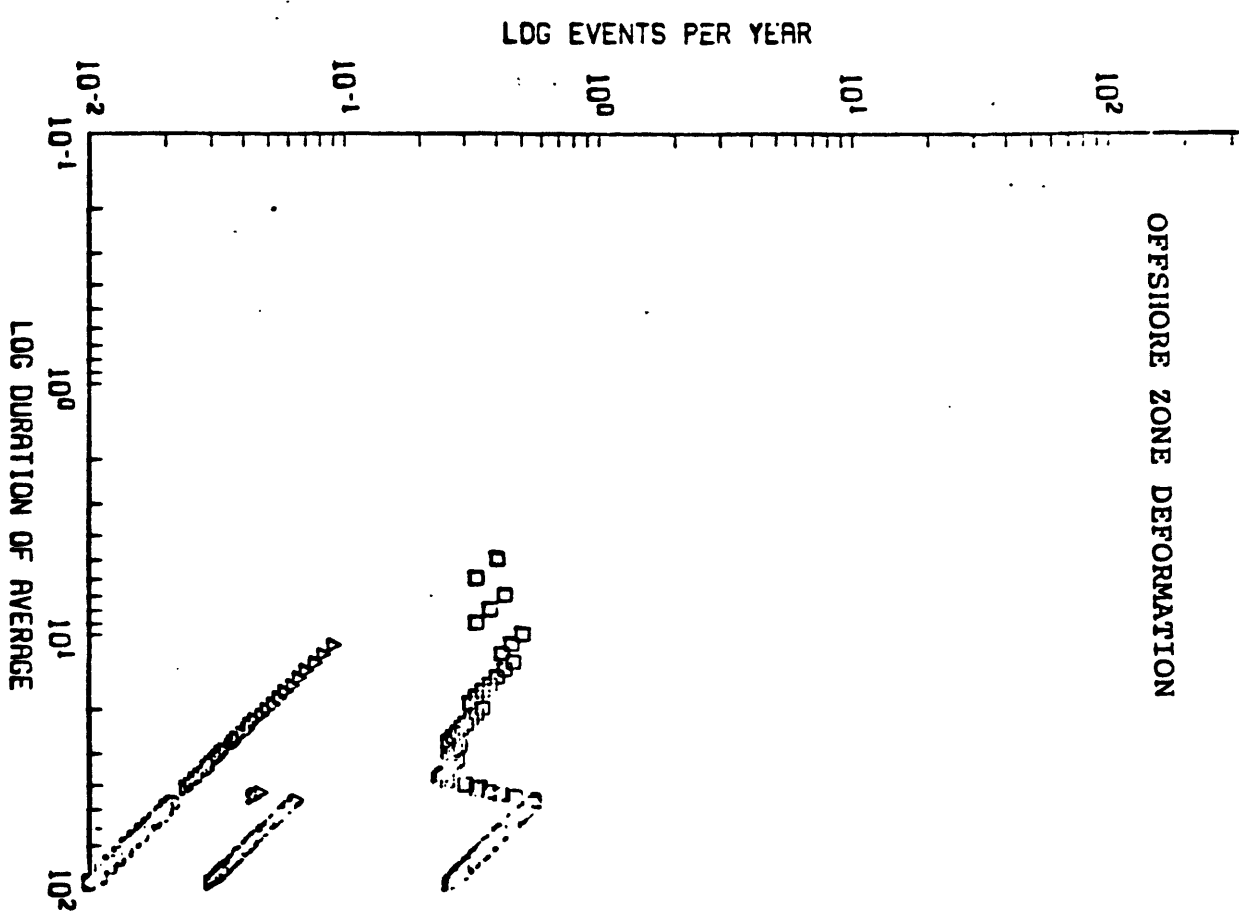


APPENDIX I-1

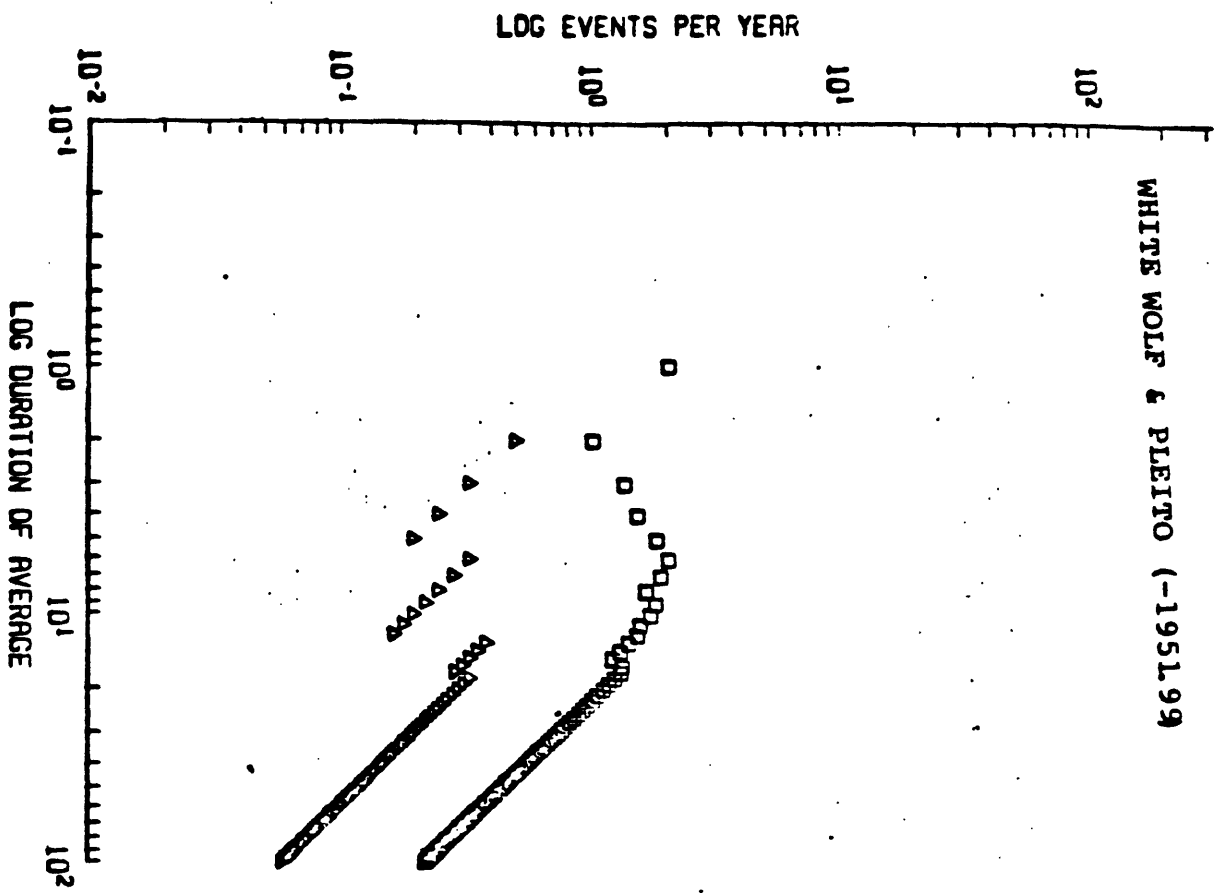
NEWPORT - INGLEWOOD



OFFSHORE ZONE DEFORMATION

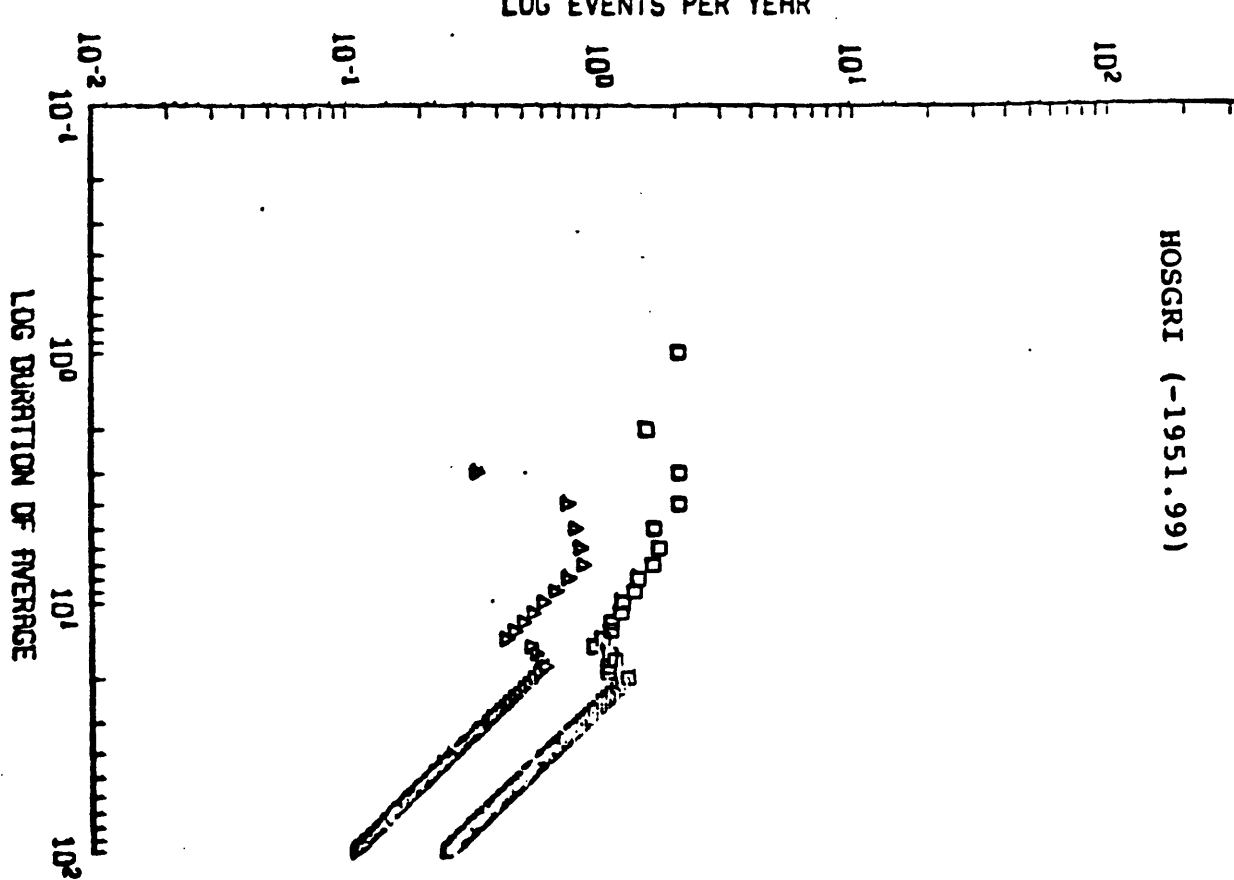


WHITE WOLF & PLEITO (-1951.99)

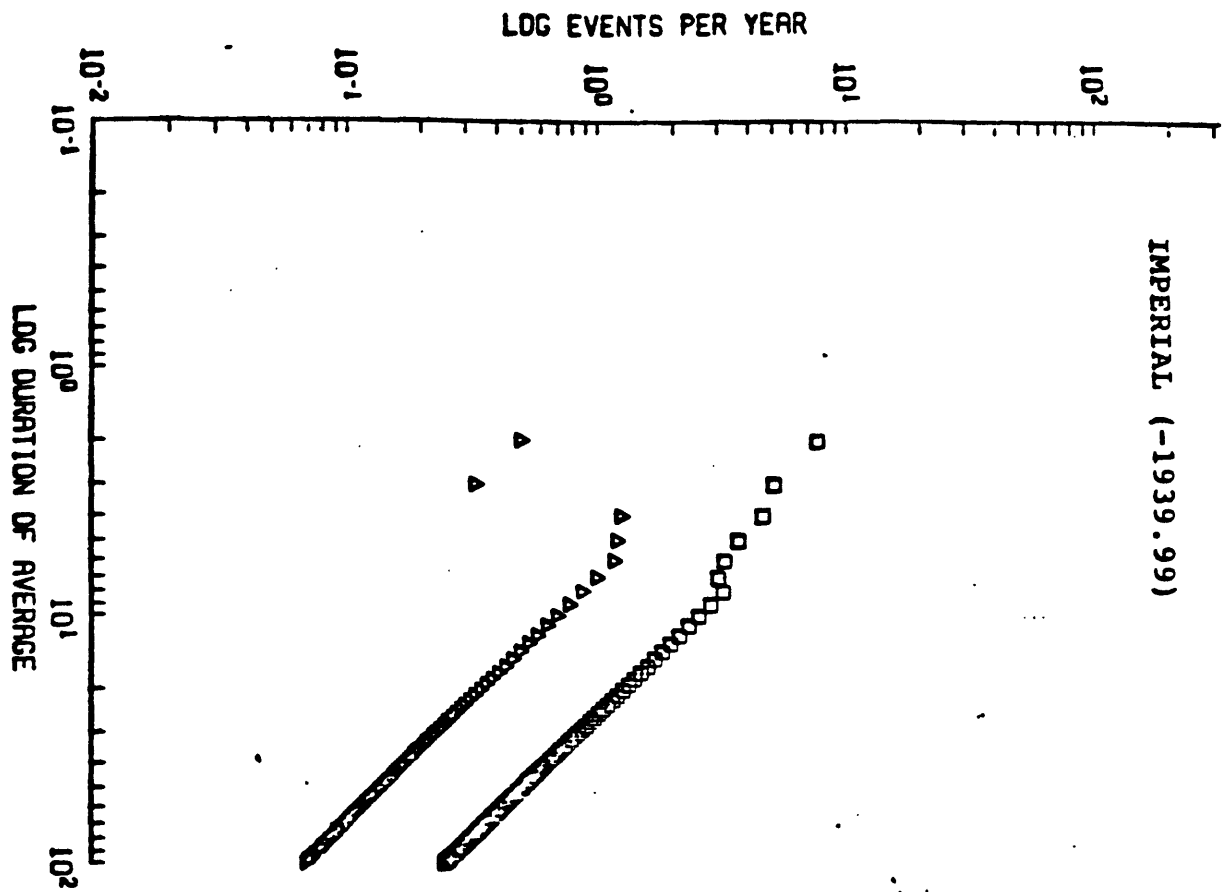


APPENDIX I-1

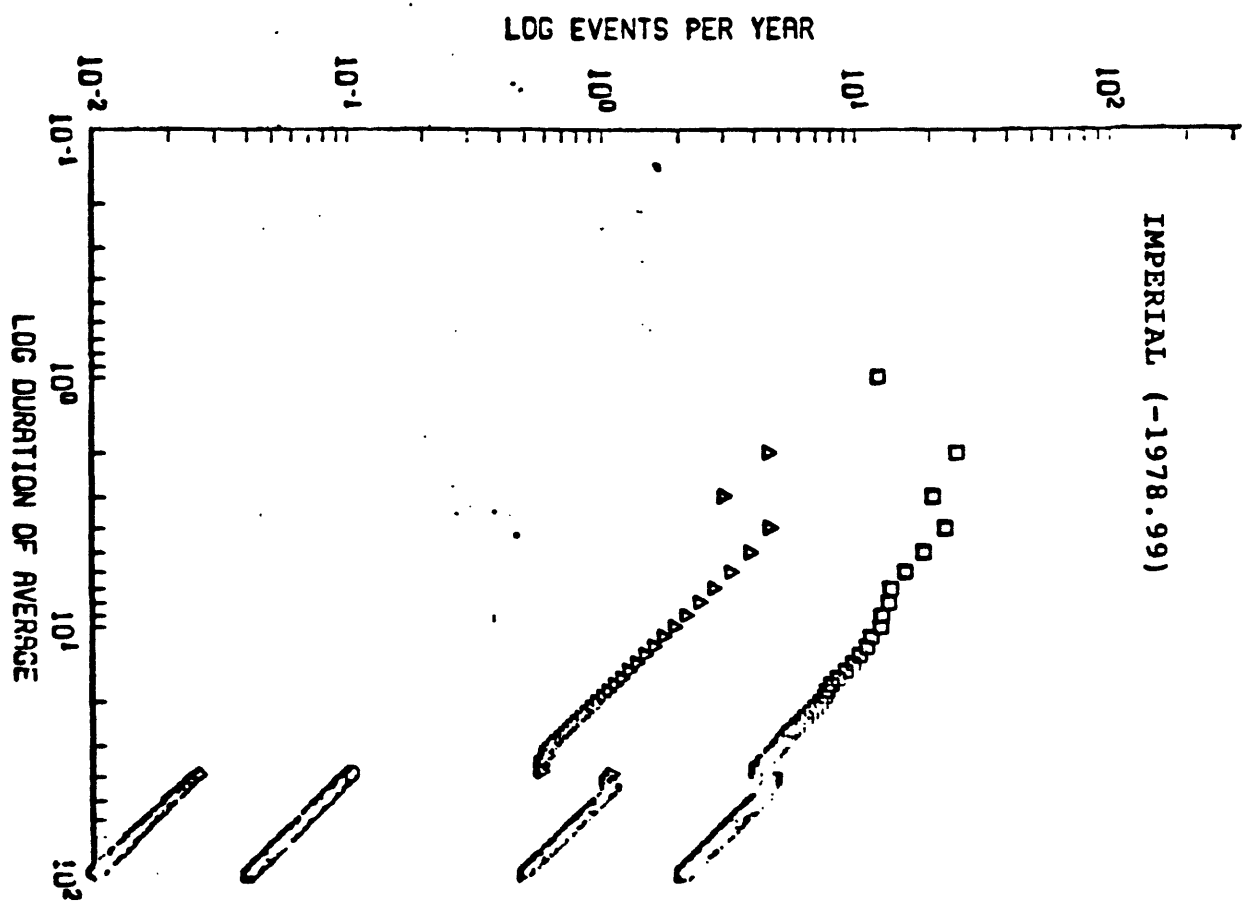
HOSGRI (-1951.99)



IMPERIAL (-1939.99)

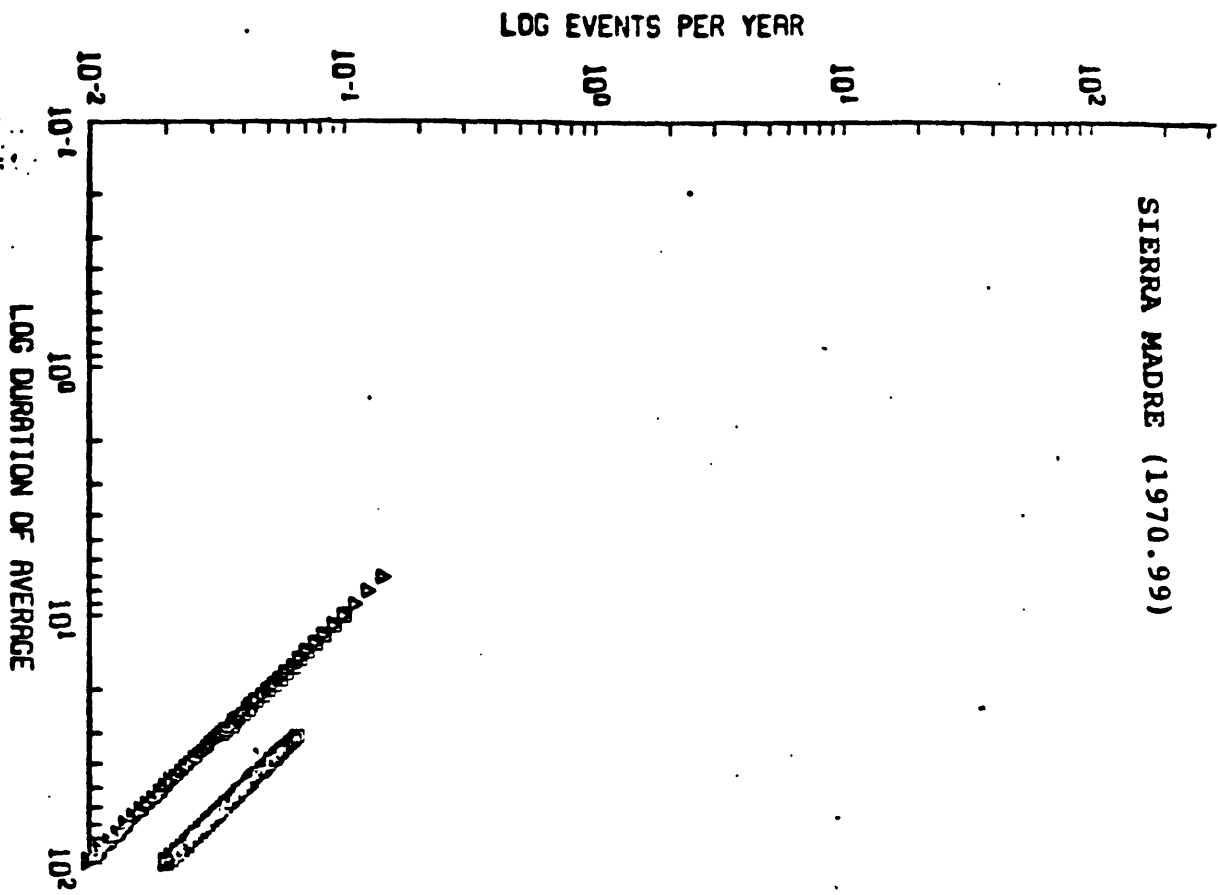


IMPERIAL (-1978.99)



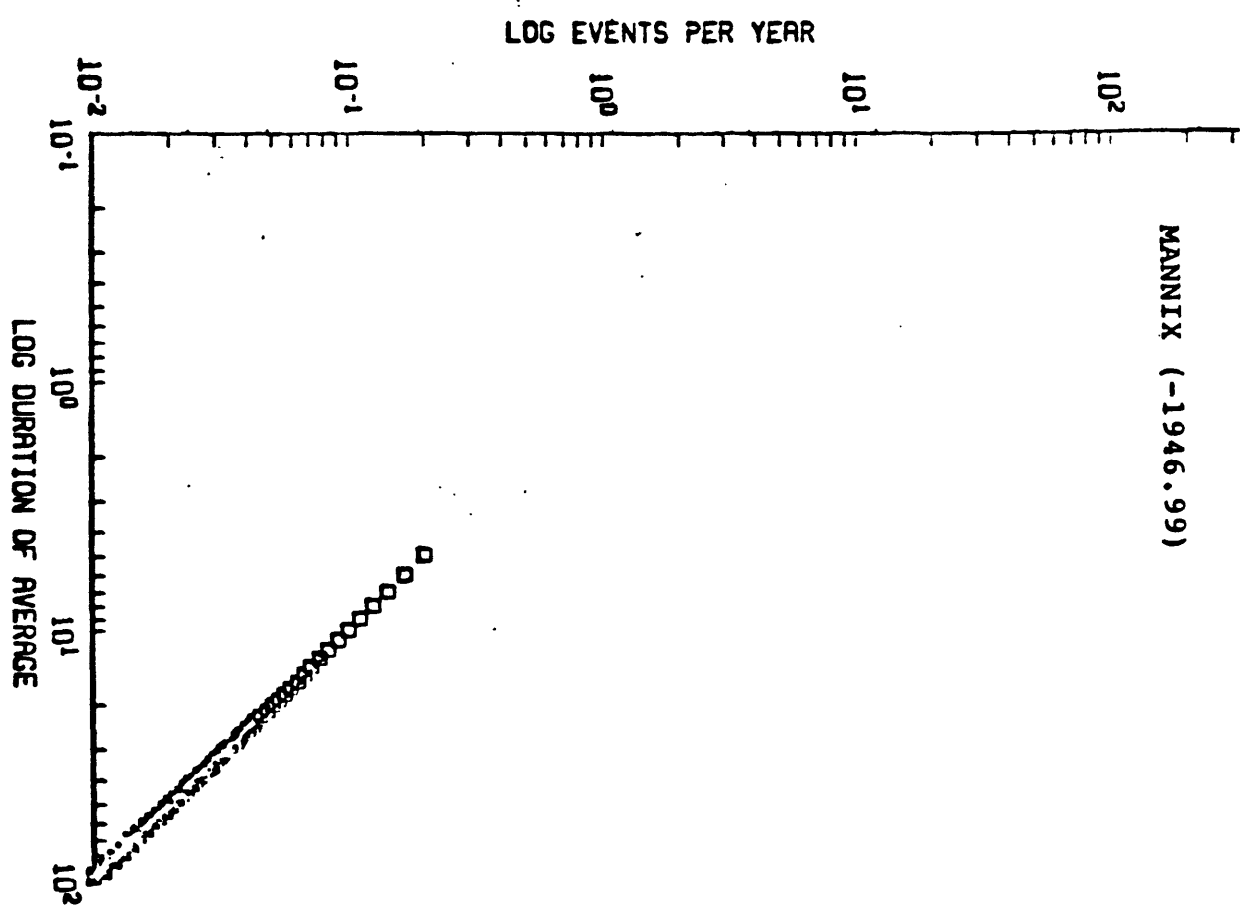
APPENDIX I-1

SIERRA MADRE (1970-99)

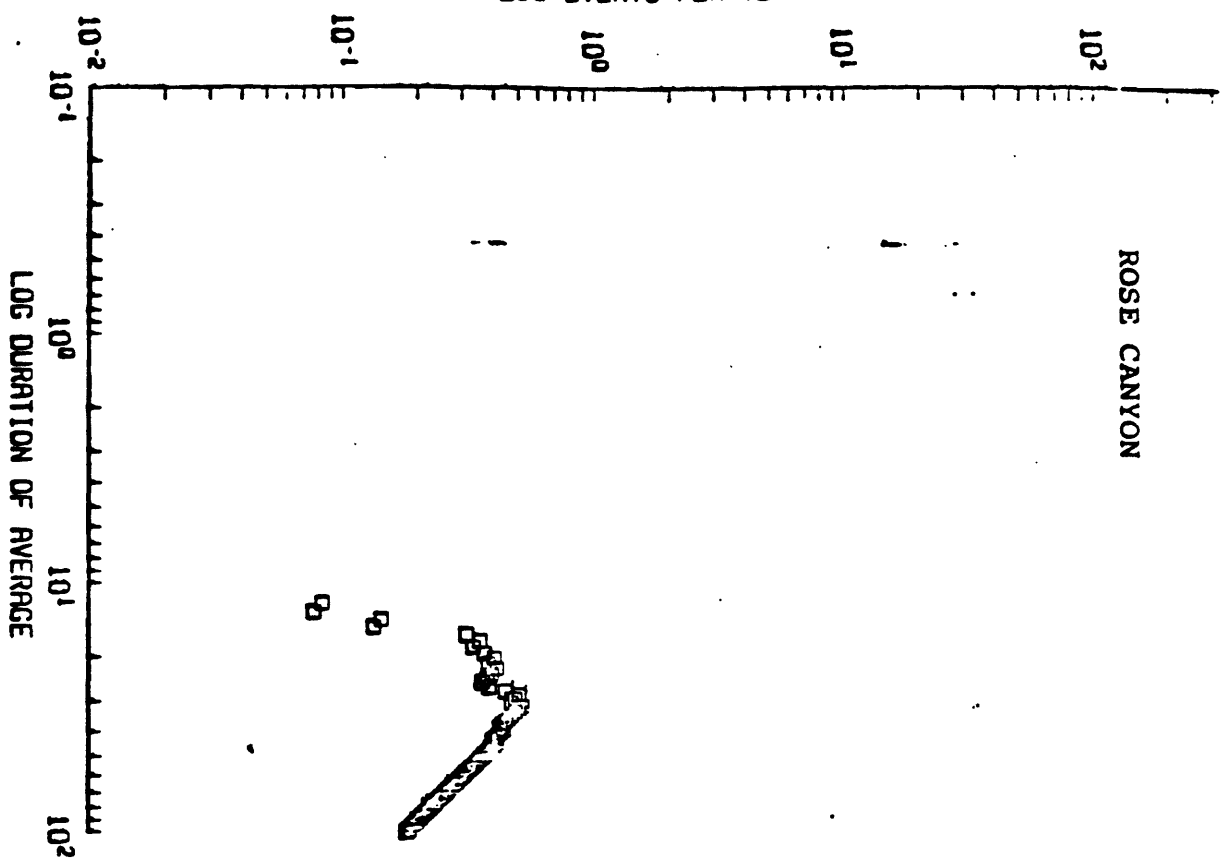


APPENDIX I-1

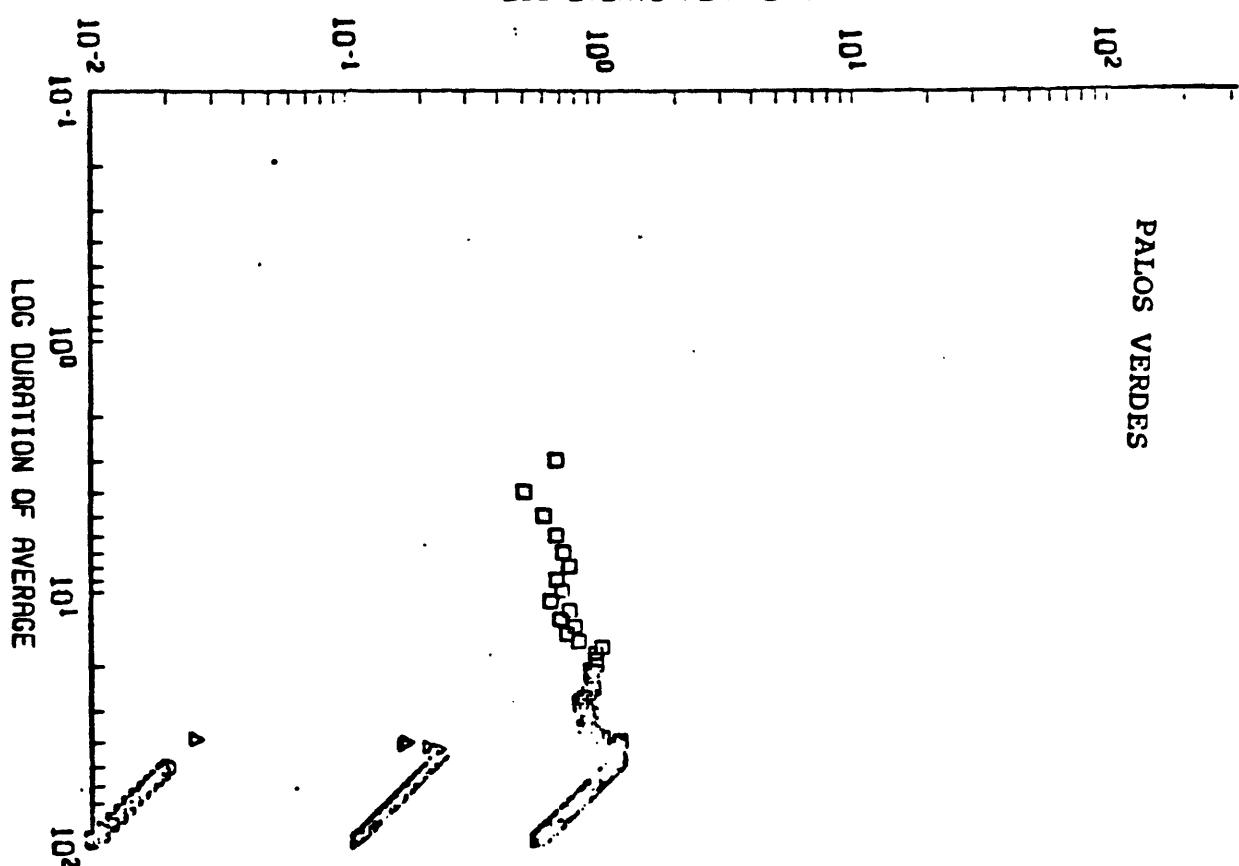
MANNIX (-1946-99)



LOG EVENTS PER YEAR

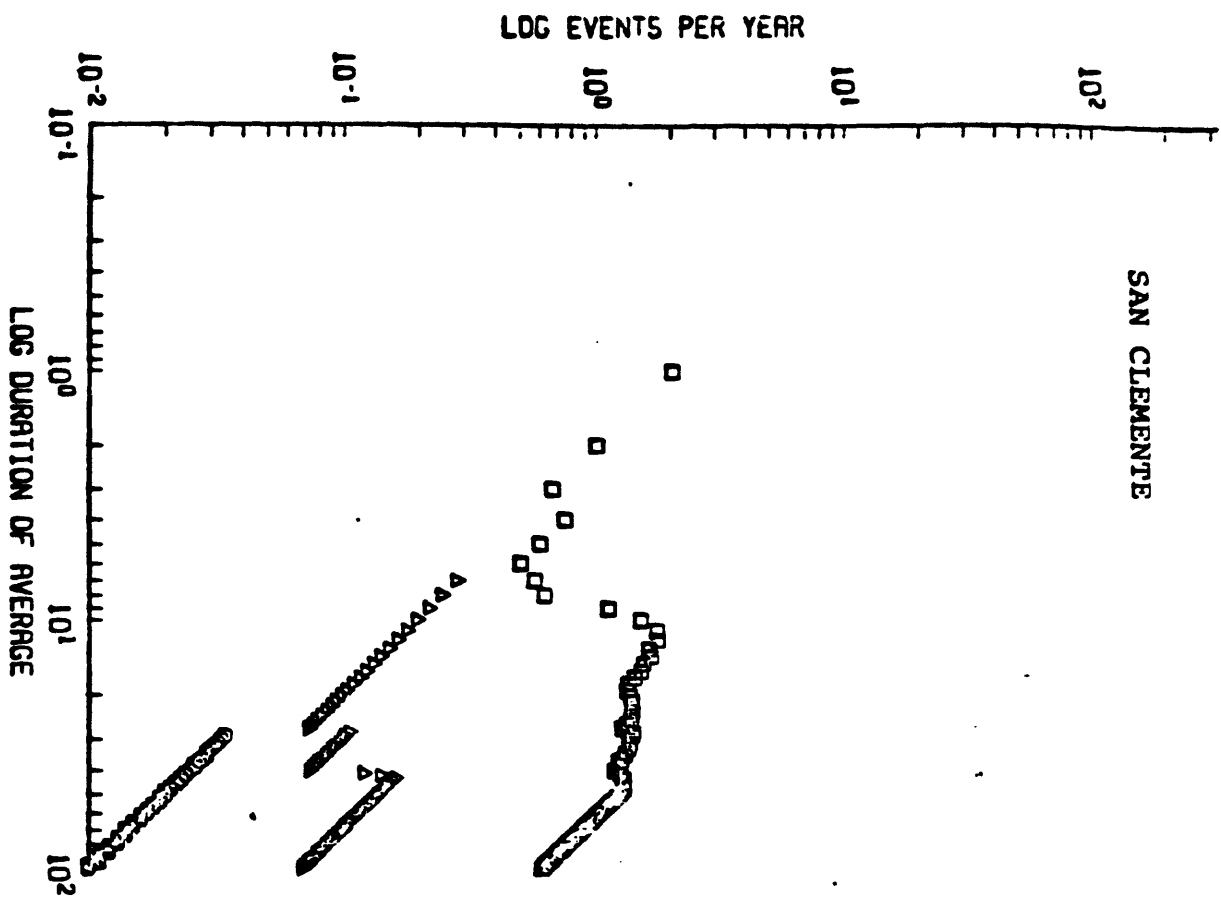


LOG EVENTS PER YEAR

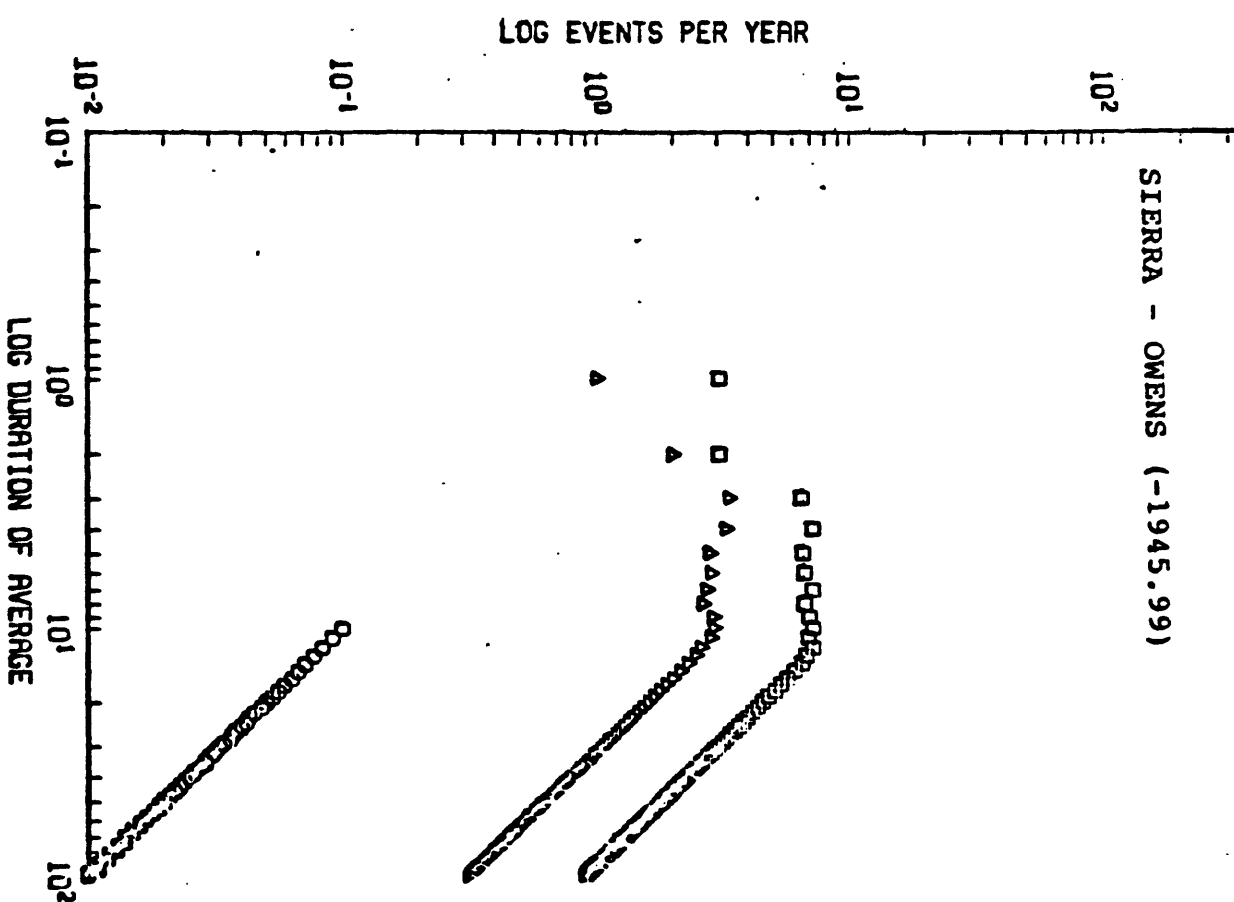


APPENDIX I-1

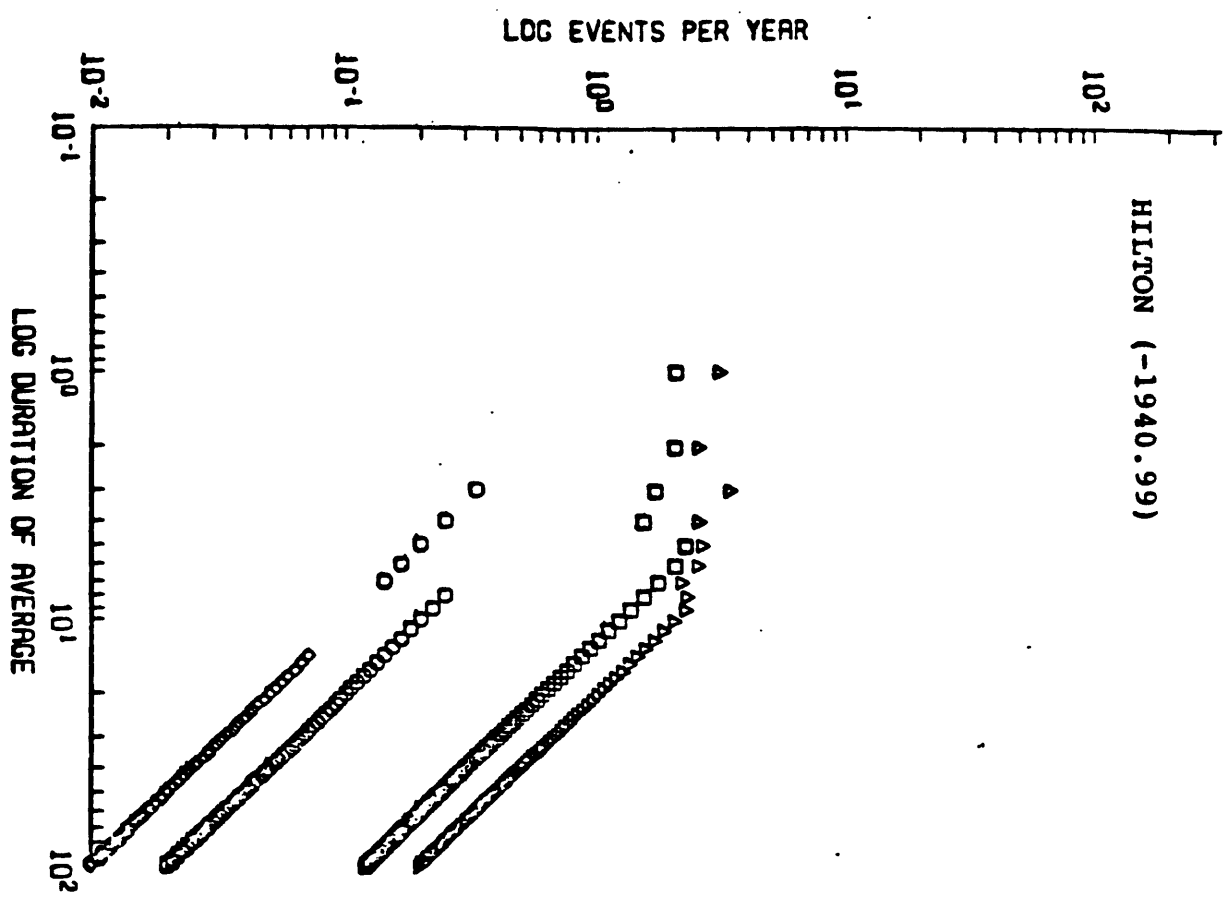
SAN CLEMENTE



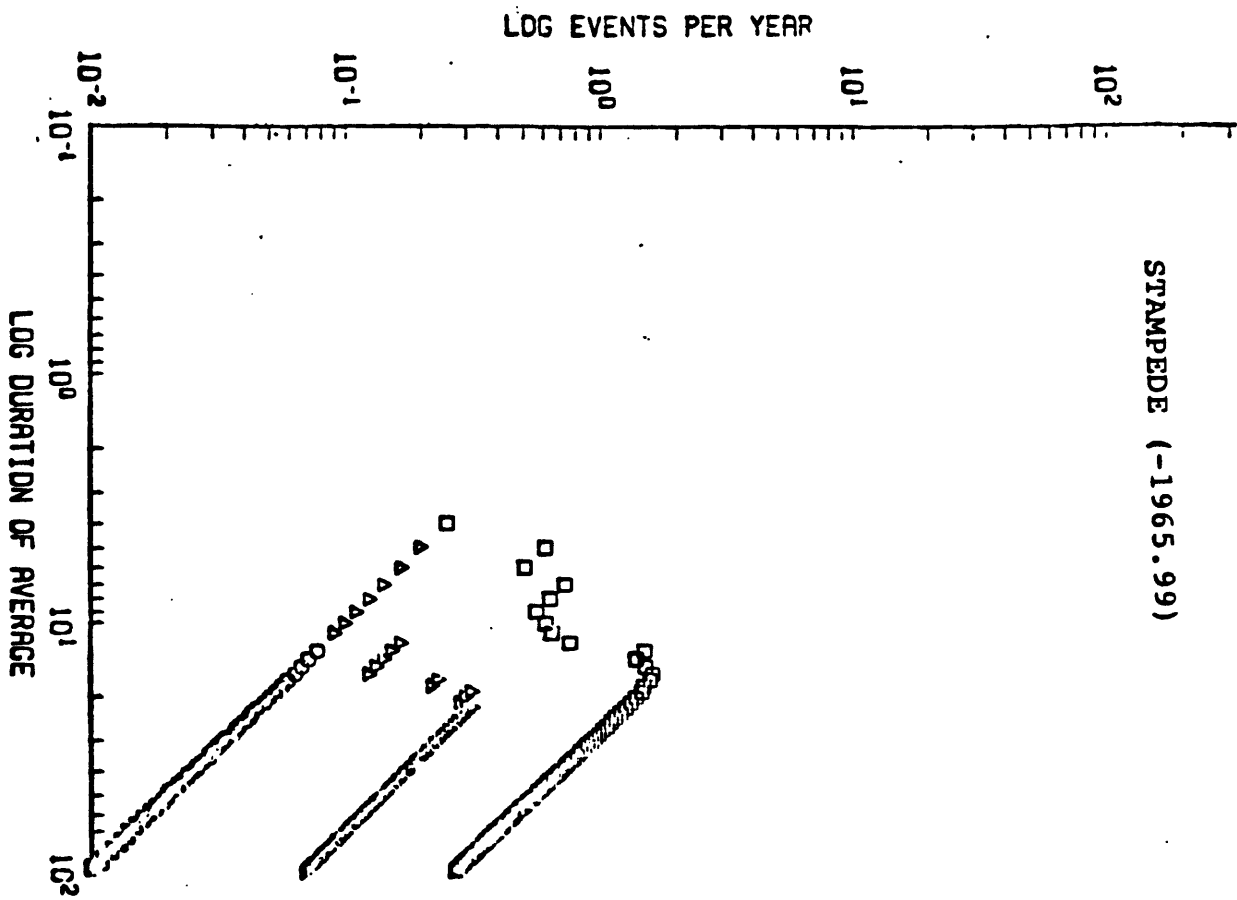
SIERRA - OWENS (-1945.99)



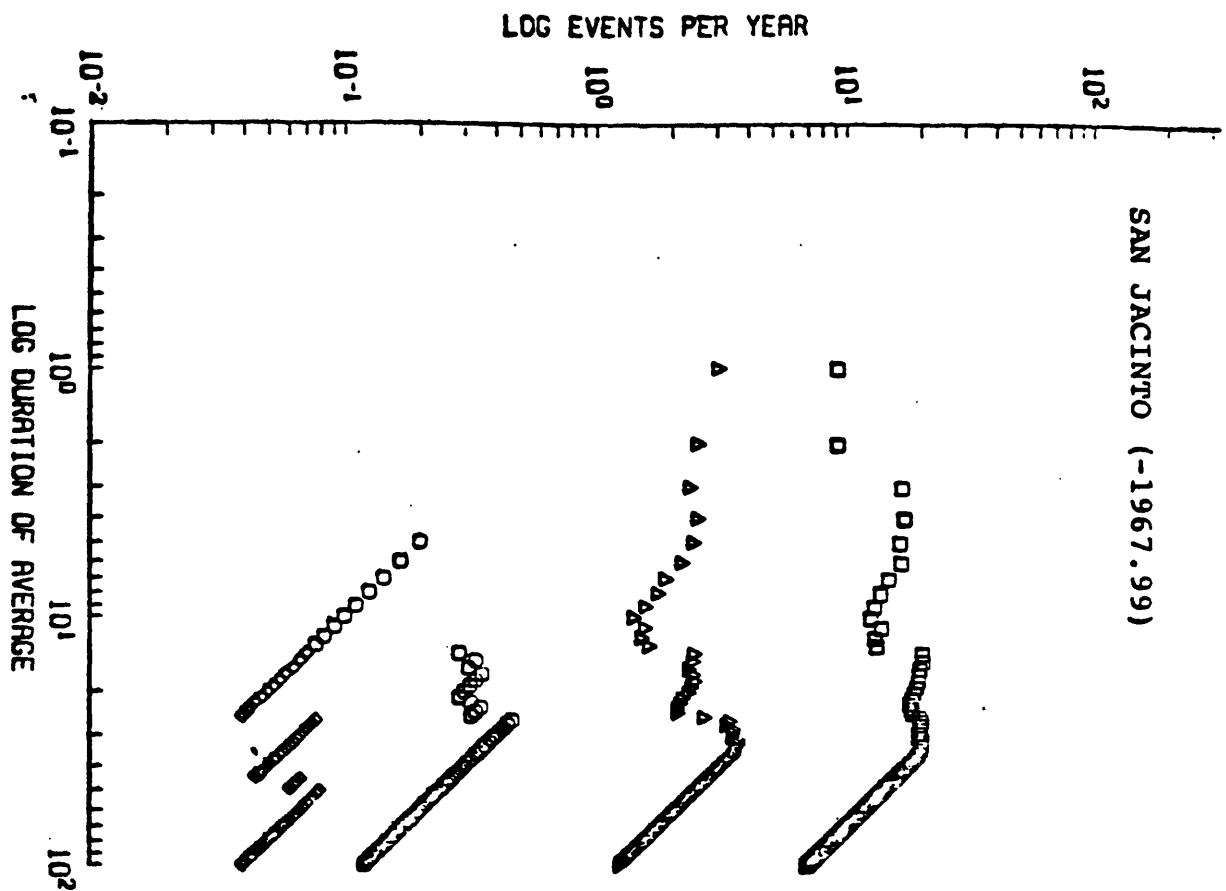
APPENDIX I-1



APPENDIX I-1

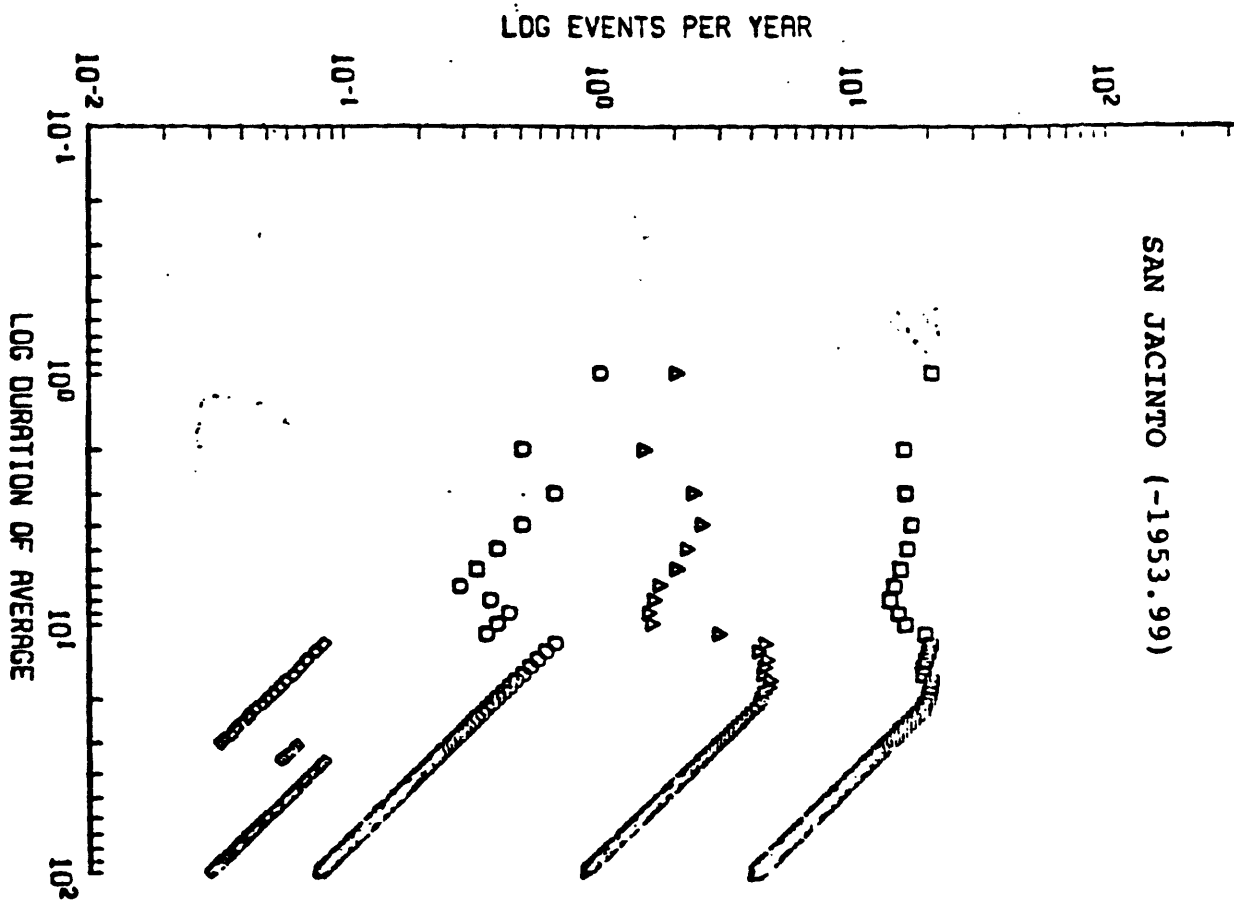


SAN JACINTO (-1967.99)

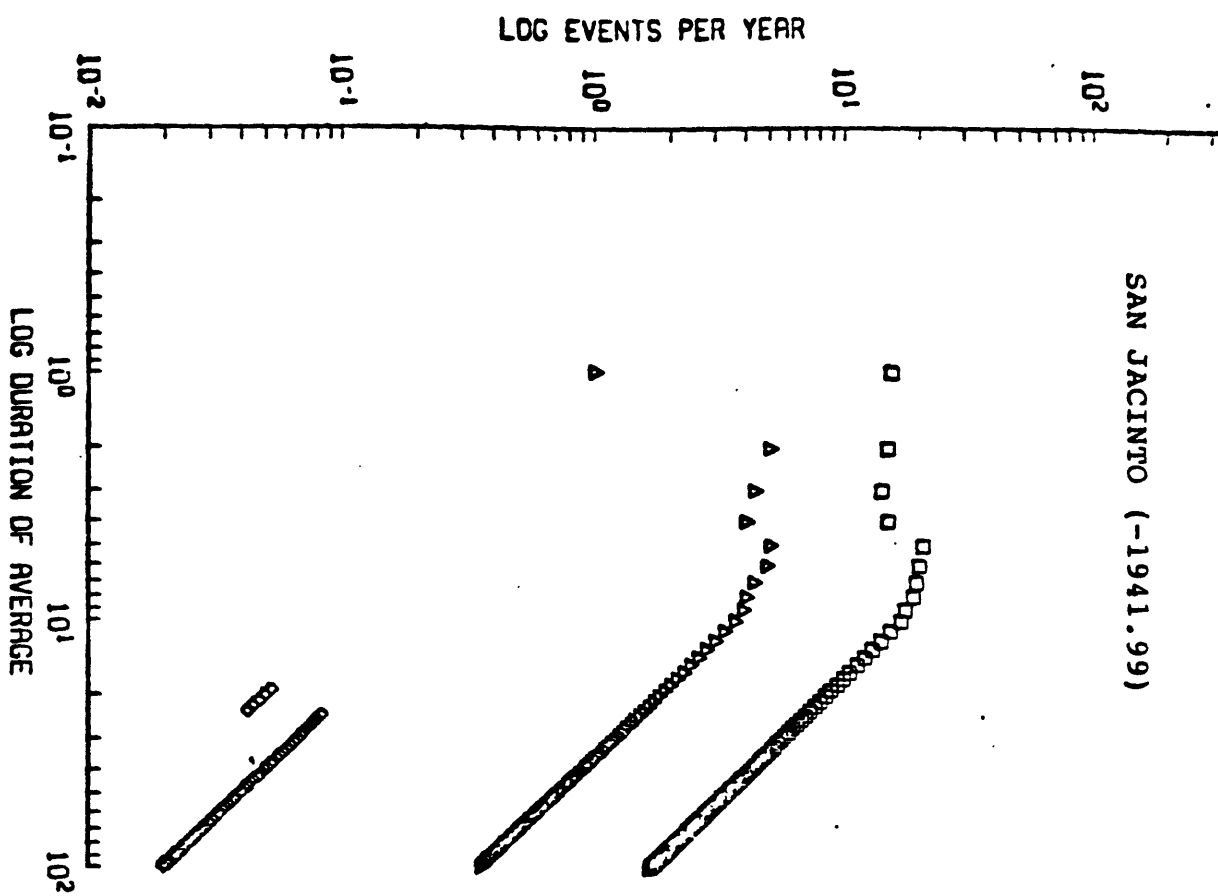


APPENDIX I-1

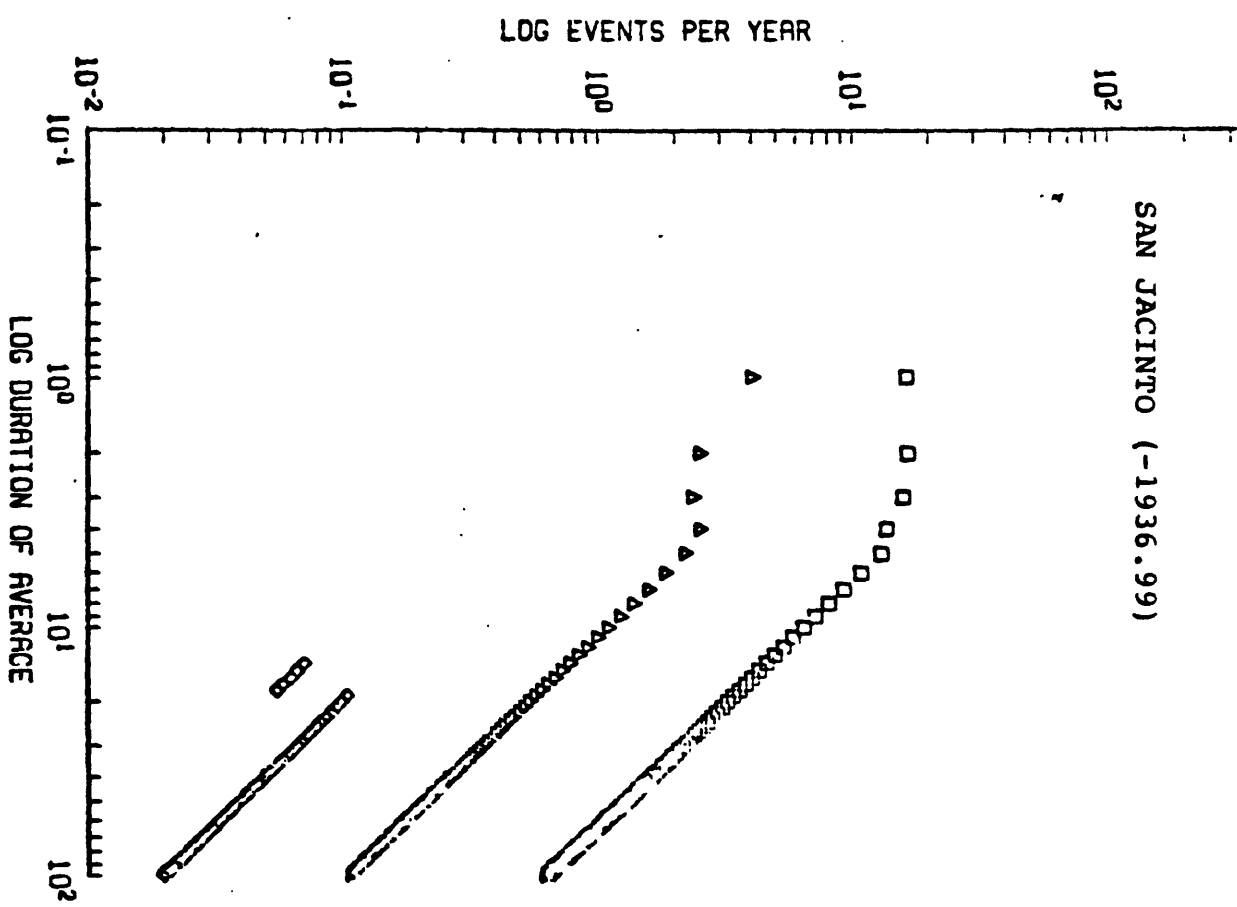
SAN JACINTO (-1953.99)



SAN JACINTO (-1941.99)

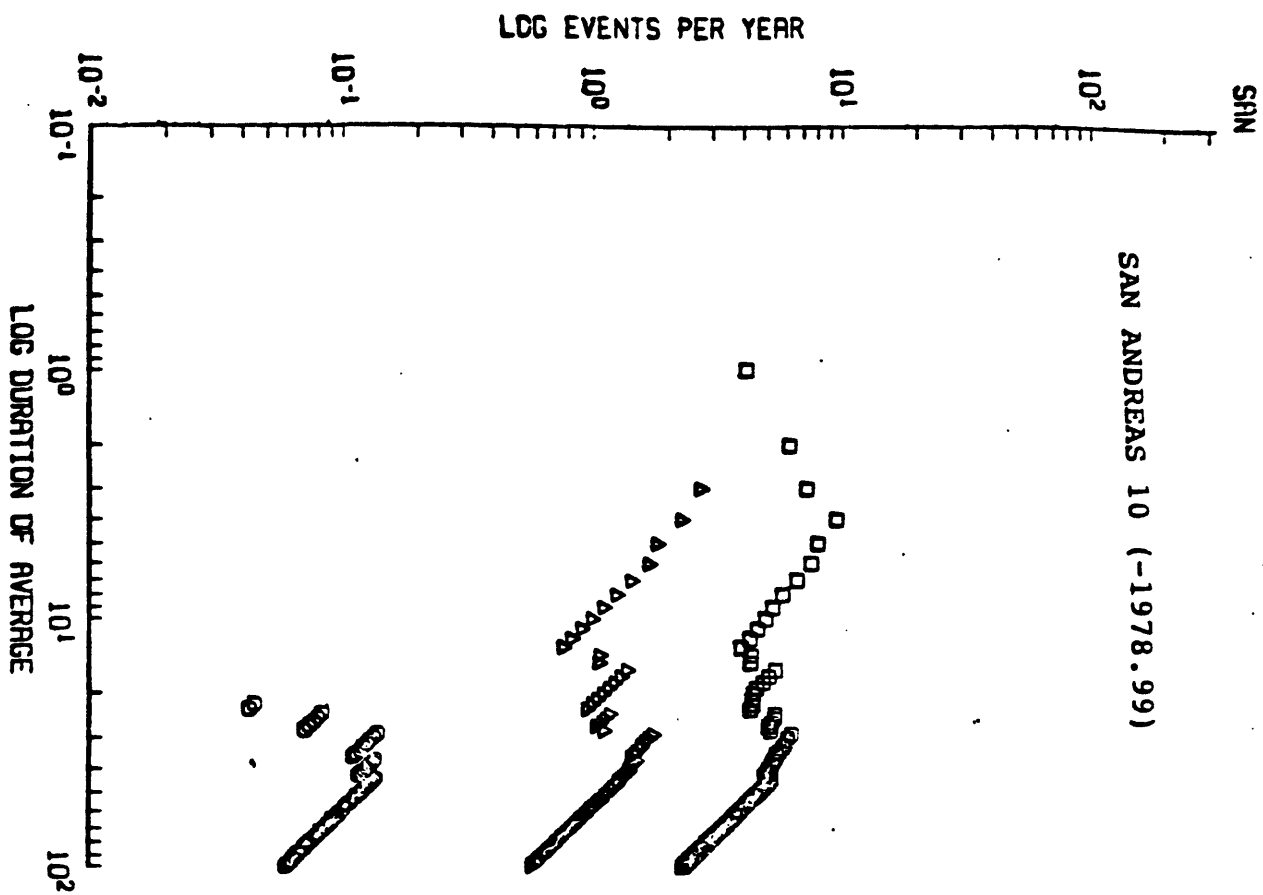


SAN JACINTO (-1936.99)

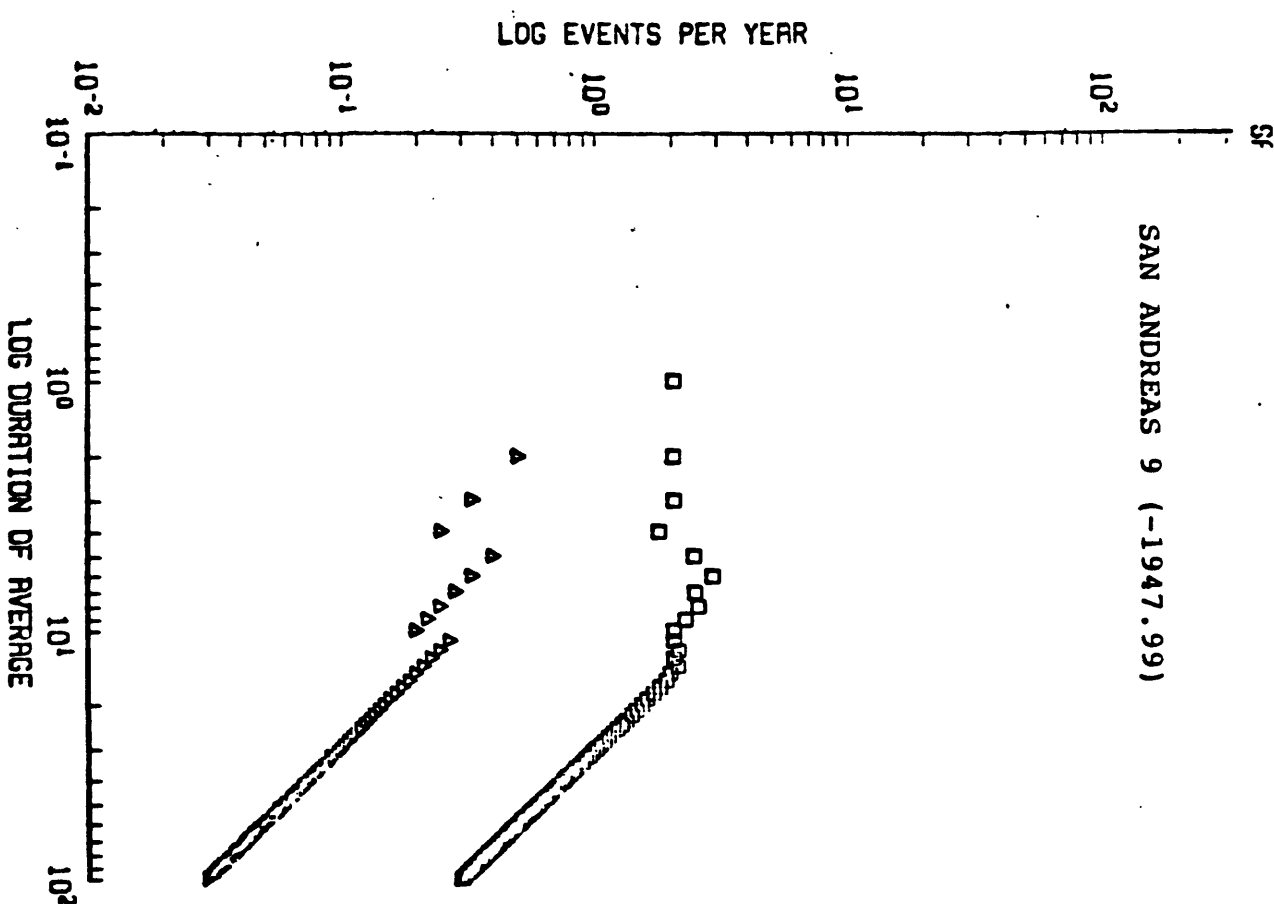


APPENDIX I-1

SAN ANDREAS 10 (-1978.99)



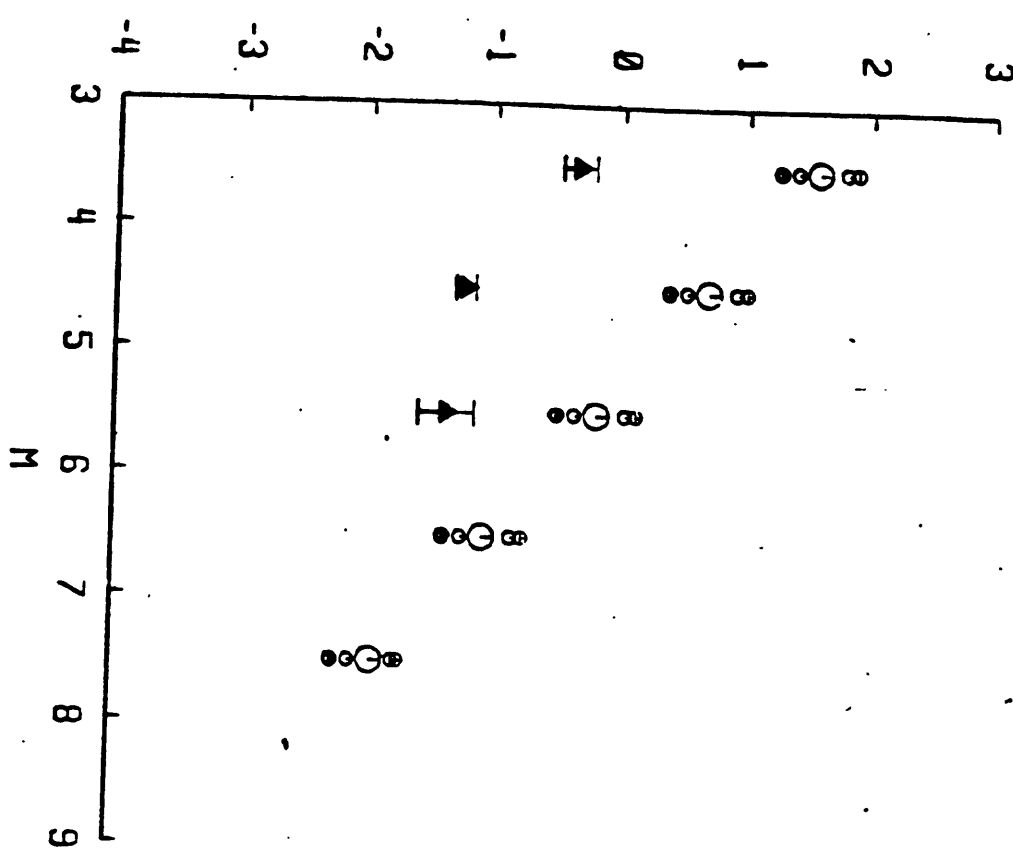
SAN ANDREAS 9 (-1947.99)



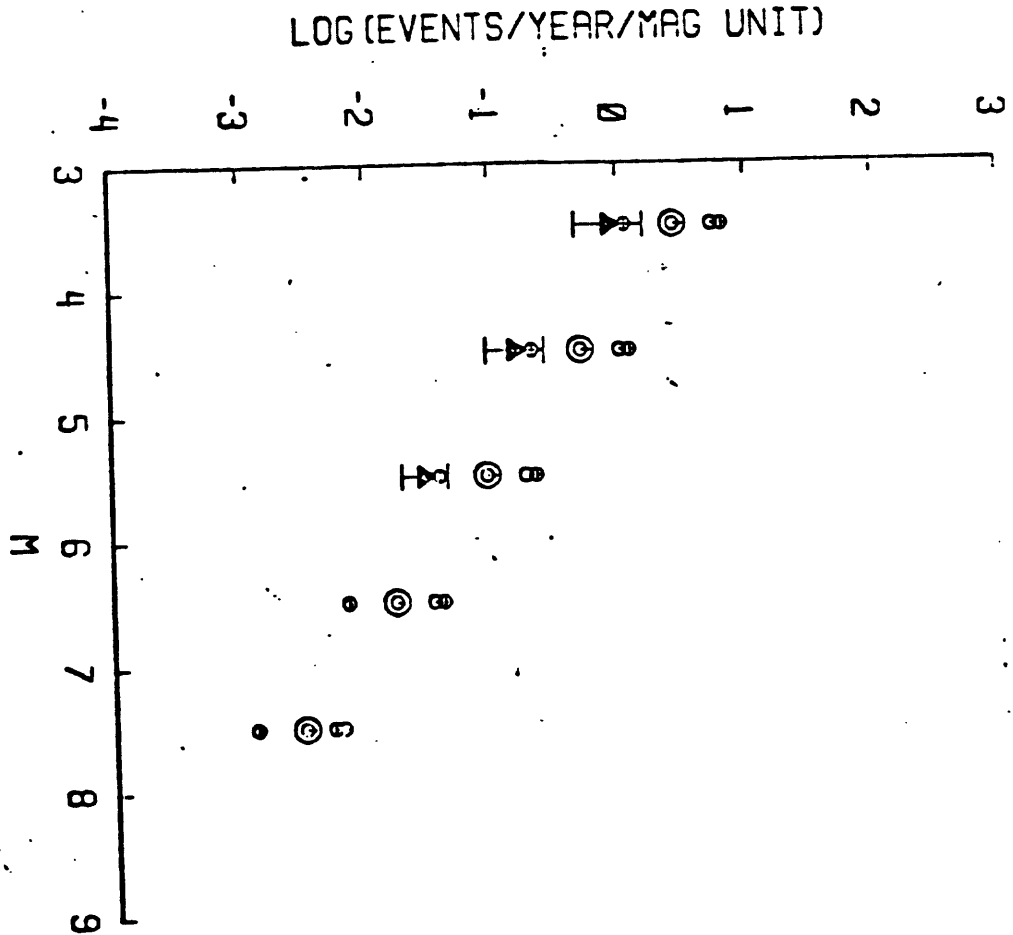
APPENDIX I-2

Plots of observed incremental occurrence rates of earthquakes (solid triangle) and of predicted occurrence rates based on the slip rates. Large open symbols give best slip rate estimate; smaller symbols correspond to estimates for extreme ranges of proposed slip rates in Table 4, and to estimates for best slip rate but with a 0.5 magnitude unit increase or decrease in theoretical maximum magnitude from the values listed in Table 4.

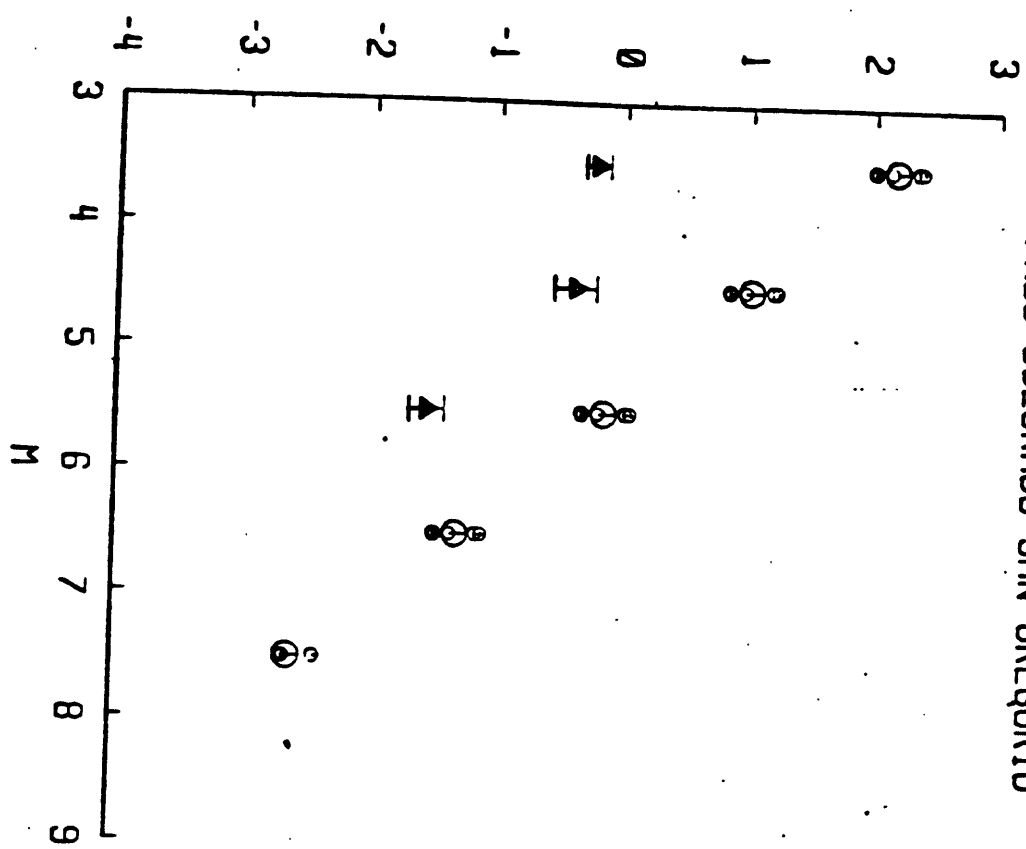
SAN ANDREAS 1



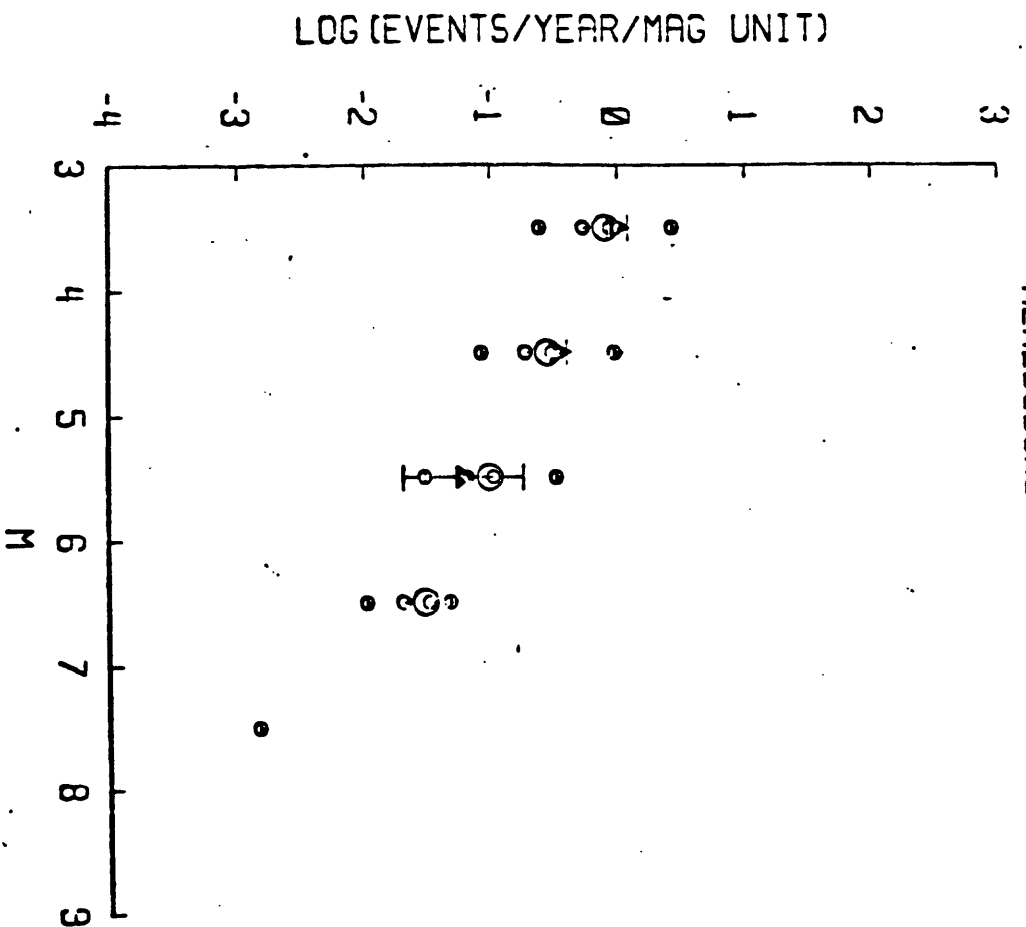
SAN ANDREAS 2

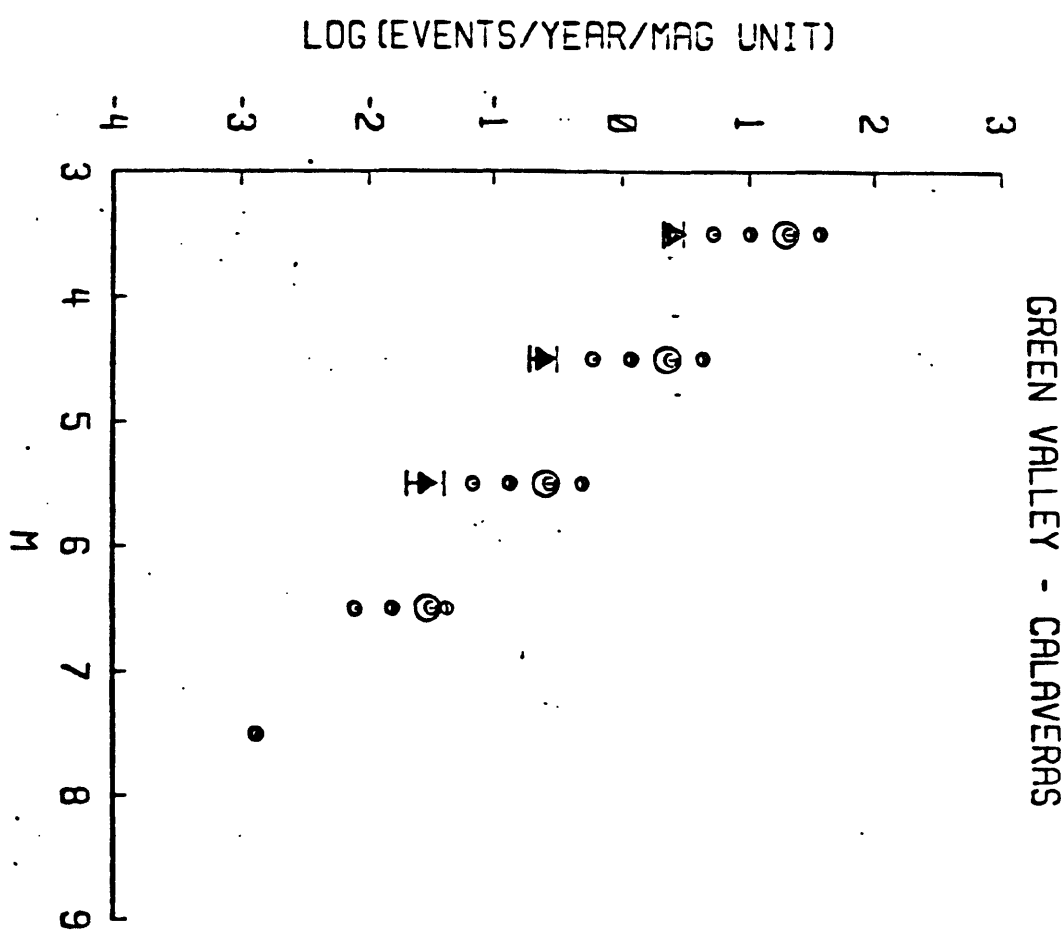
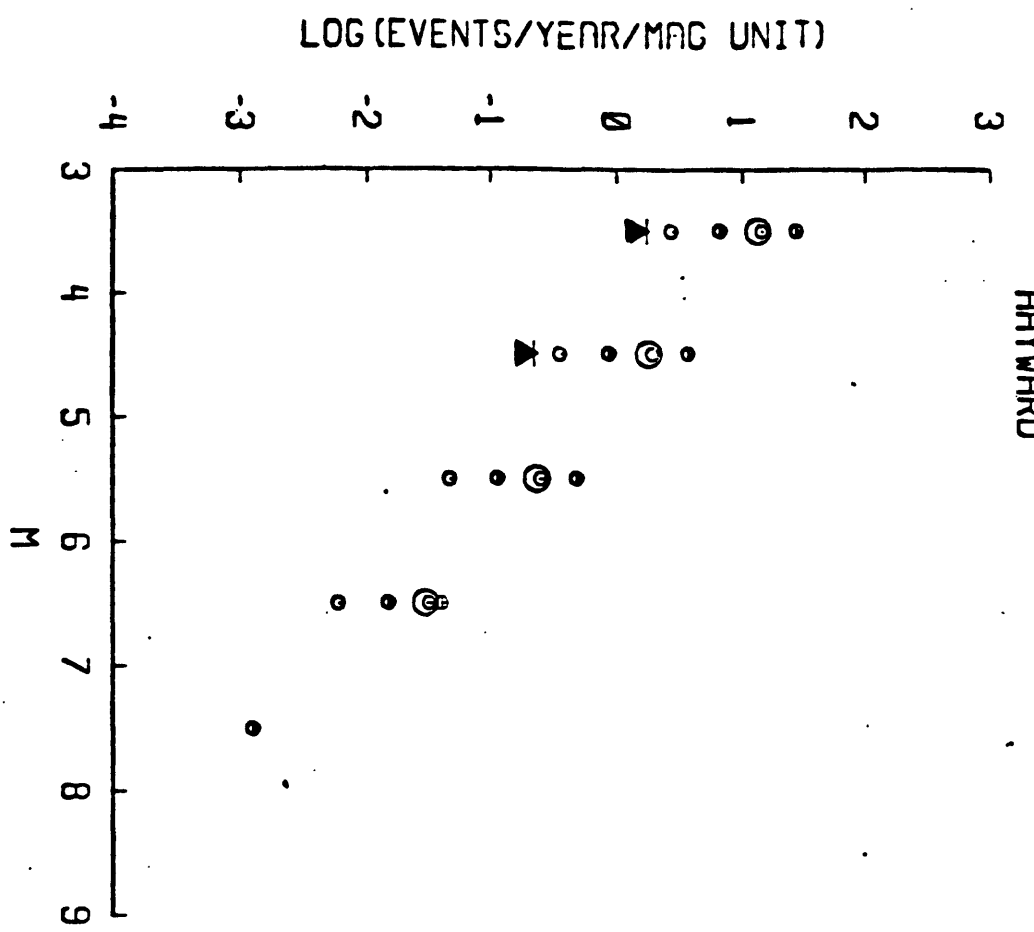


PALO COLORADO-SAN GREGORIO

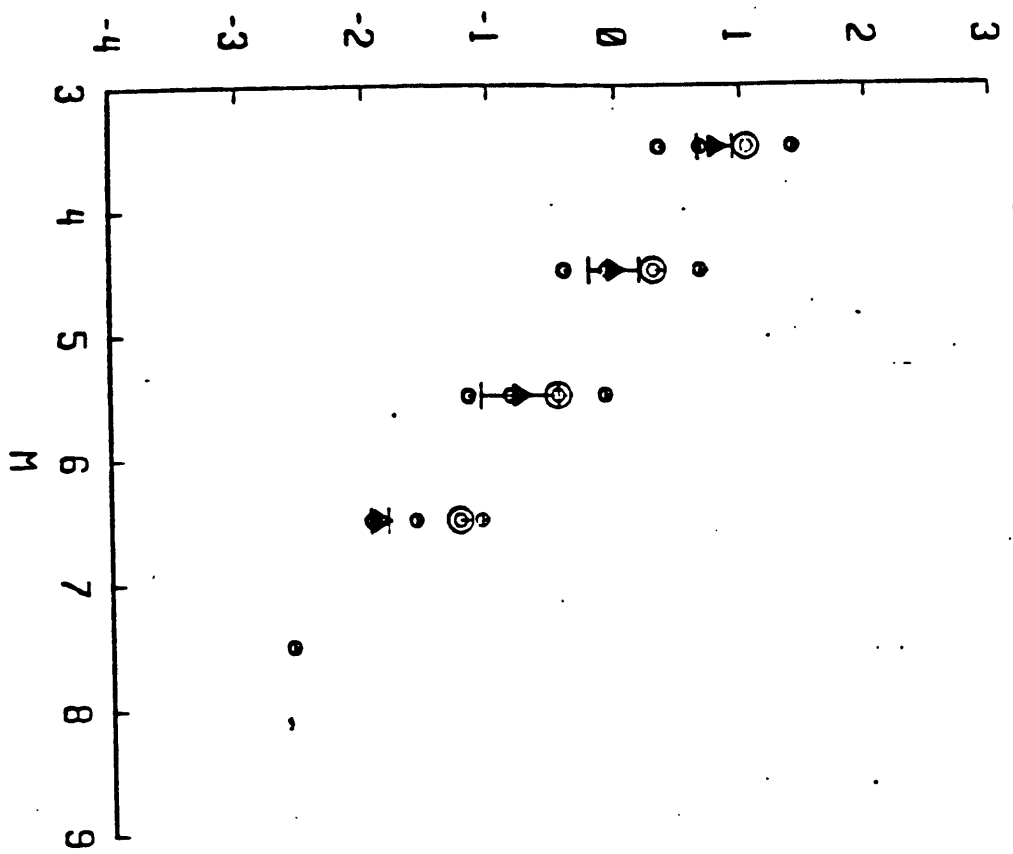


HEALDSBURG - ROGERS CREEK





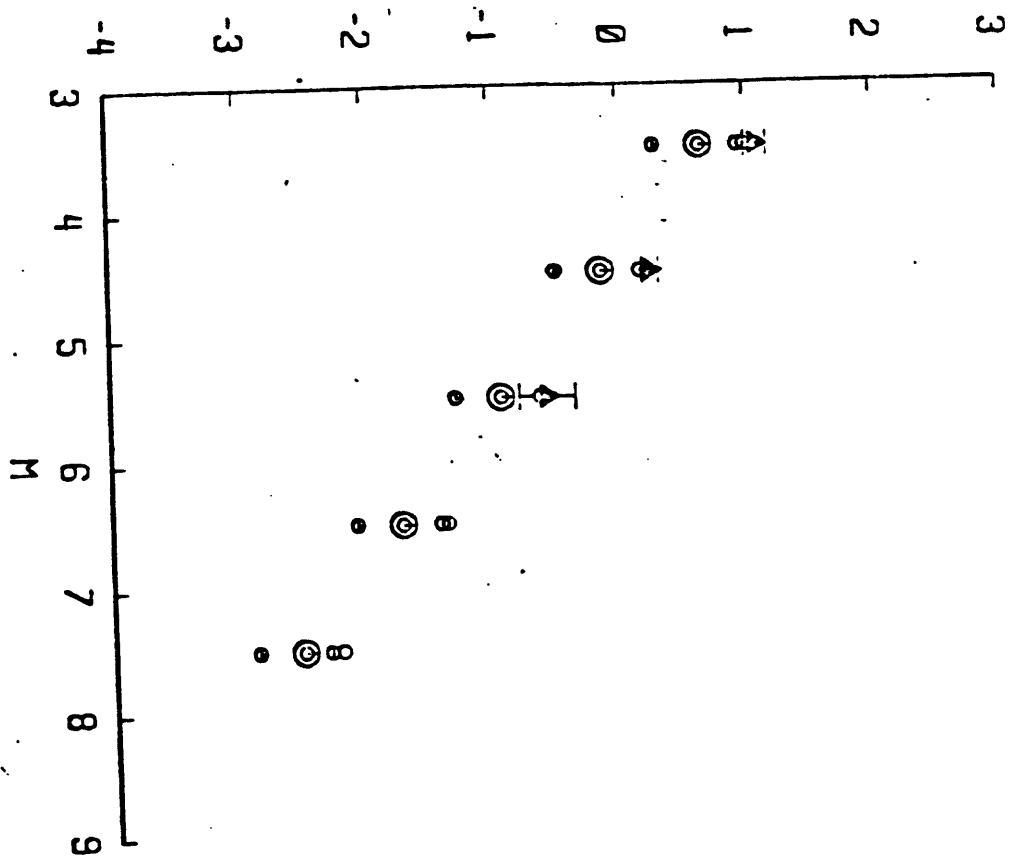
LOC (EVENTS/YEAR/MAG UNIT)



CALAVERAS - HAYWARD

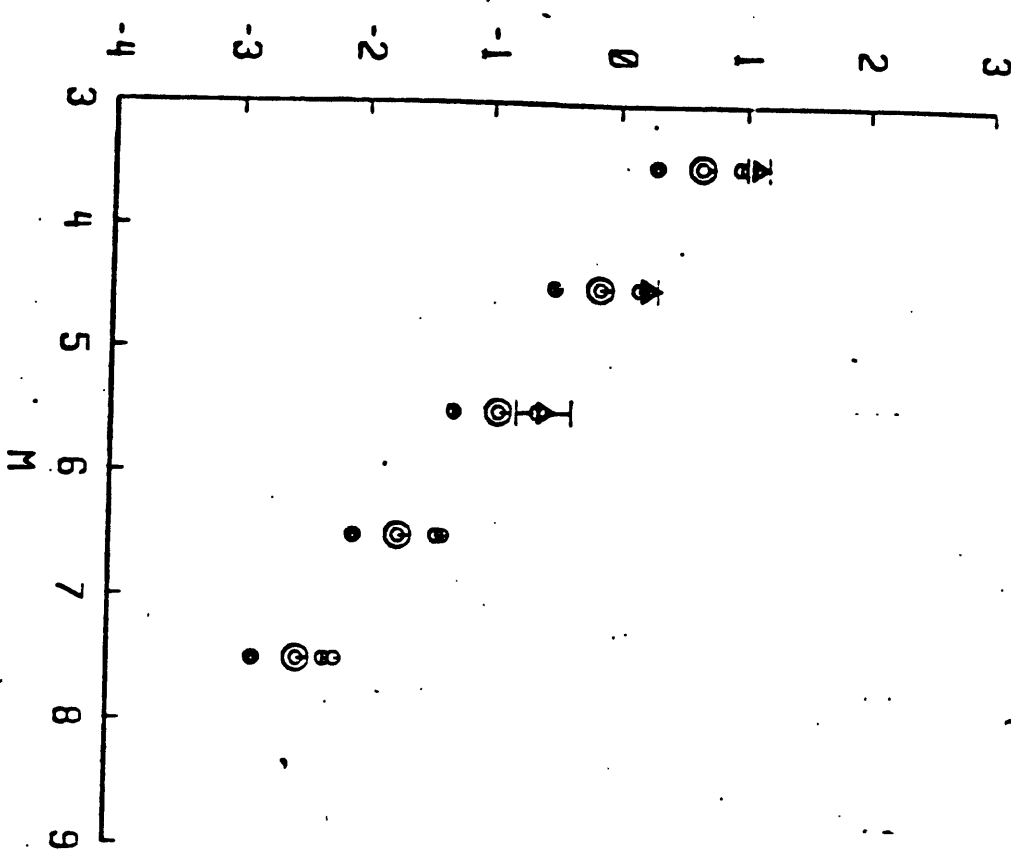
APPENDIX I-2

LOG (EVENTS/YEAR/MAG UNIT)

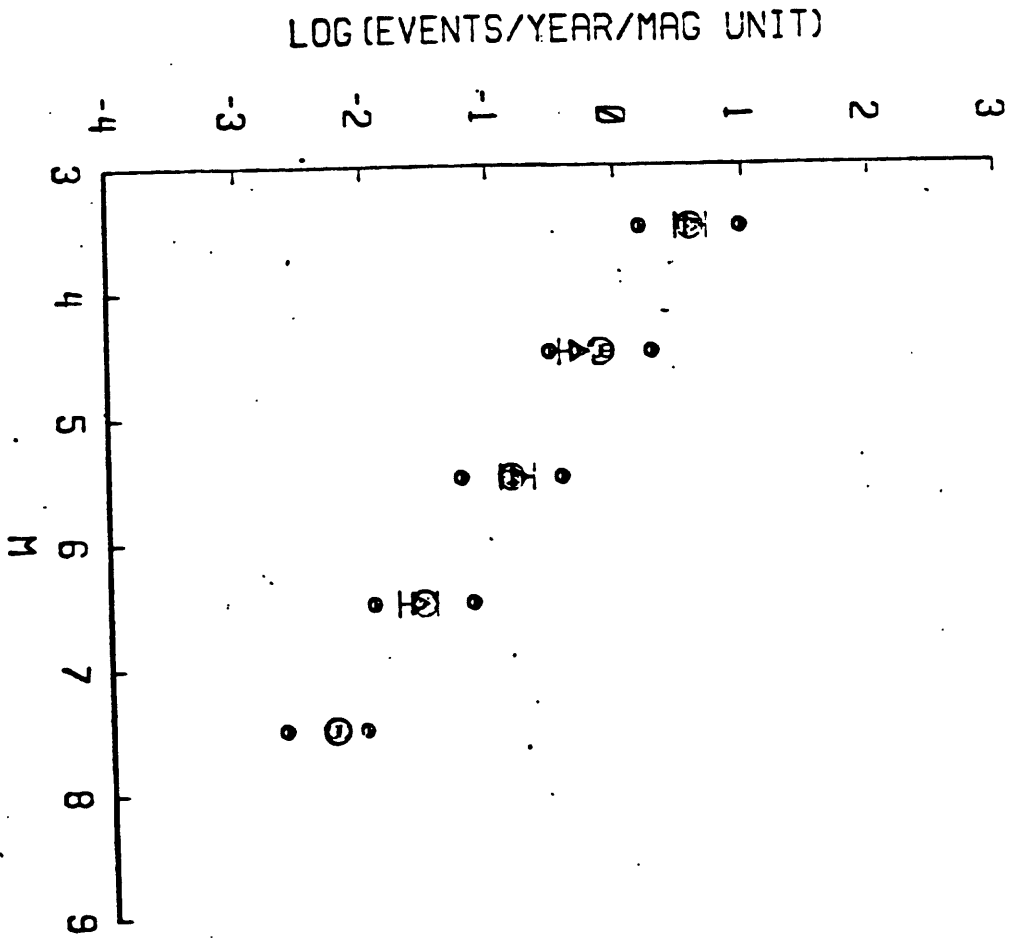


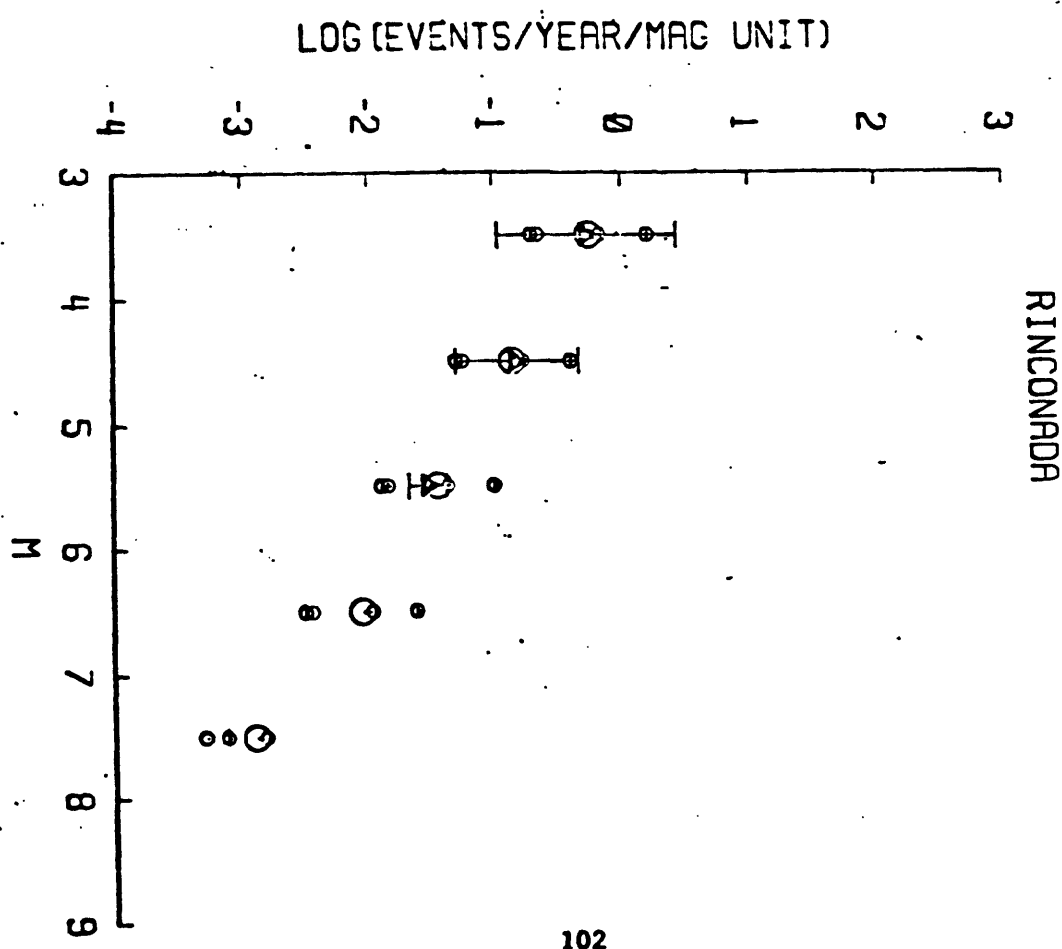
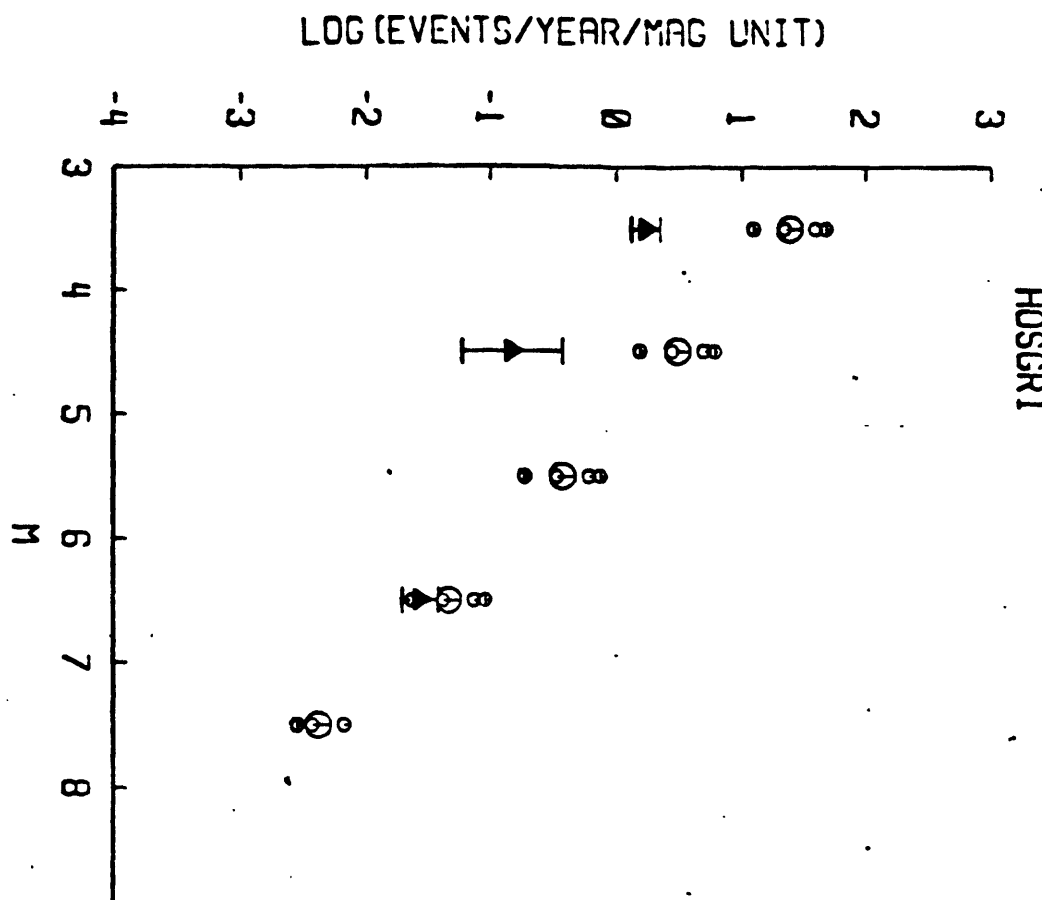
SAN ANDREAS

SAN ANDREAS 3

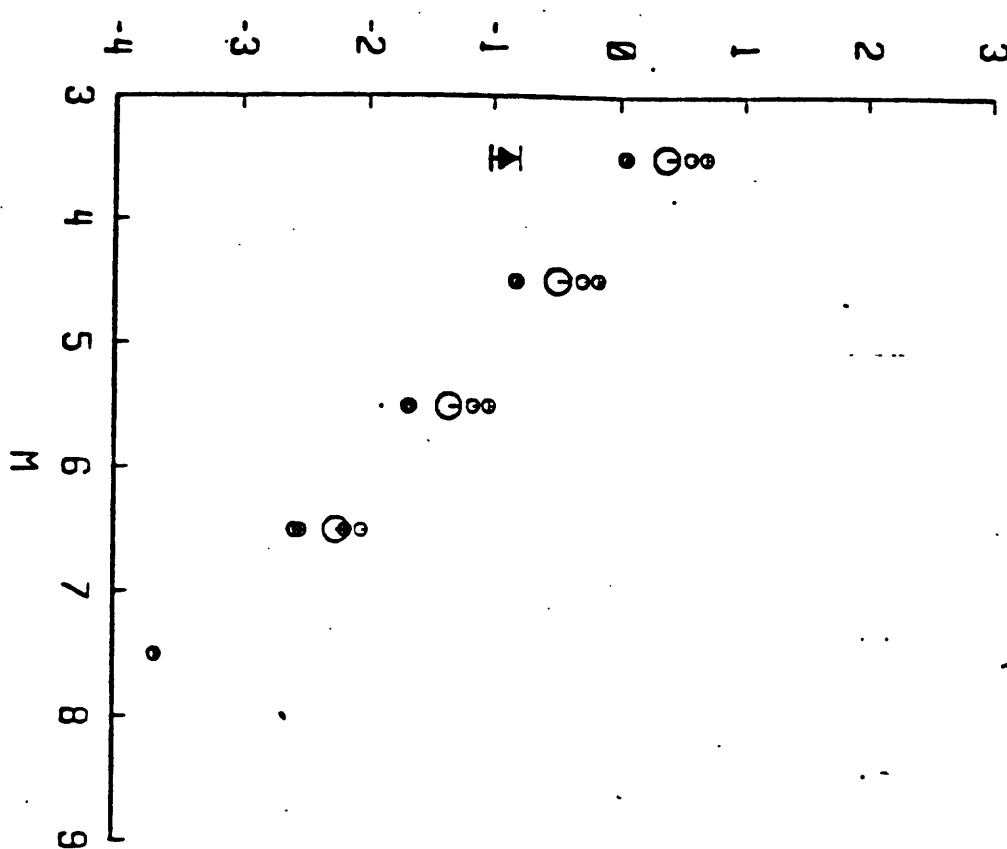


SAN ANDREAS

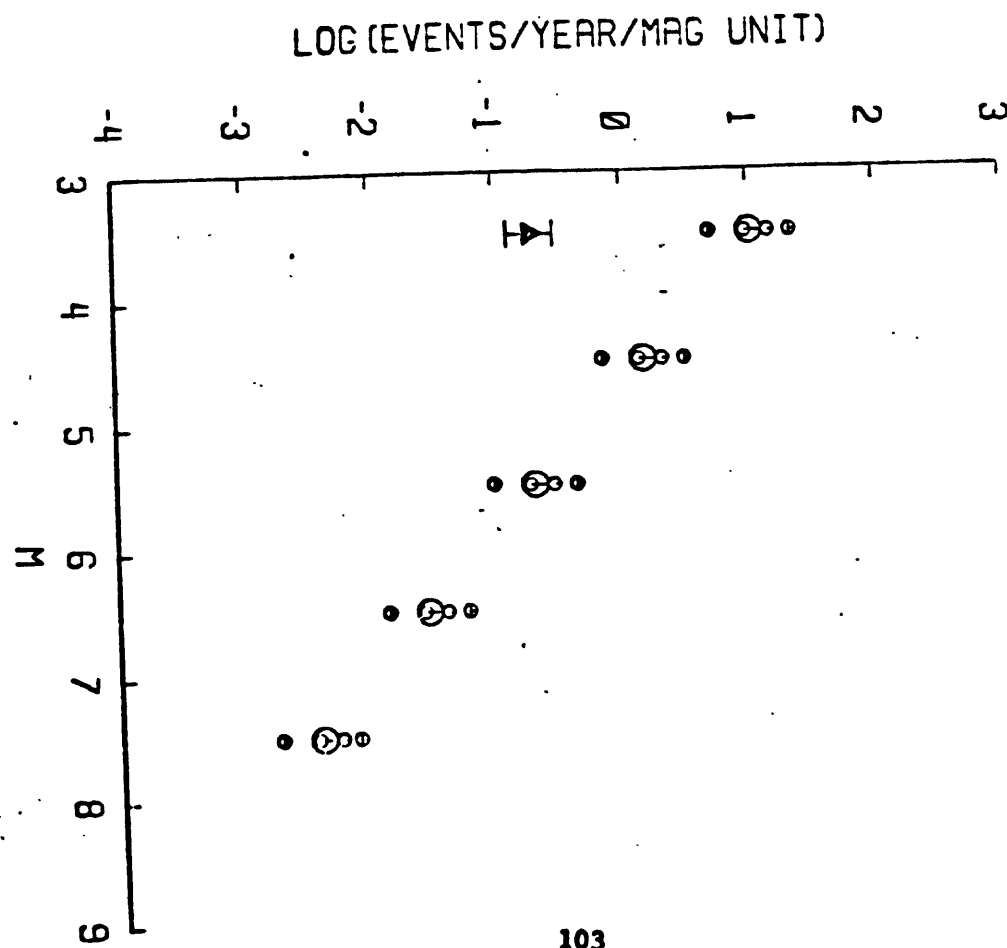




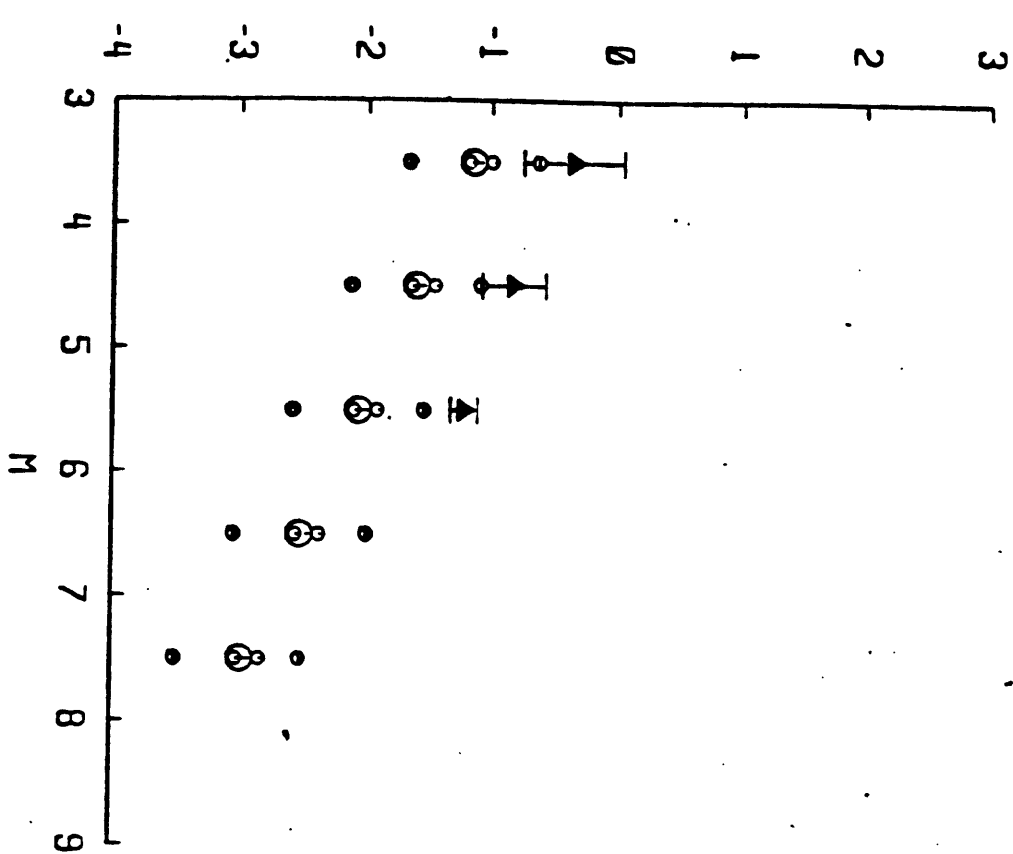
SAN JUAN



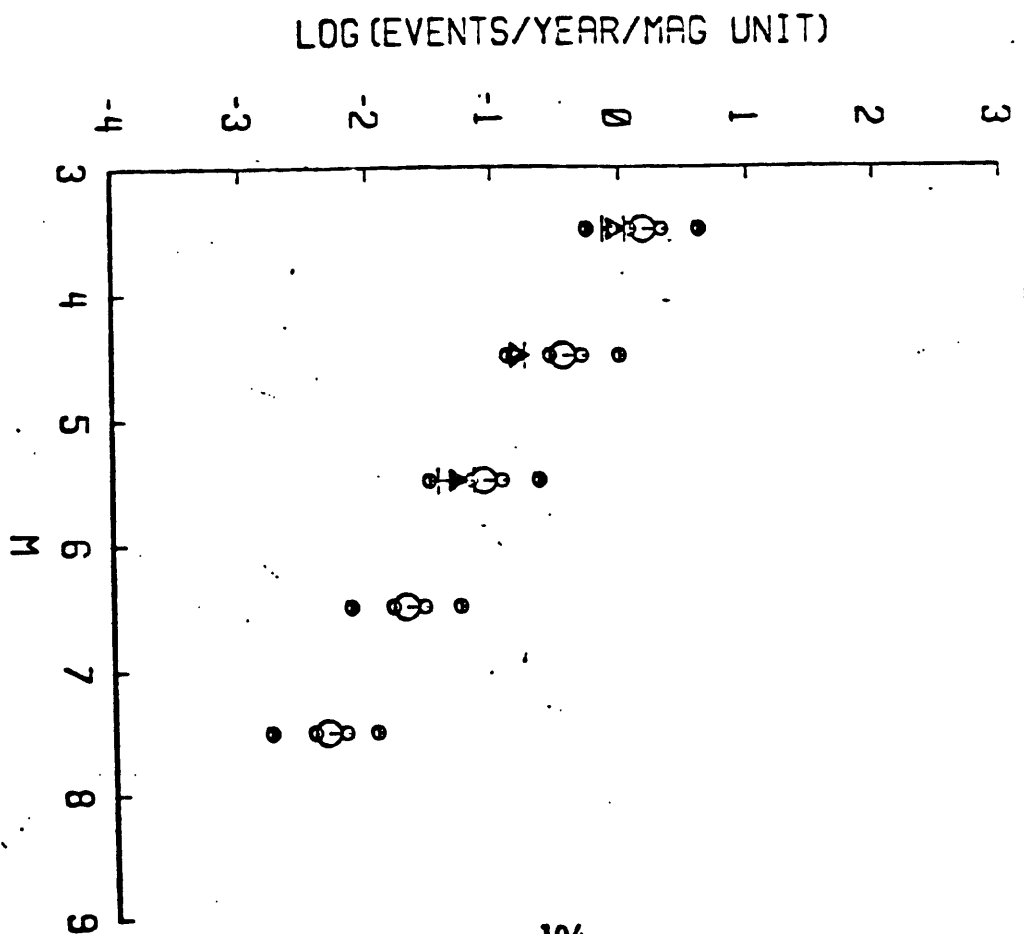
SAN ANDREAS



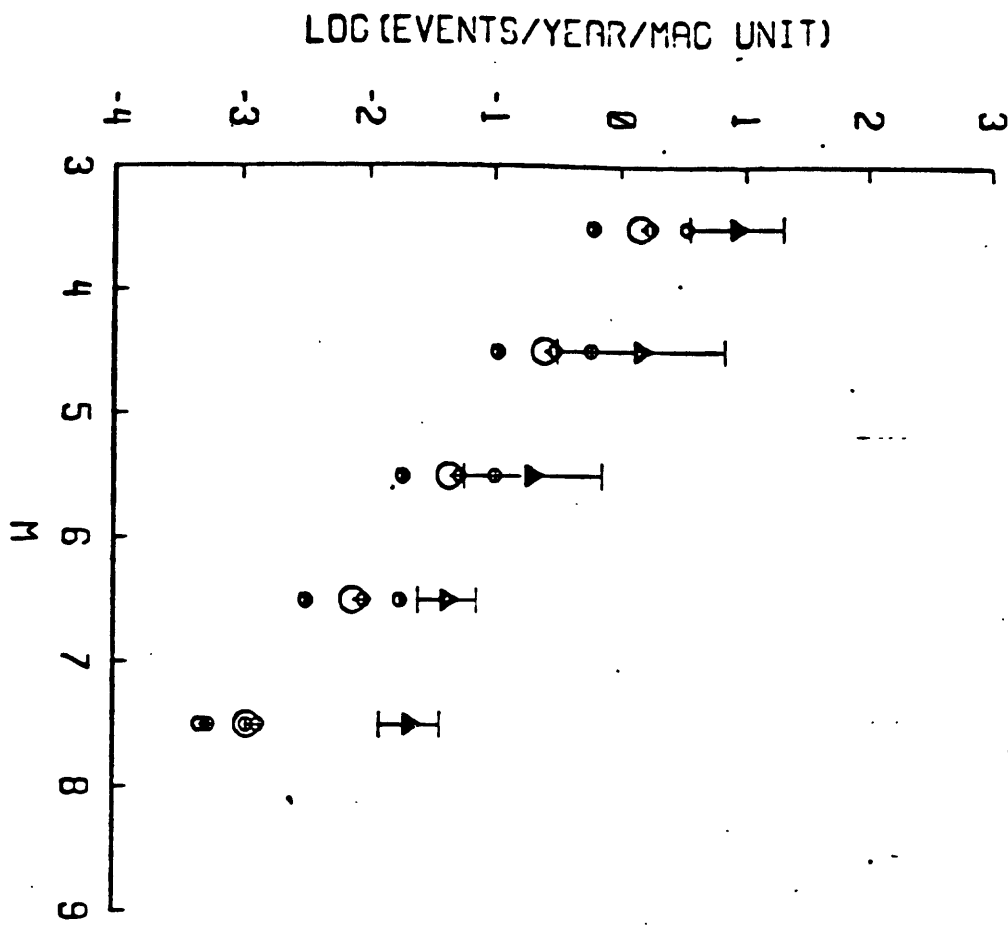
SAN ANDREAS



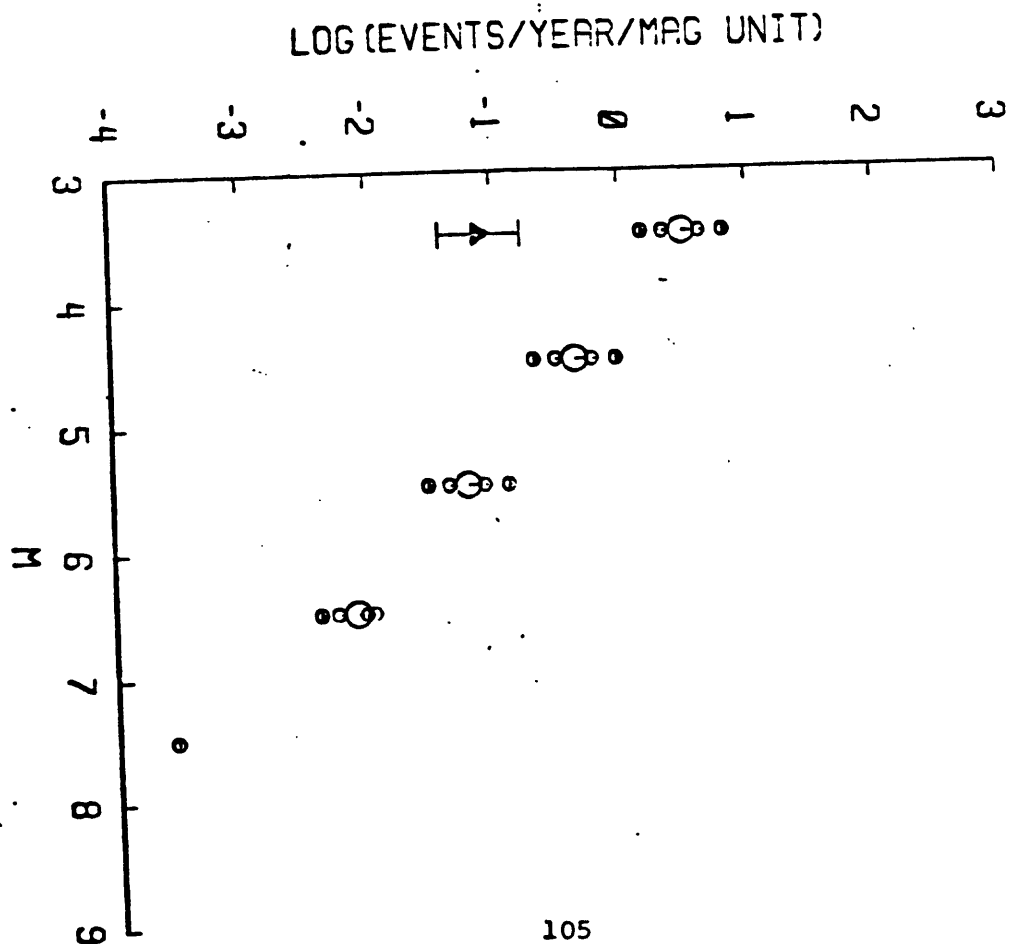
SAN ANDREAS



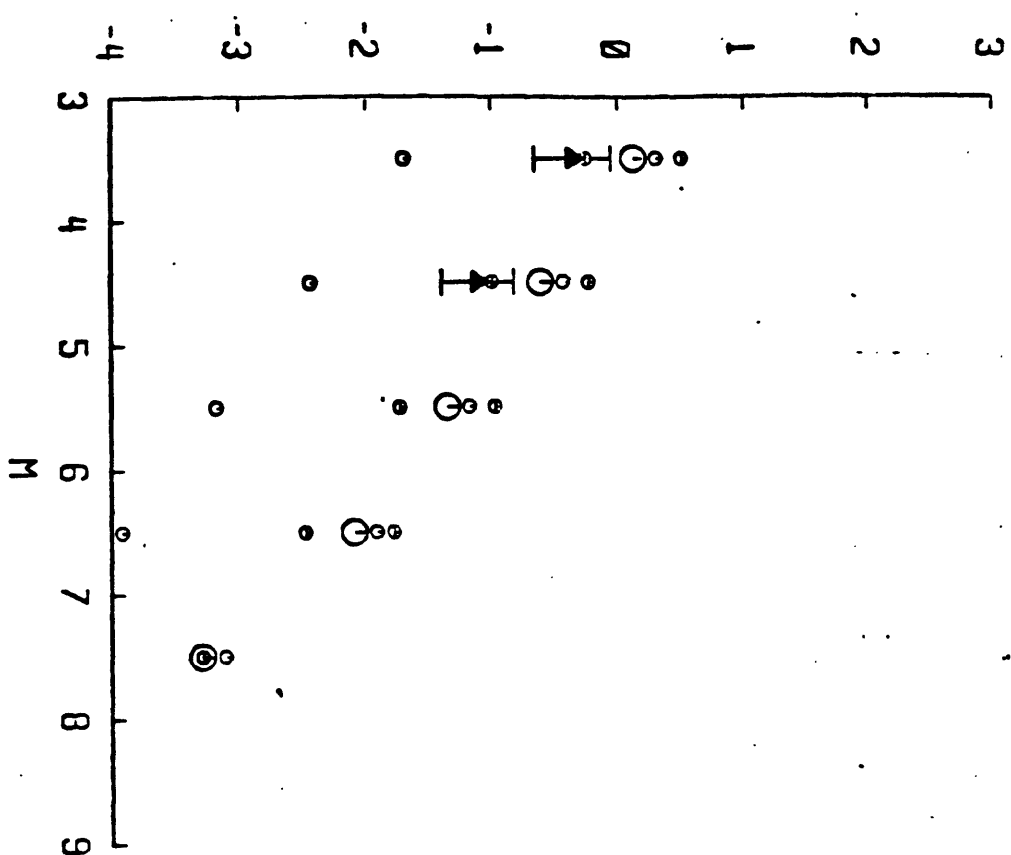
PLEITO - WHITE WOLF



BIG PINE

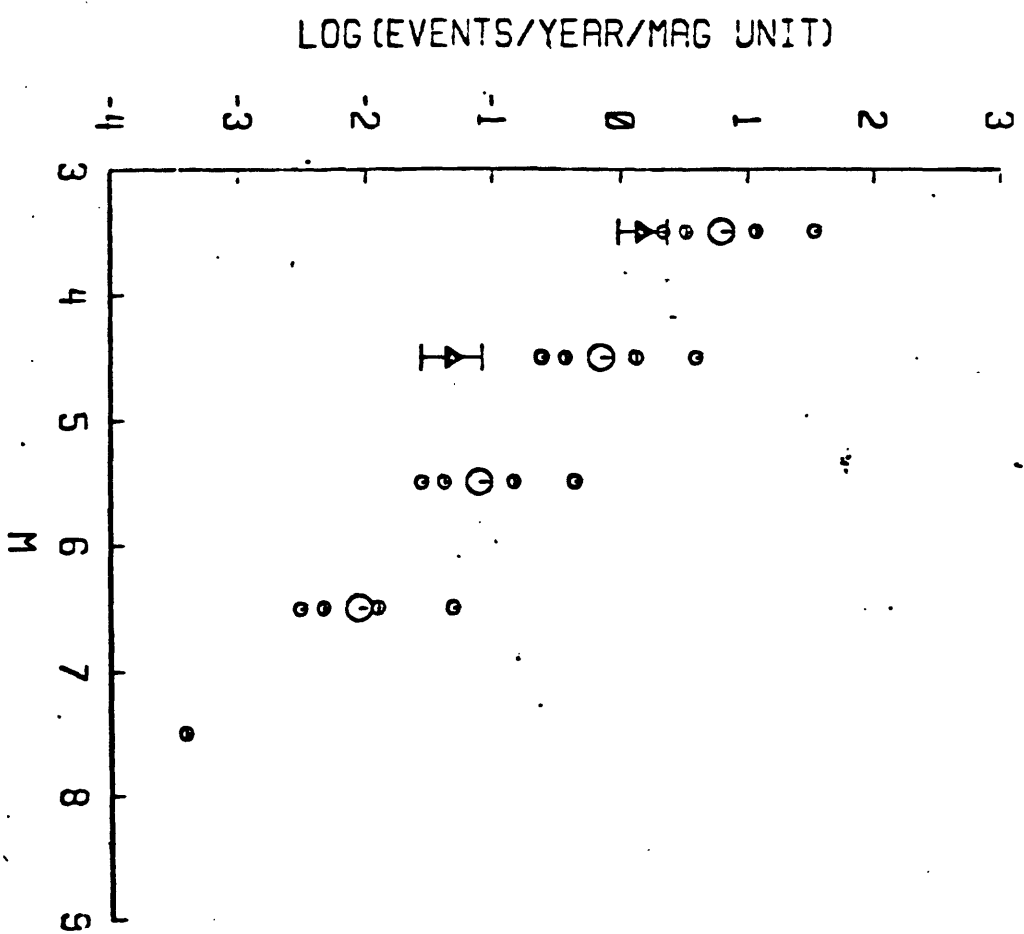


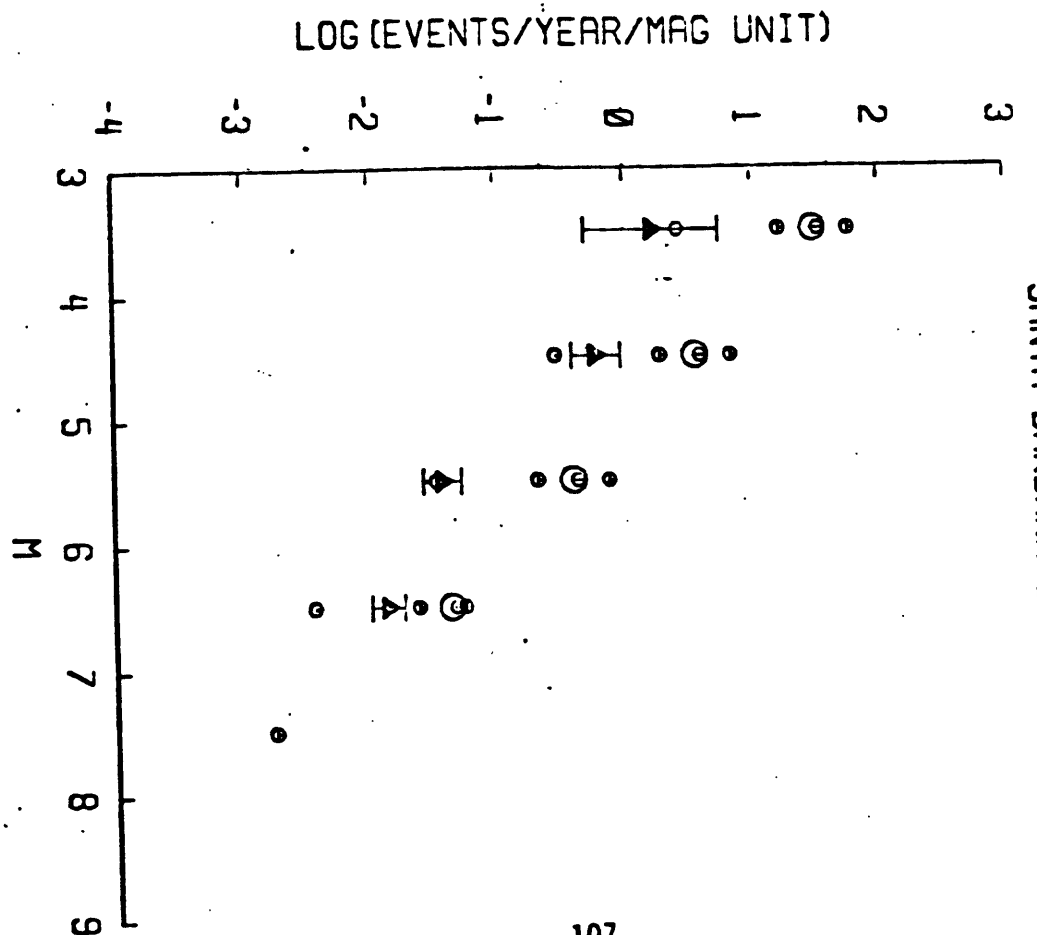
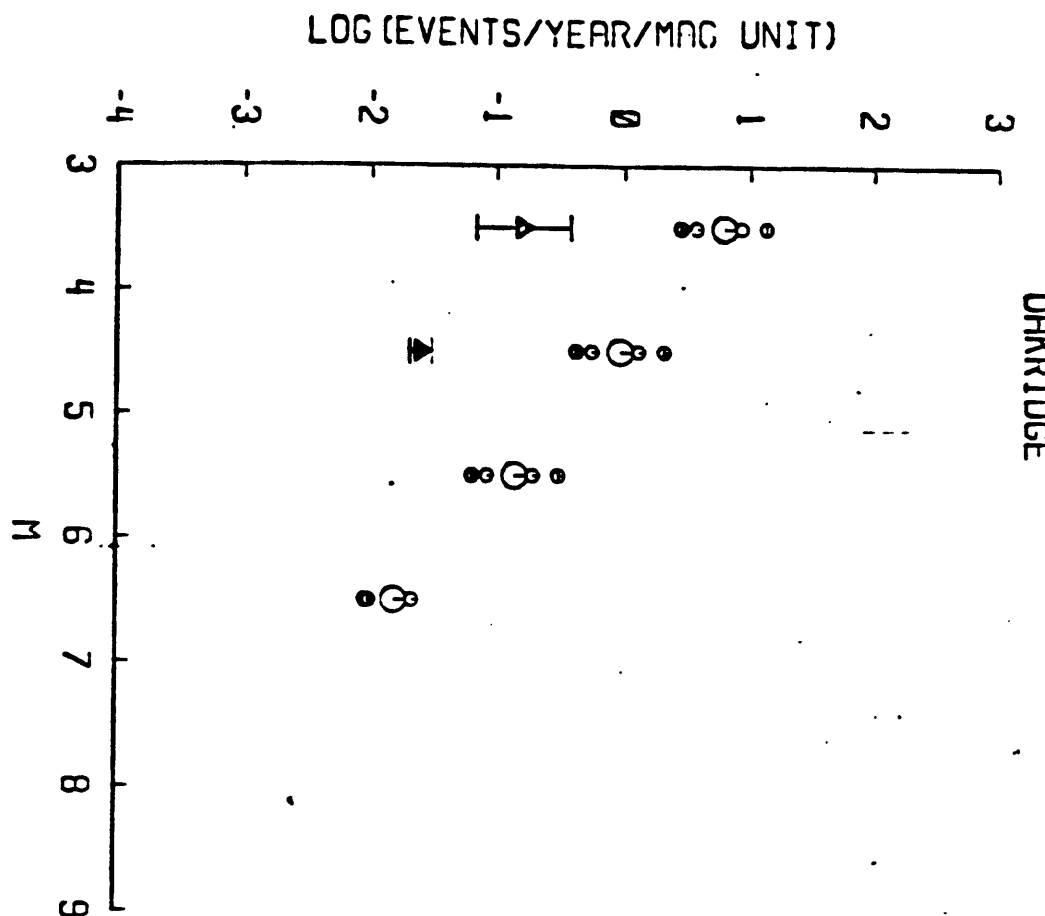
SANTA YNEZ



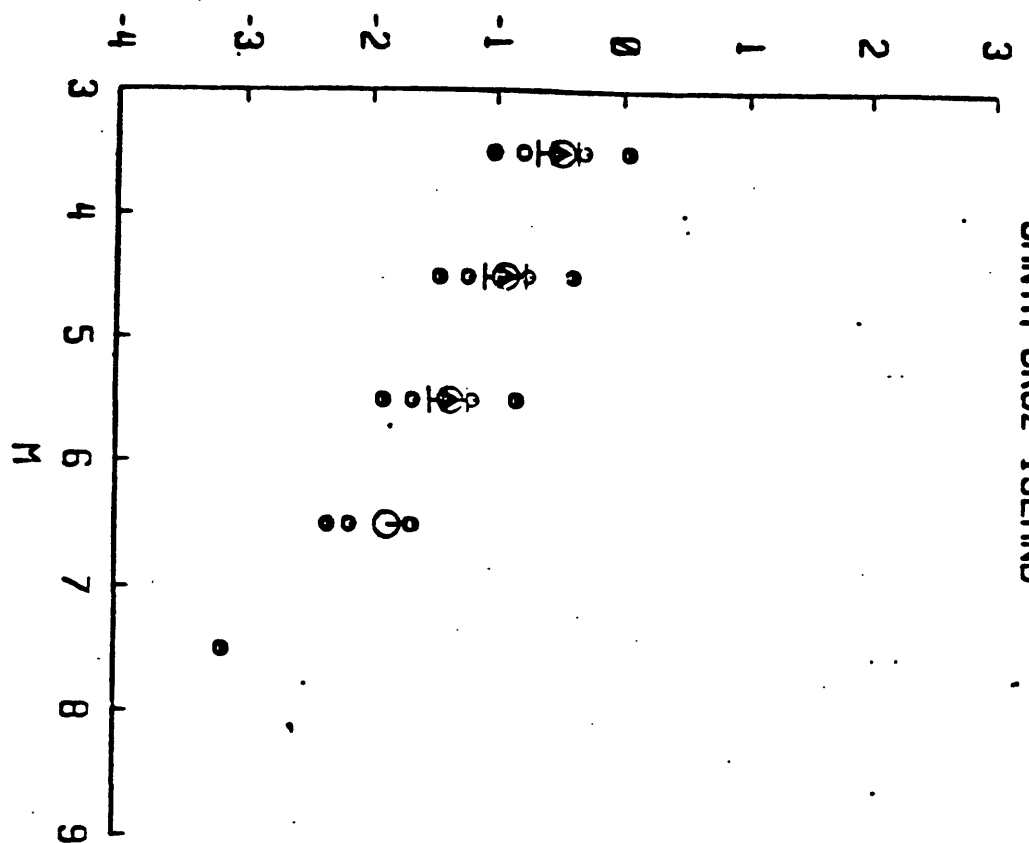
ARROYO

PARADISE





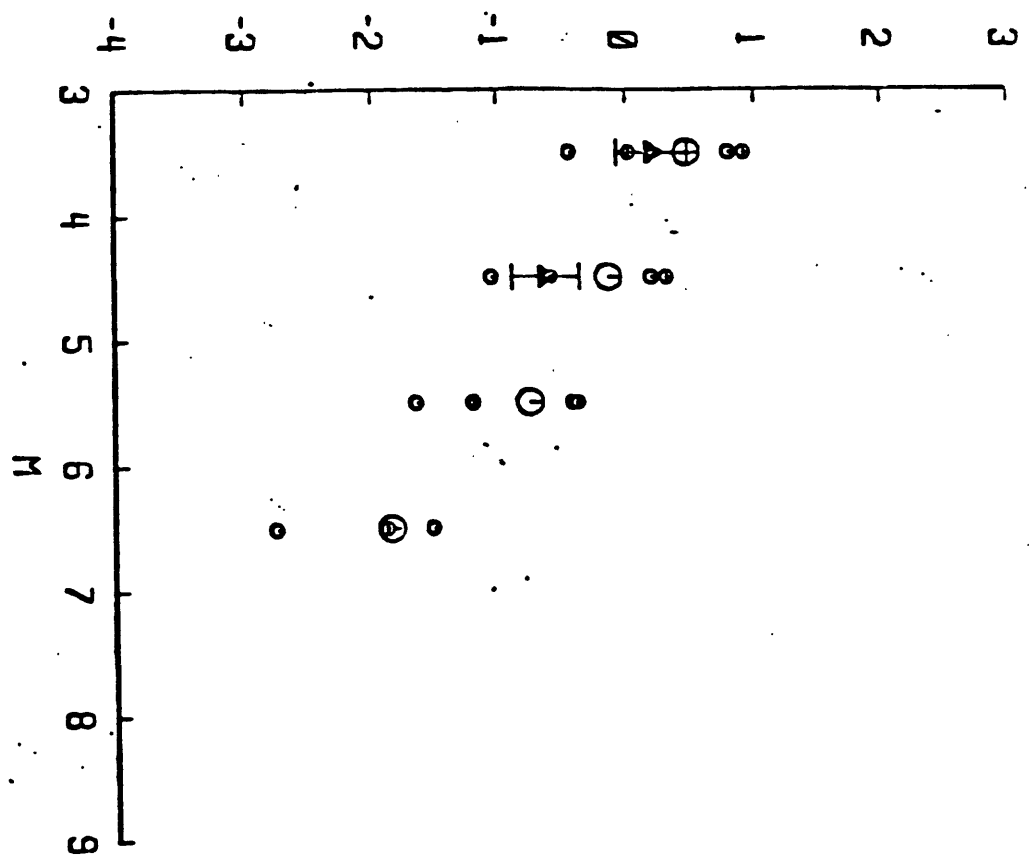
LOG (EVENTS/YEAR/MAG UNIT)



SANTA CRUZ ISLAND

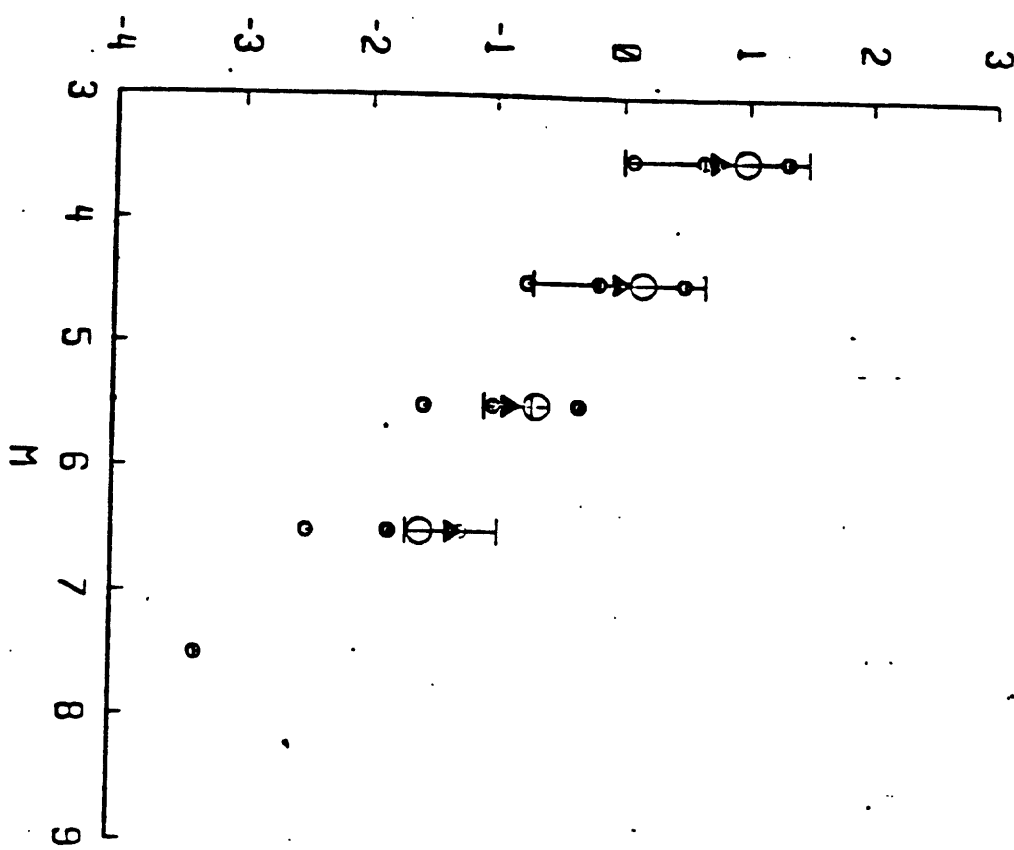
APPENDIX I-2

LOG (EVENTS/YEAR/MAG UNIT)

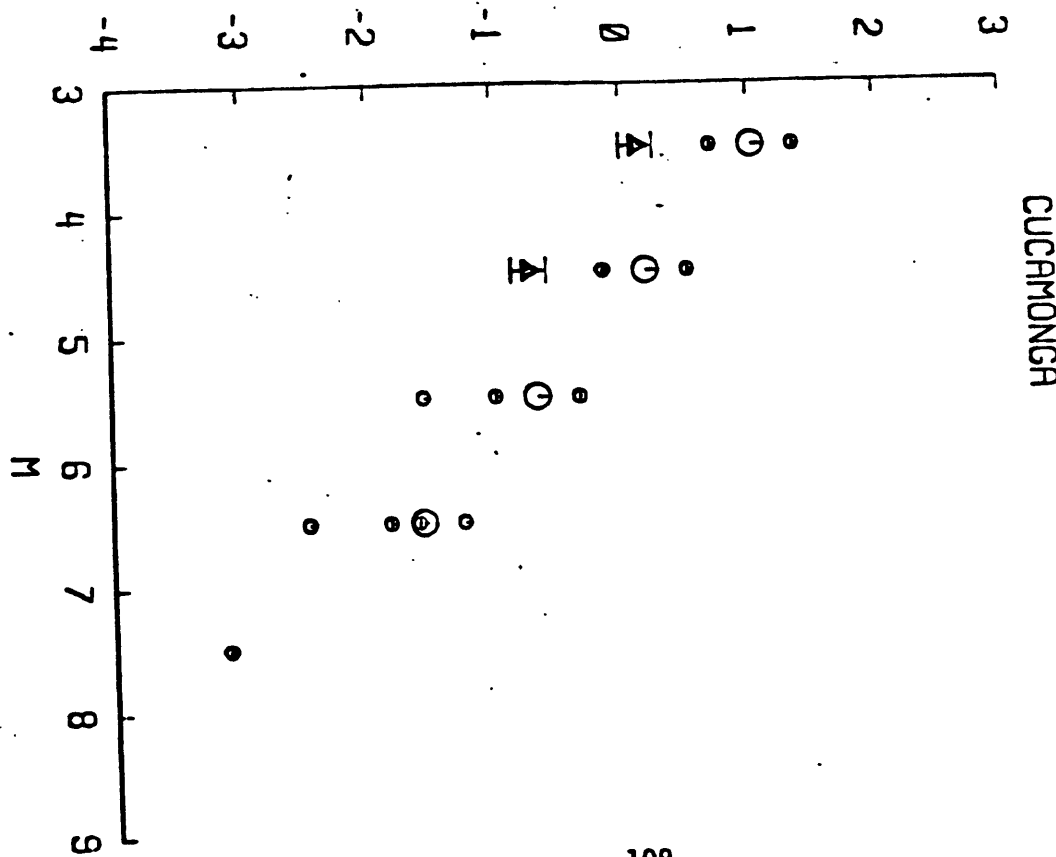


SANTA SUSANA

SIERRA MADRE

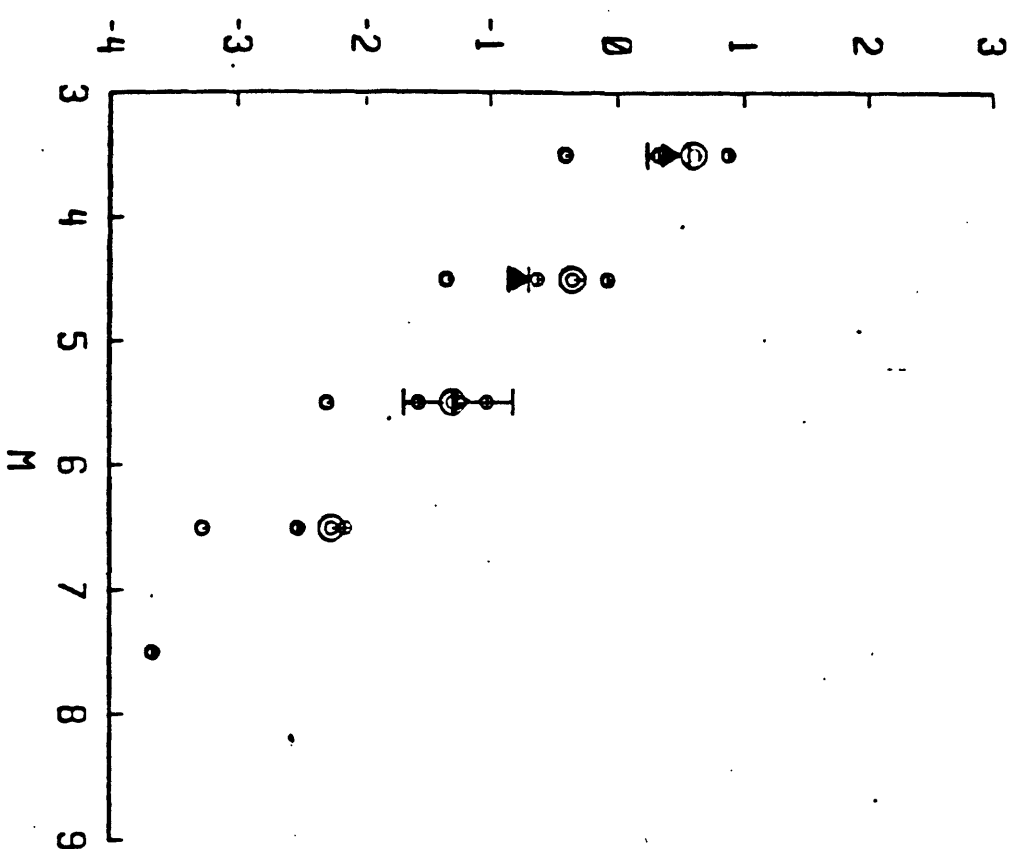


LOG (EVENTS/YEAR/MAG UNIT)

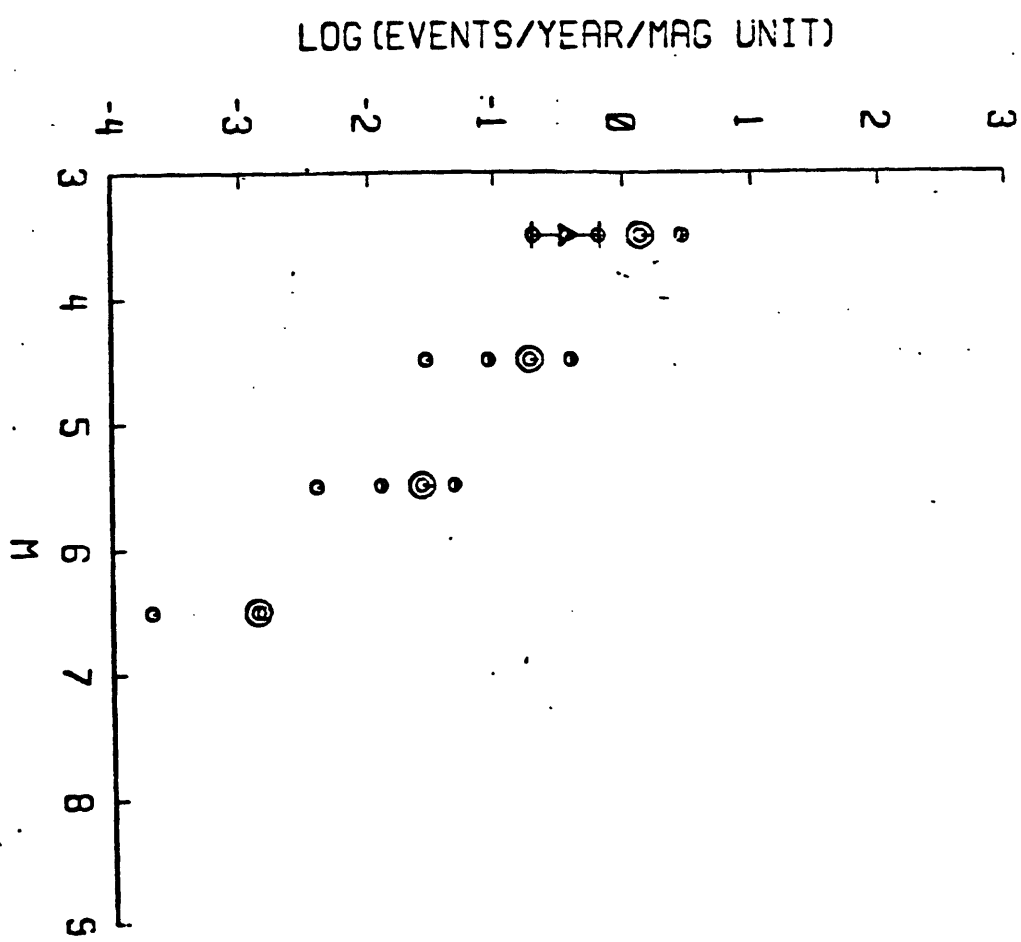


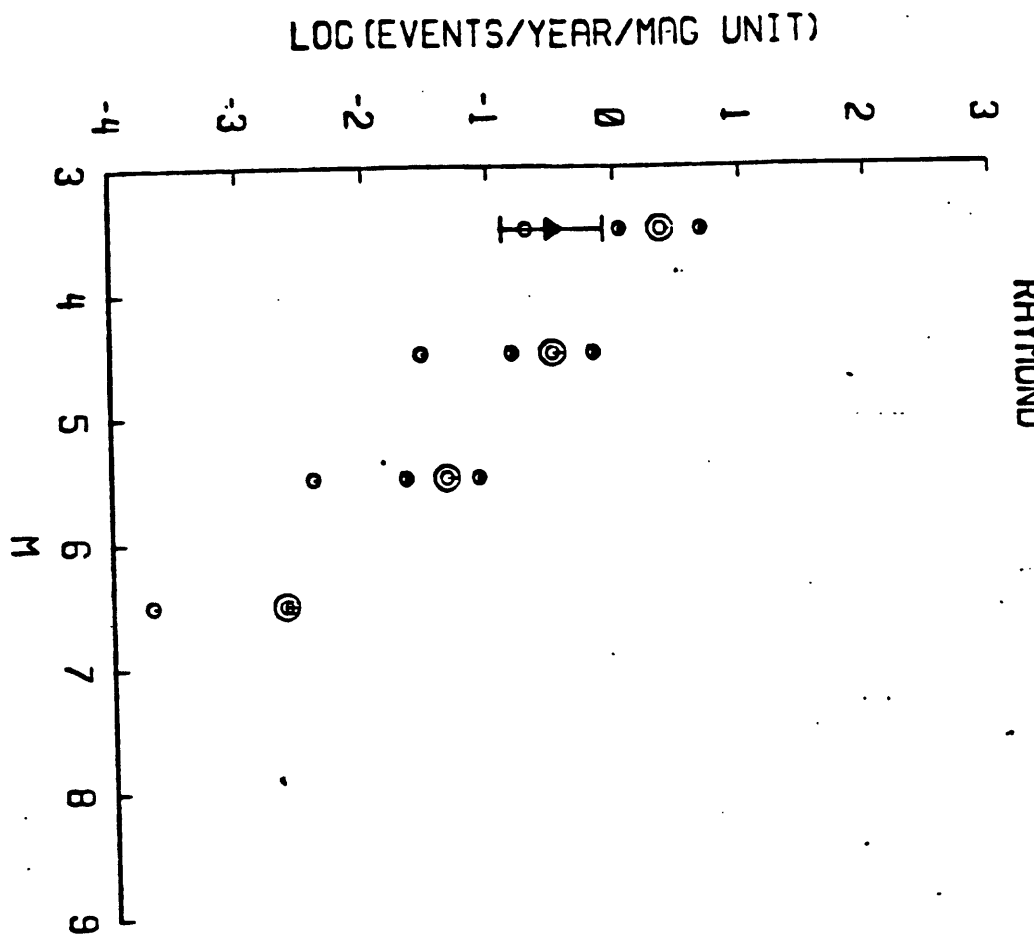
APPENDIX 1-2

MALIBU COAST (extended)

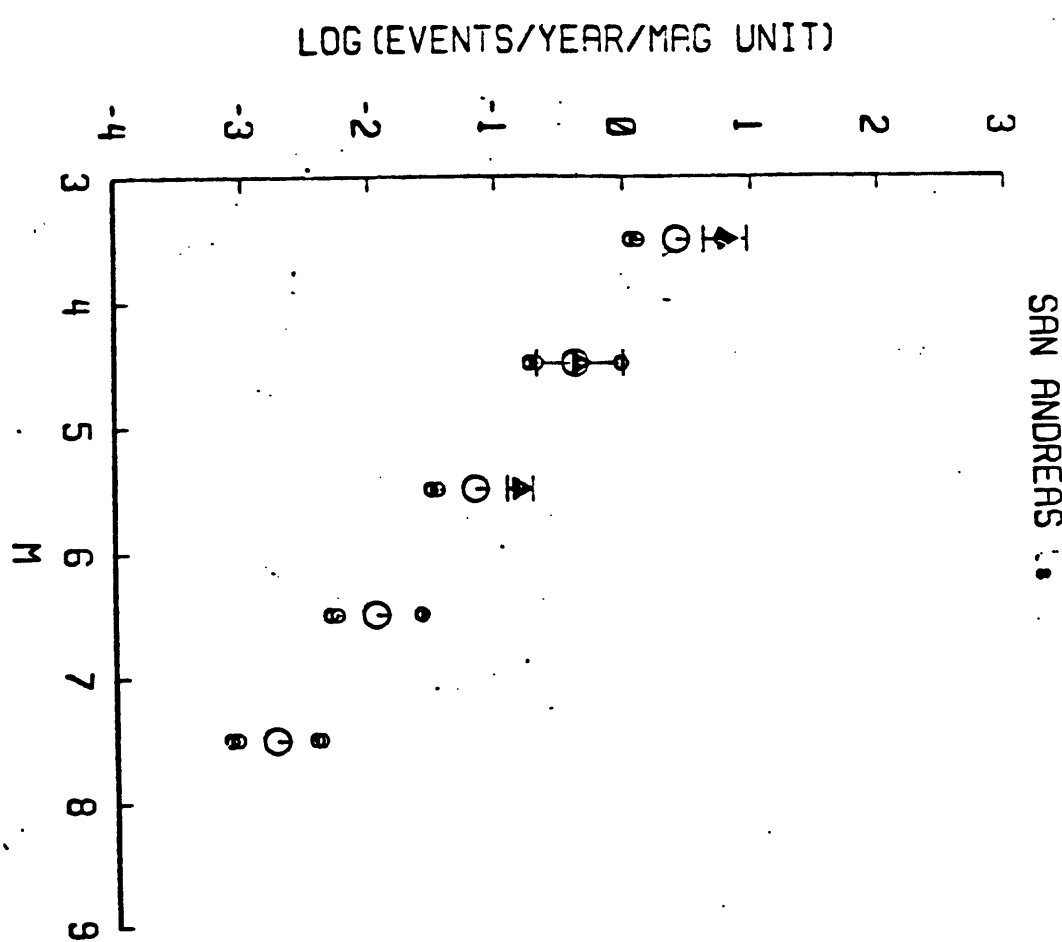


SANTA MONICA

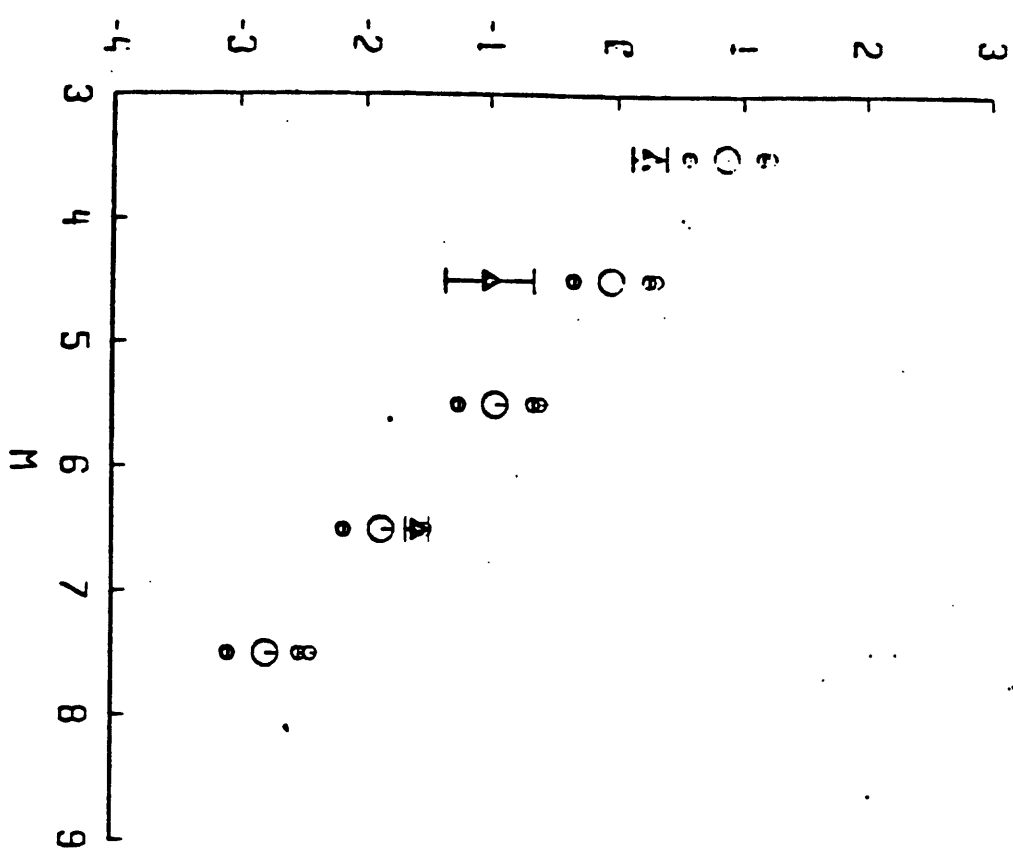




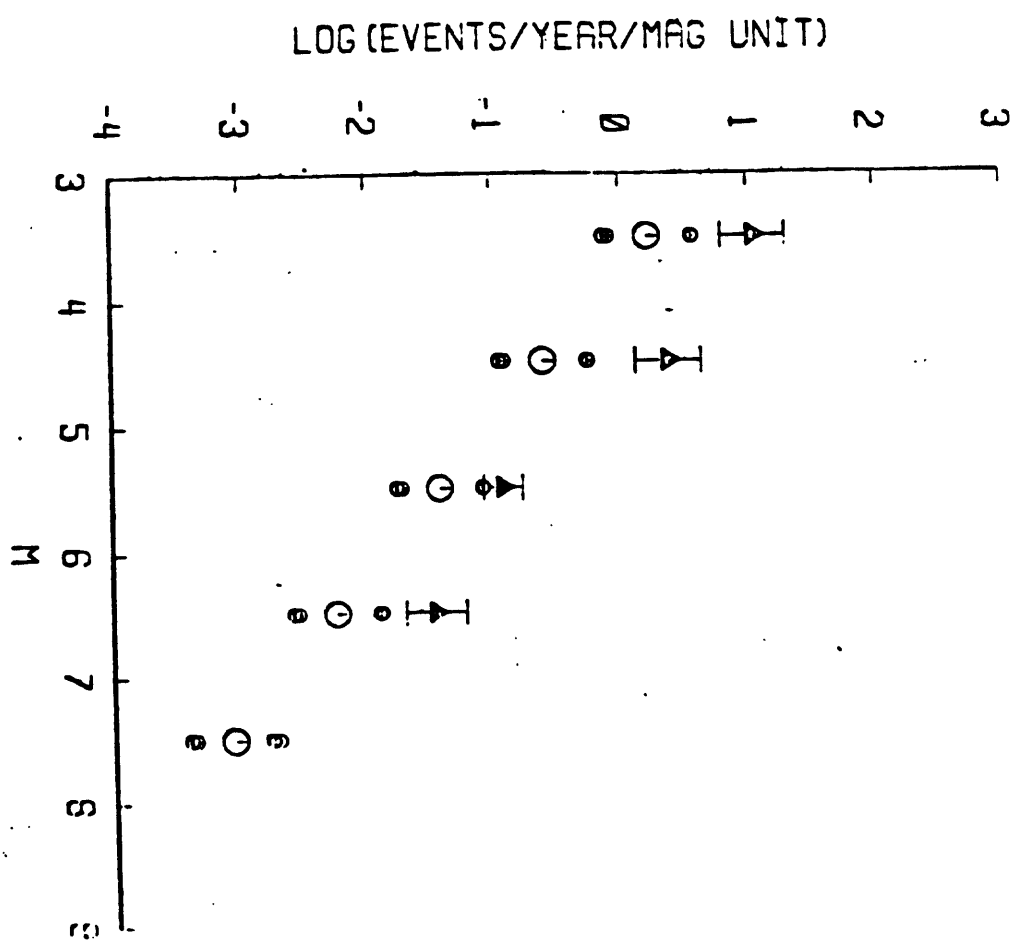
APPENDIX I-2



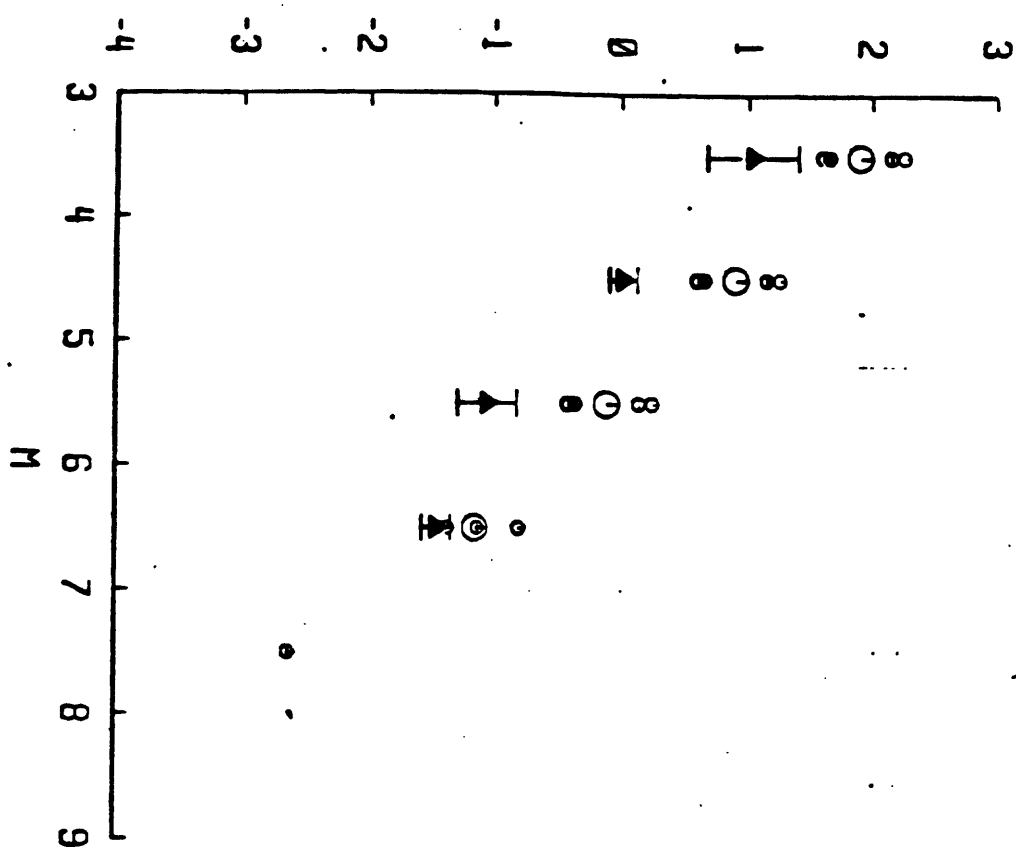
SAN ANDREAS 9



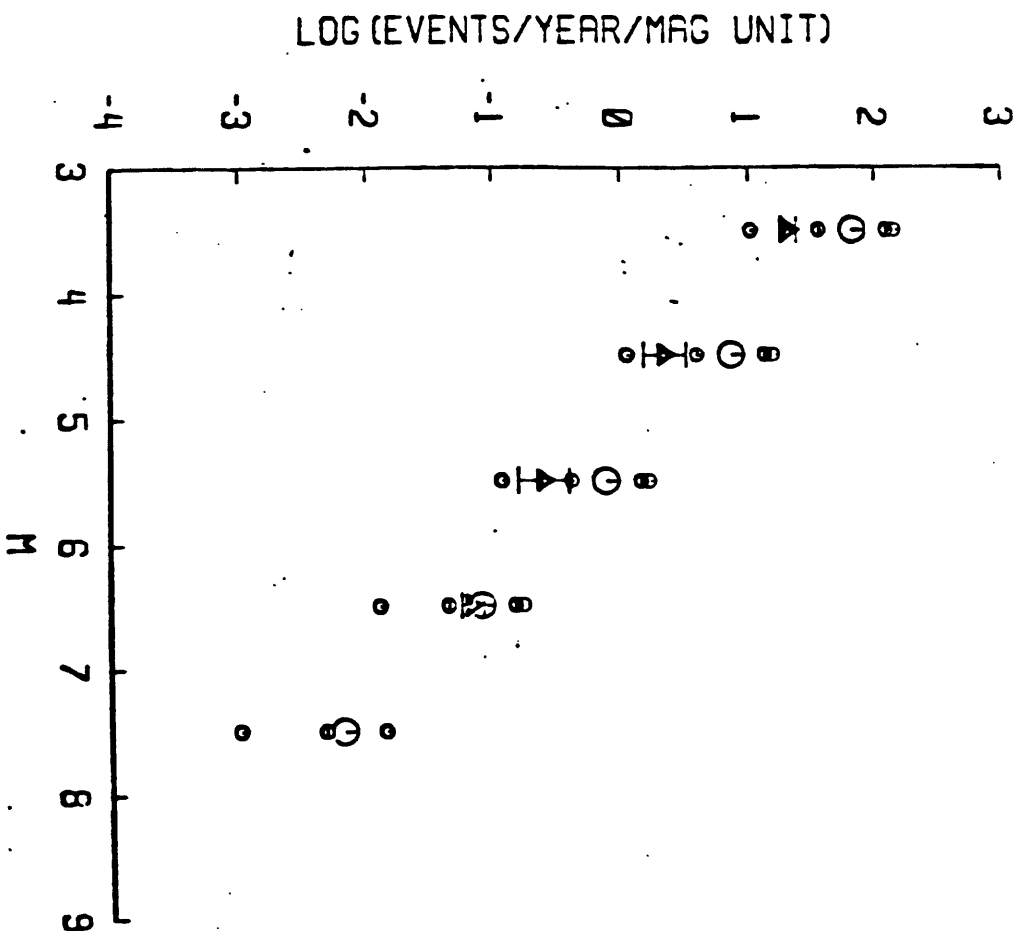
SAN ANDREAS 10



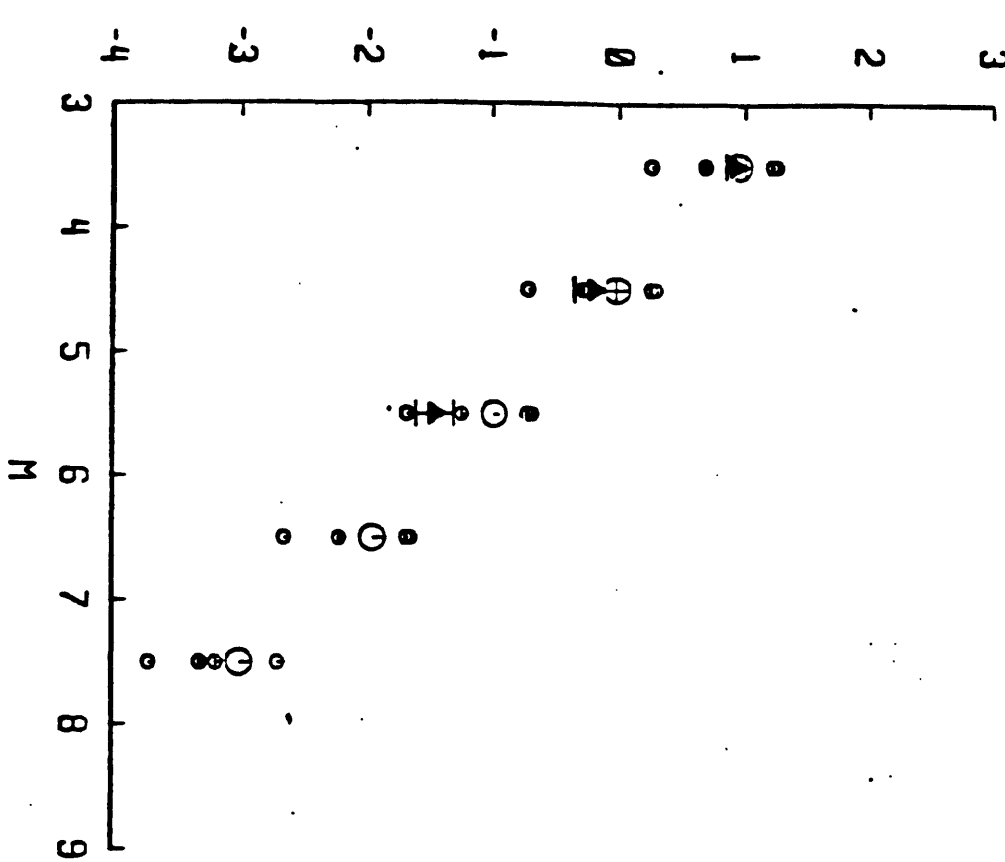
IMPERIAL



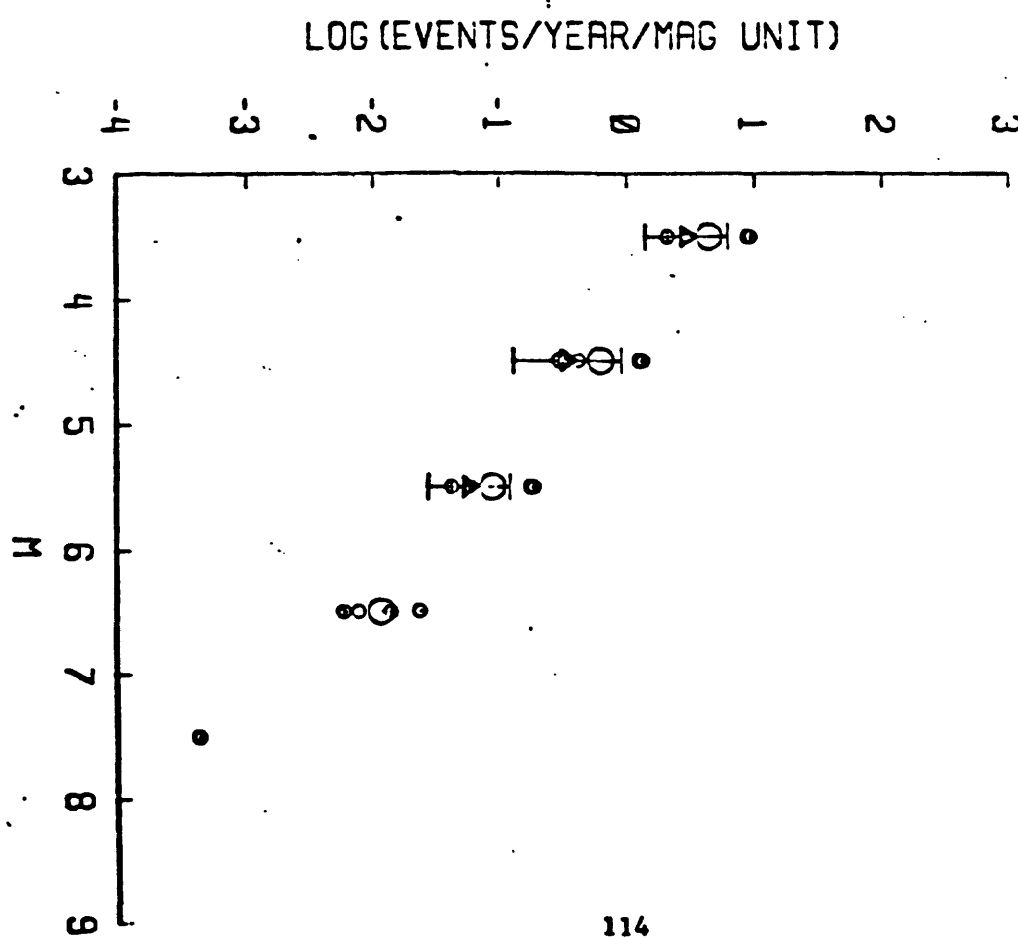
SAN JACINTO ZONE



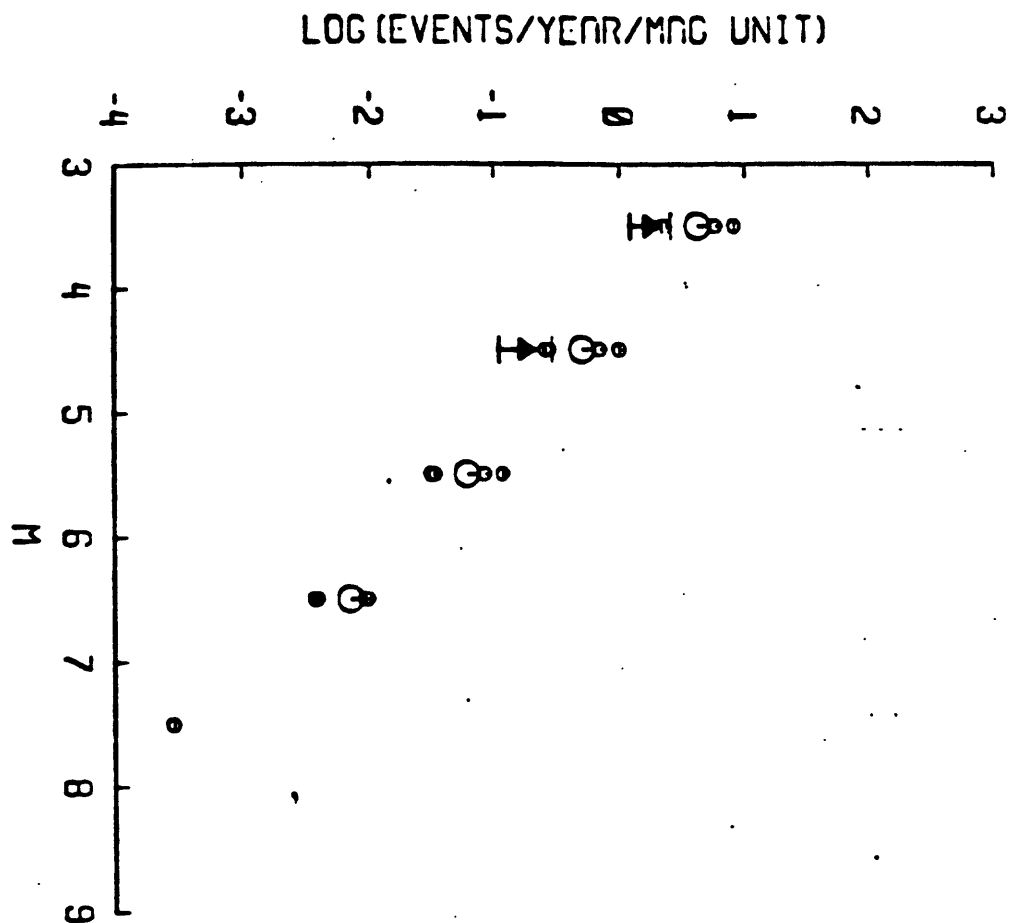
EL SINORE



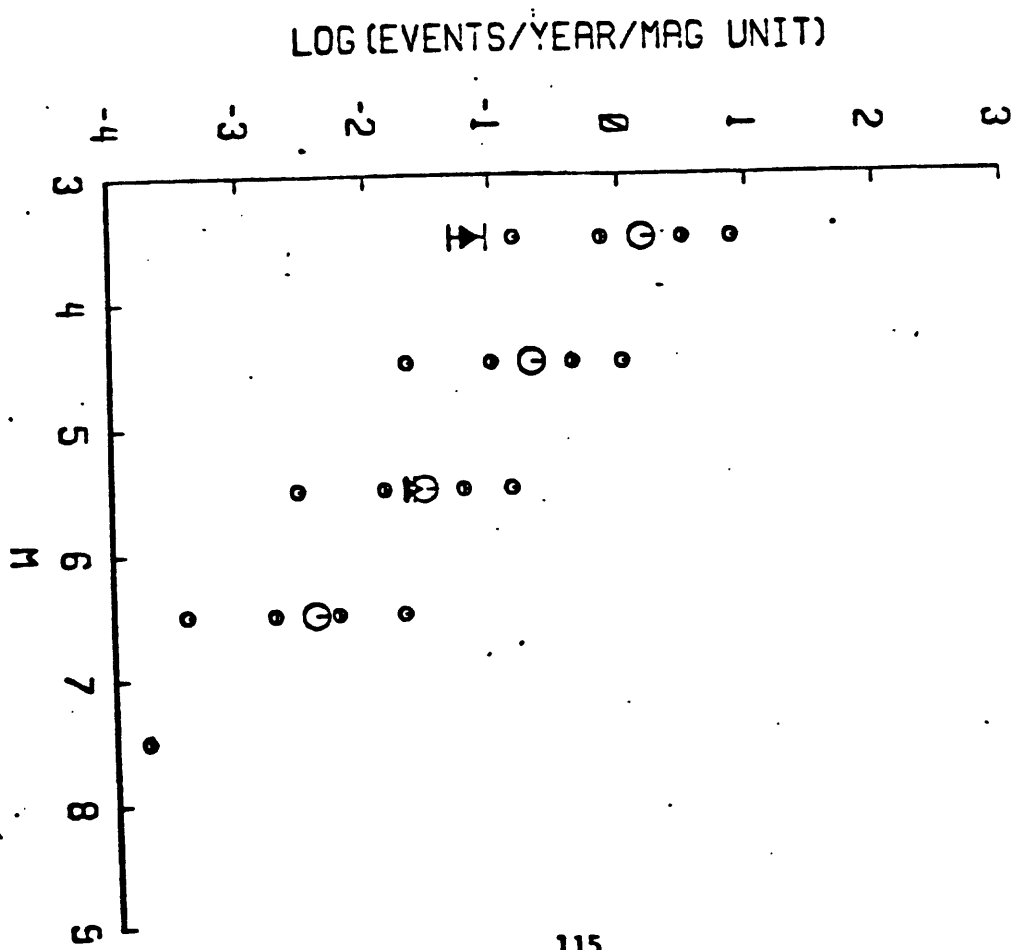
PINTO MOUNTAIN



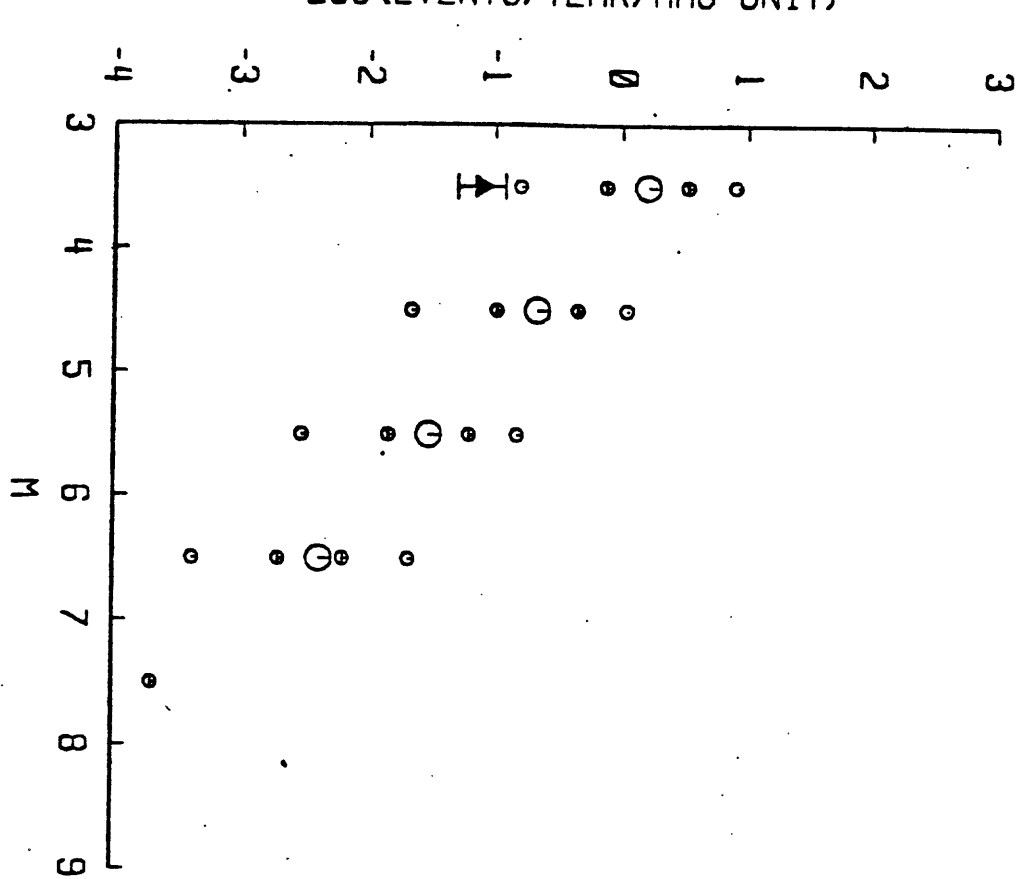
BLUE CUT



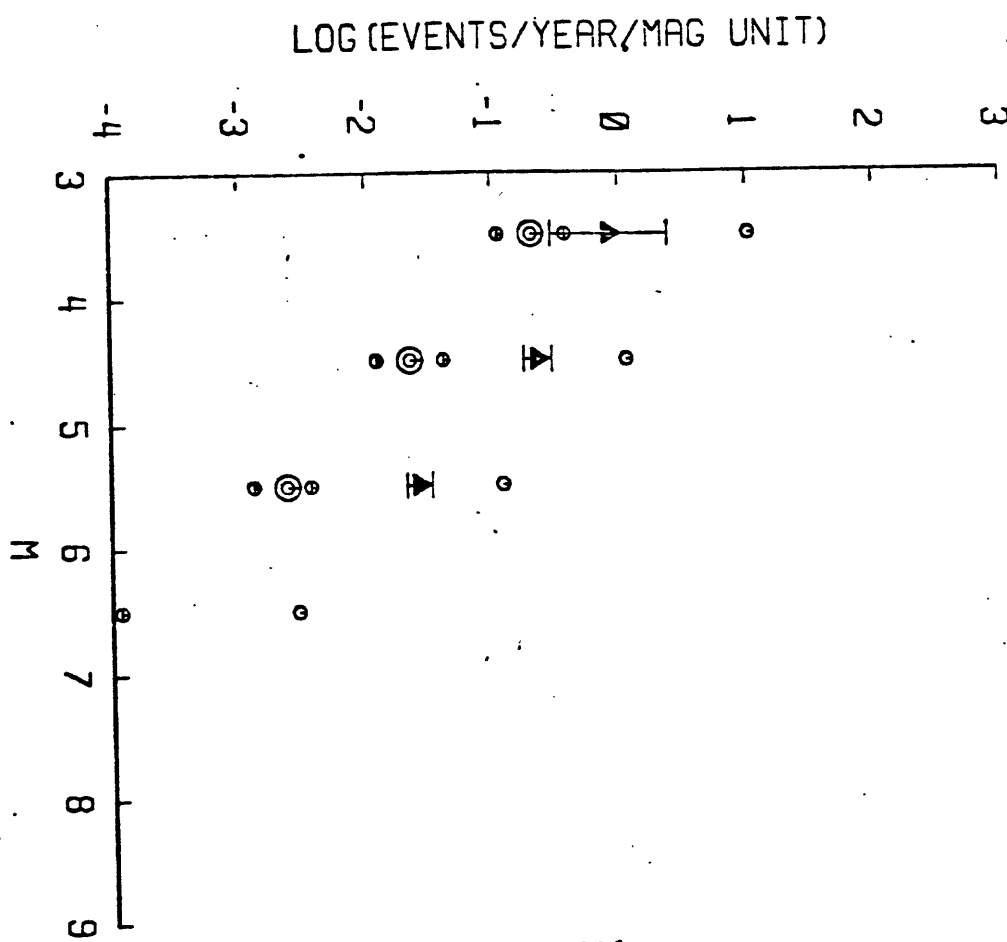
SURPRISE VALLEY



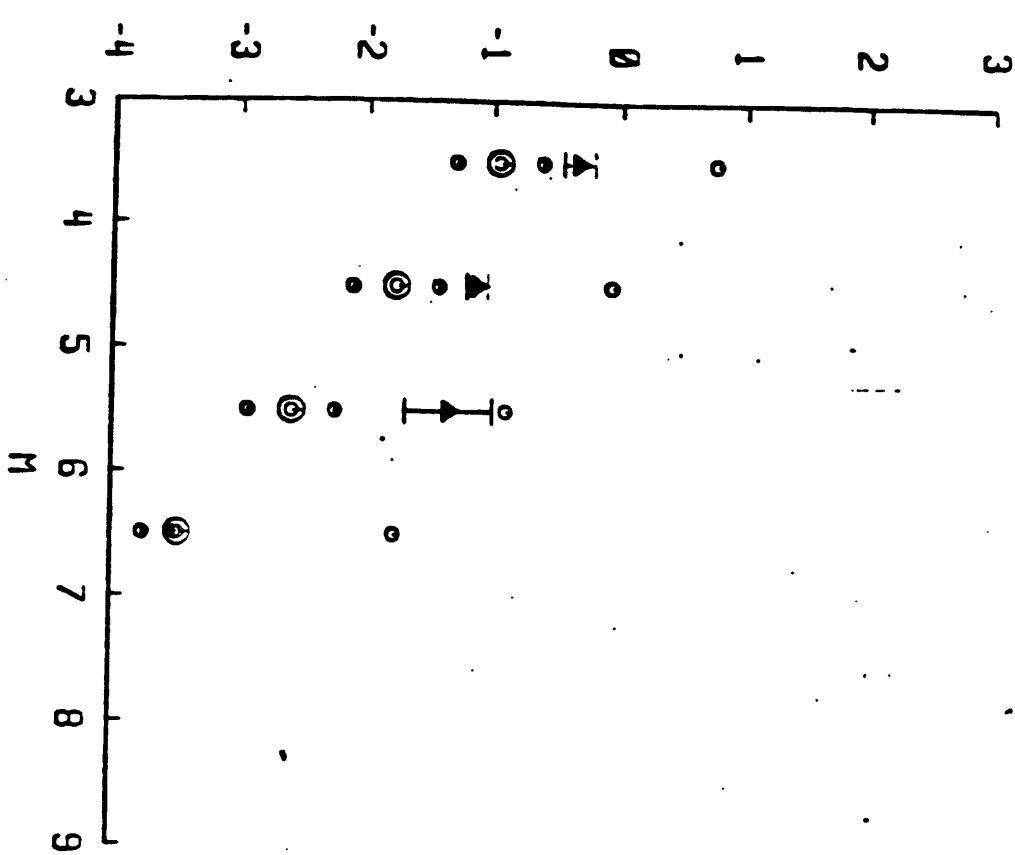
LIKEI



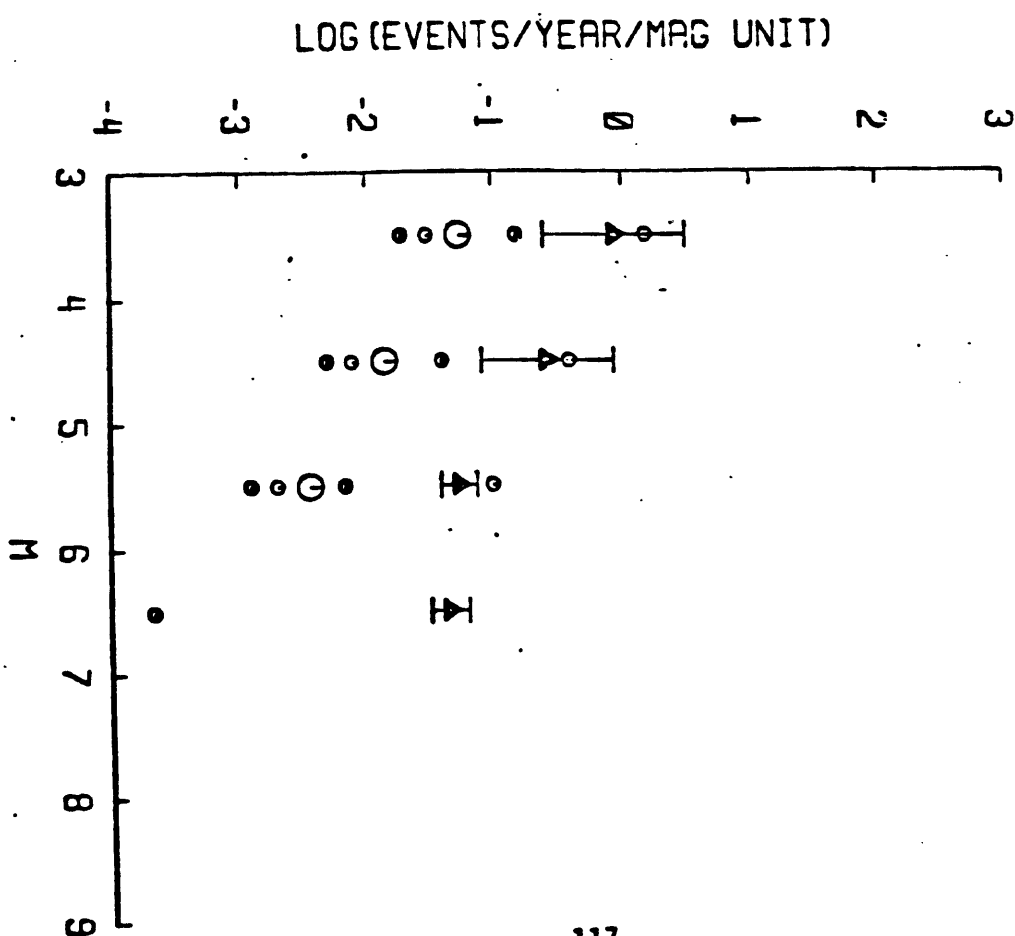
HONEY LAKE VALLEY



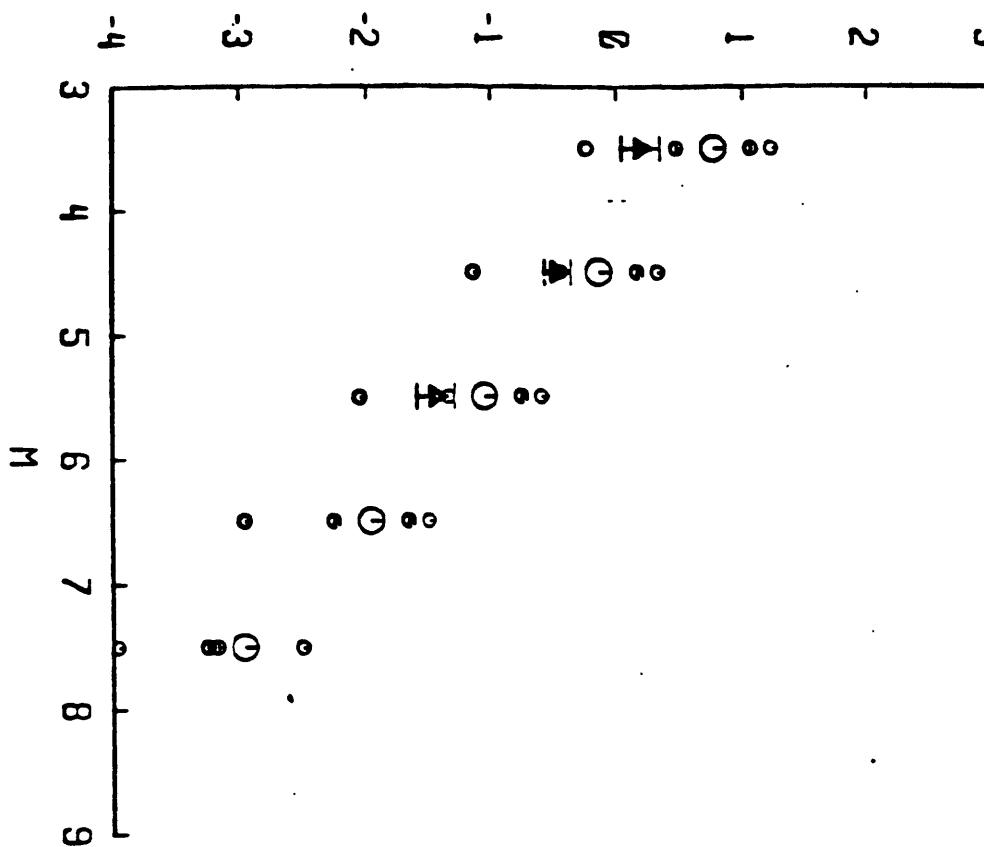
HONEY LAKE



STAMPEDE RESERVOIR

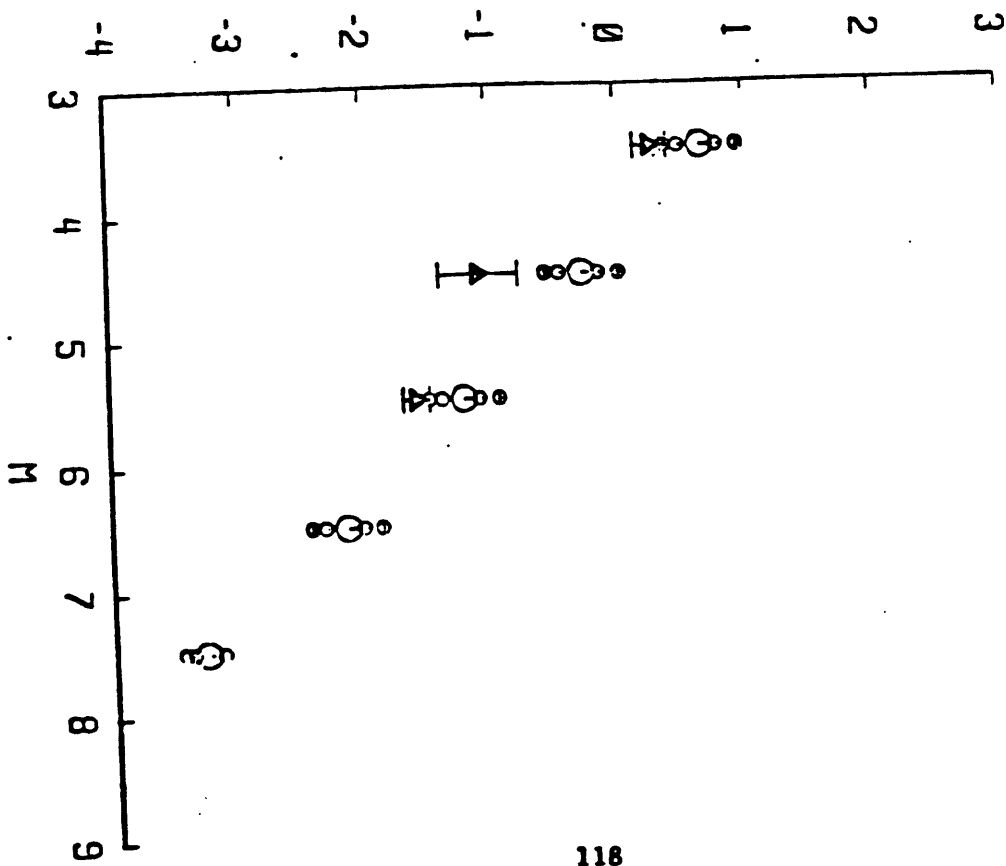


LOG (EVENTS/YEAR/MAG. UNIT)



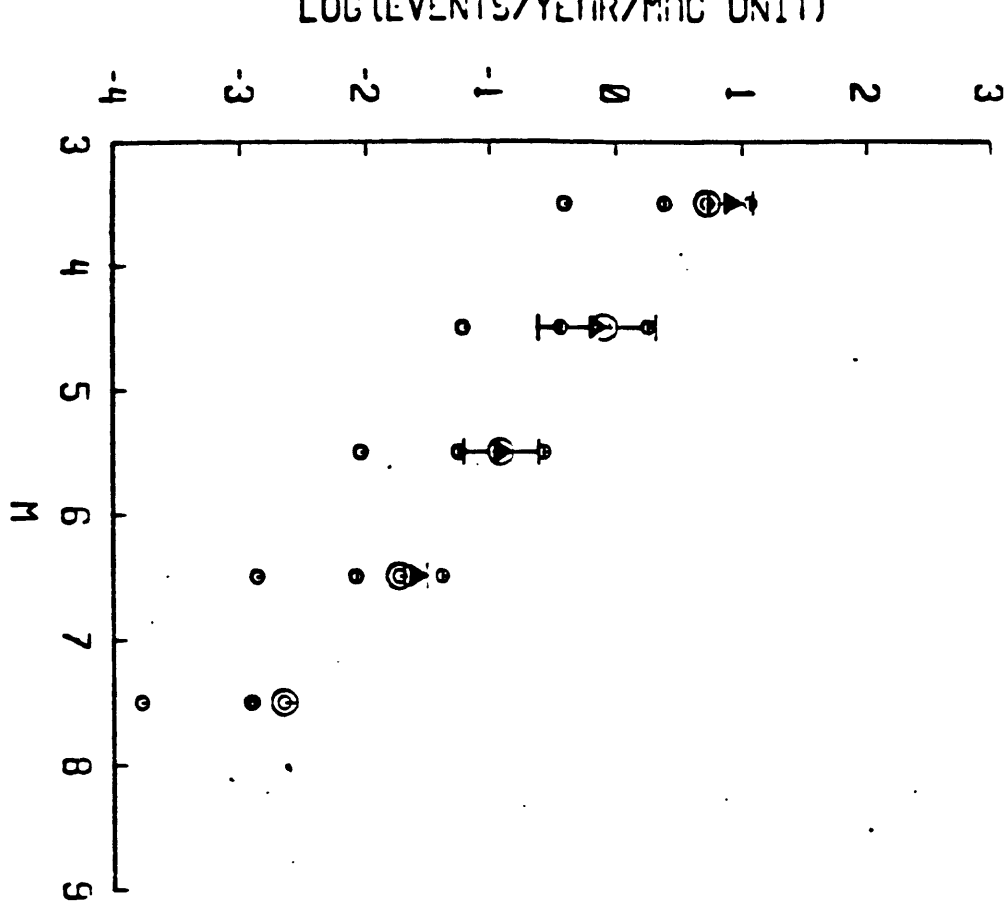
DEATH VALLEY

LOG (EVENTS/YEAR/MAG. UNIT)

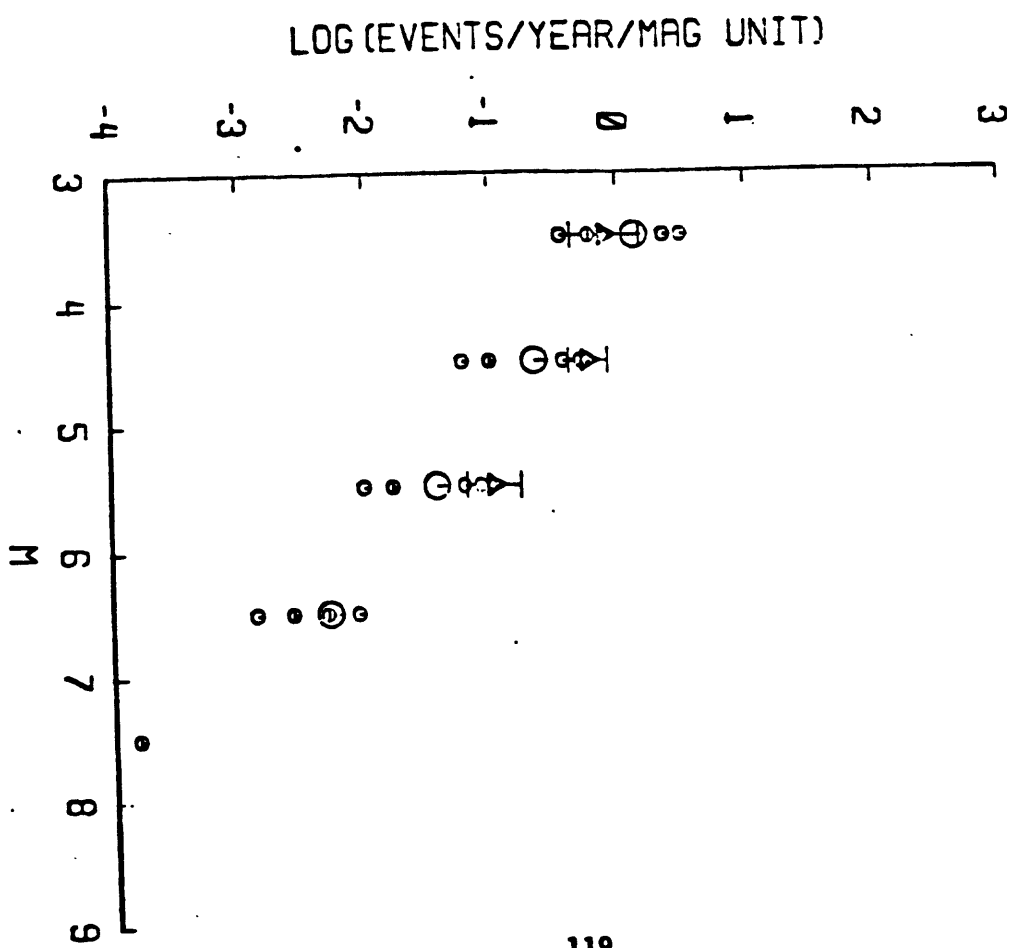


PANAMINT VALLEY

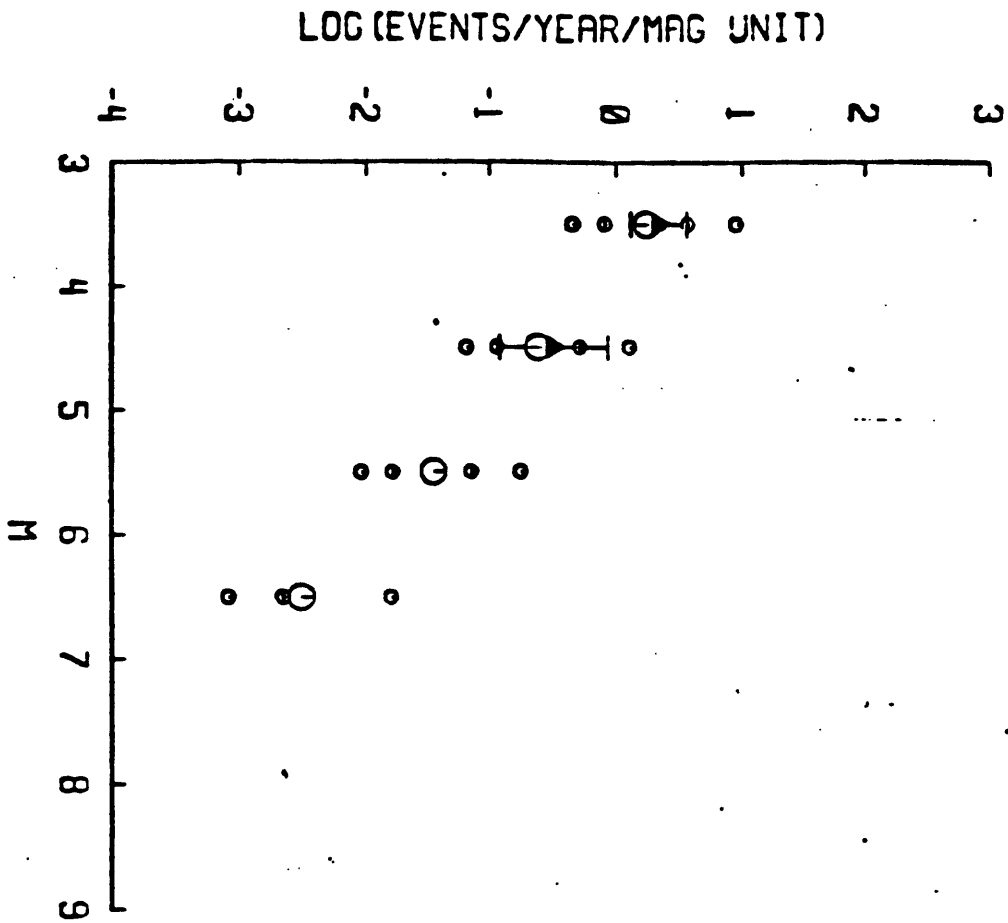
SIERRA NEVADA - OWENS VALLEY



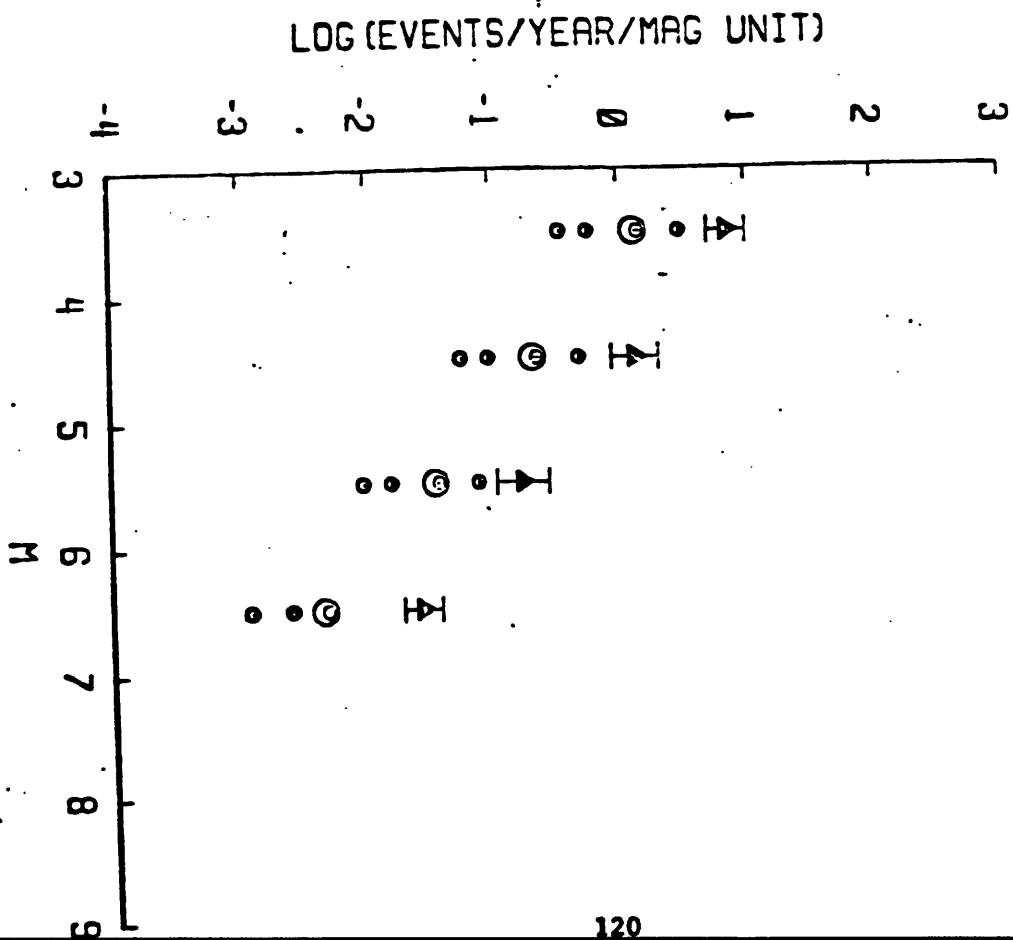
MONO LAKE REGION



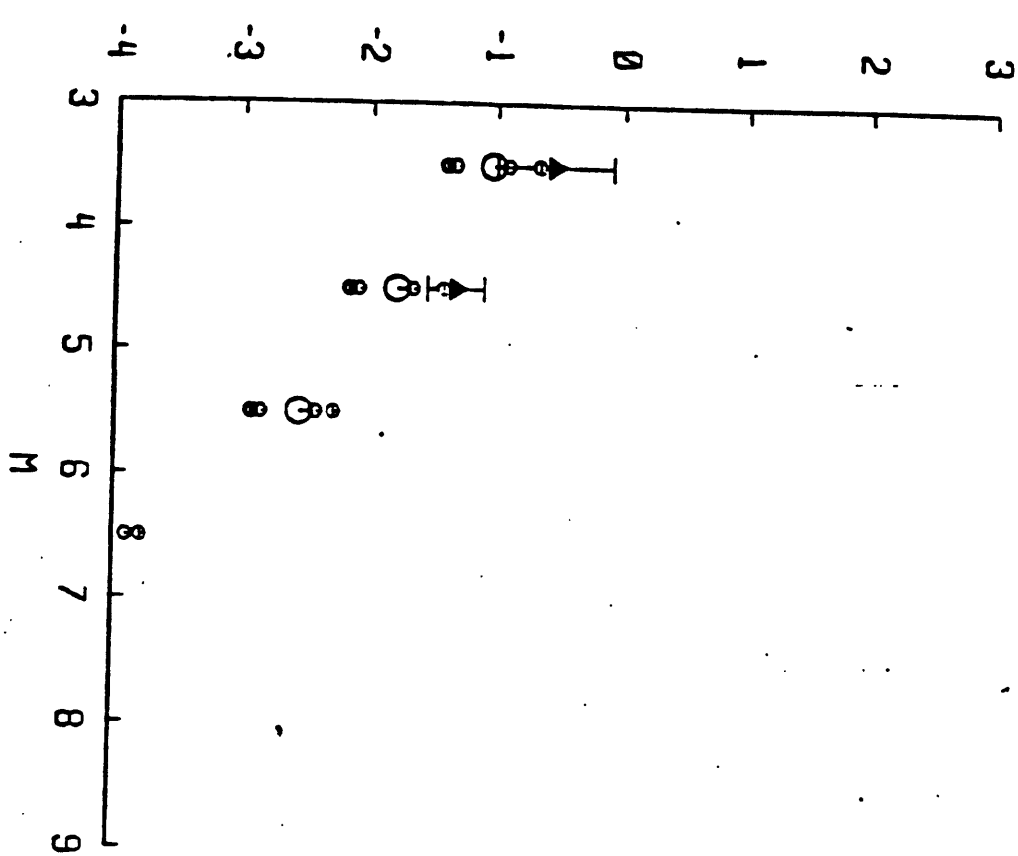
JUNE LAKE REGION



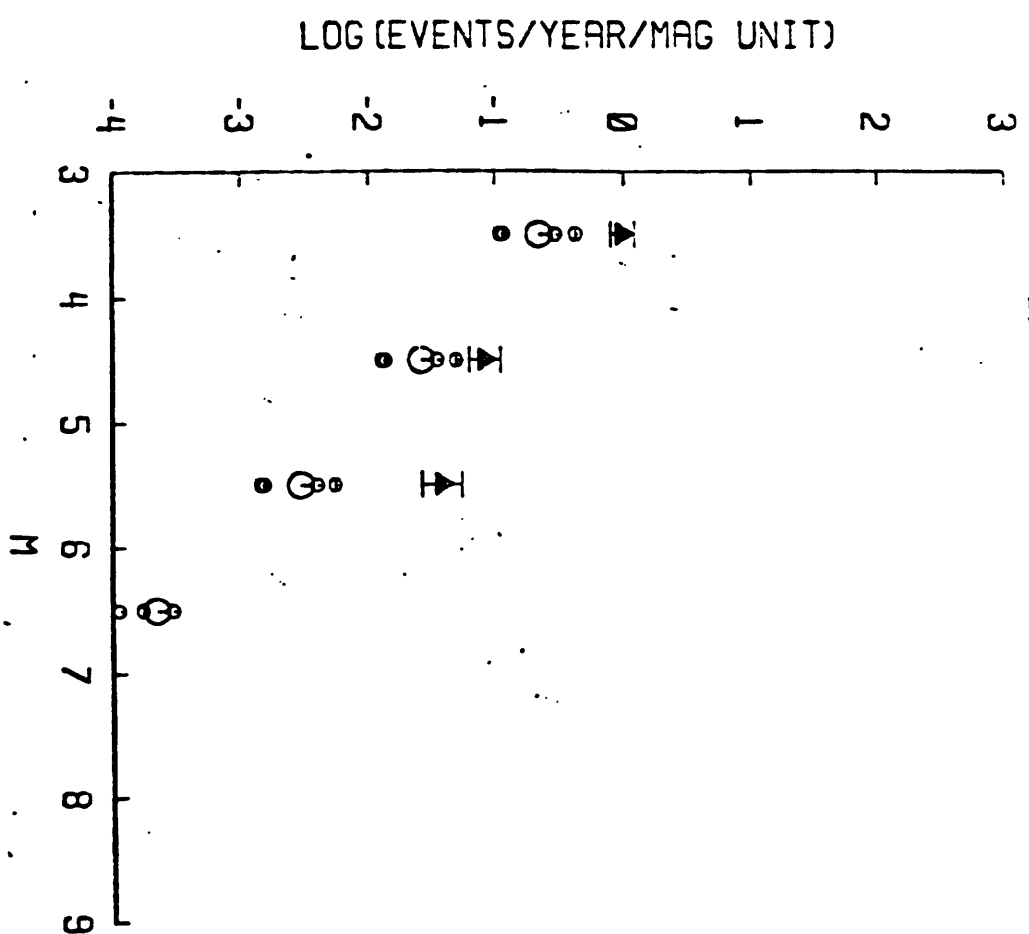
HILTON CREEK REGION



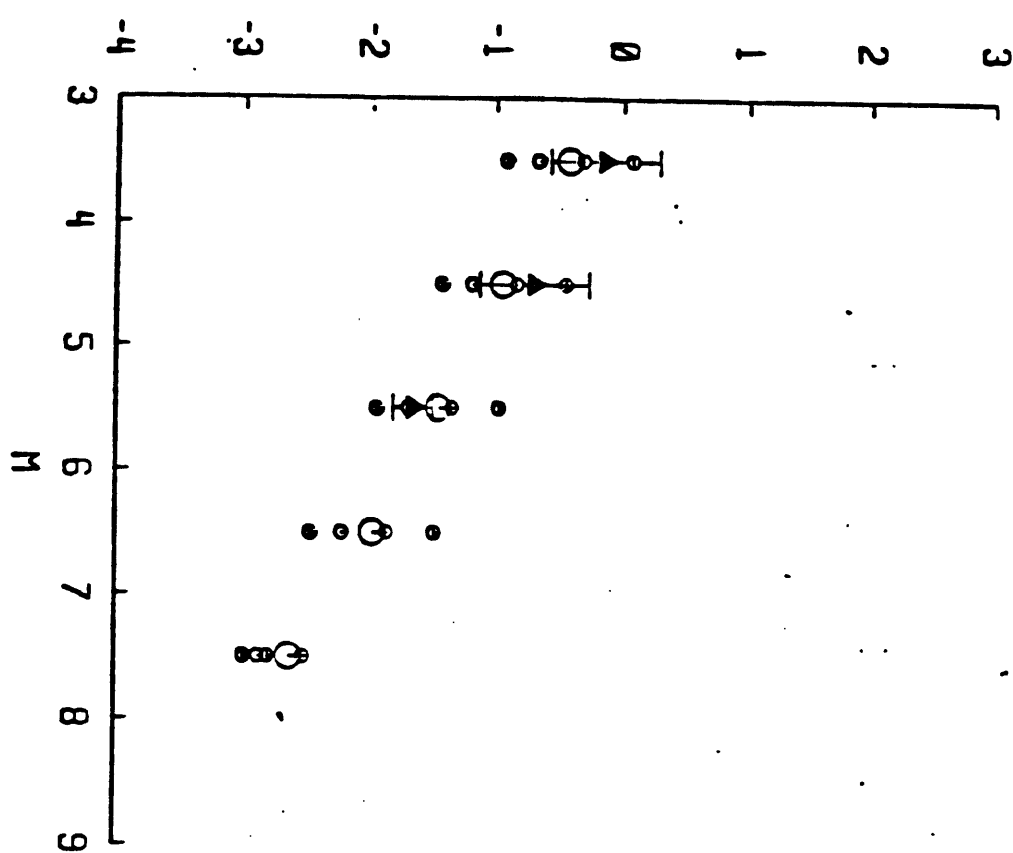
TOPAZ *



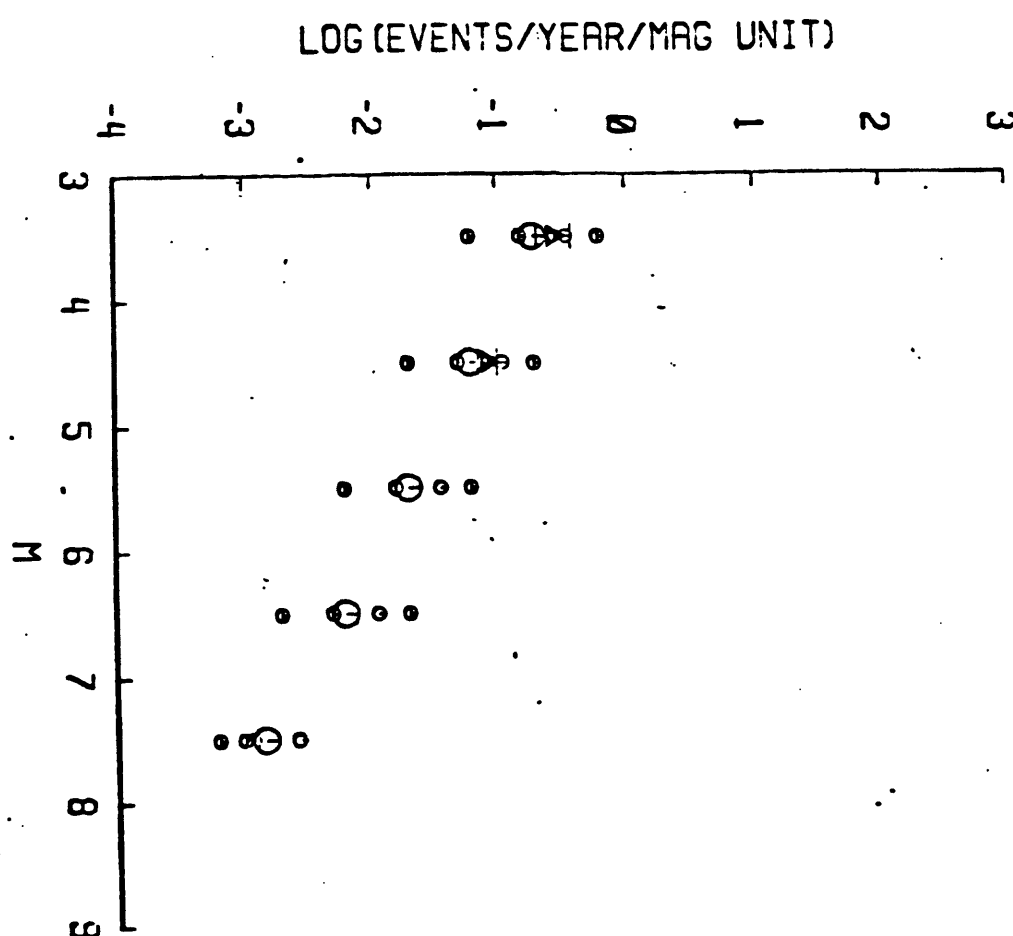
GENOA *



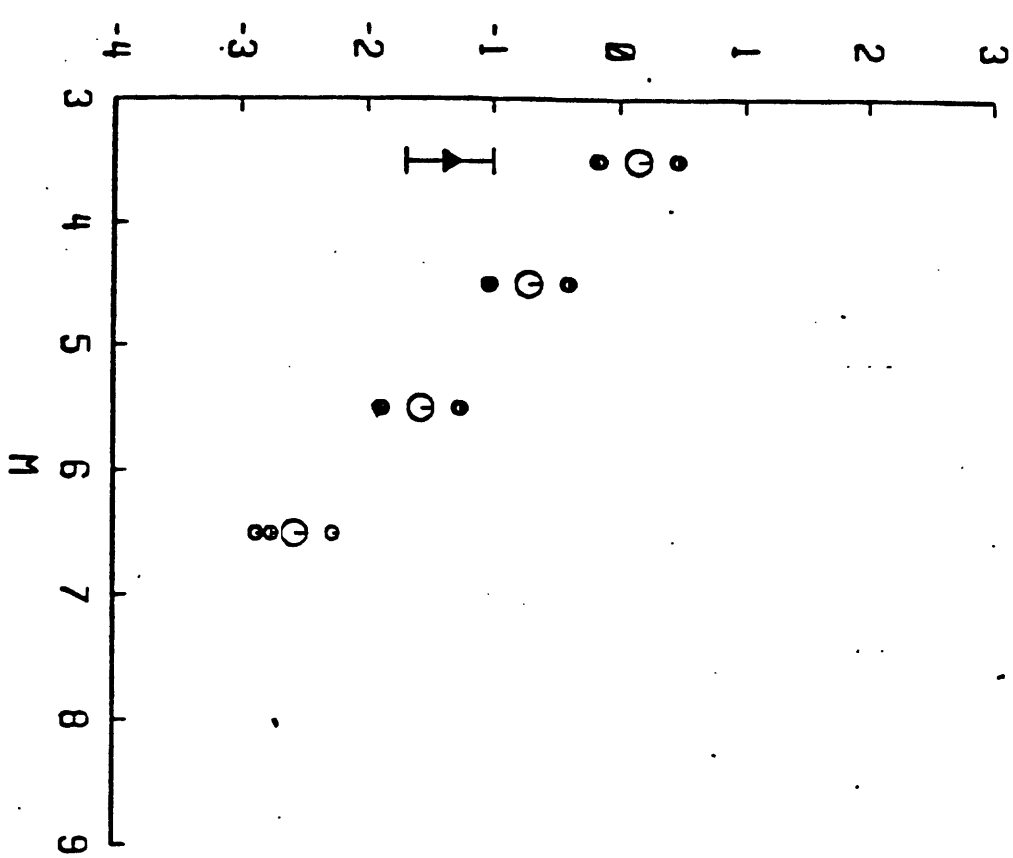
GARLOCK WEST



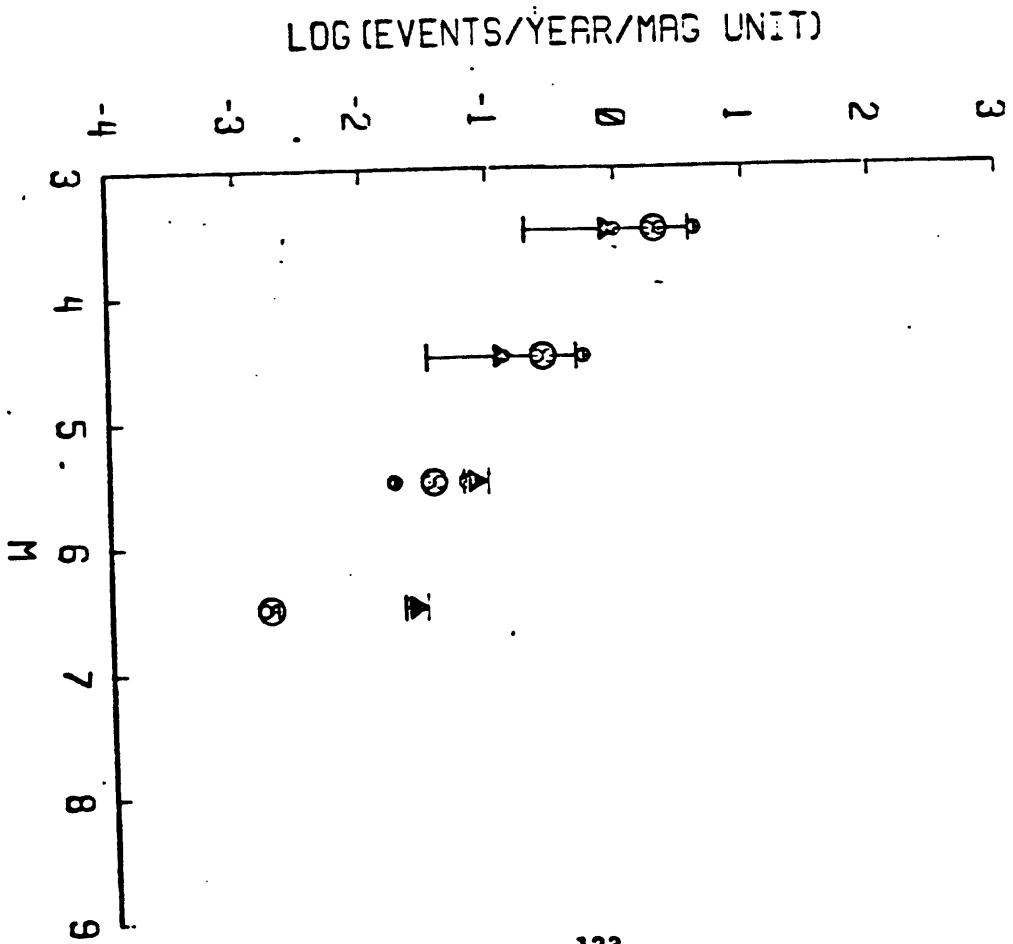
GARLOCK EAST

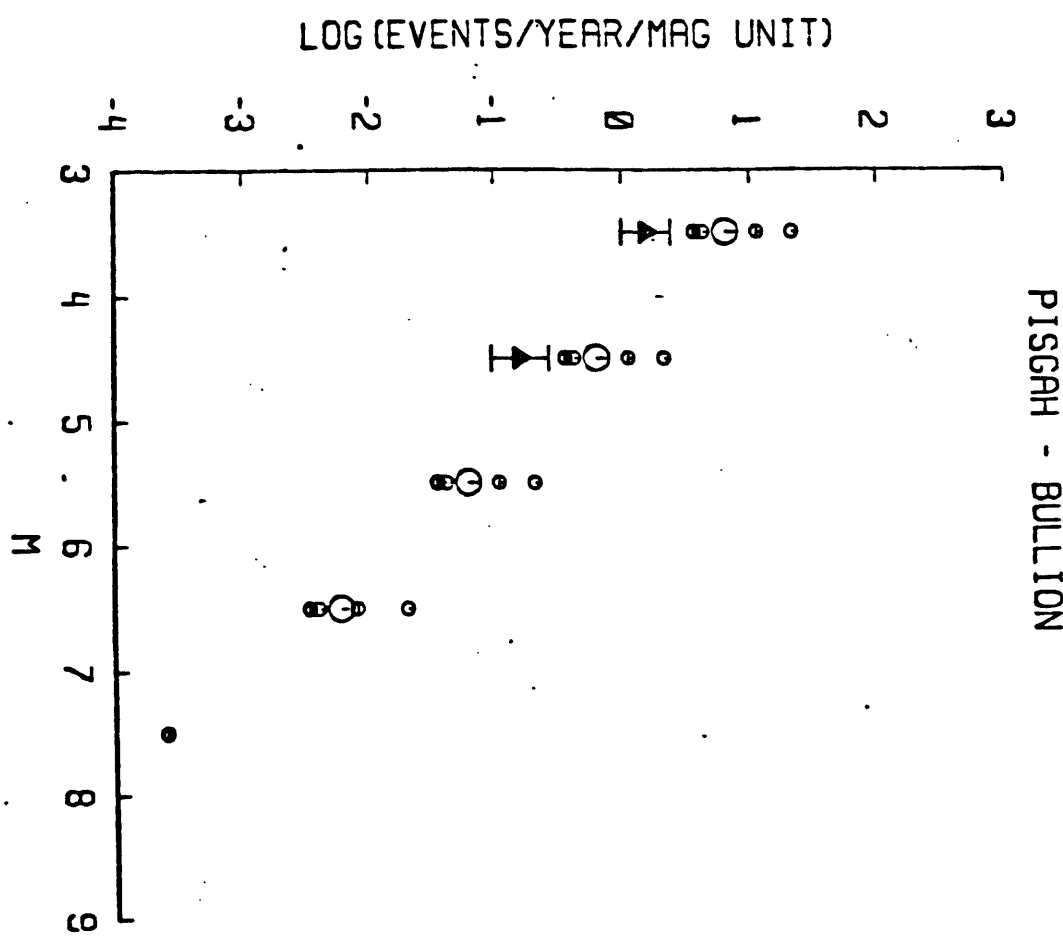
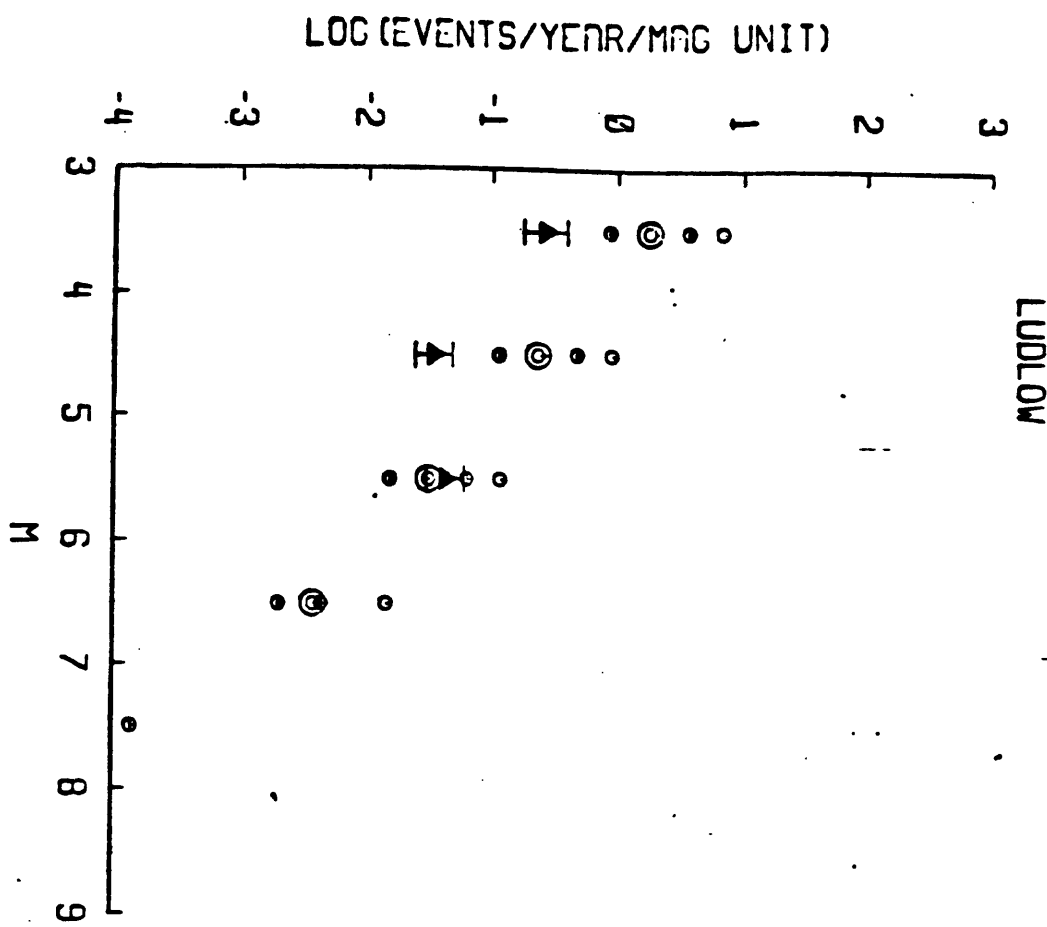


BICYCLE LAKE *

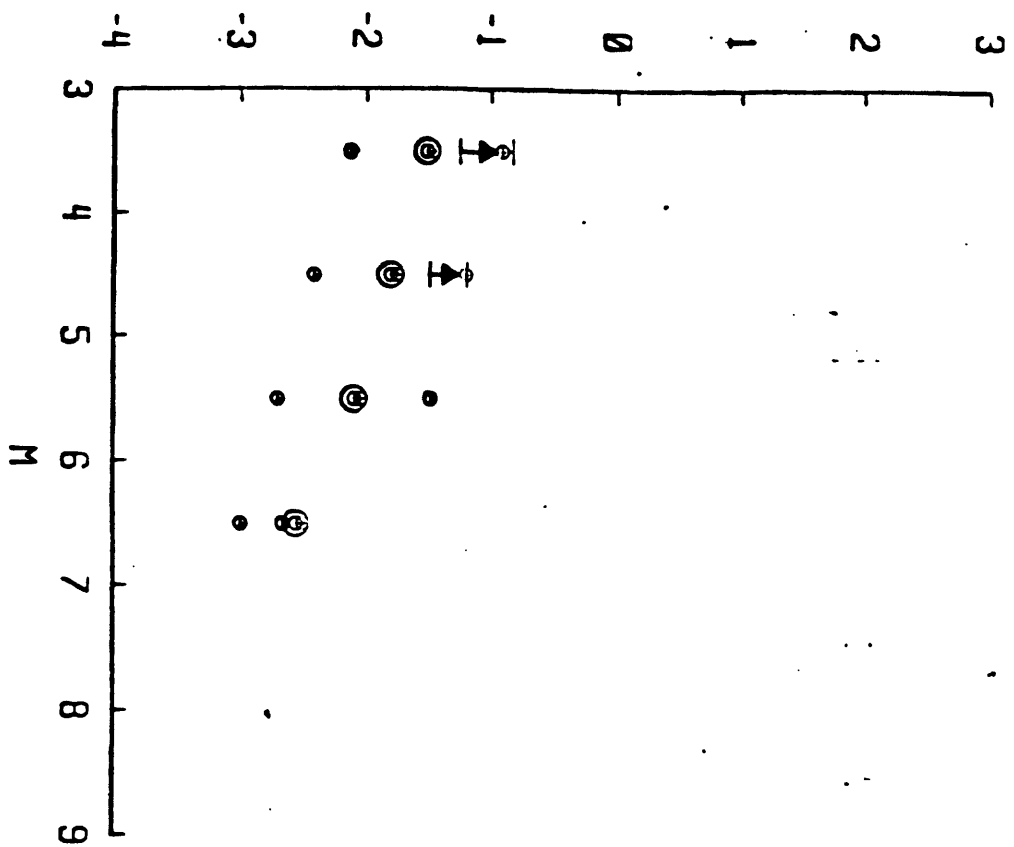


MANNIX



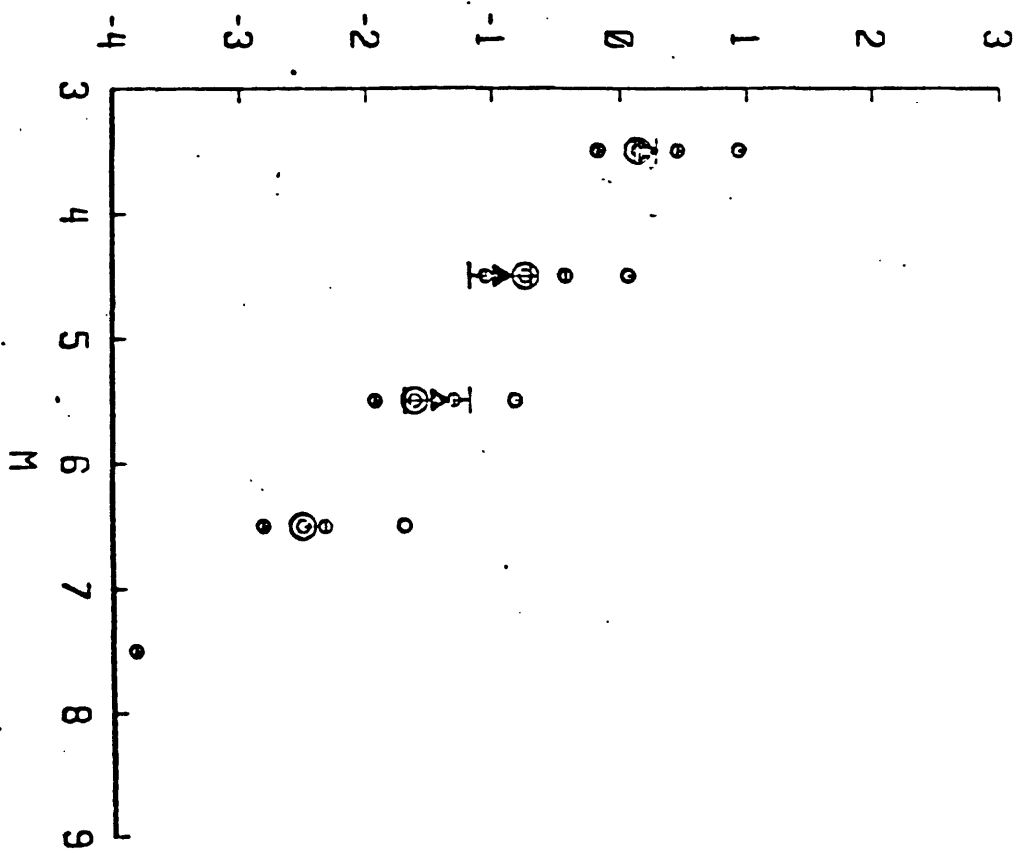


LOG (EVENTS/YEAR/MAG UNIT)

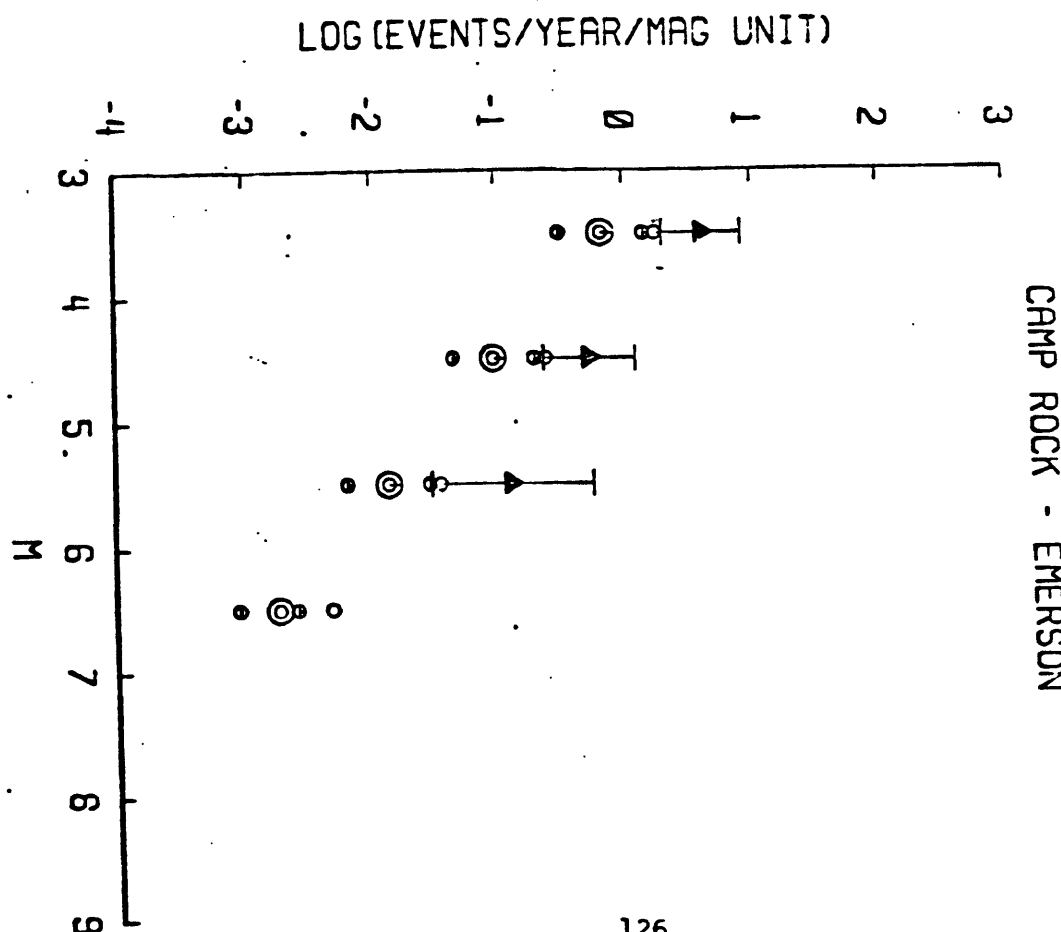
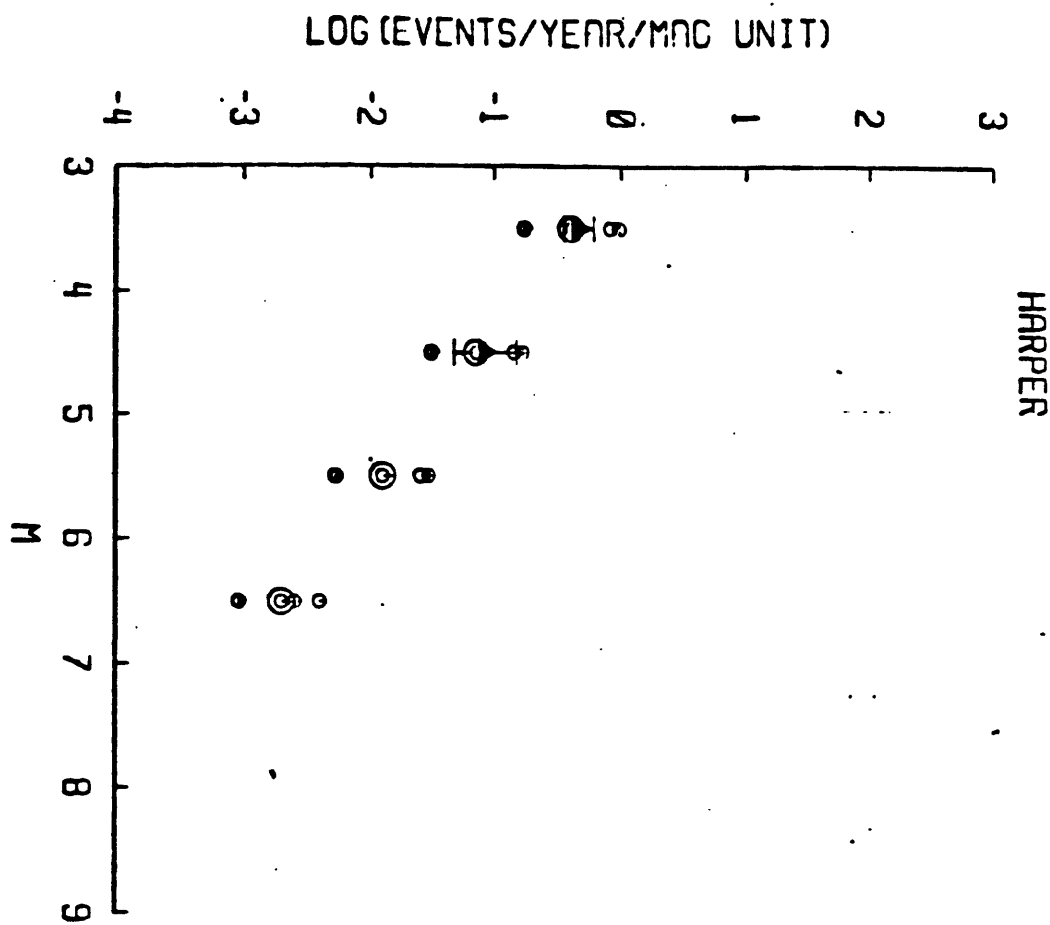


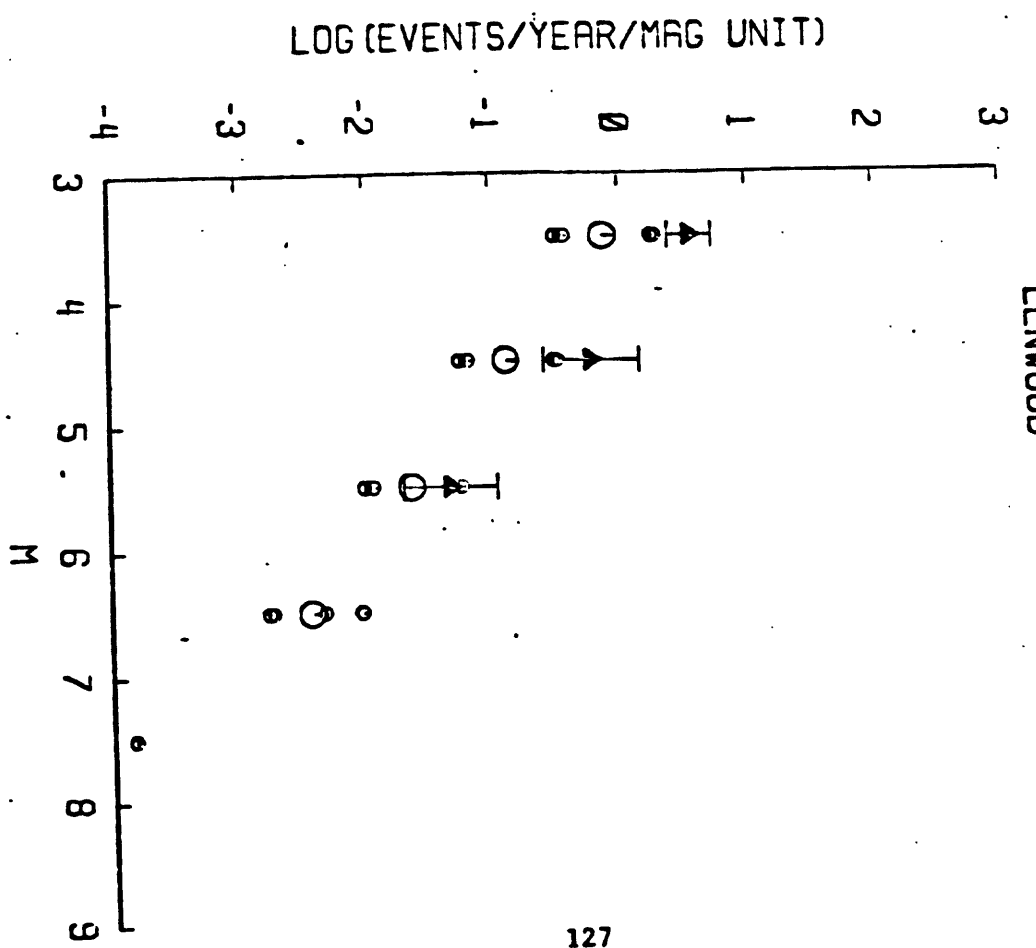
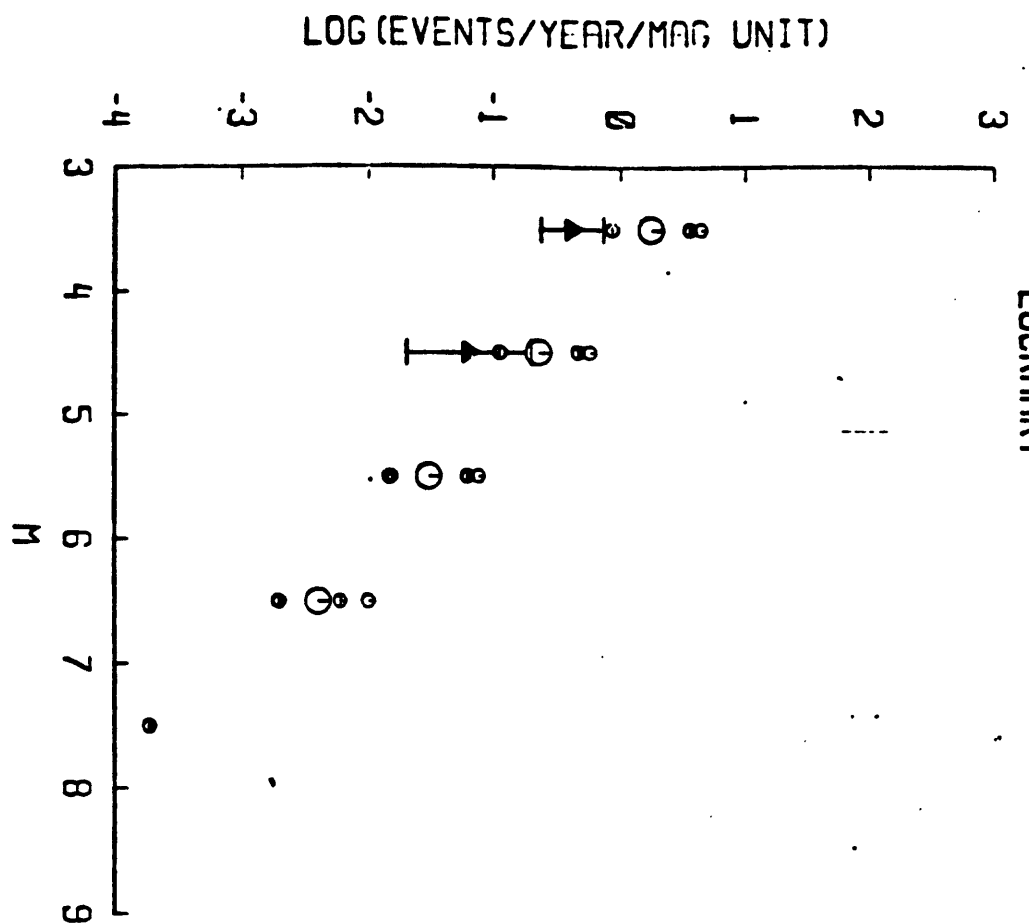
BLACKWATER

LOG (EVENTS/YEAR/MAG UNIT)

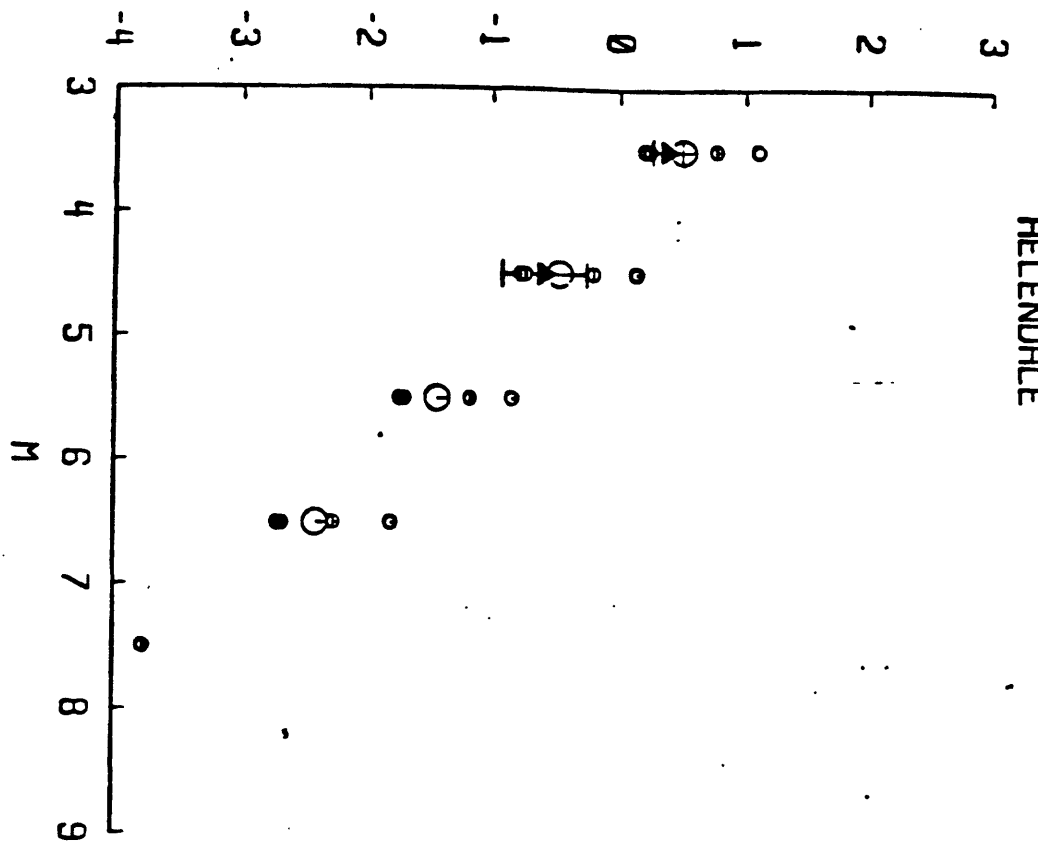


CALICO





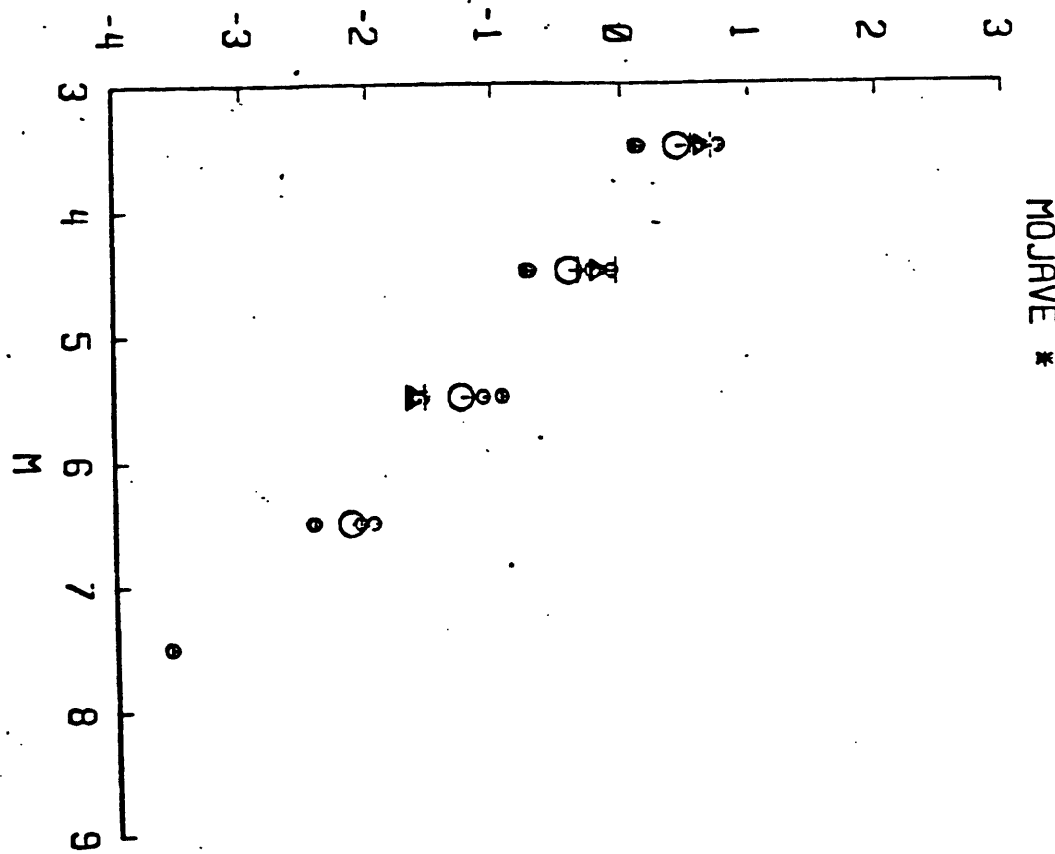
LOG (EVENTS/YEAR/MAG UNIT)



HELENDALE

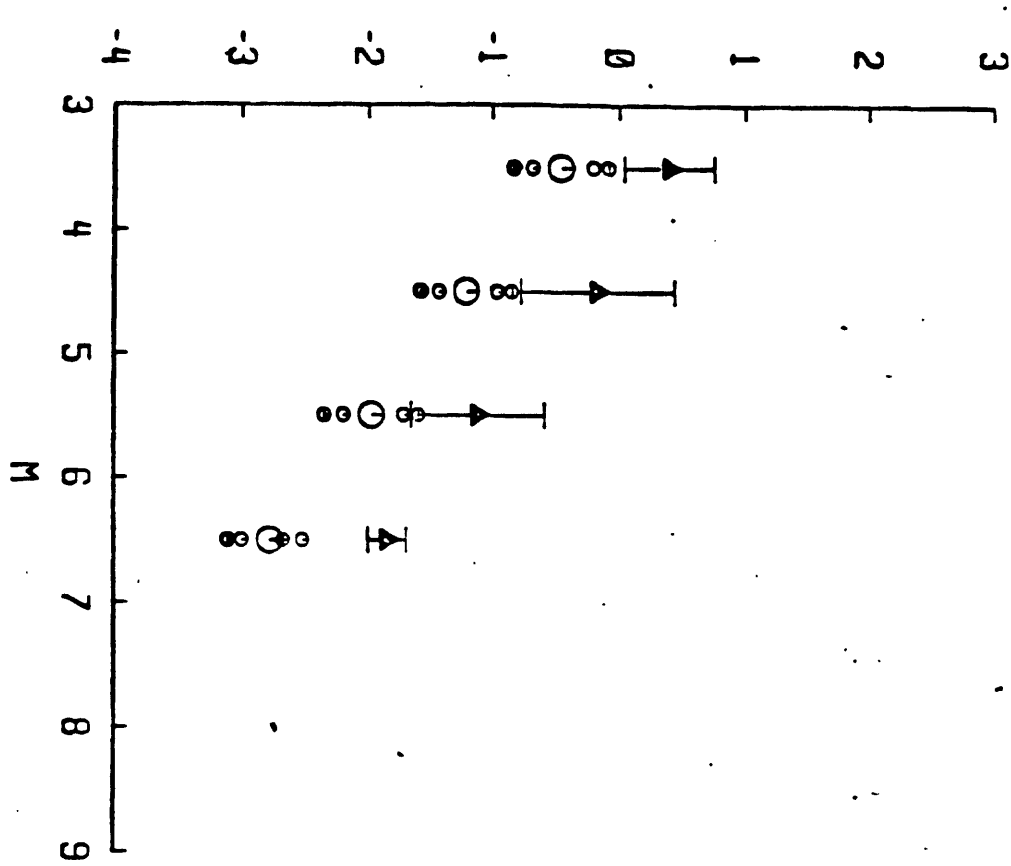
APPENDIX I-2

LOG (EVENTS/YEAR/MAG UNIT)

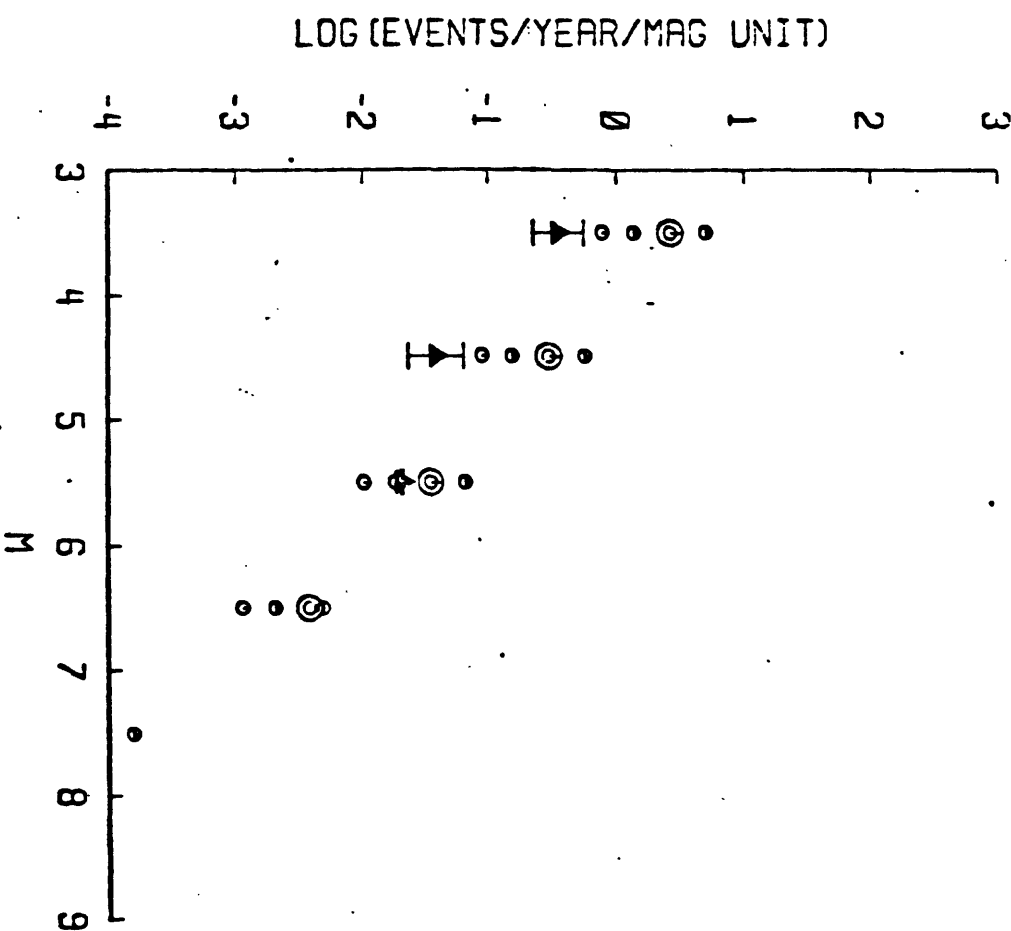


MOJAVE *

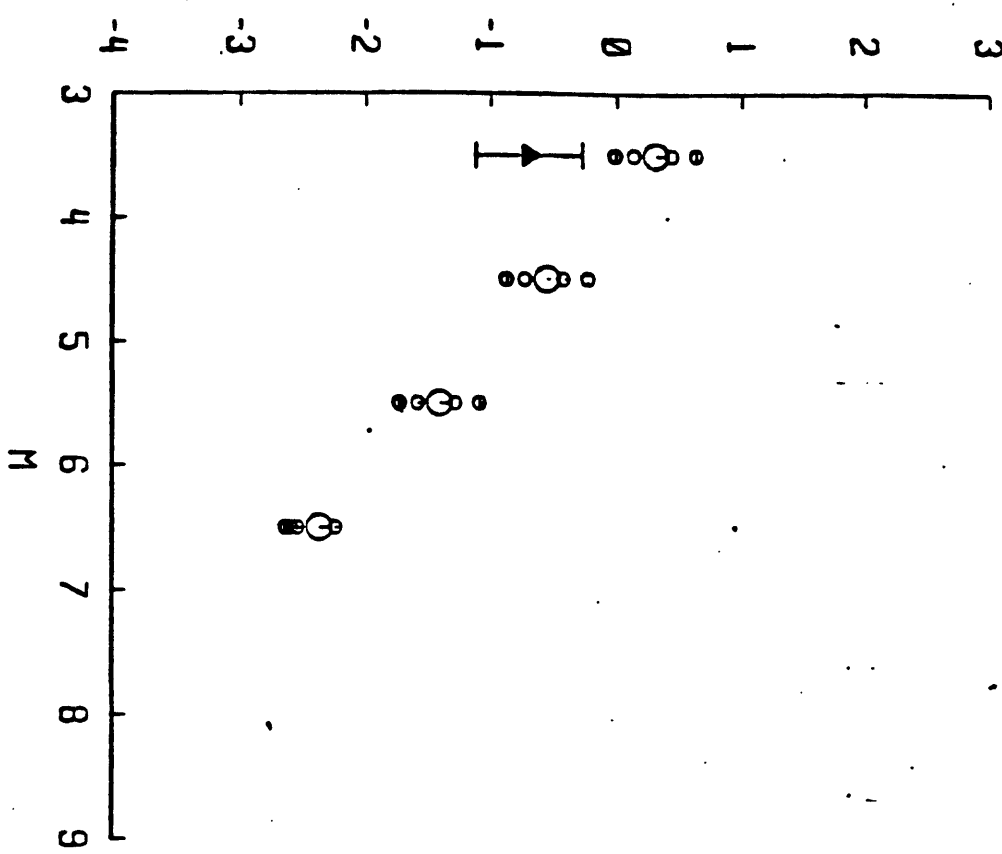
NEWPORT-INGLEWOOD



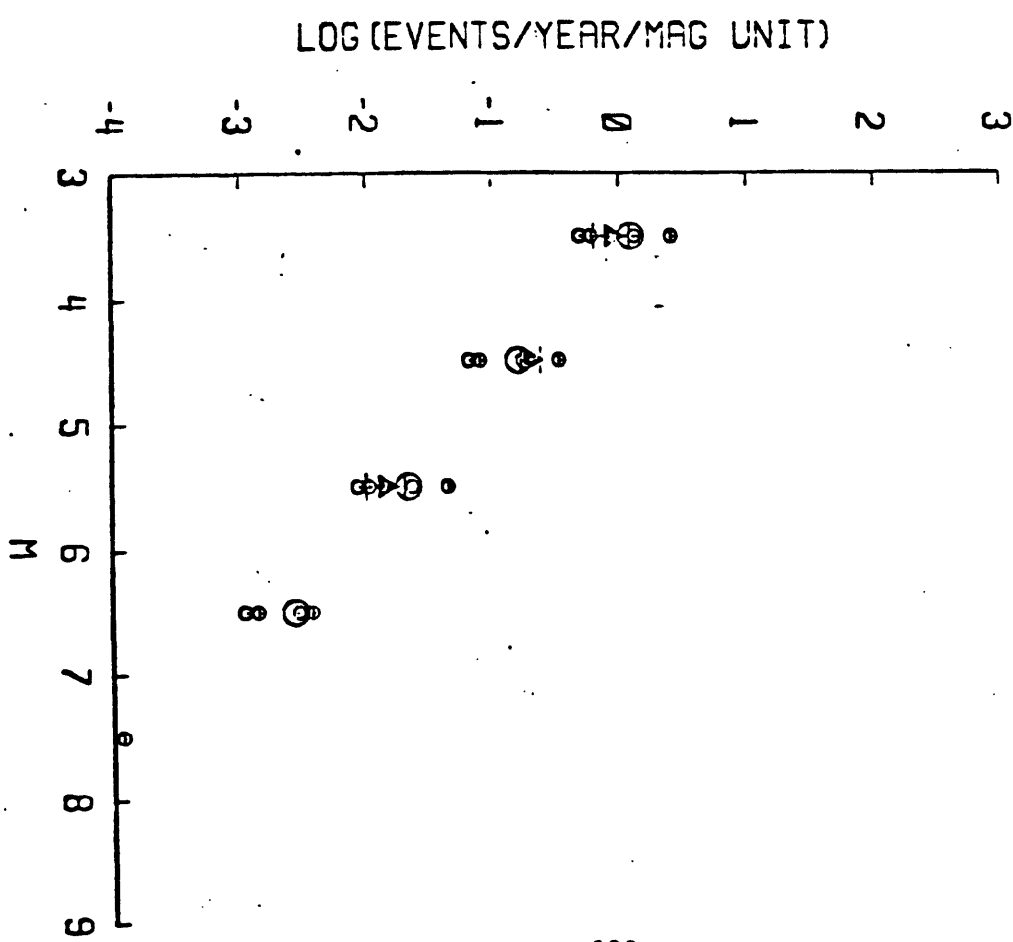
OFFSHORE ZONE DEFORMATION



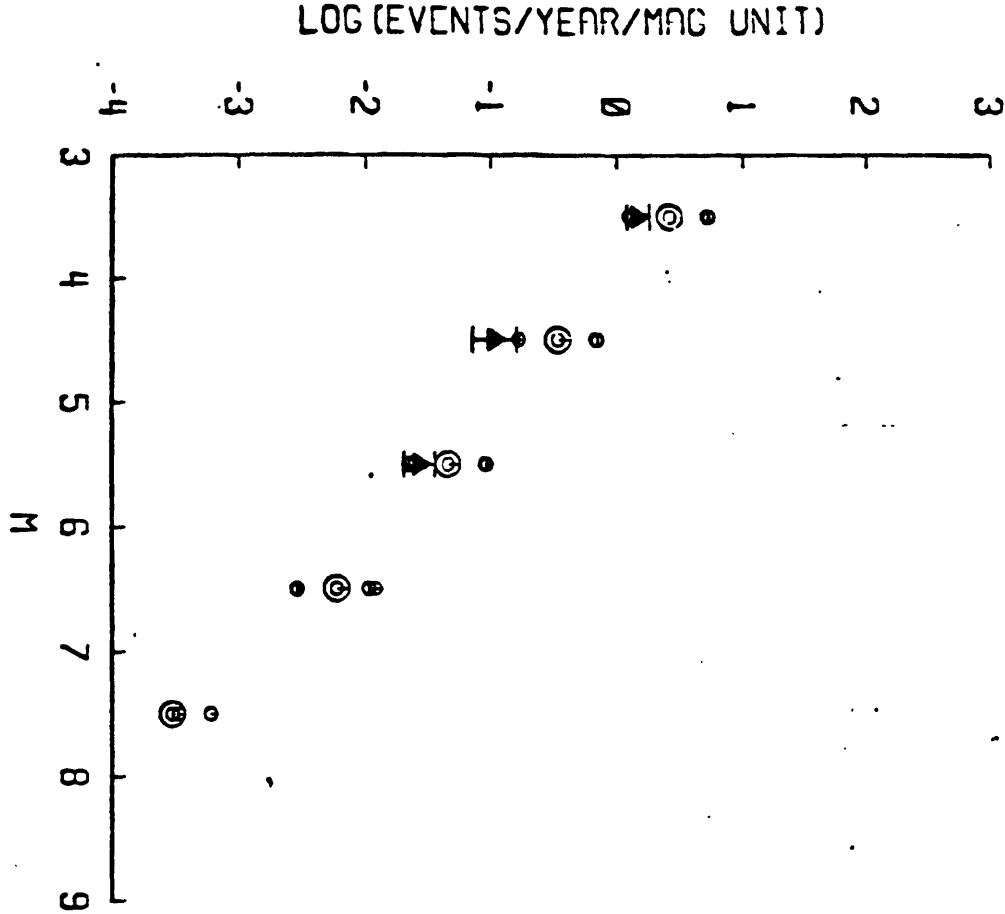
ROSE CANYON



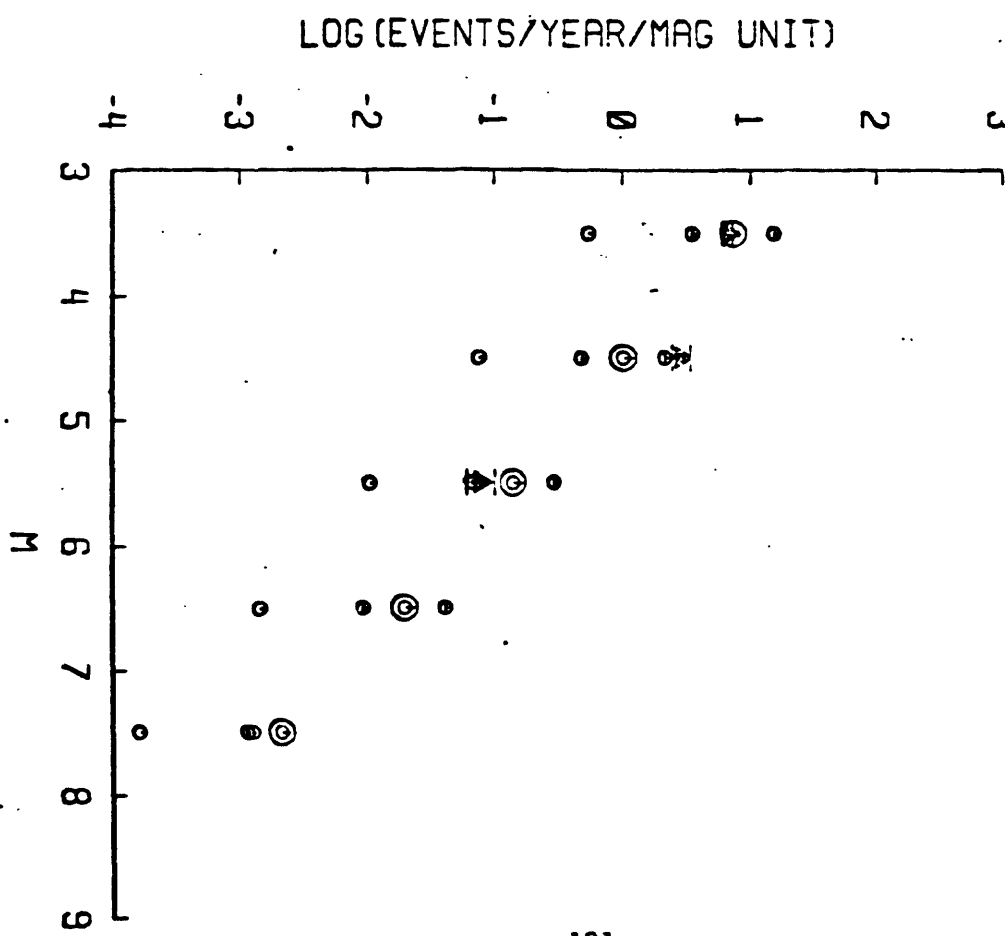
PALOS VERDES



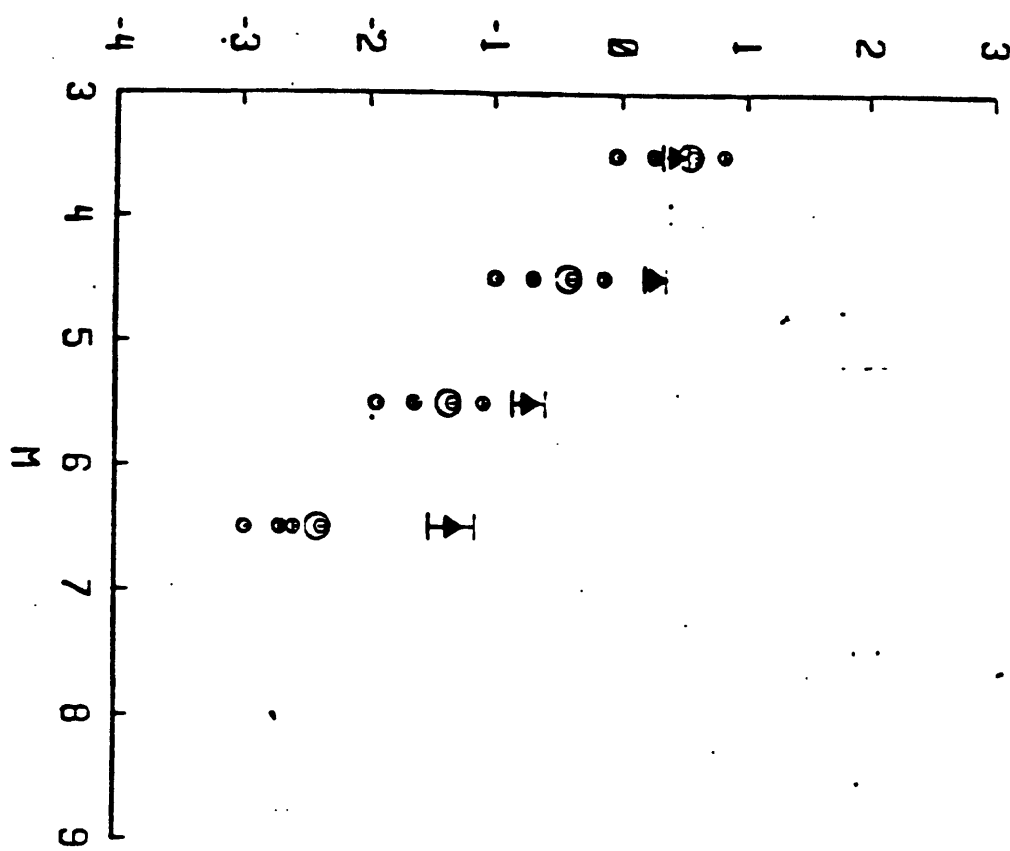
SAN CLEMENTE



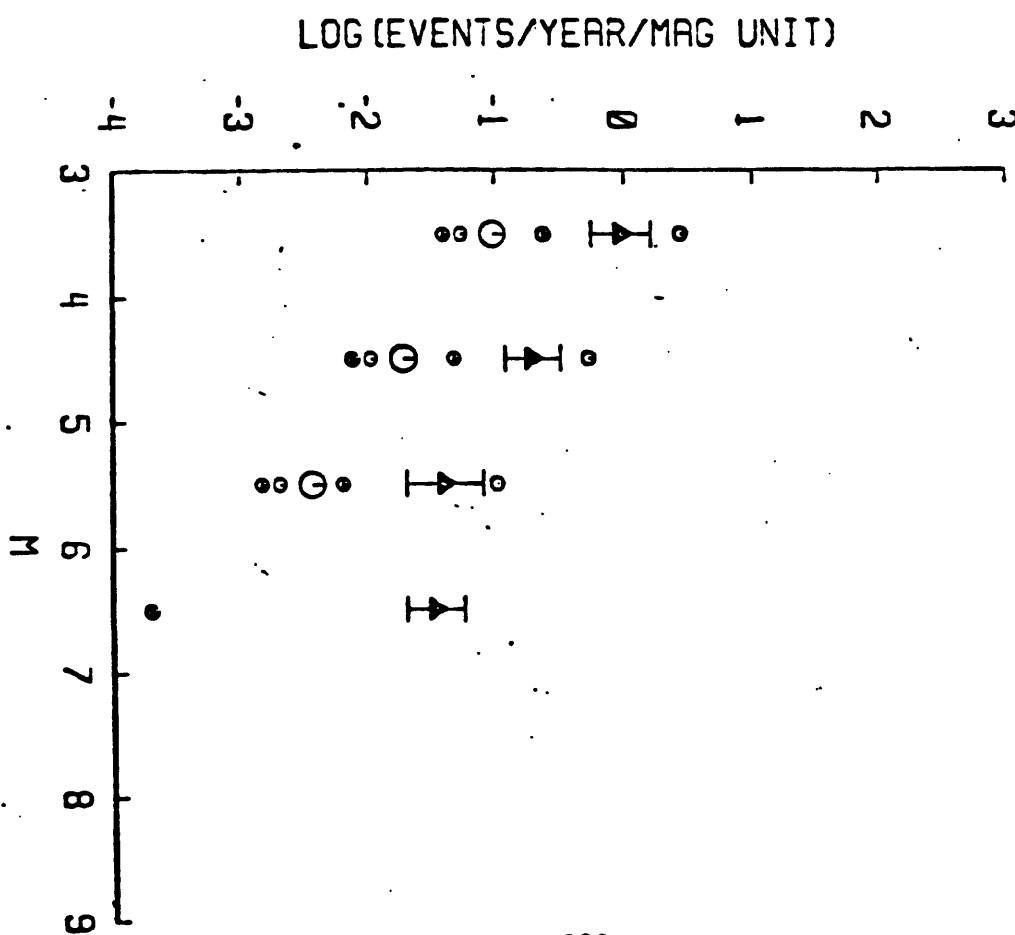
SIERRA-OWENS (-1945.99)



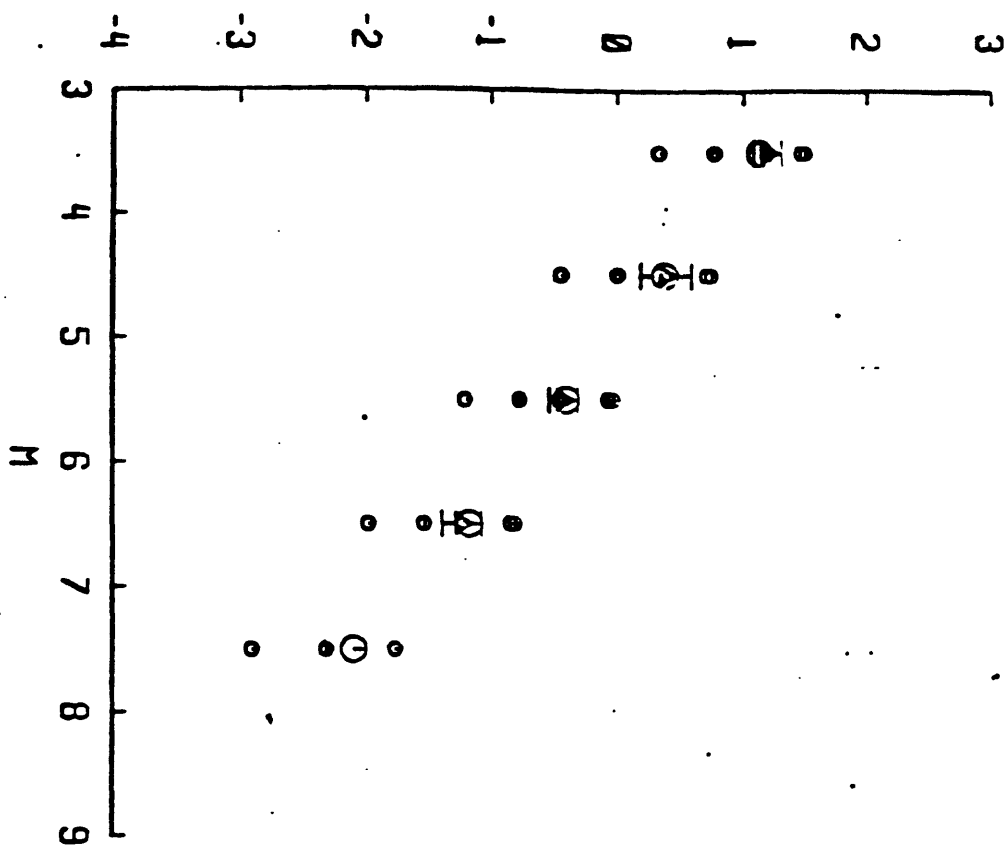
HILTON (-1940.99)



STAMPEDE (-1965.99)



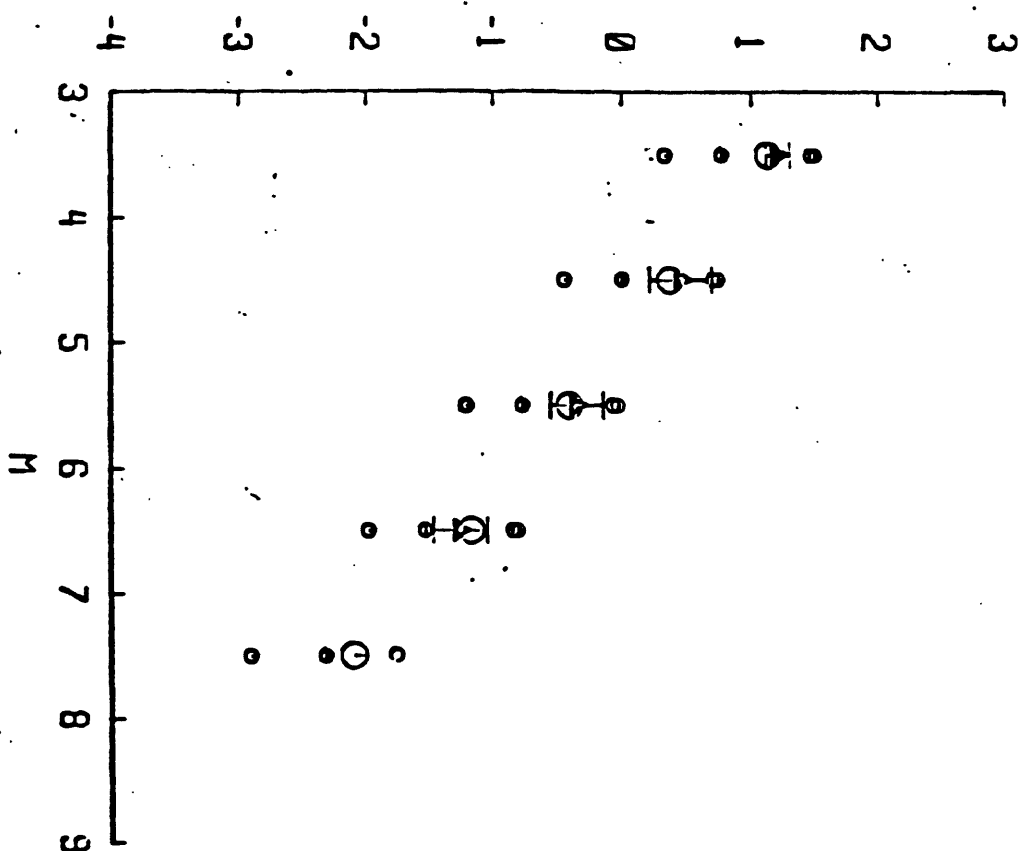
LOG (EVENTS/YEAR/MAG UNIT)



SAN JACINTO (1967.99)

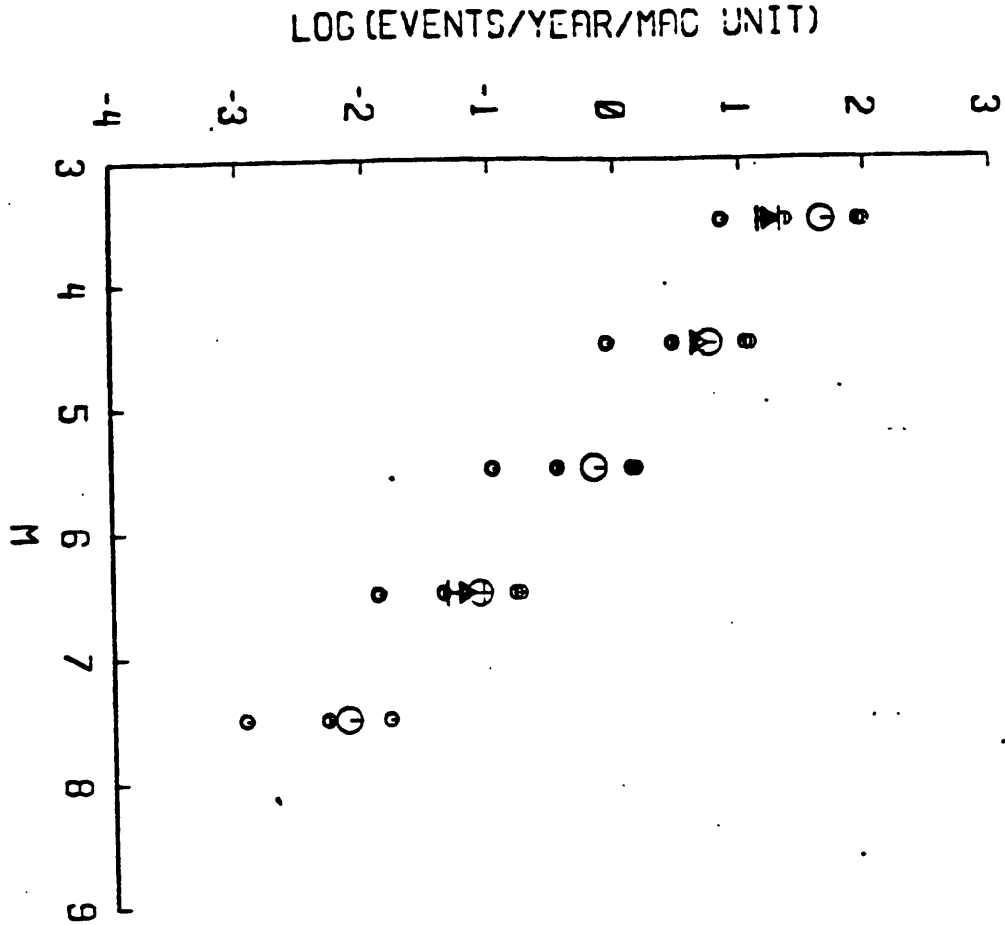
APPENDIX I-2

LOG (EVENTS/YEAR/MAG UNIT)

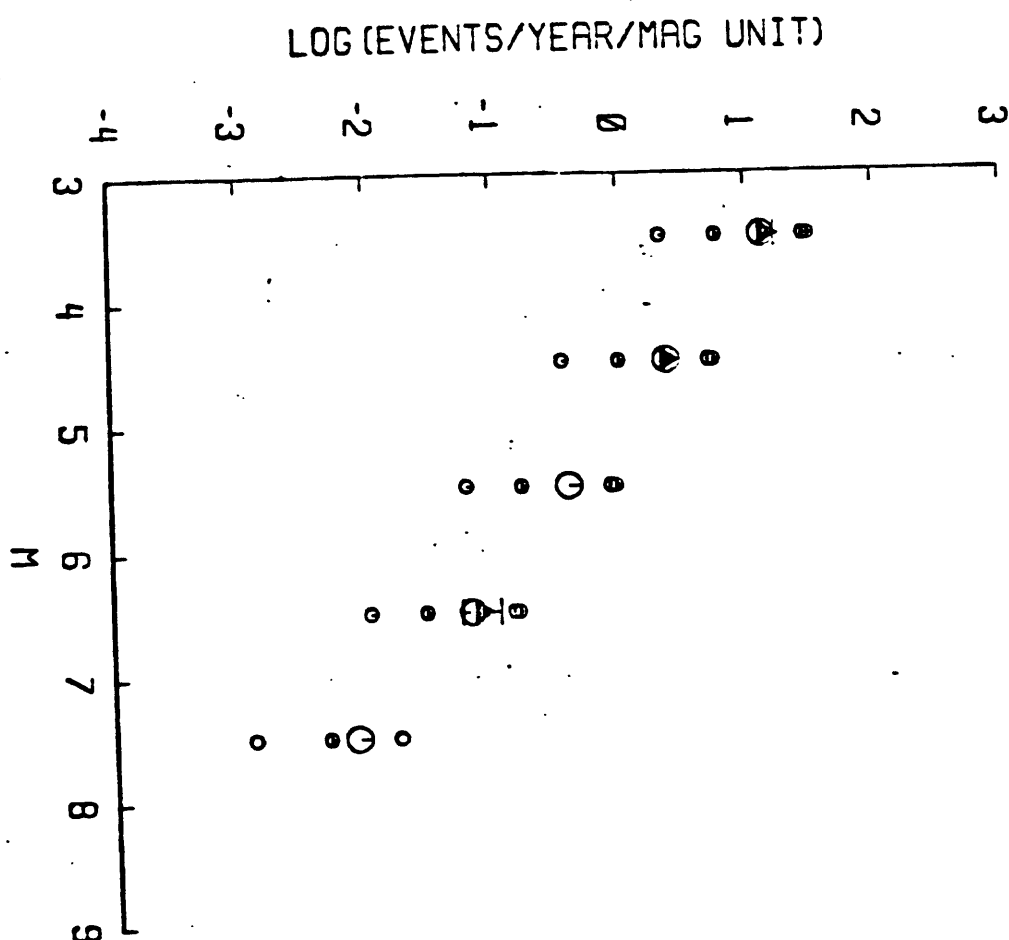


SAN JACINTO (1953.99)

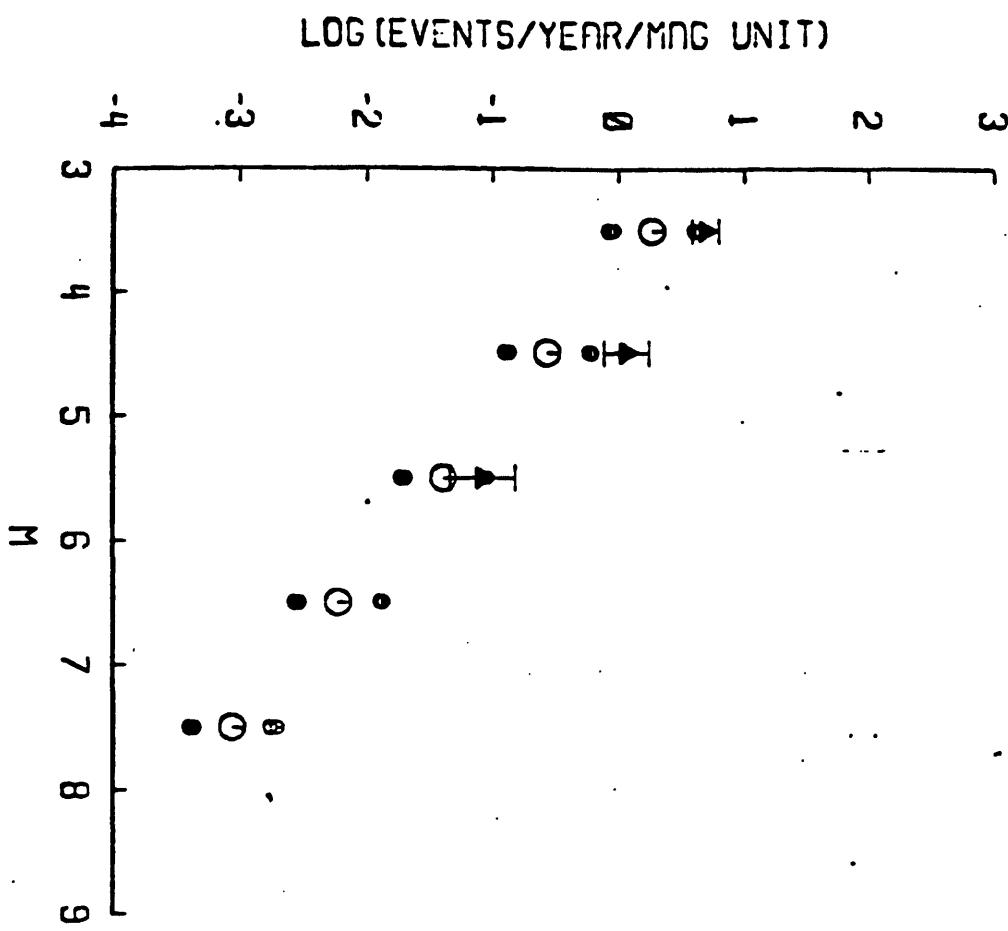
SAN JACINTO (-1941.99)



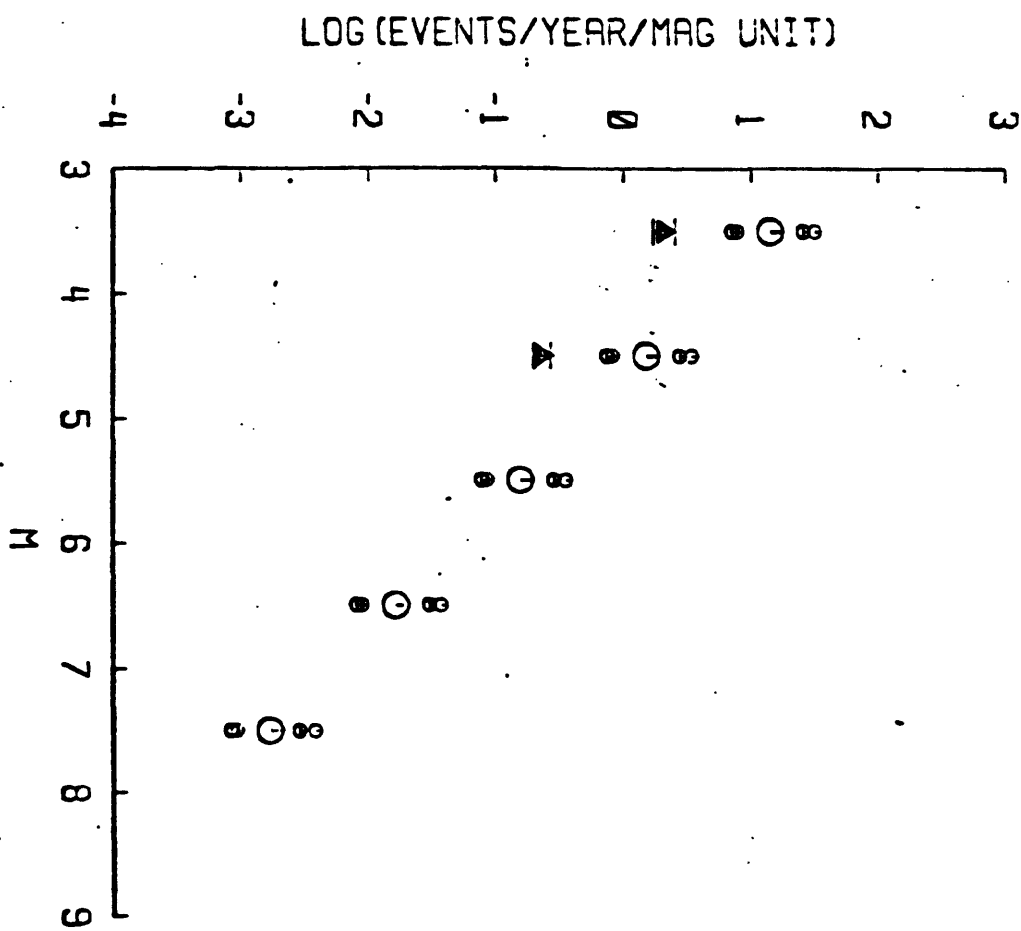
SAN JACINTO (-1936.99)



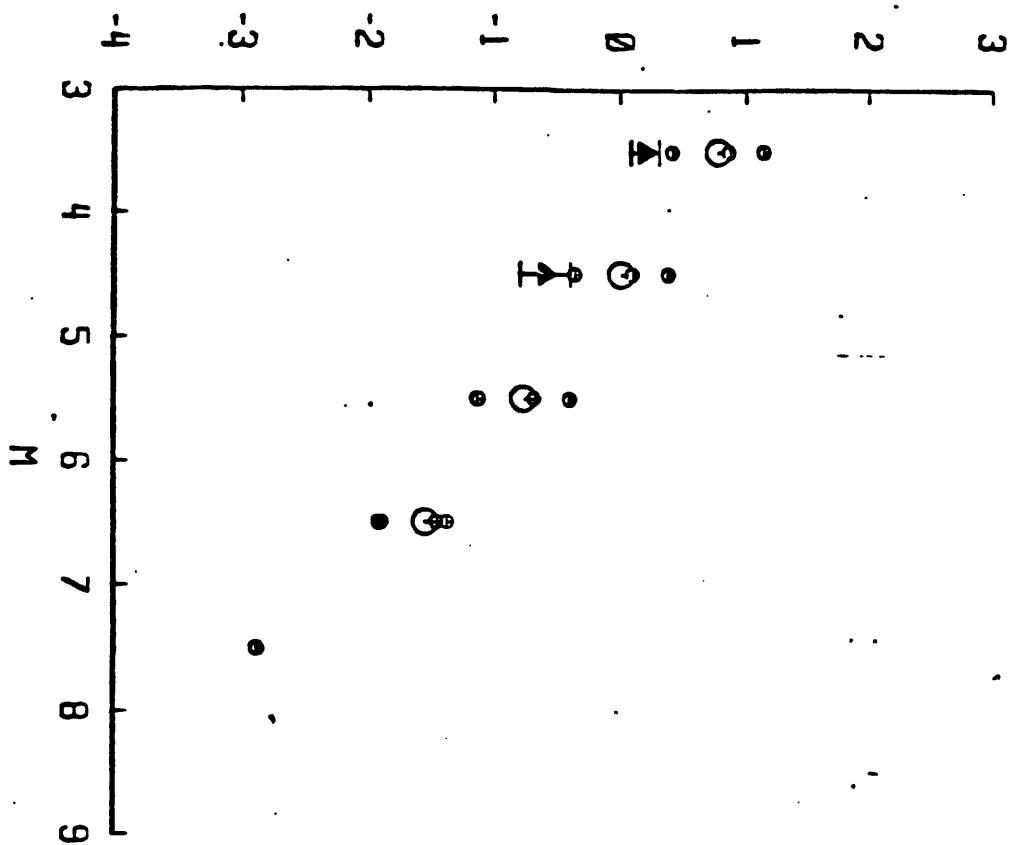
SAN ANDREAS 10 (-1978.99)



SAN ANDREAS 9 (-1947.99)

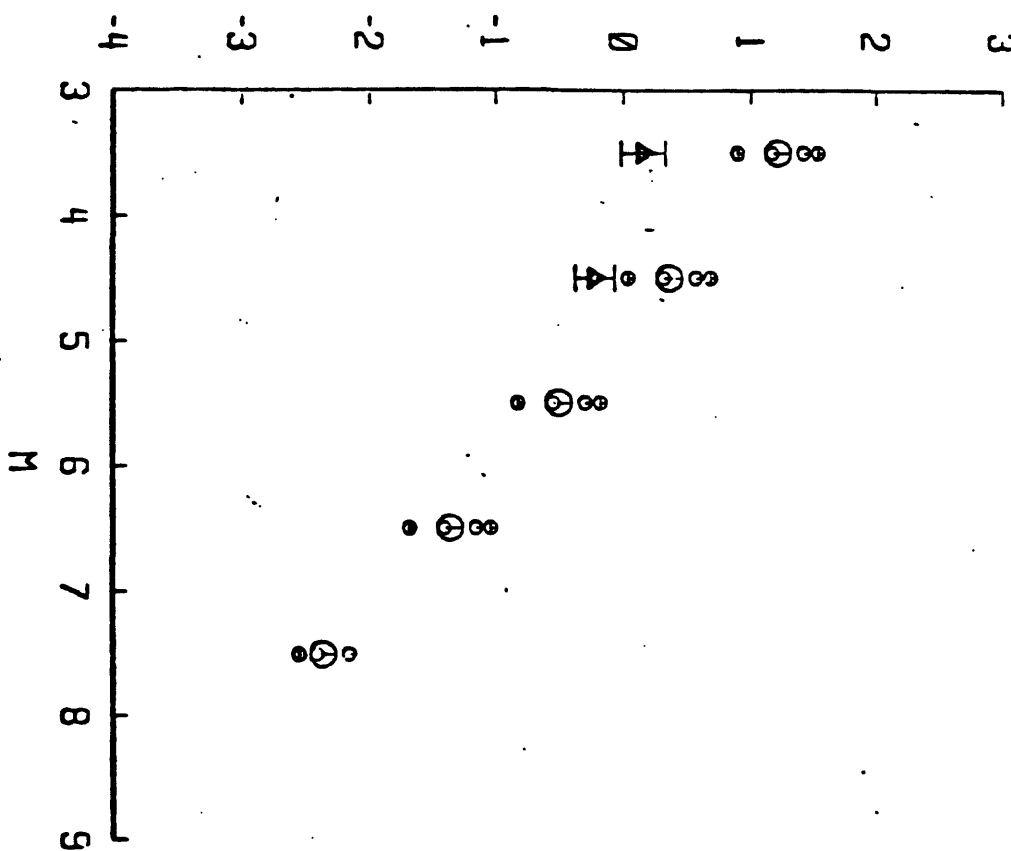


LOG (EVENTS/YEAR/MAG UNIT)



WHITE WOLF (-1951.99)

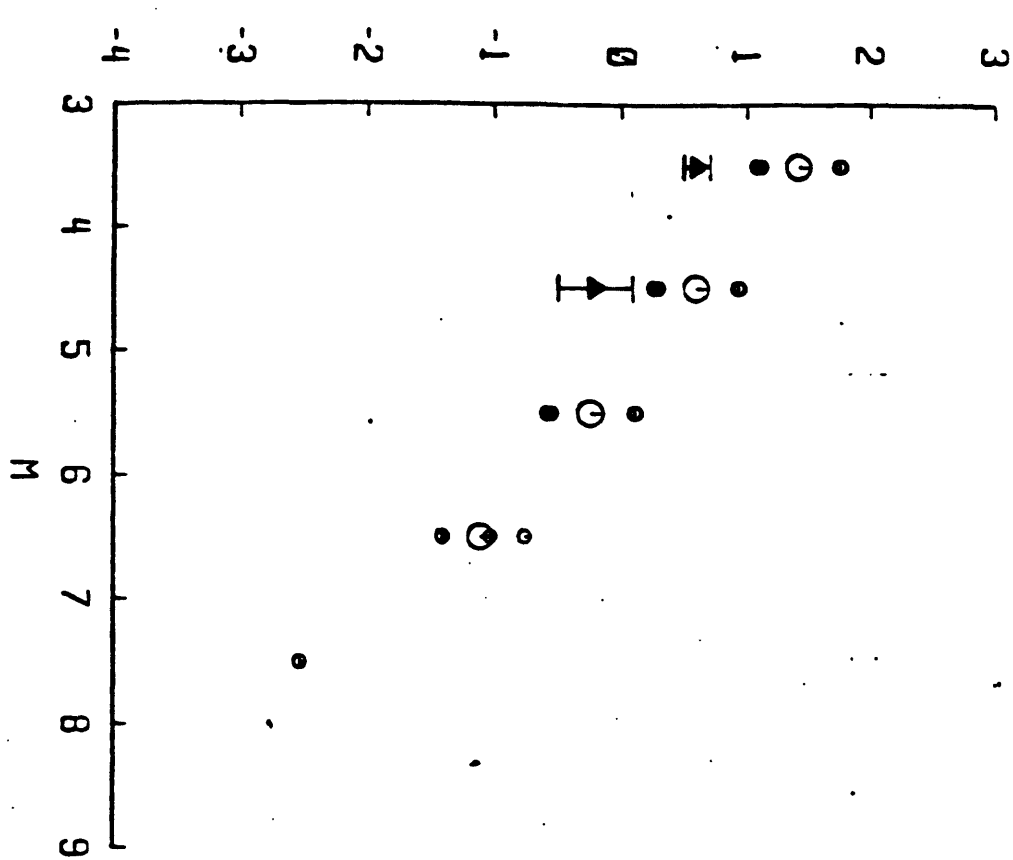
LOG (EVENTS/YEAR/MAG UNIT)



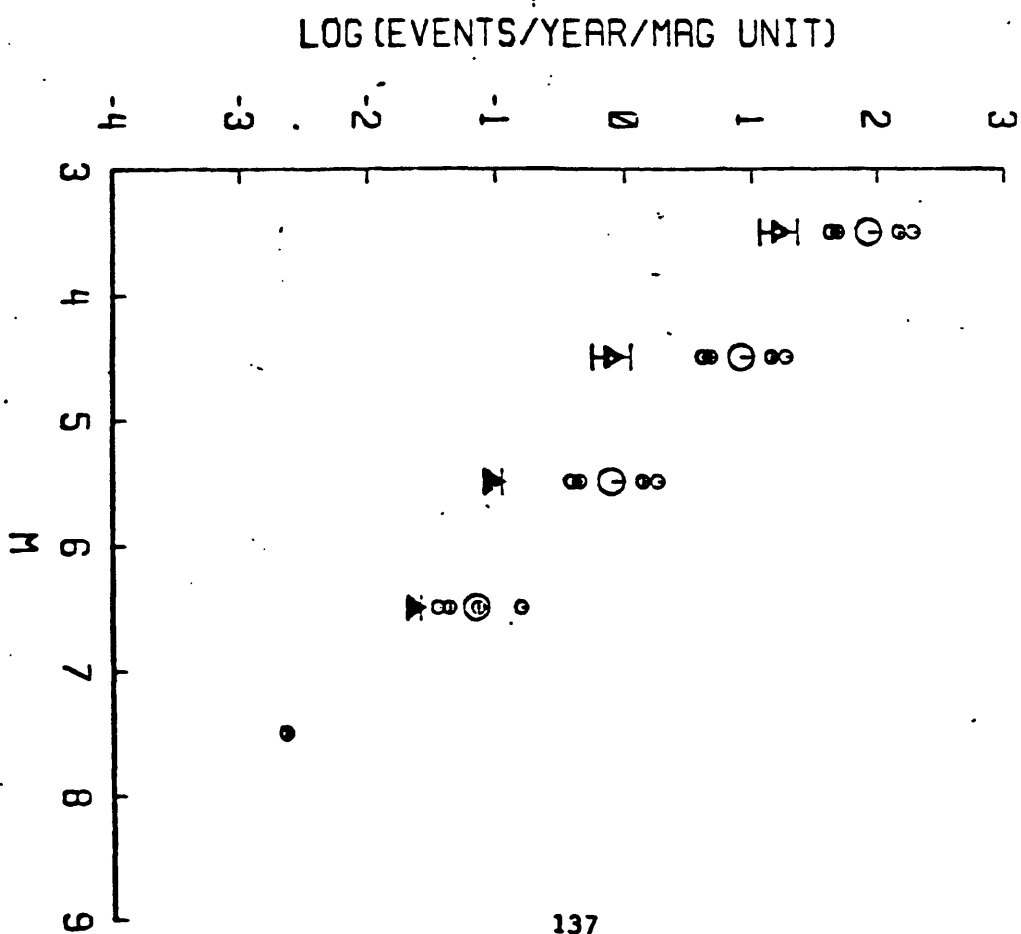
HOSSGRI (-1951.99)

APPENDIX I-2

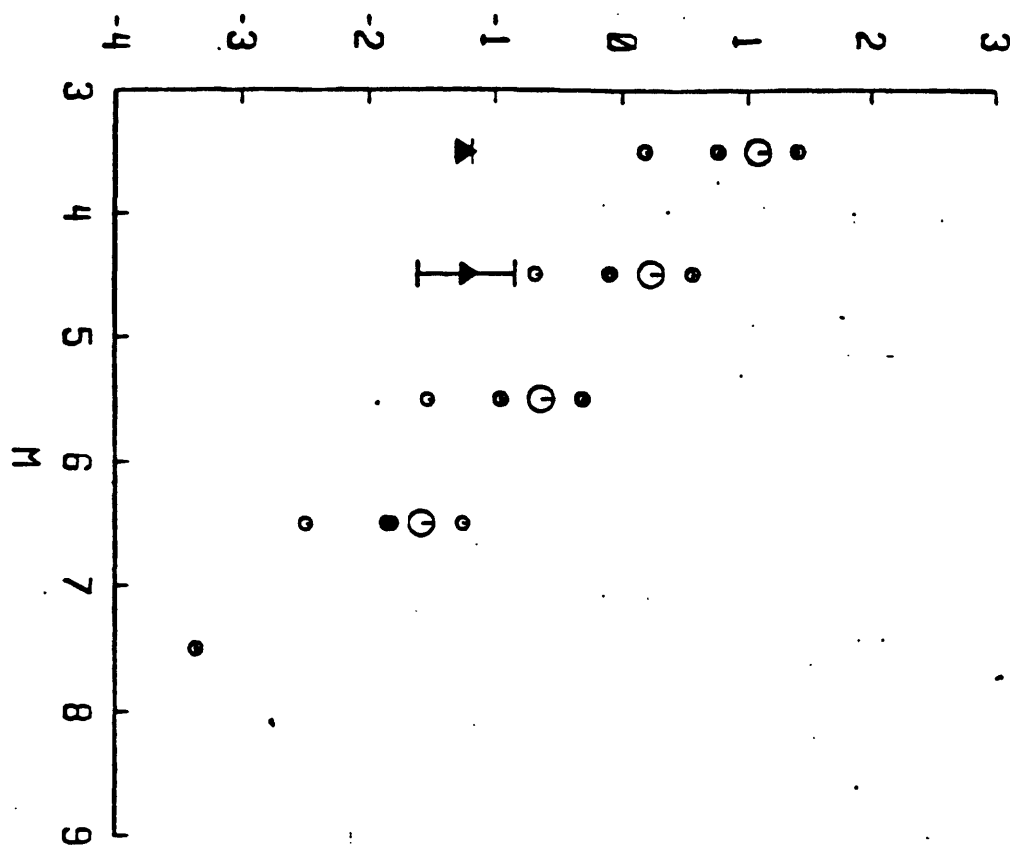
IMPERIAL (-1939.99)



IMPERIAL (-1978.99)



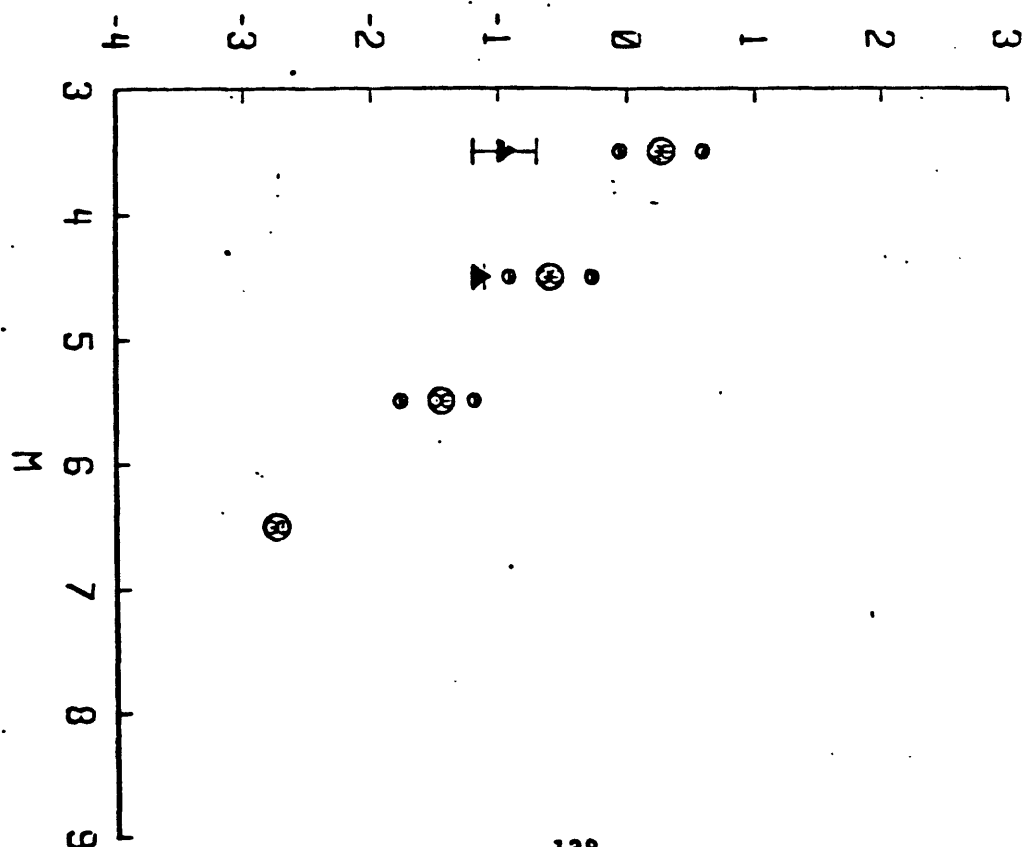
LOG (EVENTS/YEAR/MAG UNIT)



SIERRA MADRE (1970.99)

APPENDIX I-2

LOG (EVENTS/YEAR/MAG UNIT)



MANNIX (-1946.99)

CONSEQUENCES OF SLIP RATE CONSTRAINTS ON EARTHQUAKE OCCURRENCE RELATIONS

by John G. Anderson and J. Enrique Luco

ABSTRACT

Three functional forms for earthquake occurrence relations are compared, and slip rate constraints on each are derived. Constrained occurrence relations referred to total fault area, to rupture area of the maximum magnitude earthquake, and to a particular site along the fault are presented and discussed. The slip rate constraints provide a means to estimate M_{\max} from occurrence rates of small magnitude earthquakes, or a means to estimate the threshold of observations in a qualitative earthquake catalog, as well as a means to estimate occurrence rates when M_{\max} is obtained from other considerations. This paper shows examples of these three types of applications.

The relations considered are: $N_1(M)$ is such that the cumulative occurrence rate of earthquakes with magnitude greater than M is an exponential function truncated at M_{\max} , $N_2(M)$ is such that the corresponding incremental occurrence rate is a truncated exponential function, and $N_3(M)$ is such that the corresponding incremental occurrence rate is an exponential function plus a constant which causes the rate to go to zero at M_{\max} . A speculative model for the magnitudes of the earthquakes at Pallett Creek observed by Sieh (1978a) suggests that $N_2(M)$ is more appropriate than $N_1(M)$ or $N_3(M)$ for these earthquakes.

Institute of Geophysics and Planetary Physics University of California, San Diego, La Jolla, CA 92093 (JGA).

Department of Applied Mechanics and Engineering Sciences, University of California, San Diego, La Jolla, CA 92093 (JGA and JEL).

Preprint submitted for publication May 1982. Revised September 1982.

INTRODUCTION

Earthquake occurrence relations are used extensively in applications which require considerable accuracy, especially seismic risk analysis. It is increasingly common in seismic risk analyses to use geological slip rates or geological deformation rates to constrain the parameters of occurrence rate expressions. However, this has been done with little regard for the effect which the particular functional form of the occurrence rate relation might have on the outcome. Because earthquake occurrence rates are directly related to the rate of tectonic deformation, any of the several parametric forms which have been proposed to describe earthquake occurrence rates can be constrained to be consistent with known deformation rates. In this paper the emphasis is on occurrence relations as constrained by a slip rate on a fault. *Anderson (1979)*, *Molnar (1979)*, and *Papastamatiou (1980)* have shown how the slip rate can be easily replaced by a regional strain rate when appropriate.

The implications of the slip-rate constraint on occurrence relations have been recognized by several previous studies. *Brune (1968)* and *Davies and Brune (1971)* used the cumulative moment of events on a fault to estimate the slip rate. *Smith (1976)* used the cumulative moment, from geological studies, to try to constrain the maximum magnitude on a fault. *Anderson (1979)*, *Molnar (1979)*, and *Campbell (1977)* developed methods to obtain occurrence relations from slip rates. *Greensfelder et al. (1980)* and *Doser and Smith (1982)* have estimated long-term seismicity of various regions by this method. *Papastamatiou (1980)* used the slip rate and observed low-magnitude occurrence rates to estimate the maximum magnitude. In this paper the basic equations required for the above applications are derived for each of three functional forms for the occurrence rate relation. We also present an additional application, in which an occurrence rate derived from pre-instrumental sources may be used to estimate the magnitude threshold of the observations.

In the past, slip rate constraints on occurrence relations for individual faults have been derived on the assumption of a given fault length and width. For our purposes, two additional normalizations are convenient and lead to interesting results. As one alternative normalization the occurrence relation is taken to give the number of events over an area of the fault equal to that which ruptures in the

APPENDIX II

maximum earthquake M_{max} . The other alternative normalization gives the number of earthquakes which rupture the fault at a specific site along its surface trace. This alternative applies to the risk of direct faulting beneath a site and helps to interpret geological observations of repeated earthquakes as observed in a single trench. Results for this normalization are most easily derived from results for the first alternative. Both of these alternatives require the use of a relation between the extent of rupture and magnitude.

EARTHQUAKE OCCURRENCE RELATIONS

Campbell (1977), Anderson (1979), Molnar (1979), and Papazamiatou (1980) have all demonstrated how the parameters of earthquake occurrence relations can be selected so that the seismicity is consistent with the known crustal deformation rates. However, the selection of the particular functional form of the occurrence relation from the many which are proposed in the literature has not received scrutiny. The purpose of this section is to discuss briefly the range of proposed forms and their significance to the extension of this method. We limit the discussions to three-parameter functional forms characterized by the rate of occurrence at a magnitude of reference, a b -value, and a maximum magnitude M_{\max} . Because the assumed distribution of large earthquakes is critical, only the shape of occurrence-rate curves near M_{\max} is considered.

Richter (1958) points out that the frequency of earthquake occurrence within a region, as a function of magnitude, can be written as either a cumulative distribution function, $N(M)$, giving the number of shocks with magnitude M or greater per unit time, or as a density function $n(M)$, where

$$n(M) = - \frac{dN(M)}{dM} . \quad (1)$$

This density function is closely related to an incremental occurrence rate $n'(M) = N(M - \frac{\Delta M'}{2}) - N(M + \frac{\Delta M'}{2})$ for earthquakes in a magnitude band of width $\Delta M'$ which for sufficiently small $\Delta M'$ can be written in the form $n'(M) = n(M)\Delta M'$ (e.g. *Herrman, 1977*). *Gutenberg and Richter (1954)* plotted the worldwide data set, and found that while it approximately obeys the rule $\log n'(M) = a - bM$, there is a shortage of earthquakes relative to this rule for $M \geq 8$. *Bloom and Erdmann (1980)* reconfirm this observation. Both of these studies employ magnitude scales which correspond essentially to surface wave magnitude M_s . Several functional shapes might be used to approximate these observations (e.g. *Main and Burton, 1981; Esteve, 1976; Makjanic, 1980; Caputo, 1977*). For mathematical simplicity, we use the function

$$n_3(M) = \left(10^{a_3 - bM} - 10^{a_3 - bM_{\max}} \right) H(M_{\max} - M) . \quad (2)$$

APPENDIX II

which is a specific case of a form proposed by *Main and Burton (1981)*. In (2), $H(\cdot)$ denotes the Heaviside step function and M_{\max} is the maximum magnitude.

It could be argued that the relative 'shortage' of earthquakes with $M_s \geq 8$ is due to saturation of M_s for large events. The theoretical bases for the eventual saturation of the surface wave magnitude scale are generally accepted (Aki, 1967, 1972; Kanamori and Anderson, 1975; Geller, 1976; Kanamori, 1977; Hanks and Kanamori, 1979). Due to the relative scarcity of data for large events, the precise nature of the saturation is not well determined. In particular, Bloom and Erdmann (1980) based on a statistical analysis of events with $M_s \geq 8.0$ have concluded that, on the average, no saturation of M_s with respect to M_w (moment magnitude) is observed. On the other hand, the only four events in Kanamori's (1977) compilation with $M_w \geq 9.0$ have $M_s \leq 8.4$. It should be mentioned that Chinnery and North (1975) have corrected the world-wide cumulative occurrence rate for a plausible estimate of the effects of saturation and have found a linear relation between $\log N(M_o)$ and $\log M_o$ where M_o is the seismic moment. This implies a linear relation between $\log N(M_w)$ and M_w which differs from the cumulative occurrence rate implied by Eq. (2). Given the uncertainties involved in describing the saturation we do not rule out the possibility that occurrence rates may be described by Eq. (2) and consider this particular form as one possible alternative.

A second alternative is to employ the relationship

$$n_2(M) = 10^{a_2 - bM} \quad H(M_{\max} - M) \quad (3)$$

which has been used by Bath (1978) and Anderson (1979). *Berrill and Davis (1980)* have argued that this form works well at large magnitudes. The calculation of the cumulative occurrence rates from $n_2(M)$ and $n_3(M)$ is based on the implicit assumption that $N_3(M_{\max}) = N_2(M_{\max}) = 0$.

A third possibility is to consider the cumulative occurrence rate suggested by the work of Chinnery and North (1975), namely

$$N_1(M) = 10^{a_1 - bM} \quad H(M_{\max} - M) \quad (4)$$

Smith (1976), Campbell (1977) and Molnar (1979) have used this form in conjunction with slip rate

APPENDIX II

constraints on occurrence relations. This form, which also seems to be widely used in probabilistic seismic risk studies (e.g. *Housner*, 1969, *McGuire*, 1974, *Campbell*, 1977), is even more enriched in large magnitude earthquakes than the recurrence relation defined by Eq. (3). *Papastamatiou* (1980) discussed both forms $n_2(M)$ and $N_1(M)$, but his constraint on the occurrence relation parameters (Eq. (18) in his paper) is derived only for $N_1(M)$.

The occurrence relations defined by Eqs. (2), (3), and (4) can be summarized by the expression

$$N_i(M) = A_i \left[\left(e^{\bar{b} \Delta M} - 1 \right) + B_i \bar{b} \Delta M + C_i \right] H(\Delta M) \quad (5)$$

where $\Delta M = M_{\max} - M$. In Eq. (5) and in the sequel we use the notation $\bar{p} = p \ln 10$. From Eqs. (1) and (5) one obtains

$$n_i(M) = A_i \left[\bar{b} e^{\bar{b} \Delta M} H(\Delta M) + B_i \bar{b} H(\Delta M) + C_i \delta(\Delta M) \right] \quad (6)$$

where $\delta(\cdot)$ is the Dirac delta function. The distribution functions defined in Eqs. (4), (3), and (2) are obtained from (5) or (6) by setting

$$i = 1, \quad B_1 = 0, \quad C_1 = 1;$$

$$i = 2, \quad B_2 = 0, \quad C_2 = 0; \text{ and}$$

$$i = 3, \quad B_3 = -1, \quad C_3 = 0, \text{ respectively.}$$

The coefficient A_1 corresponds to $10^{a-bM_{\max}}$ in Eq. (4); A_2 and A_3 correspond to $\frac{1}{b} 10^{a-bM_{\max}}$ in Eqs.

(2) and (3). We note that *Smith* (1976), *Campbell* (1977), and *Papastamatiou* (1980) fail to include the term in $\delta(M_{\max} - M)$ when they differentiate Eq. (4). This error is carried throughout each of their analyses.

The three functional forms defined above are illustrated in Fig. 1 for the case $N_1(6) = N_2(6) = N_3(6) = 1.0$, $b = 1.0$ and $M_{\max} = 8.0$. In the cumulative distributions, $N_1(M_{\max})$ is greater than zero, while $N_2(M)$ and $N_3(M)$ approach zero as M tends to M_{\max} . Thus, $N_1(M)$ represents a form of the recurrence relation which is enriched in large magnitude events relative to

APPENDIX II

$N_2(M)$, and $N_3(M)$ is depleted in large magnitude events relative to $N_1(M)$. Fig. 1B shows the corresponding incremental rates $n_1'(M)$, $n_2'(M)$, and $n_3'(M)$. Based on Eq. (6), there are significant differences among the three density functions in the neighborhood of M_{max} . However, in the incremental rates these differences are obscured. The incremental rates shown in Fig. 1B correspond to 0.25 magnitude intervals centered at the quarter magnitude points [$n'(M) = N(M - 0.125) - N(M + 0.125)$]. The point plotted at $M = 8.0$ corresponds to the last interval (7.875, 8.125) which extends beyond $M_{max} = 8.0$. Since $N(8.125) = 0$, then, $n'(8.0) = N(7.875)$ which deviates from the approximation $n'(M) = n(M) \times 0.25$ valid at lower magnitudes. Although this choice accentuates some peculiar behavior near M_{max} , it is representative of the actual situation in which M_{max} is unknown.

With respect to occurrence rates on single faults some arguments, based on limited data, have been advanced which suggest that the description given by $N_1(M)$ is more appropriate than $N_2(M)$ or $N_3(M)$. In particular, Swan *et al.* (1980) and Schwartz *et al.* (1981) have suggested, based on geological observations, that a segment of a fault repeatedly ruptures with a characteristic earthquake with magnitude near M_{max} . This suggestion may be supported on the San Andreas fault in California by results of Sieh (1978a) and Bakun and McEvilly (1979). Mathematically this could be represented by an occurrence relation with form $N_1(M)$, and a very small b -value. Singh *et al.* (1981) suggest that this is the case along the subduction zone of Mexico and Lahr and Stephens (1982) suggest that a small b -value characterizes large events in Alaska. This model was adopted by Caputo (1977). Wesnousky and Scholz (1983), also, find that the recurrence relation for Japan can be generated from the distribution of fault lengths if each fault in a region ruptures with its own characteristic earthquake. Actually, the idea of "characteristic" earthquakes cannot be interpreted to mean strictly periodic repetition of identical events. Where there are observations of more than one ^{major} earthquake on a fault, the sizes usually differ somewhat. This is seen by Sieh (1978a), Bakun and McEvilly (1979), Shimazaki and Nakata (1980), Singh *et al.* (1981), Sykes and Quillmeyer (1981), and others. The variation in magnitude may be small, but the nature of that variation is unknown. It is desirable to use observations to select the appropriate mathematical form for the occurrence rate relation.

APPENDIX II

Considering the previous discussion as well as that pertaining to the issue of magnitude saturation, we shall consider the occurrence relations defined by Eqs. (5) and (6) for $i=1,2$ and 3, designated as Occurrence Relation 1, 2, and 3, respectively, and derive parallel results for these three alternative functional forms. The three forms are representative of the 3-parameter relations in the literature. There remains the possibility that more complex forms involving 4 or more parameters might sometimes be needed. *Singh et al. (1981)* and *Lahr and Stevens (1982)* suggest that a relation with a typical b -value at small magnitudes but a small b -value at large magnitudes is needed for the subduction zones of Mexico and Alaska.

Because occurrence relations 1, 2, and 3 are all truncated, extreme magnitudes will obey the third asymptotic distribution of extremes (*Gumbel, 1960*), as required by the results of *Yegulalp and Kuo(1974)*.

RELATION BETWEEN SEISMIC MOMENT RELEASE RATE AND OCCURRENCE RELATION PARAMETERS

The average cumulative moment which is released per year within a given region by earthquakes with magnitude greater than or equal to M is

$$\dot{M}_o(M') = \int_M^\infty M_o(M') n(M') dM' . \quad (7)$$

To evaluate this, we will use the relation

$$M_o(M) = 10^{c+dM} = M_o(M_{\max}) e^{-\bar{d} \Delta M} \quad (8)$$

where typically, $c = 16.0$ and $d = 1.5$ for M_o in units of dyne-cm (Hanks and Kanamori, 1979). We note that Eq. (8) defines the magnitude scale to be used in this paper. Then from Eqs. (6), (7), and (8),

$$\dot{M}_o(M) = A_i M_o(M_{\max}) \left\{ \left(\frac{\bar{b}}{\bar{d} - \bar{b}} \right) \left[1 - e^{-(\bar{d} - \bar{b}) \Delta M} \right] + \frac{\bar{b}}{\bar{d}} B_i \left[1 - e^{-\bar{d} \Delta M} \right] + C_i \right\} . \quad (9)$$

For $M \rightarrow \infty$ and $\bar{b} < \bar{d}$, one obtains the total moment per year, \dot{M}_o^T , as:

$$\dot{M}_o^T = \gamma_i A_i M_o(M_{\max}) \quad (10)$$

where

$$\gamma_i = \frac{\bar{b}}{\bar{d} - \bar{b}} + \frac{\bar{b}}{\bar{d}} B_i + C_i . \quad (11)$$

For $i = 1, 2$, and 3 , the values of these coefficients are $\frac{\bar{d}}{\bar{d} - \bar{b}}$, $\frac{\bar{b}}{\bar{d} - \bar{b}}$, and $\bar{b}^2 / \bar{d}(\bar{d} - \bar{b})$, respectively.

Smith (1975), Campbell (1977) and Papastiavrou (1980) obtained $(\frac{\bar{b}}{\bar{d} - \bar{b}})$ instead of $(\frac{\bar{d}}{\bar{d} - \bar{b}})$ for the coefficient γ , for $i = 1$ because of the error in differentiation which was pointed out earlier. Although this coefficient coincides with that for $i = 2$, these authors did not use the cumulative occurrence relation $N_2(M)$, but rather $N_1(M)$.

APPENDIX II

The fraction of the total moment which is released by earthquakes with magnitude greater than M is $\dot{M}_o(M)/\dot{M}_o^T$, and

$$\frac{\dot{M}_o(M)}{\dot{M}_o^T} = 1 - \gamma_i^{-1} \left[\left(\frac{\bar{b}}{d - \bar{b}} \right) e^{-(\bar{d} - \bar{b})\Delta M} + \frac{\bar{b}}{d} B_i e^{-\bar{d}\Delta M} \right] \quad (12)$$

The values of these fractions as a function of ΔM for three choices of b and for $d = 1.5$ are listed in Table 1. Because of the differences near M_{\max} , the distribution corresponding to $i = 1$ releases the most moment near M_{\max} , while the distribution corresponding to $i = 3$ releases the least. The ratios for $b = 0.25$ were included in Table 1 to show how such small b -values could accommodate the hypothesis by Schwartz *et al.* (1981) of a characteristic magnitude earthquake for a given fault. For $i = 1$, and $b = 0.25$, 95% of the moment is released by earthquakes with magnitude within 0.5 of M_{\max} .

For a given seismic moment release rate \dot{M}_o^T , and, after M_{\max} and b have been selected, Eqs. (10) and (8) can be used to obtain estimates of the parameters A_i in Eqs. (5) and (6). This is the procedure used by Anderson (1979) and Molnar (1979). The resulting distribution functions for the case of $\dot{M}_o^T = 8.1 \times 10^{25}$ dyne-cm/year, $b = 1.0$ and $M_{\max} = 8.0$ are compared in Fig. 2. For this choice of b , at $M \ll M_{\max}$, occurrence relation 2 gives 1.5 times as many small earthquakes as occurrence relation 1, and occurrence relation 3 gives 2.25 times as many small earthquakes as occurrence relation 1. For M close to M_{\max} , occurrence relations 2 and 3 include a smaller number of earthquakes than occurrence relation 1.

RELATION BETWEEN SLIP RATE, OCCURRENCE RELATION PARAMETERS AND MAXIMUM MAGNITUDE EARTHQUAKE

Relations Referred to the Entire Fault. Following Brune (1968) and Anderson (1979), if all the slip on the fault occurs seismically, the slip rate on the fault, S , is related to the moment which is released by

$$S = \frac{\dot{M}_o^T}{\mu \Sigma} \quad (13)$$

APPENDIX II

where μ is the shear modulus ($\mu = 3.3 \times 10^{11}$ dyne/cm²) and Σ is the area of the fault surface over which the total seismic moment is released. Anderson hypothesized that \dot{M}^T must be averaged over several cycles of large earthquakes for Eq. (13) to be valid. Eqs. (10) and (13) give

$$A_i = \frac{\mu \Sigma S}{\gamma_i M_o (M_{\max})} . \quad (14)$$

If the total area, Σ , of the fault is known and the occurrence rate is referred to the area Σ , then, Eqs. (5) and (14) can be used to obtain several useful relationships. If $T_i(M) = 1/N_i(M)$ ($i = 1, 2, 3$) represent the estimates of the return period of earthquakes with magnitudes equal or greater than M over the fault area Σ , then,

$$T_i(M) = \gamma_i \left(\frac{M_o(0)}{\mu \Sigma S} \right) e^{\bar{b} M + (\bar{d} - \bar{b}) M_{\max}} \cdot \left[1 - (1 - C_i - B_i \bar{b} \Delta M) e^{-\bar{b} \Delta M} \right]^{-1} \quad (15)$$

where $M_o(0) = 10^c$. From Eq. (15) one can find also the threshold magnitude M corresponding to a return period $T(M)$ and the assumed maximum magnitude. Alternatively, if Σ , S and the return period $T(M)$ of earthquakes with magnitudes equal or greater than M are known, then the maximum magnitude M_{\max} can be estimated. Equations for n_i , N_i , T_i , M , and M_{\max} are given in Tables 2, 3, and 4 for $i = 1, 2$, and 3 respectively. These equations are given in explicit form where possible, but for some of the results, only an implicit solution is possible. In particular, setting $M = M_{\max}$ in Eq. (15) for $i = 1$ leads to

$$M_{\max} = \left(\frac{1}{d} \right) \ln \left[\left(\frac{\bar{d} - \bar{b}}{\bar{d}} \right) \frac{\mu \Sigma S T_1(M_{\max})}{M_o(0)} \right] \quad (16)$$

which can be used to obtain an estimate of M_{\max} if Σ , S , and $T_1(M_{\max})$ are known. Finally, given M , $T(M)$, M_{\max} , Σ , and S , Eq. (15) can be used to obtain estimates of the parameter b .

Relations Referred to the Rupture Area of the Maximum Earthquake. An important special case of the above equations occurs when the area of reference is taken to be equal to area ruptured by the maximum earthquake [$\Sigma = \Sigma(M_{\max})$]. In this case, the fault area does not appear explicitly in the

APPENDIX II

relations involving slip rate, occurrence rates, and maximum magnitude earthquake. The average slip over the rupture area of the maximum magnitude earthquake is

$$\bar{u}(M_{\max}) = \frac{M_o(M_{\max})}{\mu \Sigma(M_{\max})} \quad (17)$$

Equation (17) can be combined with Eq. (14) to give

$$\hat{A}_r = \frac{S}{\gamma_r \bar{u}(M_{\max})} \quad (18)$$

where A_r in Eq. (14) has been replaced by \hat{A}_r in Eq. (18) to denote the value applicable to this special case. The occurrence rates, corresponding to Eqs. (5) and (6), will similarly be denoted as $\hat{N}_r(M)$ and $\hat{n}_r(M)$ for this special case.

At this point it is convenient to introduce a relationship between the average slip on the fault and magnitude. Based on historical data of Sykes and Quittmeyer (1981), Scholz (1982) proposes that to a good approximation, the average slip \bar{u} in a large earthquake (i.e., a earthquake which ruptures the total width, W , of the fault), is proportional to the length of the rupture L_r . For strike slip events, he finds that the average value of $\frac{\bar{u}}{L_r} = \alpha = 1.25 \times 10^{-5}$; for thrust faults, $\alpha = 2 \times 10^{-5}$. Based on this, the definition of seismic moment ($M_o = \mu L_r W \bar{u}$), and Eq. (8), we derive the following relationships:

$$\bar{u}(M) = \beta 10^{\frac{d}{2} M} \quad (19)$$

$$L_r(M) = \frac{\beta}{\alpha} 10^{\frac{d}{2} M} \quad (20)$$

where β is a constant with dimensions of length defined by $\beta = \sqrt{\frac{\alpha M_o(0)}{\mu W}}$. The coefficient of M in eq. (19), for $d = 1.5$, is 0.75, which is 10 percent smaller than Slemmons (1977) worldwide average of 0.833. We note that Slemmons compiled the maximum observed surface offsets, while Eq. (19) is for the average offset over the rupture area. Since these two parameters are different and not necessarily simply related, the discrepancy does not seem to us to be a serious matter at this time. Eq. (19) does

APPENDIX II

suggest an explanation for the scatter in Siemmons data in terms of variations of the parameter $\alpha = \frac{u}{L}$ and of the width W of the fault.

Substitution from Eq. (19) into Eq. (18) leads to an estimate of $\hat{\lambda}_i$, as

$$\hat{\lambda}_i = \frac{S}{\beta \gamma_i} e^{-\frac{2}{3} M_{\max}} \quad (21)$$

thus defining the level of seismicity on the fault consistent with S and M_{\max} . If $\hat{T}_i(M) = 1/\hat{N}_i(M)$ ($i = 1, 2, 3$) denotes the return period of earthquakes with magnitude larger or equal to M over an area equal to the rupture area for the maximum magnitude earthquake, $\Sigma(M_{\max}) = W L_r(M_{\max})$, then Eqs. (21) and (5) give

$$\hat{T}_i = \frac{\beta \gamma_i}{S} e^{\bar{b} M - (\bar{b} - \frac{2}{3}) M_{\max}} \cdot \left[1 - (1 - C_i - B_i \bar{b} \Delta M) e^{-\bar{b} \Delta M} \right]^{-1} \quad (22)$$

Particular expressions for $\hat{\lambda}_i$, \hat{T}_i , M , and M_{\max} for $i = 1, 2$ and 3 are given in Tables 2, 3, and 4.

Relations Referred to a Specific site on the Fault. To evaluate the probability of rupture at a selected site along the trace of a fault, and to evaluate geological observations of the chronology of ruptures at a site, an extension of the above equations is needed. Some of the large earthquakes with magnitude M ($M < M_{\max}$) which occur over the length of $L_r(M_{\max})$ will not rupture the surface at the specific observation site. We estimate the fraction $q(M)$ which cause rupture at the observation site by

$$q(M) = \frac{L_r(M)}{L_r(M_{\max})} = e^{-\frac{2}{3} \bar{b} M} \quad (23)$$

where we have assumed that the rupture length scales according to Eq. (20).

Now let $N_s(M)$ ($i = 1, 2, 3$) be the number of events with magnitude greater than or equal to M which rupture the fault at the site. We obtain

$$N_s(M) = \int_M^{M_{\max}} q(M) \hat{n}_i(M) dM \quad (24)$$

Since the magnitude dependence of $q(M)$ and $\hat{n}_i(M)$ is through $\Delta M = M_{\max} - M$, it is convenient to define

$$\frac{N_s(M)}{\hat{N}_i(M)} = F_i(\Delta M) . \quad (25)$$

We note that F_i is the ratio of the number of events with magnitude $\geq M$ which rupture the site to the number of events with magnitude $\geq M$ over L , (M_{\max}). From Eqs. (6), (21), (23), (24) and (25), we derive

$$F_i(\Delta M) = \left[1 - e^{-\bar{b}\Delta M} + B_i \bar{b} \Delta M e^{-\bar{b}\Delta M} + C_i e^{-\bar{b}\Delta M} \right]^{-1} \cdot \left\{ \left(\frac{2\bar{b}}{2\bar{b} - \bar{d}} \right) \left[1 - e^{-(\bar{b} - \frac{\bar{d}}{2})\Delta M} \right] - \frac{2\bar{b}}{\bar{d}} B_i \left[1 - e^{\frac{\bar{d}}{2}\Delta M} \right] e^{-\bar{b}\Delta M} + C_i e^{-(\bar{b} - \frac{\bar{d}}{2})\Delta M} \right\} \cdot e^{-\frac{\bar{d}}{2}\Delta M} \quad (26)$$

The functions $N_s(M)$ differ significantly from $N_i(M)$. Fig. 3 illustrates examples based on the same slip rate and maximum magnitude as used in Fig. 2. A notable characteristic of the occurrence relations $N_s(M)$, is that they flatten considerably as M decreases, because small magnitude events are less likely than large ones to rupture past the site. Thus the b -value, when measured from events at a single site, appears to be small. Since Schwartz *et al.* (1981) had only a few earthquakes at each trench site, the effect described here might completely account for their impression that only characteristic earthquakes repeatedly rupture a fault segment.

One can derive relations pertaining to the sizes and recurrence intervals of earthquakes which rupture a specific site along the fault similar to those presented earlier. If $T_s(M) = 1/N_s(M)$ ($i = 1, 2, 3$) denotes the average return period of earthquakes with magnitude M or larger to rupture past the site, we obtain

$$T_s(M) = \hat{T}_i(M)/F_i(\Delta M) , \quad (27)$$

where $\hat{T}_i(M)$ was defined in Eq. (22).

APPENDIX II

Although it is not possible to solve Eq. (27) explicitly for either the threshold magnitude M corresponding to $T_s(M)$ or for M_{\max} , either of these quantities may be obtained by a numerical solution as a function of the parameter ΔM . The particular equations for M_{\max} and M for $i = 1, 2$ and 3 are given in Tables 2, 3, and 4.

APPLICATIONS

Relationship of M_{\max} , M , and Recurrence Time of Magnitude M . In the previous section relations between maximum magnitude and "average recurrence time" of events with magnitude larger than an arbitrary magnitude M were presented. In these relations, "average recurrence time" was defined in three different ways : (A). $T(M)$, the average recurrence time over a fault of known length; (B). $\hat{T}(M)$, the average recurrence time over a section of a fault whose length is equal to the rupture length of the maximum earthquake; and (C). $\hat{T}_i(M)$, the average time between earthquakes which offset the fault at one particular point. We first explore the behavior of these relations.

The average recurrence times, in the three different meanings, are illustrated in Fig. 4, as a function of M_{\max} . Figure 4A shows $T(M)$, 4B shows $\hat{T}(M)$, and 4C shows $T_i(M)$ for $M = 5, 6, 7$ and 8. Figure 4A shows that in general as M_{\max} increases, the repeat times for smaller events on the same fault segment also increases. This is a consequence of the maximum magnitude event, and events close to it, releasing most of the moment, so that little is left over for the smaller earthquakes. Curves for occurrence relations 2 and 3 show a segment for M close to M_{\max} in which the repeat time decreases as M_{\max} increases; then as M_{\max} continues to increase, the curve becomes parallel to the curve for occurrence relation 1. This decreasing section of the curve corresponds to the portion of the occurrence rate curve which is plunging rapidly to zero (Fig. 2). While on this decreasing section, most of the seismic moment is released by events with magnitude smaller than M rather than by events with magnitude larger than M . For occurrence relation 2, the repeat times are smaller than for occurrence relation 1 when $M_{\max} \geq M + 0.5$. This results because a higher level of small magnitude activity is necessary to compensate for the smaller moment released by earthquakes with magnitude near M_{\max} .

$\hat{T}(M)$, in Fig. 4B is referred to a fault segment of length L , (M_{\max}), rather than to a previously assigned length. One sees that $\hat{T}(M)$ is, for this b -value, a gradually decreasing function of M_{\max} . In particular, for $b = \frac{d}{2}$ and $i = 1$, the return period $\hat{T}_1(M)$ becomes independent of M_{\max} . If $\hat{T}(M)$ were constant, one would find about the same total number of small magnitude earthquakes in the rupture area of the maximum earthquake, regardless of the dimension of the maximum earthquake.

APPENDIX II

The average repeat times for rupture past a site, $T_s(M)$, are shown in Fig. 4C. This figure shows that $T_s(M)$, like $T(M)$ is generally an increasing function of M_{\max} .

Figure 5 shows the estimates for the magnitude, M , of the T-year earthquake (where T may be T_i , or \hat{T}_i , or $T_s, i = 1, 2, 3$) which are found under the condition of known b -value and slip rate, but unknown M_{\max} . Examples are shown for T_i (Eq. 15) in 5A, B, and C, for \hat{T}_i (Eq. 22) in 5D, E, and F, and for T_s (Eq. 27) in 5G, H, and I. Figure 5A, for $s T_1(M) = 10^3$ mm on a fault which is 500 km long by 15 km wide, shows that as M_{\max} increases, the magnitude of the T-year earthquake decreases. This results because the maximum earthquake releases most of the required slip, and thus little needs to be released by smaller events. Figure 5B shows that for large M_{\max} , occurrence relation 2 exhibits similar behavior, when $M_{\max} \gg M$, but when M is close to M_{\max} , M increases with increasing M_{\max} . This increase corresponds to the portion of the occurrence curve where $N_2(M)$ is rapidly plunging toward zero and most of the slip is released at smaller magnitudes, as previously noted. In Figure 5C, the curves behave in a manner similar to 5B, except that the peaks in the curves are now at large magnitudes.

Figure 5D, E and F show that when the reference area is equal to the area of rupture zone of the maximum earthquake, the slopes of all the curves become more positive. For slip at a site, Figure 5G, H and I are qualitatively similar to 5A, B, and C.

Estimates of M_{\max} from Recurrence Time and Slip Rate. Expressions for estimates of the maximum magnitude are given by Eq. (16) in the text and by several other expressions in Tables 2, 3, and 4. These expressions are for the three different normalizations considered.

The following discussion on estimates of M_{\max} is based on occurrence relation 1 for which $T(M_{\max})$, $\hat{T}(M_{\max})$, and $T_s(M_{\max})$ are all finite, as opposed to the recurrence times for occurrence relations 2 and 3, which tend to infinity as M approaches M_{\max} . Estimates of M_{\max} for occurrence relation 1 are shown in Figure 6 as a function of slip rate, for five choices of recurrence time of M_{\max} between 10^2 years and 10^6 years. The results on Figure 6A, derived from Eq. (10), are shown specifically for a fault with area $\Sigma = 10^4 \text{ km}^2$; results in Figure 6B, derived from Eq. 1.13, are independent of the fault area, but do depend on the assumption that $W = 10 \text{ km}$ and $\alpha = 1.25 \times 10^{-5}$.

APPENDIX II

However, these assumptions about W and α are of only second order importance.

The results in Figure 6B are of considerable interest when compared with results of Woodward-Clyde Consultants (1979). They have observed that for strike-slip faults, the maximum magnitude which has been observed on each fault appear to be bounded by a line with larger M_{\max} for faults with larger slip rates. In fact, values of M_{\max} calculated from Eq. (I.13) in Table 2, with $W = 10$ km, $\alpha = 1.25 \times 10^{-3}$ and $\bar{T}_1 = 2000$ years nearly coincide with the proposed bound. This can be interpreted in either of two ways. The first would be that there is some physical mechanism which requires that the recurrence time of the maximum earthquake over a fault length equal to L , (M_{\max}) is less than about 2000 years on all faults. The existence of such a mechanism is unlikely, however. At low slip rates there are examples of faults with recurrence intervals of 10^5 years (Knuepfer et al., 1981; Bull et al., 1981; Menges et al., 1982). Furthermore, rock mechanics results indicate that the strength of a fault increases with the time which has elapsed since the last event, so that on faults with slow slip rates, one might even expect larger earthquakes than on faults with large slip rates. The alternative explanation, which we prefer, is that the apparent bound for the data results from the lack of observations at slow slip rates, because of the short sampling interval.

Figures 6A and 6B are predicated on the validity of occurrence relation 1. For occurrence relations 2 and 3, M_{\max} appears as a mathematical limit which may be approached but not attained. One can, however, derive similar results in which M_{\max} is replaced by $M_{\max} - \Delta M$, where ΔM is constant, and the lines are drawn for $T(M_{\max} - \Delta M) = \text{constant}$ or $\bar{T}(M_{\max} - \Delta M) = \text{constant}$. From Eq. (II.6) and (II.1), (III.6), (III.10), such lines would appear parallel to those in Figures 6A and 6B.

Comparison with Smith (1976). Eq. (16) gives an estimate of M_{\max} on a fault for which the slip rate, the total area, and the recurrence time of the maximum earthquake are known. The expression which Smith (1976) derived for M_{\max} is, except for the derivational error, equivalent to Eq. (16). To obtain this equivalence, one must associate $S \bar{T}_1(M_{\max})$ with one third of the maximum Holocene (2 to 4×10^4 years) fault slip in Smith's paper. The factor of one third was inserted by Smith because of his assumption that the maximum observed displacement is greater than the average.

APPENDIX II

Smith (1976) argues that 2×10^4 years is long enough for at least one maximum earthquake to occur along each of the faults he considered. If the maximum magnitude does not occur in that time interval, then one should use Eq. (I.6) in Table 2 instead of Eq. (16) to evaluate M_{\max} . For the sake of comparisons, Eqs (I.6) and (16) were applied to the numerical values described by Smith as applicable to a "third order fault." Smith used a total Holocene moment of 0.7×10^{26} dyne-cm on a fault with $L = 80$ km and $W = 10$ km. This implies a slip rate less than 0.02 mm/year. Using $b = 0.86$, $d = 1.5$, and our Eq. (16), one obtains $M_{\max} = 6.3$, identical to M_{\max} derived by Smith. Supposing, however, that because of the small slip rate the largest earthquake on the fault in the late Quaternary time period was only $M = 6.0$, then Eq. (I.6) gives $M_{\max} = 6.7$; if the largest Holocene earthquake was $M = 5.5$, then $M_{\max} = 7.4$, and if the largest was $M = 5.0$, then $M_{\max} = 8.1$. Thus the estimate of M_{\max} is quite sensitive to the hypothesis that the maximum earthquake has occurred on the fault in the Holocene. This hypothesis has the same problems as the conjecture that the maximum earthquake occurs with a repeat time over L , (M_{\max}) of less than 2000 years, as discussed in connection with Figure 6.

M_{\max} in California. The motion of the Pacific Plate relative to the North America Plate is, in total, about 60 mm/year (Bird, 1981), and the length of the San Andreas system from the Gulf of California to Cape Mendocina is about 1300 km. We will treat all the seismicity along this complex plate boundary as if it originated along a single fault 15 km wide, and use Eqs. (I.6) (II.6) and (III.6) to estimate M_{\max} . To accomplish this, we have plotted in Fig. 7 the predicted return periods for earthquakes with $M \geq 5, 6, 7$ and 8 versus M_{\max} for this particular selection of model parameters. On Fig. 7, we have superimposed average occurrence rates for earthquakes associated with the entire plate boundary. These included all the events listed on the Earthquake Data File (Meyers and von Hake, 1976) through Dec. 1979, bounded by a quadrilateral with corners at the following coordinates: (41° N, 128° W), (41° N, 121° W), (31° N, 190° W), and (31° N, 112° W). Average occurrence rates are sensitive to the time interval over which the average is derived; the uncertainty is at least a factor of 2. We estimate the following bounds on average recurrence times within this region : $M \geq 7$, 7.7 to 17 years; $M \geq 6$ 1.0–2.0 years; $M \geq 5$, 0.11 to 0.22 years. These bounds on recurrence times have been superimposed

APPENDIX II

on Fig. 7. From the intersection of these bounds with the theoretical curves, one can estimate M_{\max} . For occurrence relation 1, estimates for M_{\max} range from 7.8 to 8.4. For occurrence relation 2, they range from about 8.2 to 8.7. These estimates are reasonable. Although the values of M_{\max} consistent with assumption 3 (8.6 to 9.2) may seem too large to be physically realized, we note that in this case M_{\max} is a mathematical limit which would never be reached and would only rarely be closely approached.

Papastamatiou (1980) used a similar technique to estimate M_{\max} for the San Andreas fault between 36° N and 39° N, and obtained $M_{\max} = 8.83$. This result was based on the occurrence rates of magnitude 2 or larger earthquakes. The longer extrapolation introduces more sensitivity to choice of b and greater reliance on the completeness of the earthquake catalog at small magnitudes. For an individual fault, furthermore, this method of estimating M_{\max} requires great caution because occurrence rates are subject to cycles of activity with periods longer than the duration of instrumental catalogs. Such a cycle may well affect the results in Fig. 7, also.

Threshold of Observations Along the Mexico Subduction Zone. *Singh et al. (1981)* give a chronology of earthquakes along the Mexican subduction zone. The magnitudes of most of the events are known, providing the opportunity to compare some theoretical calculations with data. *Singh et al.* identified six segments of the subduction zone which appear to rupture in distinct earthquakes, and for which the date and magnitude of at least two earthquakes is known.

We note that if adjacent zones do not coalesce into single ruptures, then each zone has a dimension equal to the length of its corresponding maximum earthquake, and the relations which are referred to the rupture area of the maximum earthquake can be used. In particular, based on this assumption we attempted to estimate the magnitude of the smallest earthquake tabulated by *Singh et al. (1981)* within each of the six zones from the average recurrence interval in the zone. We used Eqs. (I.12), (II.11), and (III.11) with the parameters $S = 65$ mm/year, $W = 70$ km, $\mu = 3.3 \times 10^{11}$ dyne-cm, and $\alpha = 1.33 \times 10^{-5}$. This value of α is averaged from estimates for the 1973 Colima earthquake and the 1978 Oaxaca earthquake, based on data in *Sykes and Quittmeyer (1981)*. As seen in Fig. 5D, the estimates of the threshold of observation, M , are nearly independent of M_{\max} for the normal range of

APPENDIX II

δ -values. The results are listed in Table 5 for $b = 1.0$ and $M_{\max} = 8.0$. Estimates for M increase when the parameters M_{\max} , S , μ , or W are increased, and estimates for M decrease when the parameters b or α are increased. However, considerable changes are needed to change M by more than 0.1, and thus the choice of parameters is not critical. The greatest discrepancy in Table 2 is 0.2 magnitude units, for the San Marcos region. In the other regions, M agrees with the smallest of the observed magnitudes to within 0.1. We consider this agreement satisfactory, although the range of calculated and observed magnitudes is not large enough to provide an adequate test.

Implications of the San Andreas Fault Data from Pallett Creek. Sieh (1978a) studied sediments in a trench across the San Andreas fault at Pallett Creek. These sediments had been disrupted by several earthquakes, and, based on radiocarbon dating, Sieh derived a chronology of the events. The events and estimated year of occurrence are : D, 545; F, 665; I, 860; N, 965; R, 1190, T, 1245; V, 1470, X, 1745; Z, 1857. Except for event Z, the uncertainty in date is typically ± 50 years. The extent of sediment disruption does not require events R, or I to be as large as the 1857 event. Events V and N generated somewhat deeper troughs than the 1857 earthquake, and thus might have been associated with greater right lateral slip, but Sieh (1978a) considered all the events, except R and I, were comparable to the 1857 earthquake. The variable trough depths, and the smaller size of events R and I suggest that there is a distribution of event sizes represented at the site. The average waiting time between events is $T_s = 164$ years, based on 8 intervals between 545 and 1857.

This Pallett Creek record can be used to identify the form of the occurrence relation by means of a speculative procedure to estimate the magnitude of each of the earthquakes. The time-predictable and slip-predictable models described by Shimazaki and Nakata (1980) were used to estimate the slip in each of the earthquakes. In the time predictable model, the slip in one earthquake, and the slip rate, determine the waiting time to the next earthquake; in the slip predictable model the waiting time from the previous earthquake and the slip rate determines the slip in the next earthquake. The slip in each earthquake, as predicted by the two models, is listed in Table 6, based on a slip rate of 37 mm/year. Equation (19) was used to convert each average slip to magnitude. The consequent empirical cumulative magnitude distribution is shown in Fig. 8 A and B. We note that both the time-predictable model

APPENDIX II

and the slip-predictable model lead to the same magnitude distribution, even though the magnitude estimates for each earthquake differ. Since aftershocks are not recognized in the geological record, these magnitudes measure the total effect of the earthquake sequences rather than the size of the main shock of the sequence. We note that if events R and I were smaller than most, as indicated by Sieh (1978a), this would tend to support the time predictable model.

Fig. 8 also shows the theoretical forms for $N_i(M)$ ($i = 1, 2, 3$) for two choices of b -value ($b = 0.86$, Fig. 8A; $b = 0.20$, Fig. 8B). In Fig. 8 we used $M_{\max} = 8.3$ for Occurrence Relations 1 and 2, and $M_{\max} = 8.6$ for occurrence relation 3. Over the magnitude range illustrated in Fig. 8, theoretical curves for $b < 0.2$ are not significantly different from the curves, shown, for $b = 0.2$. The comparisons in Fig. 8 show that our Pallett Creek magnitude estimates seem to obey occurrence relation 2 with b near zero much better than they obey occurrence relation 1, and slightly better than they obey relation 3. There is no choice of M_{\max} which can alter the conclusion that occurrence relation 2 fits better. Changes in the other scaling parameters (S , α , W) require that the magnitudes in Table 6 also be modified for internal consistency, and thus systematically modify both the data and the theoretical curves in Fig. 8 without affecting the conclusion. We cannot rule out the possibility that random errors affecting each datum could change the conclusion. Significant random errors might arise from uncertainty in event dates, variations in scaling parameters from event to event, deviations from the time-predictable or slip-predictable model, and possible incompleteness in the geological record. The $N_{i2}(M)$ in Fig. 8B is slightly lower than the data because it allows some slip ($\approx 10\%$) to be released in smaller events, while the magnitude estimates in Table 6 require that all the slip occurred in these 8 events. Large aftershocks of the main events might or might not affect the shape of the distribution curves as measured from seismograph observations, in the magnitude range shown.

The equations in Tables 2, 3 and 4 for the case of rupture past the site can be used to estimate the smallest main shock magnitude in the Pallett Creek record as a function of M_{\max} . Table 7 shows these estimates for the magnitude corresponding to a 164 year recurrence interval. Even though Table 6 suggests that M_{\max} is at least 8.3, Table 7 considers possible values between 7.8 and 8.8. Since Sieh (1978b) finds that the moment of the 1857 earthquake implies that the magnitude for that event

APPENDIX II

was 7.8 to 7.9, smaller values are not considered. The upper limit for M_{\max} , 8.8 was suggested by Fig. 7. An exceptionally large earthquake which ruptures from north of Parkfield to the Salton Sea (600 km), and which is characterized by $\alpha = 2.5 \times 10^{-5}$, $W = 20$ km, and $\mu = 3 \times 10^{11}$ dyne/cm², leads to $M = 8.5$. However, for occurrence relation 3, M_{\max} is a mathematical limit which would rarely be approached; thus values of M_{\max} to 8.8 are not necessarily disqualified.

The results in Table 7 indicate that for M_{\max} in the range 8.0 to 8.5, the threshold magnitude M would be in the range 6.5 to 7.5, depending on the occurrence relation and b -value used. In particular, a value of $M_{\max} = 8.26$ and a threshold magnitude of 7.33 as calculated for the time predictable model listed in Table 6 are not inconsistent with the results in Table 7. Since risk assessment for the southern California region depends upon the Pallett Creek record, an appreciation of this range of magnitudes will likely influence that assessment.

APPENDIX II

SUMMARY

Three earthquake occurrence relations with different functional dependence near M_{\max} have been examined. The forms considered while representing a subset of the class of 3-parameter occurrence relations are sufficient to cover the major types of expected behavior near M_{\max} . These occurrence relations relate two variables M and $T(M)$ and the parameters corresponding to the rate of occurrence at a magnitude of reference, a b -value, and, a maximum magnitude M_{\max} . Knowledge of the slip rates permits one to derive a constraint among the three parameters characterizing the occurrence relation. The resulting slip-constrained occurrence relation can be utilized to obtain one of the following estimates: (i) given S , M , M_{\max} , and b find $T(M)$, (ii) given S , $T(M)$, M_{\max} and b find M , (iii) given S , M , $T(M)$ and b find M_{\max} , (iv) given S , $T(M_{\max})$ and b find M_{\max} , and (v) given S , M , $T(M)$ and M_{\max} find b . The slip-rate constraints and the equations necessary for the above applications have been derived for three occurrence relations of different functional form. Specific application of estimates (i) through (iv) have been illustrated.

We have addressed also the problem of normalization of the earthquake occurrence relations. We have considered three types of normalization corresponding to: (i) occurrence over a prescribed fault area, (ii) occurrence over an area equal to the rupture area during the maximum magnitude earthquake, and, (iii) occurrence such that the earthquake rupture area includes a specific point.

Acknowledgements

The authors have benefitted from discussions with J.N. Brune and C.H. Scholz, and from a review of the manuscript by M. Reichle. This research was supported by the United States Geological Survey Contract No. 14-08-0001-19766.

REFERENCES

Aki, K. (1967). Scaling law of seismic spectrum, *Journal of Geophysical Research* 72, 1217-1231.

Aki, K. (1972). Scaling law of earthquake source time-function, *Geophysical J.* 31, 3-25.

Anderson, J. G. (1979). Estimating the seismicity from geological structure for seismic-risk studies, *Bull. Seism. Soc. Am.* 71, 827-843.

Bakun, W.H. and McEvilly, T.V. (1979). Earthquakes near Parkfield, California : comparing the 1934 and 1966 sequences, *Science* 205, 1375-1477.

Bath, M. (1978). A Note on recurrence relations for earthquakes, *Tectonophysics* 51, T23-T30.

Berrill, J.B. and R.O. Davis (1980). Maximum entropy and the magnitude distribution, *Bull. Seism. Soc. Am.* 70, 1823-1831.

Bird, P. Kinematics of present crust and mantle flow in southern California, *Bull. Geological Soc. Am.* (in press).

Bloom, E. D. and R. C. Erdmann (1980). The observation of a universal shape regularity in earthquake frequency-magnitude distributions, *Bull. Seism. Soc. Am.* 70, 349-362.

Brune, J. N. (1968). Seismic moment, seismicity, and slip rate along major fault zones, *Journal of Geophysical Research* 73, 777-784.

Bull, W.B., S.S. Calvo, P.A. Pearthree and J. Quade (1981). Frequencies and magnitudes of surface rupture along the Pitayachi fault, northwestern Sonora, Mexico (abstract), *Abstracts with programs 1981, 77th Annual Meeting, Cordilleran Section, Geological Society of America, Hermosillo, Sonora, Mexico*, 47.

Campbell, K. W. (1977). The use of seismotectonics in the Bayesian estimation of seismic risk, Report No. UCLA-ENG-7744, School of Engineering and Applied Sciences, University of California, Los Angeles.

APPENDIX II

Caputo, M. (1977). A mechanical model for the statistics of earthquakes, magnitude, moment, and fault distribution, *Bull. Seism. Soc. Am.* 67, 849-861.

Chinnery, M.A. and R.G. North (1975). The frequency of very large earthquakes, *Science* 190, 1197-1198.

Davis, G. F. and J. N. Brune (1971). Regional and global fault slip rates from seismicity, *Nature Physical Science* 229, 101-107.

Doser, D.I. and R.B. Smith (1982). Seismic moment rates in the Utah region, *Bull. Seism. Soc. Am.* 72, 525-551.

Esteva, L. (1976). Seismicity, in *Seismic Risk and Engineering Decisions*, C. Lomnitz and E. Rosenblueth, editors, Elsevier Scientific Publishing Company, Amsterdam, 179-224.

Geller, R.J. (1976). Scaling relations for earthquake source parameters and magnitudes, *Bull. Seism. Soc. Am.* 66, 1501-1523.

Greensfelder, R.W., F.C. Kintzer and M.R. Somerville (1980). Seismotectonic regionalization of the Great Basin, and comparison of moment rates computed from Holocene strain and historic seismicity, in *Proceedings of Conference X. Earthquake hazards along the Wasatch and Sierra-Nevada frontal fault zones, Open file Report 80-801*, United States Department of the Interior Geological Survey, Menlo Park, California, p. 433-493.

Gumbell, E.J. (1960). *Extreme value Statistics*, Columbia University Press, 375 pp.

Gutenberg, B. and C. F. Richter (1954). *Seismicity of the Earth and Associated Phenomena*, 2nd edition, Princeton University Press, Princeton, N. J., 310 p.

Hanks, T.C. and H. Kanamori (1979). A moment magnitude scale, *Journal of Geophysical Research* 84, 2348-2350.

Herrmann, R. B. (1977). Recurrence relations, *Earthquake Notes* 48, Nos. 1-2, 47-49.

APPENDIX II

Housner, G. W. (1969). Engineering estimates of ground shaking and maximum earthquake magnitude, Proc. 4th World Conference on Earthquake Engineering, Santiago, Chile, Vol. 1, 1-13.

Kanamori, H. (1977). The energy release in great earthquakes, *Journal of Geophysical Research* 82, 2981-2987.

Kanamori, H. and D.L. Anderson (1975). Theoretical basis of some empirical relations in seismology, *Bull. Seism. Soc. Am.* 65, 1073-1095.

Knuepfer, P.L., K.J. Coppersmith and L.S. Cluff (1981). A framework for classifying faults based on their relative degree of activity (abstract), *Earthquake Notes* 52, 70-71.

Lahr, J.C. and C.D. Stephens (1982). Alaska seismic zone: possible example of non-linear magnitude distribution for faults (abstract), *Earthquake Notes* 53 No. 1, 66.

Main, I.G. and P.W. Burton (1981). Rates of crustal deformation inferred from seismic moment and Gumbel's third distribution of extreme magnitude values, in J.E. Beavers, ed., *Earthquakes and Earthquake Engineering - eastern United States*, Ann Arbor Science Publishers, Inc., 937-951.

Makjanik, B. (1980). On the frequency distribution of earthquake magnitude and intensity, *Bull. Seism. Soc. Am.* 70, 2253-2260.

McGuire, R.K. (1974). Seismic Structural Response Risk Analysis, Incorporating Peak Response Regressions on Earthquake Magnitude and Distance, Research Report R74-51, Department of Civil Engineering, Massachusetts Institute of Technology, Cambridge, Mass. 371 pp.

Menges, C.M., P.A. Pearce and S. Calvo (1982). Quaternary faulting in southeast Arizona and adjacent Sonora, Mexico (abstract), *Abstracts with programs 1982, 78th Annual Meeting, Cordilleran Section, Geological Society of America, Anaheim, California*, 215.

Meyers, H. and C.A. von Hake (1976). Earthquake Data File summary, National Geophysical and Solar-Terrestrial Data Center, Boulder, Colorado.

APPENDIX II

Molnar, P.E. (1979). Earthquake Recurrence Intervals and Plate Tectonics, *Bull. Seism. Soc. Am.* **69**, 115-133.

Papastamatiou, D. (1980). Incorporation of crustal deformation to seismic hazard analysis, *Bull. Seism. Soc. Am.* **70**, 1321-1335.

Richter, C.F. (1958). *Elementary Seismology*, W.H. Freeman, San Francisco, California.

Schwarz, D.P., K.J. Coppersmith, F.H. Swan III, P. Somerville, and W.U. Savage (1981). "Characteristic" earthquakes on interpolate normal faults (Abstract), *Earthquake Notes* 52, No. 1, 71.

Scholz, C.H. (1982). Scaling laws for large earthquakes: consequences for physical models, *Bull. Seism. Soc. Am.* **72**, 1-14.

Shimazaki, K. and T. Nakata (1980). Time-predictable recurrence model for large earthquakes, *Geophysical Research Letters* **7**, 279-282.

Sieh, K.E. (1978a). Prehistoric large earthquake produced by slip on the San Andreas fault at Pal-lett Creek, California, *J. Geophys. Research* **83**, 3907-3939.

Sieh, K. (1978b). Slip along the San Andreas fault associated with the great 1857 earthquake, *Bull. Seism. Soc. Am.* **68**, 1421-1448.

Singh, S.K., L. Astiz, and J. Havskov (1981). Seismic gaps and recurrence periods of large earthquakes along the Mexican subduction zone: a re-examination, *Bull. Seism. Soc. Am.* **71**, 827, 843.

Slemmons, D.B. (1977). State-of-the-art for Assessing Earthquake Hazards in the United States Report 6, *Faults and Earthquake Magnitude*, Miscellaneous Paper S-73-1, Mackay School of Mines, University of Nevada, Reno.

Smith, S.W. (1976). Determination of maximum earthquake magnitude, *Geophysical Research Letters*, **33**, 351-354.

Sykes, L.R. and R.C. Quittmeyer (1981). Repeat times of great earthquakes along simple place boundaries, in D.W. Simpson and P.G. Richards, eds., *Earthquake Prediction, An International Review*, American Geophysical Union, Washington, D.C., p. 217 to 247.

Swan, F.H., III, D.P. Schwartz and L.S. Cluff (1980). Recurrence of moderate to large magnitude earthquakes produced by surface faulting on the Wasatch fault zone, Utah, *Bull. Seism. Soc. Am.* 70, 1431-1462.

U. S. Geological Survey (1981). *Scenarios of Possible Earthquakes Affecting Major California Population Centers, with Estimates of Intensity and Ground Shaking*, Open File Report 81-115, Menlo Park, California.

Wallace, R.E. (1970). Earthquake recurrence intervals on the San Andreas fault, *Geological Society of America Bulletin* 81, 2875-2890.

Wesnousky, S.G. and C.H. Scholz (1983), in preparation.

Woodward-Clyde Consultants (1979). *Report of the Evaluation of Maximum Earthquake and Site Ground Motion Parameters Associated with the Offshore zone of Deformation San Onofre Nuclear Generating Station*, prepared for Southern California Edison, Rosemead, California.

Yegulap, T.M. and J.T. Kuo (1974). Statistical prediction of the occurrence of maximum magnitude earthquakes, *Bull. Seism. Soc. Am.* 64, 393-414.

FIGURE CAPTIONS

Figure 1 A. Cumulative magnitude distribution functions $N_1(M)$, $N_2(M)$, and $N_3(M)$ (Eq. 5) for $b = 1.0$, $M_{\max} = 8.0$, normalized so that $N_1(6) = N_2(6) = N_3(6) = 1.0$. B. Corresponding incremental rates $n_1^f(M)$, $n_2^f(M)$ and $n_3^f(M)$ in 0.25 magnitude unit intervals. Each datum is plotted at the center of its magnitude interval.

Figure 2 A. Cumulative magnitude distribution functions $N_1(M)$, $N_2(M)$ and $N_3(M)$ (Eq. 5) for $b = 1.0$ and $M_{\max} = 8.0$, normalized so that on the average the seismic moment released by the earthquakes is 8.1×10^{25} dyne-cm/year. B. Corresponding incremental rates $n_1^f(M)$, $n_2^f(M)$, and $n_3^f(M)$ in 0.25 magnitude unit intervals. Each datum is plotted at the center of its magnitude interval.

Figure 3 A. Cumulative magnitude distribution functions $N_{s1}(M)$, $N_{s2}(M)$ and $N_{s3}(M)$ (Eq. 25) giving the frequency of a magnitude M or larger earthquake causing ground rupture at a single site on a fault. Curves are generated for $b = 1.0$, $M_{\max} = 8.0$, $\alpha = 1.25 \times 10^{-5}$, $\mu = 3 \times 10^{11}$ dyne/cm², $W = 15$ km, $S = 40$ mm/year, and the magnitude-rupture length scaling assumptions given by Eq. 20 B. Corresponding incremental rates in 0.25 magnitude unit intervals. Each datum is plotted at the center of its magnitude interval.

Figure 4 A. Average recurrence times $T(M)$ (Eq. 15) for magnitude M or greater earthquakes on a fault with $L = 1000$ km, $W = 10$ km, and $S = 40$ mm/year, as a function of M_{\max} . Other parameters are $b = 1.0$, $\alpha = 1.25 \times 10^{-5}$, $\mu = 3 \times 10^{11}$ dyne/cm². B. Average recurrence times $\bar{T}(M)$ (Eq. 22) for magnitude M or greater earthquakes on a fault with $L = L(M_{\max})$ as a function of M_{\max} . Other parameters as in fig. 4A. C. Average recurrence times $T_s(M)$ (Eq. 27) for magnitude M or greater earthquakes rupturing a single site on a fault, as a function of M_{\max} . Other parameters as given above.

APPENDIX II

Figure 5 Magnitude thresholds of observation consistent with the product (slip rate) \times (recurrence time of events exceeding thresholds) = 10^3 mm. These thresholds are shown as a function of maximum magnitude, and for four b -values. Parameters held constant for all curves are $\alpha = 1.25 \times 10^{-5}$, $\mu = 3 \times 10^{11}$ dyne/cm 2 , $W = 15$ km. A) Occurrence rate curve has form $N_1(M)$, and recurrence time applies to events occurring any place on the segment of the fault with $L = 500$ km. B) Equivalent of A for occurrence rate curve $N_2(M)$. C) Equivalent of A for occurrence rate curve $N_3(M)$. D) Occurrence rate curve has the form $N_1(M)$, and recurrence time applies to events occurring on a segment of the fault ruptured by the maximum magnitude earthquake. E) Equivalent of D for occurrence rate curve $N_2(M)$. F) Equivalent of D for occurrence rate curve $N_3(M)$. G) Occurrence rate curve has the form $N_1(M)$ and recurrence time applies to events which rupture the fault at a single site. H) Equivalent of G for occurrence rate curve $N_2(M)$. I) Equivalent of G for occurrence rate curve $N_3(M)$.

Figure 6 M_{\max} as a function of slip rate S for several choices of recurrence times $T_1(M_{\max})$ (6A) and $T_{s1}(M_{\max})$ or $\bar{T}_1(M_{\max})$ (6B). M_{\max} in 6A is for a fault area $\Sigma = 10^4$ km 2 . M_{\max} in 6B is for a fault with $W = 10$ km. Other parameters are $b = 0.86$, $\mu = 3 \times 10^{11}$ dyne/cm 2 , and $\alpha = 1.25 \times 10^{-5}$. Curves only apply if seismicity obeys occurrence relation $N_1(M)$, but parallel curves for $M_{\max} - \Delta M$, ΔM fixed, can be derived for occurrence relations $N_2(M)$ and $N_3(M)$.

Figure 7 Repeat times $T_i(M)$ ($i = 1, 2, 3$) for $M = 5, 6, 7$ and 8 when $S = 60$ mm/year, $\alpha = 1.25 \times 10^{-5}$, $b = 0.91$, $W = 15$ km, $L = 1300$ km, and $\mu = 3 \times 10^{11}$ dyne/cm 2 . Superimposed are bounds for the observed repeat times of events with $M \geq 5, 6$ and 7 for the California plate boundary region from the Gulf of Mexico to Cape Mendocino. Intersections of these observations and theoretical curves are projected down to near the horizontal axis to infer appropriate range of M_{\max} corresponding to each form of the occurrence relation.

APPENDIX II

Figure 8 Cumulative magnitude distribution functions $N_{s1}(M)$, $N_{s2}(M)$ and $N_{s3}(M)$ (Eq. 25) giving the theoretical frequency of a magnitude M or larger earthquake causing rupture at a single site on a fault. Curves are generated for $b = 0.86$ (8A) or $b = 0.20$ (8B), and for $\alpha = 1.25 \times 10^{-5}$, $\mu = 3 \times 10^{11}$ dyne/cm², $W = 10.0$ km, and $S = 37$ mm/year. $N_{s1}(M)$ and $N_{s2}(M)$ have $M_{\max} = 8.3$, and $N_{s3}(M)$ has $M_{\max} = 8.6$. Superimposed on each figure is the distribution of magnitudes inferred for the Pallett Creek site on the San Andreas fault. Inferred magnitudes (Table 3) are based on chronology given by Sieh (1978a), time-predictable or slip-predictable model of Shimazaki and Nakata (1980), and earthquake scaling relations of Scholz (1982).

Table 1
 Fraction of Moment Released by Earthquakes with
 Magnitude between $M_{max} - \Delta M$ and M_{max}

ΔM	$b = 0.25$			$b = 0.85$			$b = 1.0$		
	O. R. 1	O. R. 2	O. R. 3	O. R. 1	O. R. 2	O. R. 3	O. R. 1	O. R. 2	O. R. 3
0.0	0.83	0.0	0.0	0.43	0.0	0.0	0.33	0.0	0.0
0.1	0.88	0.25	0.04	0.51	0.14	0.02	0.41	0.11	0.02
0.25	0.92	0.51	0.19	0.61	0.31	0.11	0.50	0.25	0.09
0.35	0.94	0.63	0.30	0.66	0.41	0.18	0.55	0.33	0.15
0.5	0.96	0.76	0.47	0.73	0.53	0.30	0.63	0.44	0.25
1.0	0.99	0.94	0.82	0.87	0.78	0.63	0.79	0.68	0.54
2.0	1.00	1.00	0.99	0.97	0.95	0.91	0.93	0.90	0.85
3.0	1.00	1.00	1.00	0.99	0.99	0.98	0.98	0.97	0.95
4.0	1.00	1.00	1.00	1.00	1.00	1.00	0.99	0.99	0.99

Table 2

Summary of Equations which Result when
Occurrence Relation 1 is Considered by Slip Rate.

$$\begin{aligned} M_1(M) &= A_1 e^{\delta_1 M} H(\Delta M) & (1.1) \\ n_1(M) &= A_1 \left[\delta e^{\delta_1 M} H(\Delta M) + \theta(\Delta M) \right] & (1.2) \\ \Delta M &= M_{\max} - M & (1.3) \end{aligned}$$

ARBITRARY		RUPTURE PAST SITZ	
$\Sigma = \Sigma(M_{\max})$		$\Sigma = \Sigma(M_{\max})$	
$A_1 = \left[\frac{\bar{\delta} - \bar{\delta}}{\bar{\delta}} \right] \frac{\mu \Sigma S}{M_0(M_{\max})}$	(1.4)	$\lambda_1 = \left[\frac{\bar{\delta} - \bar{\delta}}{\bar{\delta}} \right] \frac{\mu \Sigma S}{\beta} e^{-\frac{\bar{\delta}}{\beta} M_{\max}}$	(1.9)
$\tau(M) = \frac{\bar{\delta}}{\bar{\delta} - \bar{\delta}} \frac{M_0(M_{\max})}{\mu \Sigma S} e^{-\delta_1 M}$	(1.5)	$\tau(M) = \left[\frac{\bar{\delta}}{\bar{\delta} - \bar{\delta}} \right] \frac{\mu}{S} e^{\frac{\bar{\delta}}{\beta} M_{\max}} e^{-\delta_1 M}$	(1.10)
$M_{\max} = \frac{1}{\bar{\delta} - \bar{\delta}} \ln \left[\frac{\bar{\delta} - \bar{\delta}}{\bar{\delta}} \frac{\mu \Sigma S \tau(M)}{M_0(0)} e^{-\delta_1 M} \right]$	(1.6)	$M_{\max} = \frac{2}{\bar{\delta} - \bar{\delta}} \ln \left[\frac{\bar{\delta}}{\bar{\delta} - \bar{\delta}} \frac{\mu}{S \tau(M)} e^{\delta_1 M} \right]$	(1.11)
$M = M_{\max} - \frac{1}{\bar{\delta}} \ln \left[\frac{\bar{\delta}}{\bar{\delta} - \bar{\delta}} \frac{M_0(M_{\max})}{\mu \Sigma S \tau(M)} \right]$	(1.7)	$M = \frac{1}{\bar{\delta}} \ln \left[\frac{\bar{\delta} - \bar{\delta}}{\bar{\delta}} \frac{\mu \Sigma S \tau(M)}{\beta} \right] + \left[\frac{2\bar{\delta} - \bar{\delta}}{2\bar{\delta}} \right] M_{\max}$	(1.12)
$M_{\max} = \frac{1}{\bar{\delta}} \ln \left[\left(\frac{\bar{\delta} - \bar{\delta}}{\bar{\delta}} \right) \frac{\mu \Sigma S \tau(M_{\max})}{M_0(0)} \right]$	(1.8)	$M_{\max} = \frac{2}{\bar{\delta}} \ln \left[\left(\frac{\bar{\delta} - \bar{\delta}}{\bar{\delta}} \right) \frac{\mu \Sigma S \tau(M_{\max})}{\beta} \right]$	(1.13)
		$F_1(\Delta M) = \frac{2\bar{\delta}}{2\bar{\delta} - \bar{\delta}} e^{-\frac{\bar{\delta}}{\beta} M_{\max}} \left[1 - \left(\frac{\bar{\delta}}{2\bar{\delta}} \right) e^{-\frac{\bar{\delta}}{\beta} \Delta M} \right]$	(1.14)
		$T_1(M) = \tau(M)/F_1(\Delta M)$	(1.15)
		$M_{\max} = \frac{2 - \bar{\delta}}{\bar{\delta}} \frac{S T_1(M)}{\beta F_1(\Delta M)} e^{\delta_1 M}$	(1.16)
		$M = M_{\max} - \Delta M$	

Table 3
Summary of Equations which Result when
Occurrence Relation 2 is Constrained by Slip Rate.

$$N_1(M) = A_1(e^{\delta \Delta M} - 1) H(\Delta M) \quad (III.1)$$

$$n_1(M) = A_1 \delta e^{\delta \Delta M} H(\Delta M) \quad (III.2)$$

$$\Delta M = M_{\max} - M \quad (III.3)$$

ARBITRARY		RUPTURE PAST SITE	
$A_1 = \left[\frac{2-\delta}{\delta} \right] \frac{\mu \Sigma S}{M_0(M_{\max})}$	(III.4)	$\lambda_1 = \left[\frac{2-\delta}{\delta} \right] \frac{\mu}{\beta} e^{-\frac{\delta}{\beta} M_{\max}}$	(III.6)
$T(M) = \frac{1}{2-\delta} \frac{M_0(M_{\max})}{\mu \Sigma S} \frac{\delta}{(e^{\delta \Delta M} - 1)}$	(III.5)	$T(M) = \left[\frac{\delta}{2-\delta} \right] \frac{\mu}{S} e^{\frac{\delta}{\beta} M_{\max}} \left[e^{\delta \Delta M} - 1 \right]^{-1}$	(III.9)
$M_{\max} = \frac{1}{\delta} \ln \left[\frac{2-\delta}{\delta} \frac{\mu \Sigma S T(M)}{M_0(0)} \left[e^{\delta \Delta M} - 1 \right] \right]$	(III.6)	$M_{\max} = \frac{2}{\delta} \ln \left[\frac{2-\delta}{\delta} \frac{\mu T(M)}{\beta} \left[e^{\delta \Delta M} - 1 \right] \right]$	(III.10)
$M = M_{\max} - \frac{1}{\delta} \ln \left[\frac{\delta}{2-\delta} \frac{M_0(M_{\max})}{\mu \Sigma S T(M)} + 1 \right]$	(III.7)	$M = M_{\max} - \Delta M$	(III.11)
		$F_1(\Delta M) = \frac{2\delta}{2\delta - \delta} e^{-\frac{\delta}{\beta} \Delta M} \left[\frac{1 - e^{-\delta \Delta M}}{1 - e^{-\delta \Delta M}} \right]$	(III.12)
		$T_1(M) = \frac{2\delta}{2\delta - \delta} (F_1(\Delta M))$	(III.13)
		$M_{\max} = \frac{2}{\delta} \ln \left[\frac{2-\delta}{\delta} \frac{S T_1(M)}{\beta F_1(\Delta M)} (e^{\delta \Delta M} - 1) \right]$	(III.14)
		$M = M_{\max} - \Delta M$	(III.15)

Table 4

Summary of Equations which Result when
Oscillation Relation 2 is Considered by Step Rule.

$$\begin{aligned} N_1(M) &= A_1 \left[\rho_{100} - 1 - \frac{1}{2} \rho_{10} \right] M(M) & (m.1) \\ n_1(M) &= A_1 \left[\rho_{100} - 1 \right] M(M) & (m.2) \\ \Delta M &= M_{max} - M & (m.3) \end{aligned}$$

EQUILIBRIUM		RUPTURE PART STATE	
$\Sigma = \Sigma(M_{eq})$		$\Sigma = \Sigma(M_{eq})$	
$M_{eq} = \frac{2(2-\eta)}{\eta} \frac{M_0(M_{eq}-1)}{M_0(M_{eq}-\eta)}$		$M_{eq} = \frac{2(2-\eta)}{\eta} \frac{M_0(M_{eq}-1)}{M_0(M_{eq}-\eta)} \left[\frac{1}{2} \left(\rho_{100} - 1 \right) - \rho_{10} \right]$	
$M_{eq} = \frac{2(2-\eta)}{\eta} \frac{M_0(M_{eq}-1)}{M_0(M_{eq}-\eta)} \left[\frac{1}{2} \left(\rho_{100} - 1 \right) - \rho_{10} \right] - \rho_{100}$		$M_{eq} = \frac{2(2-\eta)}{\eta} \frac{M_0(M_{eq}-1)}{M_0(M_{eq}-\eta)} \left[\frac{1}{2} \left(\rho_{100} - 1 \right) - \rho_{10} \right] - \rho_{100}$	
$M_{eq} = M_{eq} - \Delta M$		$M_{eq} = M_{eq} - \Delta M$	
$M = M_{eq} - \Delta M$		$M = M_{eq} - \Delta M$	

APPENDIX II

Table 5

Region	Approx. Location	Ave. Period Years	Smallest Observed Magnitude	Calculated Threshold Magnitude ¹		
				(Eq. I.12)	(Eq. II.11)	(Eq. III.11)
1. Oaxaca	16.2°N 95.8°W	34	7.4	7.5	7.5	7.4
2. Oaxaca	16.0°N 96.8°W	54	7.8	7.7	7.6	7.5
3. Oaxaca	16.6°N 97.7°W	38	7.4	7.5	7.5	7.4
4. San Marcos	16.7°N 99.2°W	56	7.5	7.7	7.6	7.5
5. Petatlan	17.3°N 101.4°W	36	7.5	7.5	7.5	7.4
6. Colima	18.4°N 103.2°W	32	7.5	7.5	7.5	7.4

¹ For parameters $\alpha = 1.33 \times 10^{-5}$, $\mu = 3.3 \times 10^{11} \text{ dyne-cm}^{-2}$, $w = 70 \times 10^5 \text{ cm}$, $M_o(0) = 10^{16} \text{ dyne-cm}$, $b = 1.0$, $M_{\max} = 8.0$, $S = 65 \text{ mm/yr}$.

Table 6
Pallid Creek Events : Magnitude Estimates

Event	Time Inferred Model			Slip Predictable Model			
	Est. Year	Waiting Time to next Event (years)	Inferred slip in Event (m) ¹	Magnitude ²	Waiting Time from prior Event (years)	Inferred slip in Event (m) ¹	Magnitude ²
Z 1857	> 125	> 4.6 (4.5 to 4.8) ³	> 7.81 (7.8 to 7.9) ³		112	4.1 (4.5 to 4.8) ³	7.74 (7.8 to 7.9) ³
X 1745	112	4.1	7.74		275	10.2	8.26
V 1470	275	10.2	8.26		225	8.3	8.15
T 1245	225	8.3	8.15		55	2.0	7.33
R 1190	55	2.0	7.33		225	8.3	8.15
N 965	225	8.3	8.15		105	3.9	7.71
I 860	105	3.9	7.71		195	7.2	8.06
P 665	195	7.2	8.06		120	4.4	7.78
D 545	120	4.4	7.78		?	?	?

¹ Based on slip rate of 37 mm (year)

² Based on Eq. (25) for $W = 10$ km, $\frac{\bar{u}}{L} = 1.25 \times 10^{-5}$. Uncertainty is > 0.2 magnitude units.

³ Actual, (Sieh 1978b).

Table 7

Magnitude of Threshold of Observations Consistent with $S = 37$ mm/year and
 $T_s(M) = 164$ years¹ at Pallett Creek, as a function of M_{\max}

M_{\max}	$b = 0.20$			$b = 0.86$		
	Eq. I.17	Eq. II.15	Eq. III.15	Eq. I.17	Eq. II.15	Eq. III.15
7.8	-	7.50	7.30	7.43	7.32	7.18
7.9	7.83	7.52	7.36	7.37	7.34	7.21
8.0	7.23	7.53	7.39	7.31	7.34	7.24
8.1		7.48	7.41	7.21	7.32	7.26
8.2		7.40	7.42	7.10	7.29	7.27
8.3		7.19	7.40	6.95	7.24	7.27
8.4		6.60	7.40	6.77	7.17	7.26
8.5			7.28	6.58	7.08	7.23
8.6			7.13	6.35	6.96	7.19
8.7			6.85	6.08	6.81	7.13
8.8			6.15		6.64	7.05

¹ Other Parameters $\mu = 3 \times 10^{11}$ dyne/cm², $W = 10$ km, $\frac{\bar{u}}{L} = 1.25 \times 10^{-5}$.

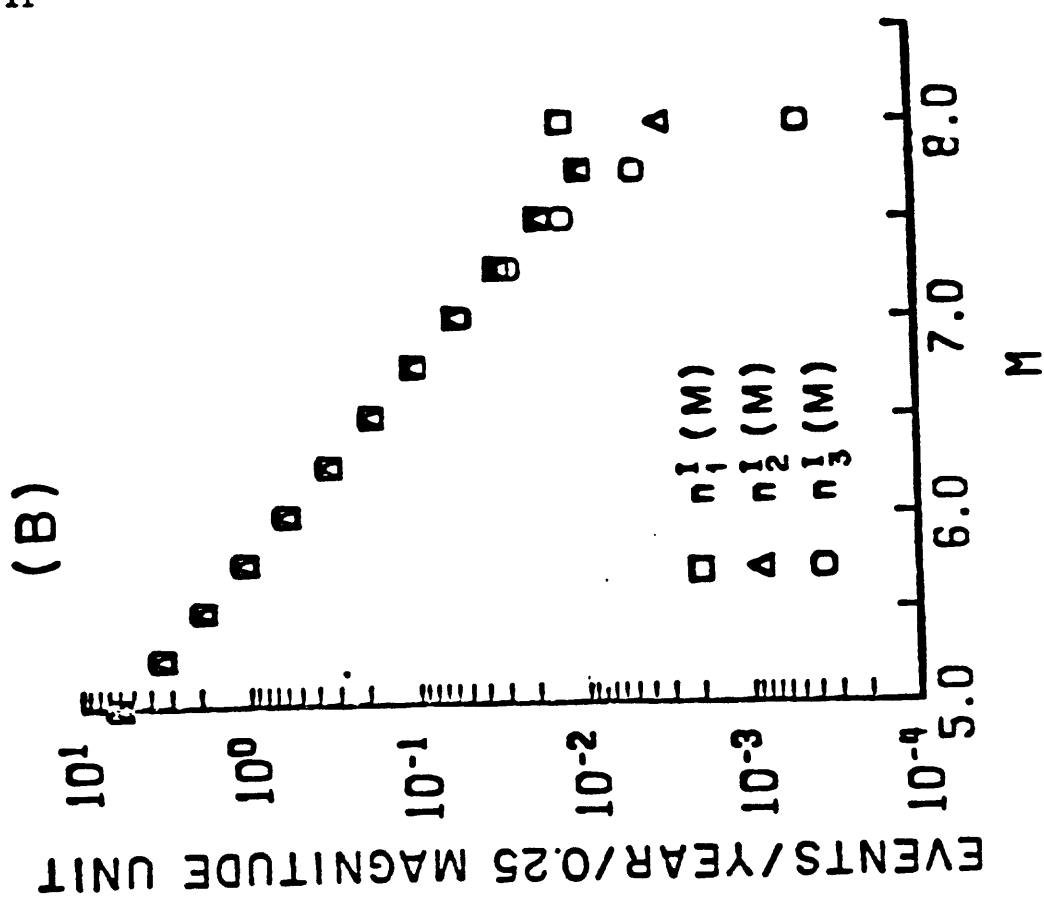
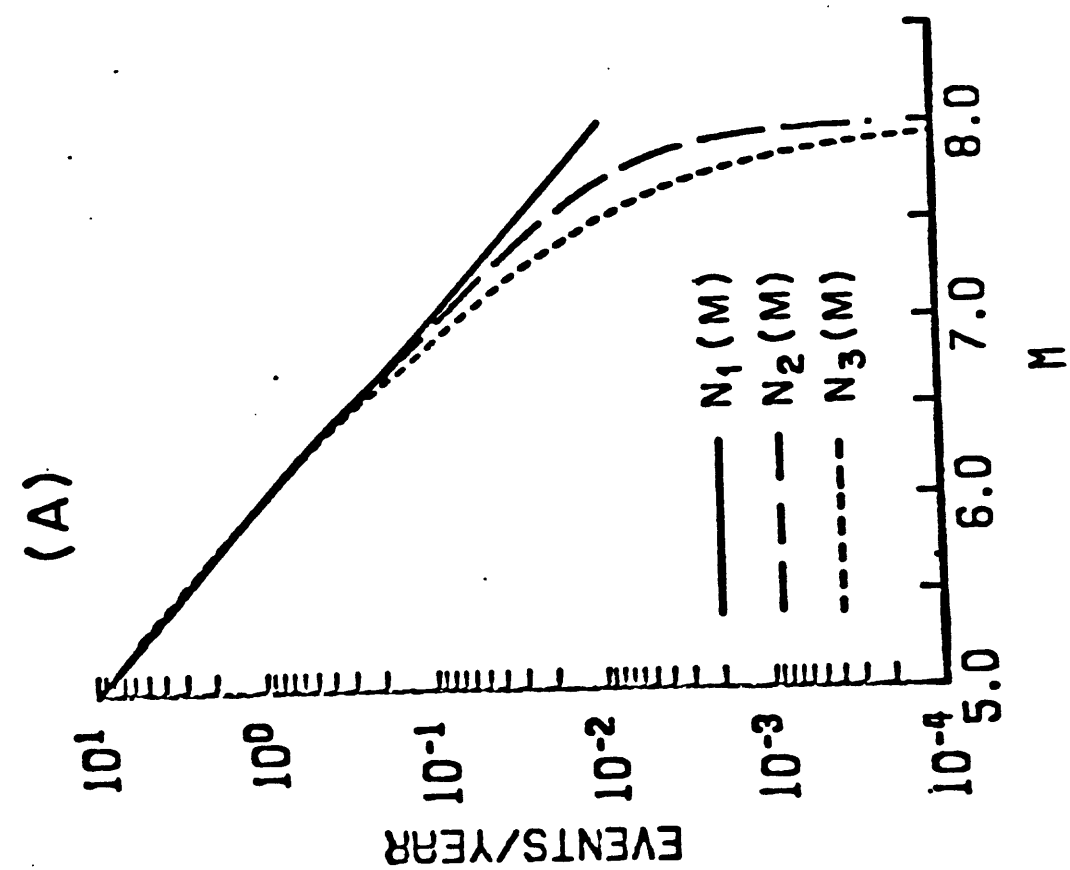


FIGURE 1

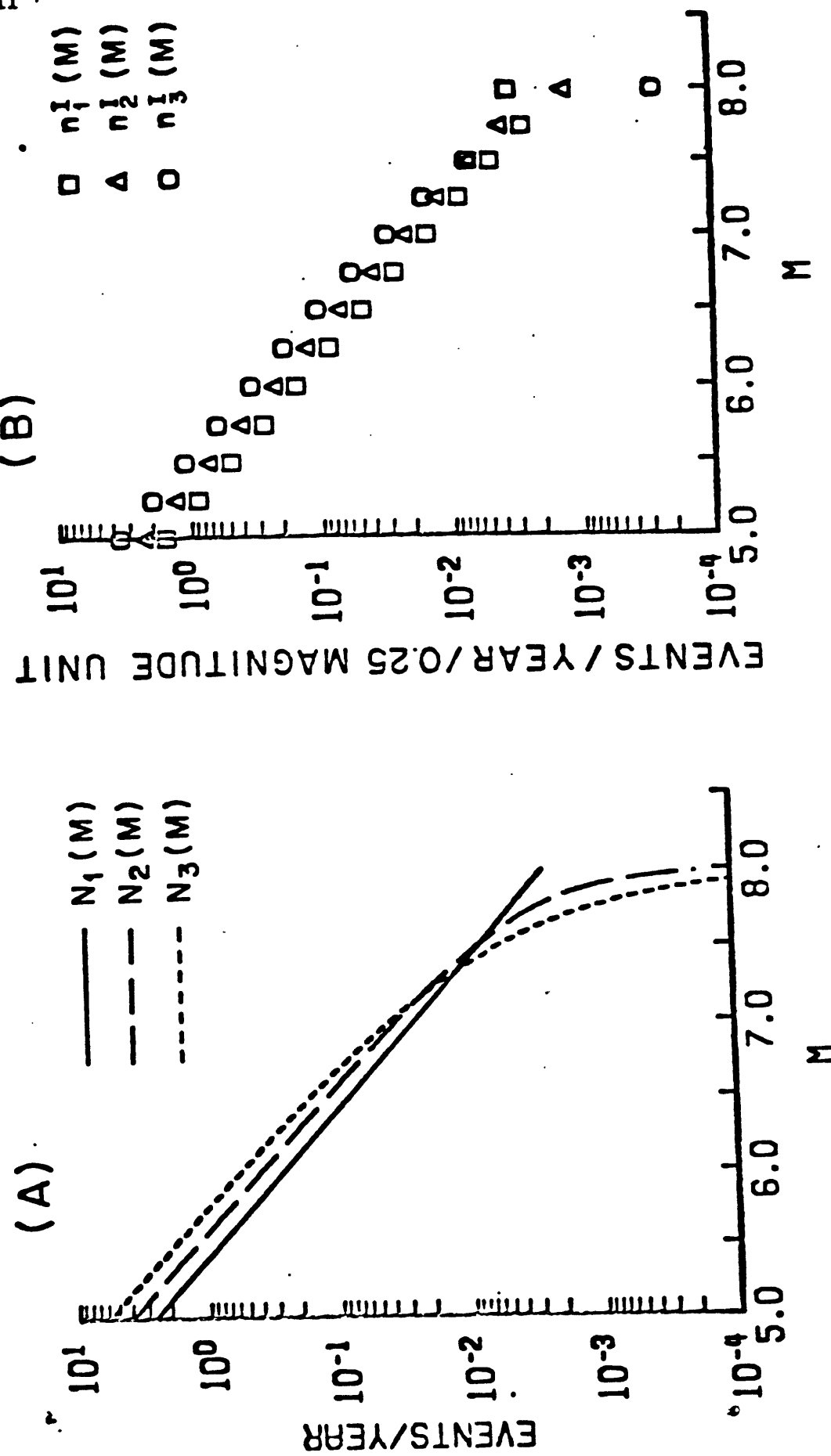


FIGURE 2

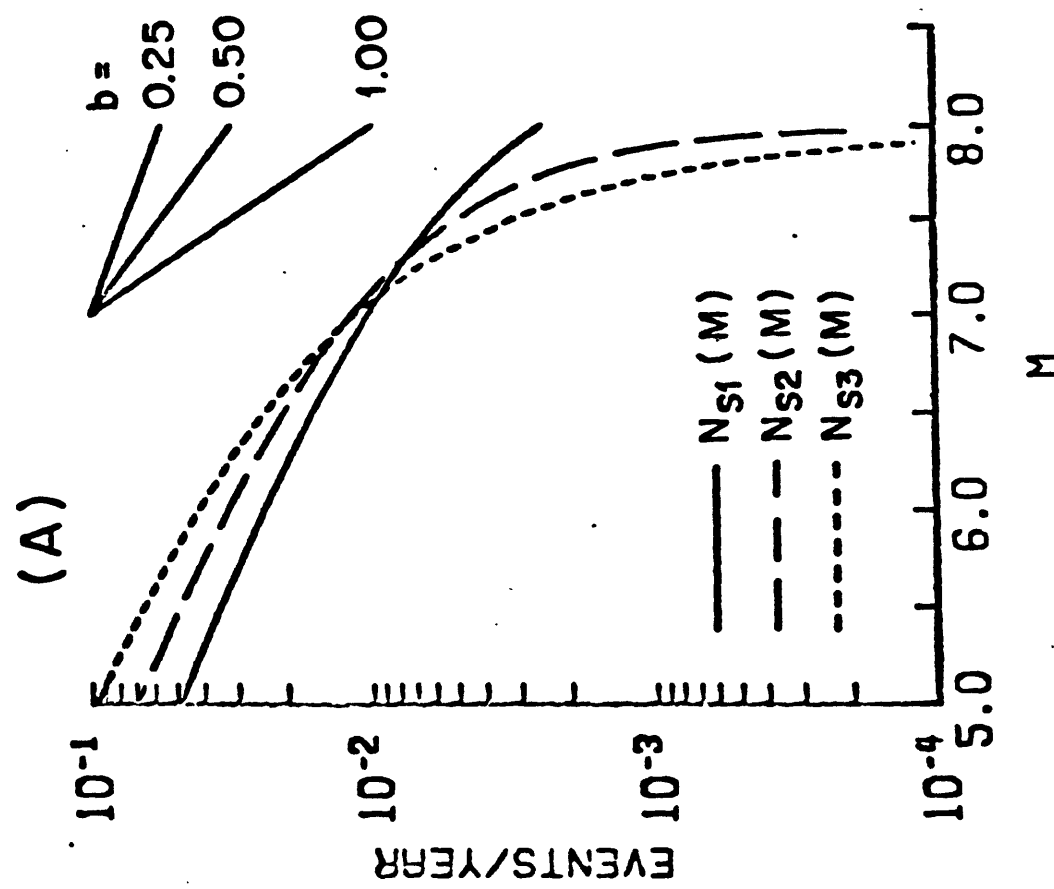
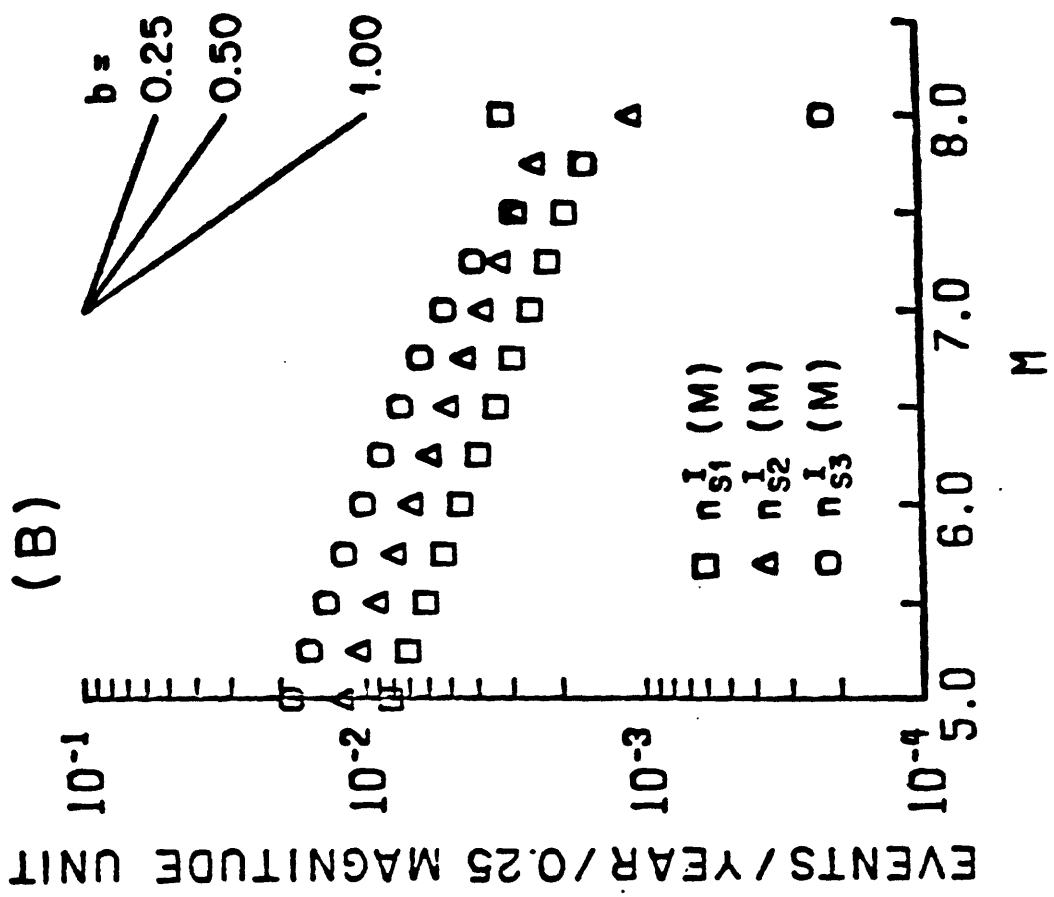


FIGURE 3

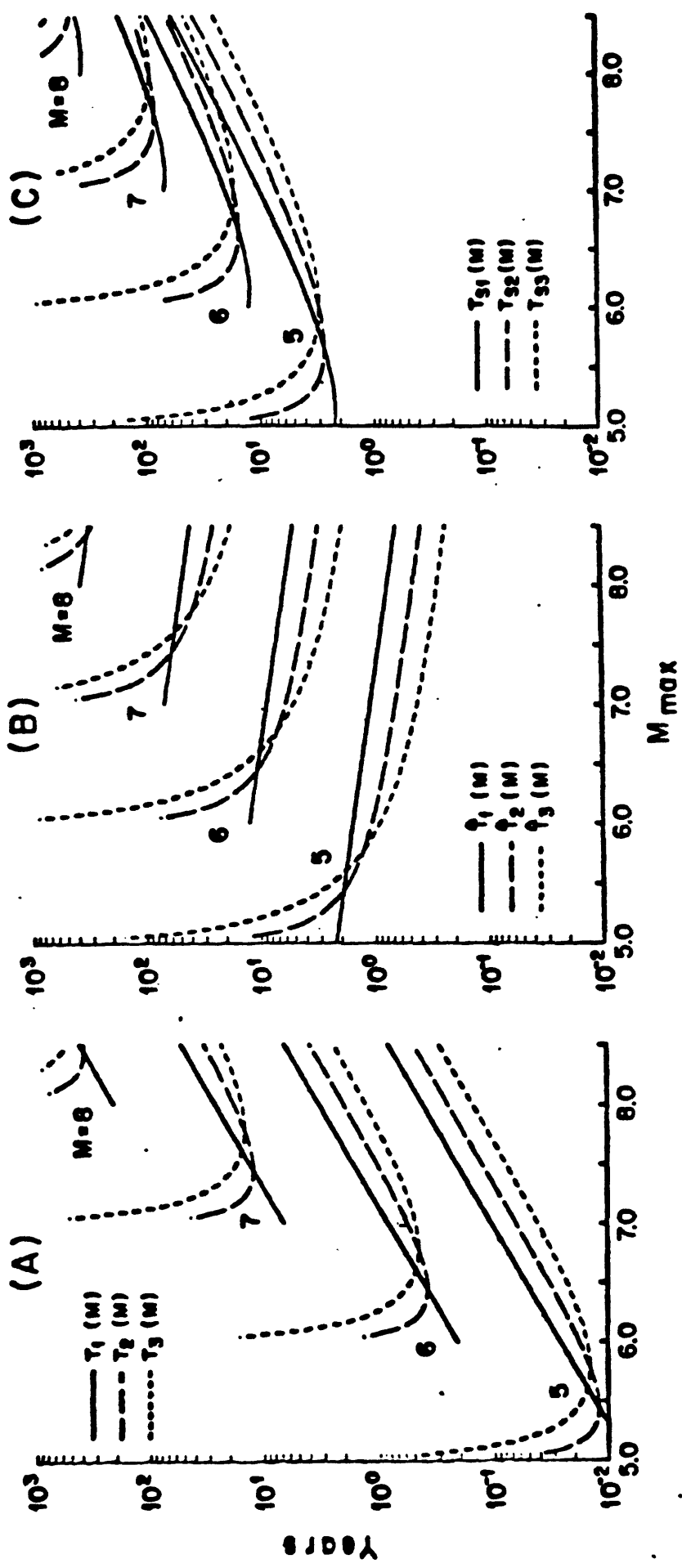


FIGURE 4

APPENDIX II

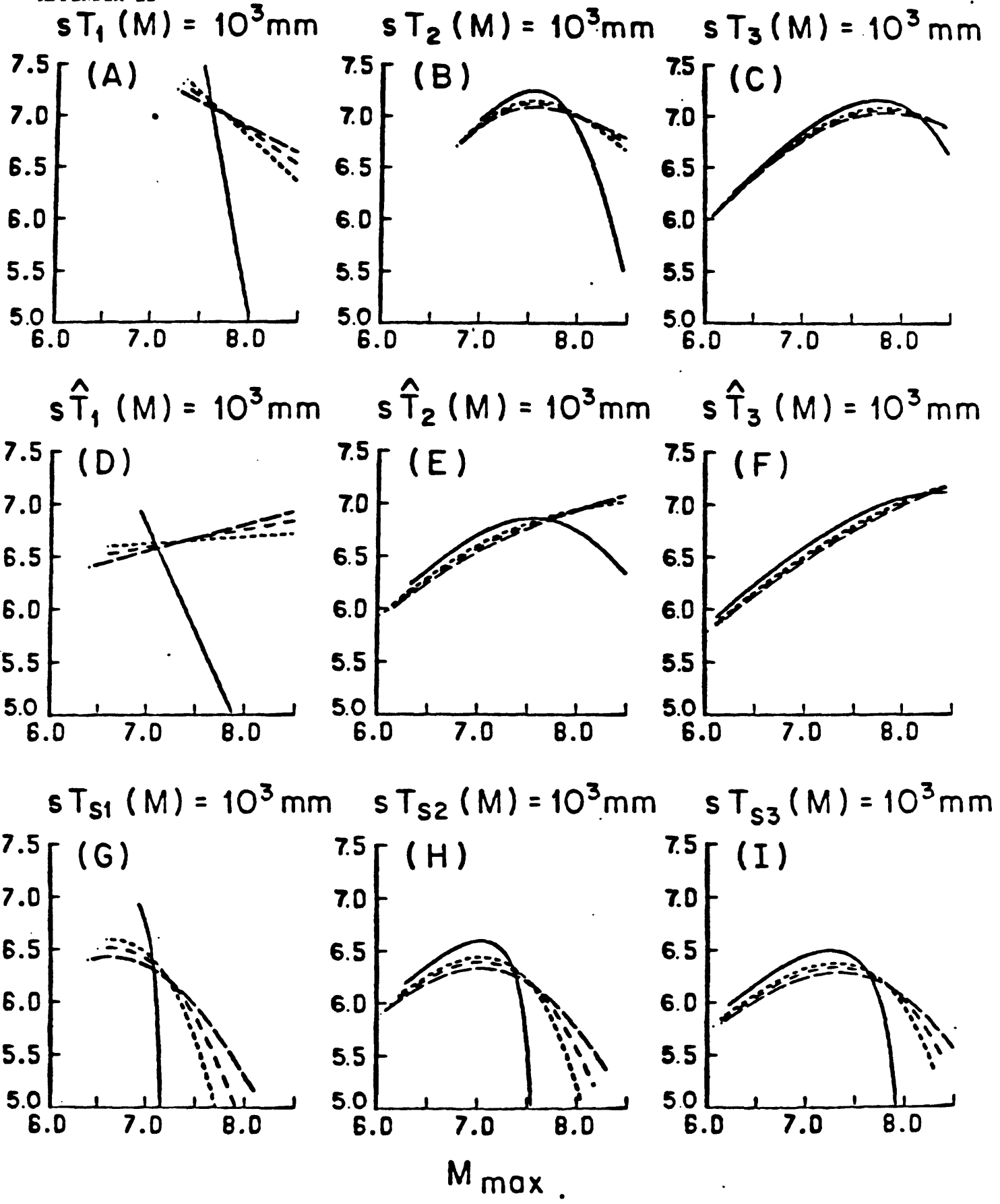


FIGURE 5

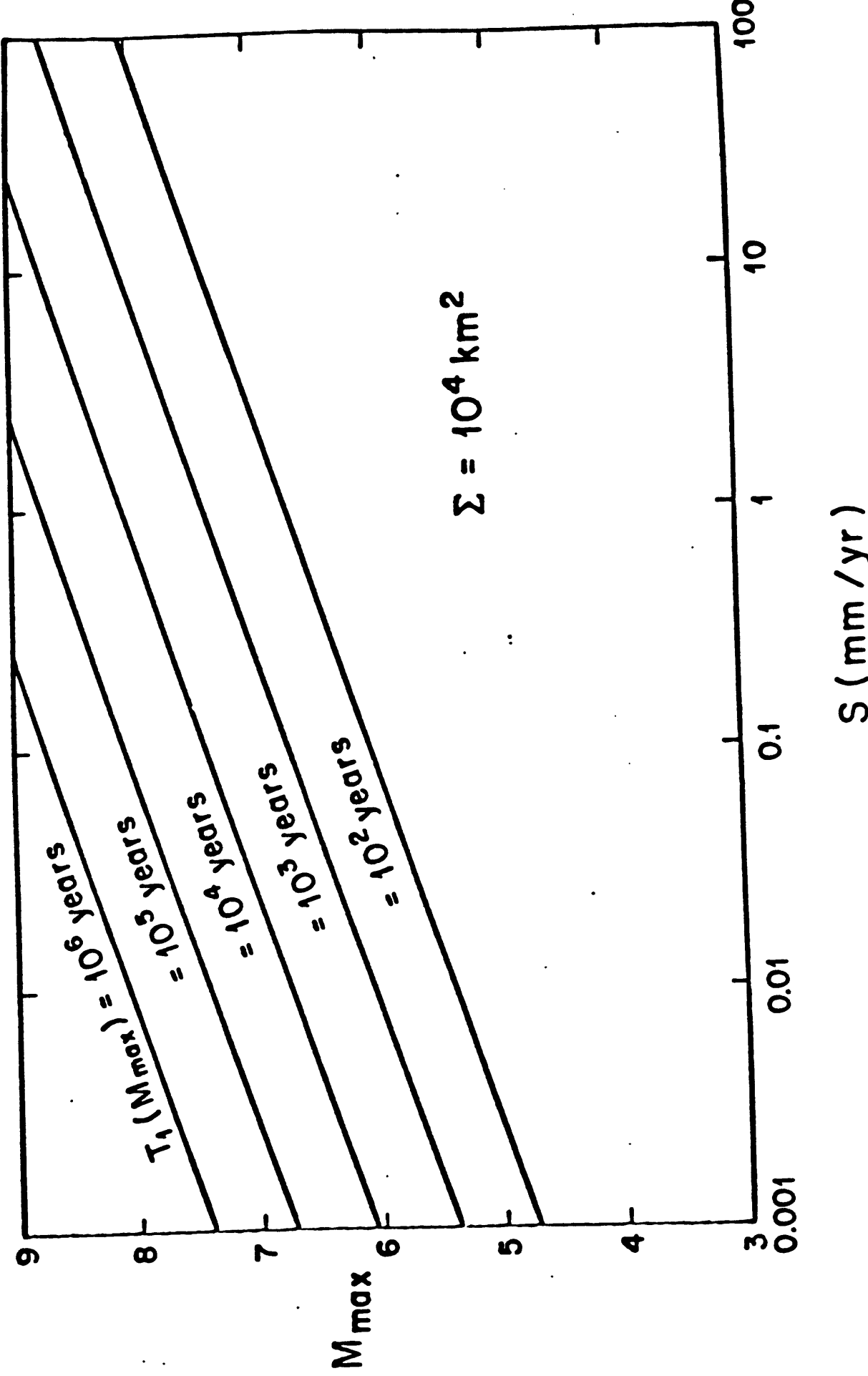


FIGURE 6A

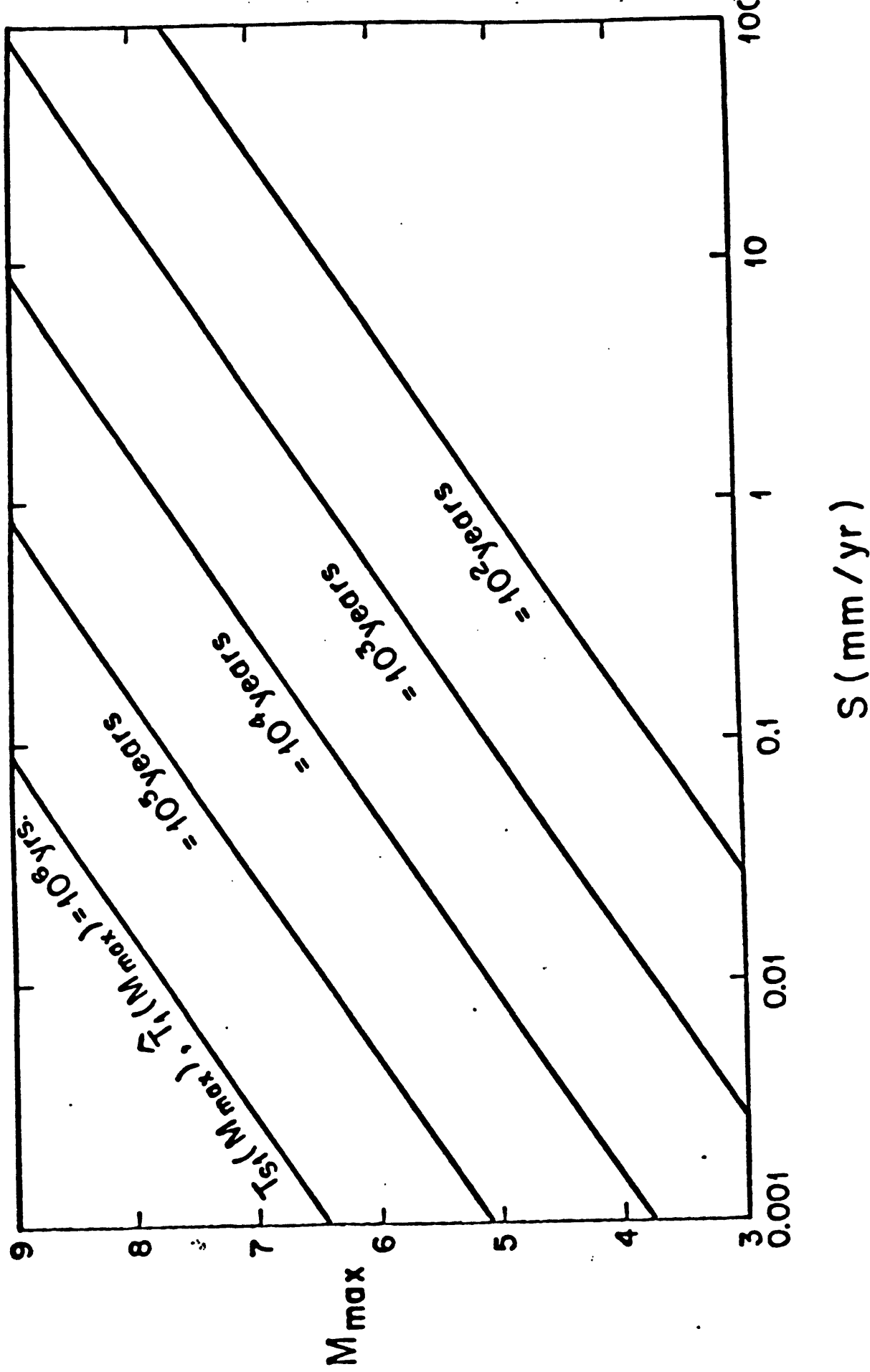


FIGURE 6B

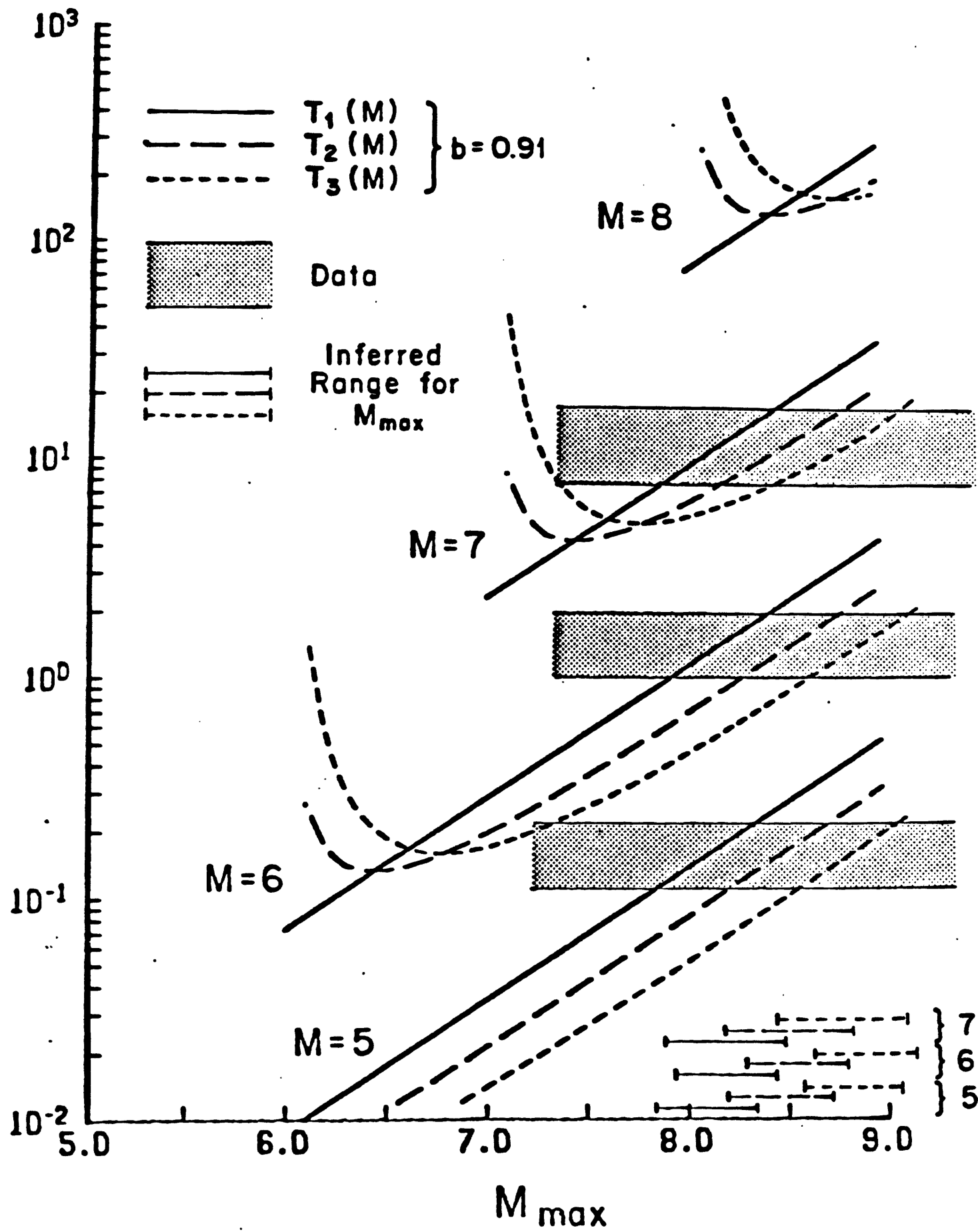


FIGURE 7

EVENTS/YEAR

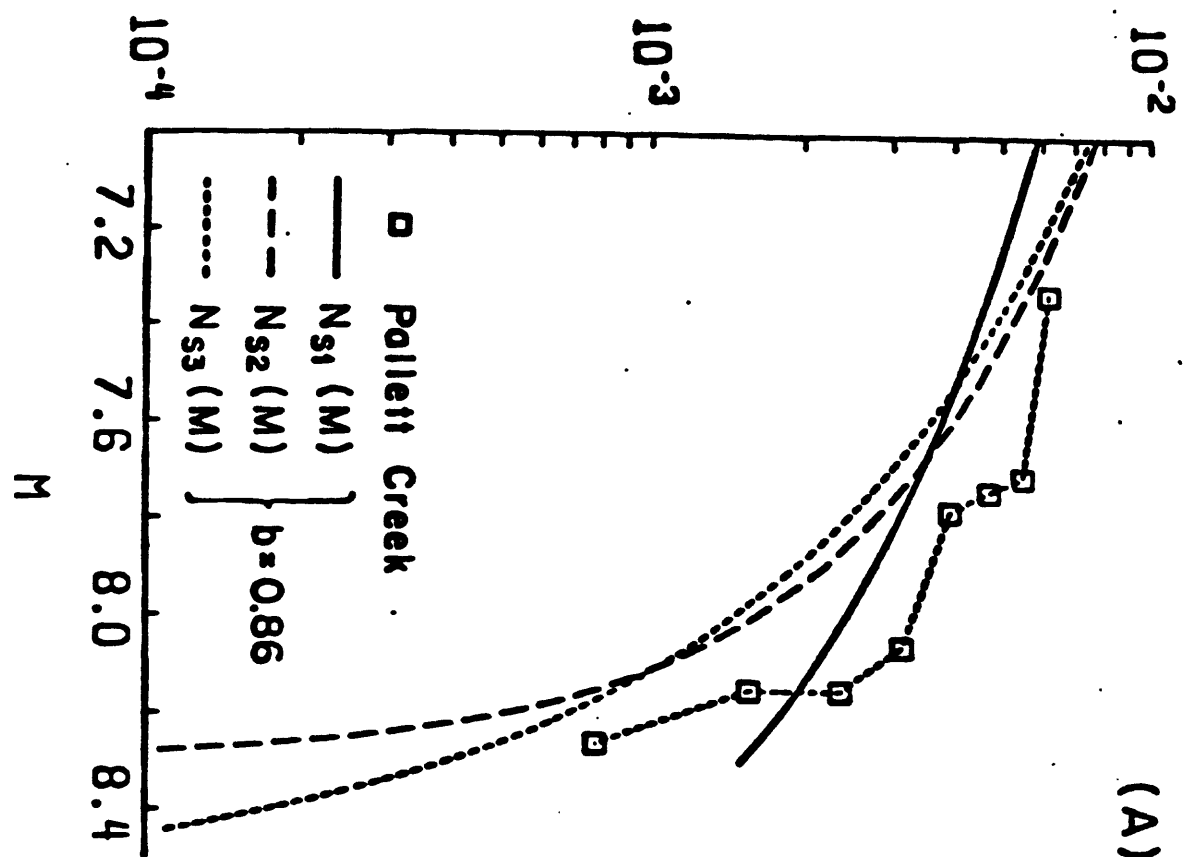


FIGURE 8

